Métallisation Electroless des Polymères Induite par des Ligands

Alexandre Garcia

Laboratoire de Chimie des
Surfaces et Interfaces

Thèse de doctorat de l'École Polytechnique

Spécialité : Science des matériaux

Présentée par

Alexandre GARCIA

Ligand Induced Electroless Plating of Polymers

Métallisation Anélectrolytique des Polymères Induite par des Ligands

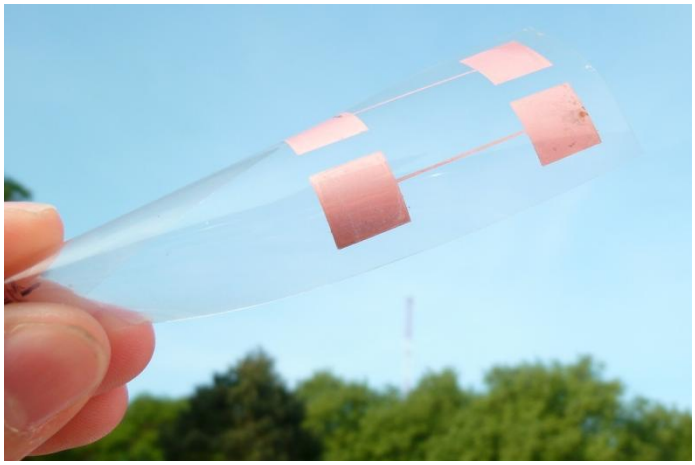

Soutenance prévue le 19 Septembre 2011 devant le jury composé de :

Pr.	**Jean-Christophe LACROIX**	*Université Paris Diderot*	Rapporteur
Pr.	**Pascal MAILLEY**	*Université Joseph Fourier Grenoble*	Rapporteur
Pr.	**Clément SANCHEZ**	*Collège de France / Université de Pierre et Marie Curie*	Examinateur
Dr.	**Thierry GACOIN**	*Ecole Polytechnique*	Examinateur
Dr.	**François BESSUEILLE**	*Université Claude Bernard Lyon*	Examinateur
Dr.	**Pascal VIEL**	*CEA Saclay*	Directeur de thèse
Dr.	**Thomas BERTHELOT**	*CEA Saclay*	Encadrant

Remerciements

Ce travail de thèse a été réalisé au Laboratoire de Chimie des Surfaces et Interfaces (LCSI) du Service de Physico-chimie des Surfaces et Interfaces (SPCSI) du CEA de Saclay en collaboration avec le Laboratoire des Solides Irradiés (LSI) au CEA et basé à l'Ecole Polytechnique.

Je tiens tout d'abord à remercier Serge Palacin qui m'a accueilli au LCSI et m'a fait entièrement confiance tant dans la réalisation de mes travaux que dans la rédaction et la présentation des résultats notamment lors de conférences internationales (Cancun, Mexico). Merci Serge pour tes conseils, tes lectures et relectures de nos différents articles et de mes chapitres de thèse.

Je remercie, avec émotion, mon directeur de thèse, Pascal Viel, toujours disponible et prêt pour parler des projets à venir, des résultats obtenus mais également de gloire, d'amour et d'eau fraîche… Et tout ça, quelque soit le jour avec grande générosité, une énorme envie et confiance. Chef, allias Maman, ces trois ans à tes côtés resteront pour moi une période incroyablement enrichissante.

Je remercie profondément, mon encadrant de thèse, Thomas Berthelot, également toujours disponible et prêt à bâtir l'avenir, toujours aller plus haut et croire en l'avenir! Le tout avec volonté, passion et envie de toujours faire mieux, viser plus haut!
Chef, allias Papa, ces trois ans où tu m'as emmené avec toi d'un laboratoire à un autre furent une vraie réussite et je pense qu'elle restera mutuelle.

Je remercie grandement Bruno et Jérôme qui m'auront apporté tout leur expérience, savoir et patience donnant lieu à une très belle production de résultats…Un grand merci Messieurs!

Je tiens à remercier tout particulièrement mes collègues et amis du LCSI, qui par leur bonne humeur, leur esprit d'équipe et leur ouverture d'esprit ont rendu ces trois années inoubliables.

Alice ma Jumelle (ou binôme), on aura bien rigolé, voyagé, partagé les pires comme les meilleurs moments! Encore merci pour ton organisation, dont il faut le dire, j'ai souvent largement profité, et surtout bon suite, comme dirait un autre compère, Federico !

Fanny, Maman dans l'âme, merci encore de la part ton fiston pour tous ces précieux conseils et autre fous rires !

Lorraine et Romain, vous avez été les piliers sur lesquels j'ai pu compter à mon arrivée et vous resterez toujours dans mon cœur.

Xavier et Adina, chers co-bureaux, merci pour toutes ces conversations endiablées autour du sport, du PSG mais aussi autour de Dalida et des complexes metalliques… Et je n'oublierai pas non plus votre soutien au quotidien, ces 2 ans en votre compagnie furent vraiment agréables !

Merci à Guy le conseiller vacances, Pascale la cacheuse d'échantillons et experte en XPS, Brigitte toujours prête à rendre service, Nabila pour tous nos fous rires et blagues , Tuan mon mentor, Amandine la copine chez les physiciens, Cécile, Olivier, Julienne, Dimitry, Cédric et les stagiaires comme on les aime Nassim, Robin (à prononcer à l'anglaise), Jenna, Mohamed, Marianne et les naines de Montpellier…

Et puis, la vie au laboratoire, c'est une chose mais la thèse, c'est aussi dans sa vie privée et à ce titre, je remercie tous mes amis qui auront subi tous ces débriefings sur la métallisation des plastiques !

Merci à ma famille qui est toujours resté à l'écoute dans les bons comme les mauvais moments, ça y est j'y suis arrivé.

Enfin, Merci à Pauline, ma louloute d'amour, pour ton soutien tous ces jours et en particulier les derniers. Merci pour ton investissement au quotidien, je n'aurai pas pu rêver meilleur support et meilleure moitié…

Table of contents

Abbreviations, Notations, Acronyms

A) Molecules and Polymers

4VP	4-vinylpyridine
ABS	Acrylonitrile-Butadiene-Styrene
ABS-PC	Acrylonitrile-Butadiene-Styrene-Polycarbonate
DNA	Deoxyribonucleic acid
EDTA	Ethylenediaminetetraacetic acid
FPI	Fluorinated polyimide
GOD	Glucose oxidase
PA	PolyAmide
PAA	Poly(acrylic acid)
PAMAM	Polyamide-amine
PAP	Polyaminophenylene
PE	Polyethylene
PET	Poly(ethylene terephtalate)
PDMS	Polydimethoxysilane
PHEMA	Polyhydroxyethylmethacrylate
PS	Polystyrene
PP	Polypropylene
PVC	Poly(vinyl chloride)
PVDF	Poly(vinylidene fluoride)
VIDz	Vinylimidazole

B) Characterizations

AFM	Atomic Force Microscopy
IR	Infra-Red
RF	Radio-Frequency
SEM	Scanning Electron Microscopy

UV	Ultra Violet
VUV	Vacuum Ultra Violet
XPS	X-ray photoelectron spectroscopy

C) Processes

AIEP	Amino-Induced Electroless Plating process
CIJ	Continuous Inkjet Printing
CVD	Chemical vapor deposition
DIAP	Diazonium Induced Anchoring Process
DOD	Drop-on-demand
LIEP	Ligand Induced Electroless Plating
µCP	Microcontact printing
PVD	Physical vapor deposition
SEEP	Surface Electroinitiated Emulsion Polymerization

D) Others

ASTM	American Society for Testing and Materials
MPT	Mixed-potential theory

I. Introduction

In everyday life, we are surrounded by products and materials that are coated by thin films which main goal is to combine the properties of the bulk material and the coating. Obviously, while using their smart phone, their computer or their car, customers cannot imagine the innovative breakthroughs that were achieved to develop and industrialize these attractive products. One of the main challenges for manufacturers is to ensure the performance durability with time. This performance is driven in part by adhesion and cohesion mechanisms. Therefore, while cohesion is depending on the intrinsic properties of the coating material, the adhesion between two materials is based on physical, chemical and mechanical interactions between those materials. And even if from the Neolithic period, coatings made of beeswax or Arabic gum have been used to give new chemical or physical properties to raw materials, we are still not able to explain exactly all the phenomenon involved in the adhesion mechanisms. The famous Geckos lizards are a good illustration of the adhesion mechanism complexity (**Figure 1**). Hence, they are able to run up a wall and hang onto ceilings of most surfaces thanks to their footpads made of spatula tipped setae which own incredible adhesive forces. Even if it was admitted that these adhesive forces are mainly based on Van der Waals interactions between the adhesive setae and the surface, complete adhesion mechanisms are still not fully understood and controversial [1-3].

Figure 1 : Pictures of a gold dust day gecko (also known as Madagascar day geckos) and a close-up of the underside of a gecko's foot as it walks on vertical glass

However, scientific community concurs to say that adherence of a coating onto a surface is the result of a very complex balance between mechanical and physico-chemical interactions between the surface and the coating that need to be optimized. This is specifically true for coatings which do not have any specific chemical or physical affinity with the raw material surface to be coated, such as metal coatings onto plastics substrates.

As such, since the end of the Second World War the use of plastics substrates has hugely increased due to their specific properties such as light weight, design flexibility and low cost of manufacturing. This has led, in a very wide range of applications, to the replacement of metals with polymers as materials of construction. Nevertheless, they are several metal properties that cannot be matched by polymers such as the reflectivity, brightness or electrical conductivity. This was a drawback when, in the early 1960's, the automobile industry was looking to replace metal with polymer substrates for manufacturing exterior and interior bright trim. At this moment, trim components were usually finished in bright electroplated nickel/chromium generally known as chromium electroplating, which provided the required high quality brightness. If plastics substrates were used as a replacement, a new coating method was therefore required to provide similar surface appearance and properties. It was soon established that only electroplated nickel/chromium would give the necessary quality that was related not only to aesthetic properties but also to other properties of this particular coating system such as good resistance to corrosion and abrasion, or ease of cleaning. The surface coatings industry was facing the problem of producing this durable and attractive metal coating on polymers components, thereby combining the advantageous properties of the substrate with those of the coating system.

Contrarily to polymer coatings onto metals that can be obtained by electrochemical or chemical processes, metal coatings onto insulating substrates such as polymers was a great challenge since very few chemical or electrochemical processes are available to promote the adhesion of a metal onto insulating polymer substrate. Additionally, the mechanical constraints generated by an inelastic metal layer onto a flexible and elastic polymer are quite high and make the process quite difficult to optimize and durability of the final coatings difficult to improve.

However, since the early days of the 1960's, the economic and technological attractiveness of the metallization (or metal finishing) of polymers & polymer-based materials has led to the development of various processes and is widely used today in various technological applications ranging from decorative coatings in general manufacturing and especially in the automobile industry to the fabrication of printed circuits in microelectronics (**Figure 2**) [4-10]. Indeed, the use of organic materials combined to metal coating in the fabrication of

microelectronics devices, bioelectronics devices and portable electronics has met a growing interest during the last few decades [10-16]. As an example, the fabrication of metallic circuit patterns on polymer substrates becomes extremely important for the manufacturing processes of flexible electronics.

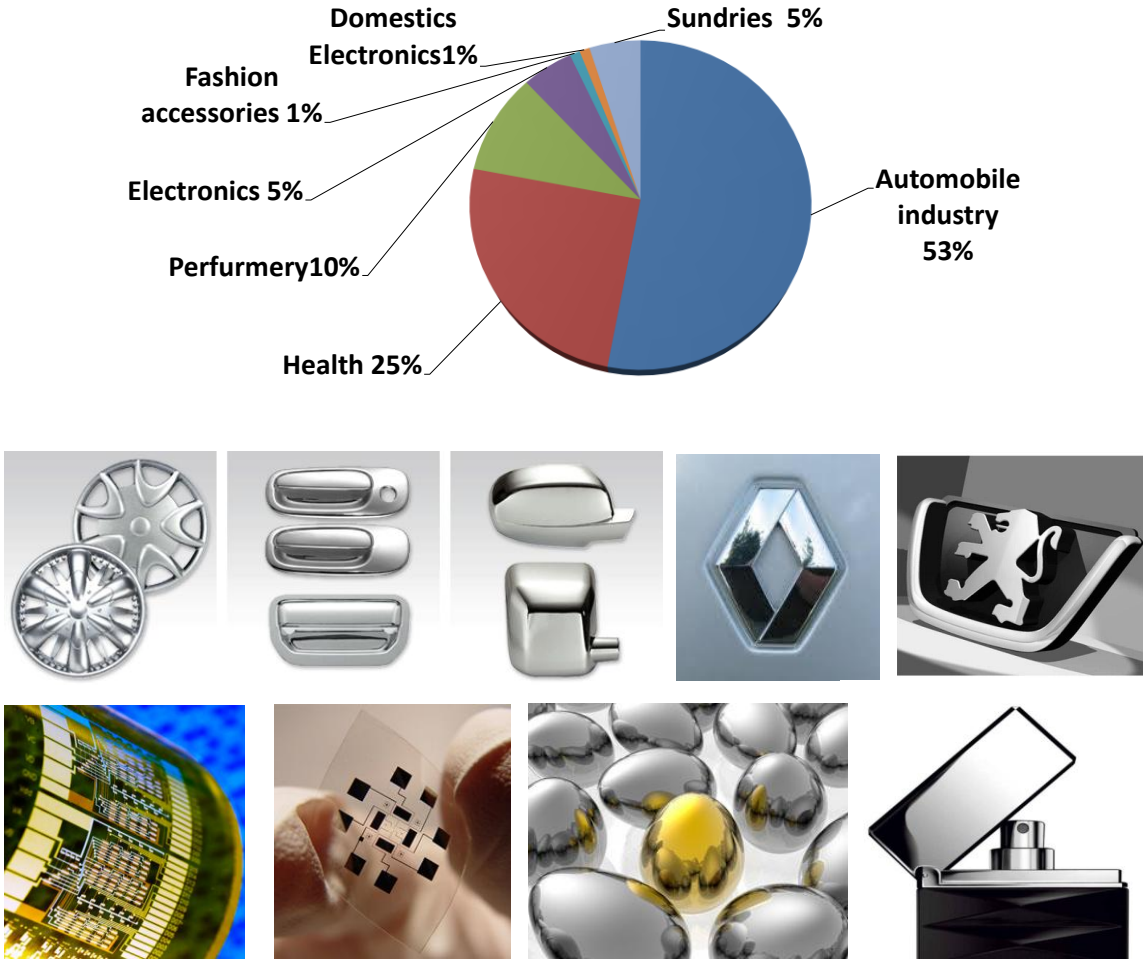

Figure 2 : Examples of polymer metallization applications

Up to now, for ABS (Acrylonitrile-Butadiene-Styrene), ABS-PC (Acrylonitrile-Butadiene-Styrene-PolyCarbonate) and PA (PolyAmide), which represent more than 90 % of the industrially metallized polymers (**Figure 3**), the best (and most widely used) method is based on the electroless metal plating growth. This process starts by a chromic acid etching, which oxidizes the bulk polymer surface. In most cases, this surface conditioning (or surface treatment) is followed by the surface seeding with a catalyst and the electroless deposition itself, which is the chemical deposition of a metal film from a solution containing a mild reducing agent and an ionic complex of the metal to be plated onto the seeded substrate [6,

9]. The main goal of the electroless deposition is to make the polymer substrates conductive (0.5 to 2 µm in thickness) and then, depending on the applications, various metal electroplating steps are achieved. Finally, the thickness of the metal coating is about a few tens microns which induces strong surface mechanical strains. Therefore, the ability of the whole metal coating to withstand mechanical strains is directly linked to the adhesion of the electroless metal layer onto the substrate. And that is how the hexavalent chromium based surface treatment step is essential in the metallization of polymers process since it is the step that guarantees the adhesion of the electroless metal layer and thereby the adhesion of the metal coating including the different electroplated layers [9, 17, 18].

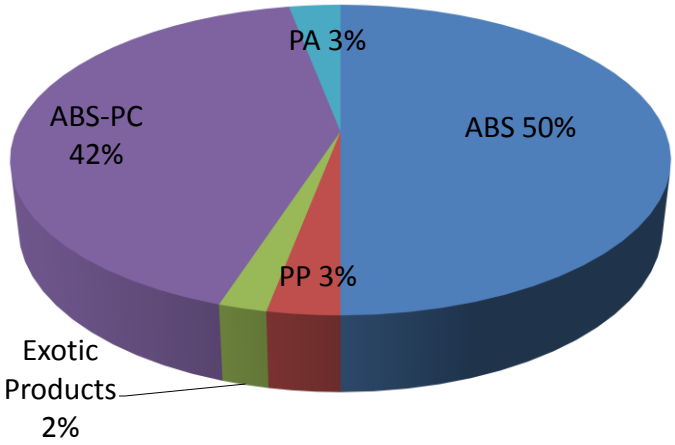

Figure 3 : Metal plated polymers distribution

Unfortunately, hexavalent chromium or chromium (VI) which is also essential for other surface treatments processes such as chromic acid anodizing [19] or hard chromium electroplating [20] is highly toxic by inhalation and is a proven carcinogen. Breathing high levels of hexavalent chromium can damage and irritate nose, lungs, stomach, and intestine (US Agency for Toxic Substances and Disease Registry, 1993). Risks linked to chromium trioxide or chromic acid based solutions are given by the INRS (Institut national de recherche et de sécurité) safety sheets. Although hexavalent chromium provides many advantageous properties, it is regulated by the European Council for its toxicity and carcinogenicity [17, 18]. As a matter of fact, hexavalent chromium waste can be generated by either industrial accidental leak or landfill products.

In order to prevent any environmental accident during the metallization process, hexavalent chromium concentration in the industrial baths and their volumes are important

factors for the industrial plants classification based on the ICPE nomenclature[a], the French equivalent European directive called, "SEVESO II"[b] [21]. More recently, another European directive[c] aims to prevent and reduce all recurrent pollution risks produced by the most polluting European plants (chemistry, metallurgy, papermaking, mechanical industry, glassworks but also industrial livestock farming …) by increasing the use of "best available techniques" (BATs) which is an obligation to ensure that industrial operators work with the most cost-effective techniques to achieve the highest level of environmental protection [22]. Besides, according to the BATSs for the waste treatment described in the BAT REFerences document (BREF), hexavalent chromium is banned from the waste and has to be reduced in trivalent chromium.

For landfill products, legislations refer to two similar European directives [17, 23].[d,e]

As a matter of fact, through all these directives, the main goal is to ban hexavalent chromium from all consumer products (in automobile industry and electrical and electronic equipments) which end-life cycle is not yet fully controlled and limit its use during the process fabrication.

Finally, in the near future, the European Commission Regulation N°143/2011 of 17 February 2011 amending Annex XIV to Regulation (EC) N°1907/2006 of the European

[a] Installations classées pour la protection de l'environnement - Inspectorate of Classified Installations

[b] Directive 1996/82/EC of the European parliament and of the council of 9 December 1996 on the control of major-accident hazards involving dangerous substances

[c] Directive 2008/1/EC of the European Parliament and of the Council of 15 January 2008 concerning Integrated Pollution Prevention and Control, which replaces the Council Directive 96/61/EC of 24 September 1996 on the same subject matter

[d] Directive 2000/53/EC of the European Parliament and of the Council of 18 September 2000 on end-of life vehicles (VHU – Véhicule Hors d'Usage) aims to minimize the impact of the end of life of vehicles on environment by restricting the use of certain heavy metals, such as hexavalent chromium, in new vehicles from 1 July 2003. The objective is to ensure that 85% of an end of life vehicle by weight will be recycled by the year 2006, increasing to 95% by the year 2015 with additional de-pollution tasks being progressively introduced.

[e] Directive 2002/95/EC of the European Parliament and of the Council of 27 January 2003 on the restriction of the use of certain hazardous substances (RoHS) in electrical and electronic equipment involves the restriction of the use of six hazardous materials in the manufacture of various types of electronic and electrical equipment and took effect on 1 July 2006, and is required to be enforced and become law in each member state. For the hexavalent chromium, the maximum concentration value which determines the maximum amount of each substance that will be allowed in order for that product to be determined to be RoHS Compliant is 0.1% by weight of homogeneous material.

Parliament and of the Council on the Registration, Evaluation, Authorization and Restriction of Chemicals ("REACH") will force the industry to give up chromium use, hence raising technological and scientific challenges. In the same time, it has to be kept in mind that another risk lies in the industrial relocation in countries without any legal rules on waste treatments, which gives to that environmental issue huge economical impact.

Thereby, even if the hexavalent chromium concentration in the etching baths was successfully reduced (from 400 $g.L^{-1}$ in the 1960's to 60 $g.L^{-1}$ nowadays) [24], the polymer metallization industry has now to work on available and economically feasible alternatives for chromium acid etching which up to now, has not been found.

Despite the fact that metallization of polymers is considered as an applied process relatively abandoned by academia researchers in the past, the recently demonstrated ability of polymers to function as semiconductors, diodes, and transistors in polymers integrated circuits has aroused attention in industry and academia for flexible electronics applications, which also require metal coatings. There are thus great challenges to take up in order to obtain a greener and competitive process than the one currently used in the industry based on a chromic acid etching and to adapt it to flexible electronics applications.

Within this socioeconomic, public health and environmental issues combined with the scientific and technological limitations, the main goals of this research project are:

i. To address an industrial problem by developing a chromium-free and efficient process for the electroless metal plating of polymers involving a new adhesion approach which could even allow to extend the polymer substrates range to be metallized
ii. To adapt this wet chemical based process for the fabrication of metal patterns by low-cost lithography techniques adapted for flexible electronics applications.
iii. To transpose this chromium-free and versatile wet process to a printing and photo-assisted process in order to improve its sustainable nature

This research project led to an important scientific production regularly validated by patents and articles published into peer-reviewed journals. Hence this thesis is essentially based on those articles, allowing the reader to have well-identified steps of the presented

work. The following state of the art is intended to give the reader the necessary background on the achieved work.

II. State of the art

Metallization of polymers is widely used today in various technological applications ranging from the fabrication of printed circuits in microelectronics to decorative coatings in general manufacturing. Through polymer metallization, the specific properties of polymers, such as light weight, design flexibility and low cost of manufacturing, are enriched by the addition of properties usually associated with metals. These include reflectivity, abrasion resistance, electrical conductivity and a variety of decorative effects. The processes used for metallizing polymers can be carried out in solid, liquid or gaseous phase, but all require an appropriate etchant system for surface conditioning in order to get an adherent metallic layer.
In a first part, we will focus on the different kinds of pretreatments starting by a brief reminder on the adhesion mechanisms, then, in a second part we will present the different methods to obtain metal coatings onto polymers, once the substrate is pretreated. At this stage, we will focus on the most used method: the electroless metal plating and we will attempt to describe its mechanism. In a third and a fourth part, we will respectively focus on the electroless plating processes based on ligands adsorption (chemisorption or physisorption) with 2D or 3D-ligation structure and how to adapt these processes to achieve selective electroless plating and obtain metal patterns onto polymers. Finally, in a fifth part, we will deal with the diazonium induced anchoring process which was the basis of this work.

1. Surface conditioning or pretreatment

First of all, in order to obtain the best available adhesion between the deposited metal layer and the substrate surface, the surface state needs to be optimized. Therefore, surface conditioning, also called pretreatment or surface treatment, is always preceded by a cleaning treatment. Indeed, polymer surfaces are generally prone to organic pollution which could be detrimental for the following steps. This cleaning treatment mostly consists in the immersion, often associated with sonication, into an industrial detergent.

Once the surface is cleaned, a pretreatment can be applied and has two main goals:

i. Increasing the bulk polymer roughness (by voids or pores creation) to promote the mechanical anchoring which is directly related to the **mechanical adhesion** of the deposited metal layer.

ii. Increasing the bulk polymer wettability by surface oxidation to promote the chemical affinity between the metallic catalyst and the substrate surface which induces a better **physico-chemical adhesion** of the final deposited metal layer.

Whereas mechanical adhesion provides adhesion at the micrometer scale, physico-chemical adhesion improves molecule/substrate interfaces interactions at the molecular scale through chemisorption or physisorption phenomena. The best adhesion of the metal layer onto the substrate is logically obtained by combining both mechanical and physico-chemical adhesions.

At the industrial scale, there are two main methods to evaluate the adhesion of the deposited metal layer, (**Figure 4**): The first method is a T-peel strength adhesion measurement, based on the standard test method for peel resistance of adhesives (T-peel test) ASTM D1876-08 (**Figures 4a and 4b**). The second method which is also more demanding is the standard Scotch® tape test based on the standard ASTM D3359 Scotch® tape test (cross-cut tape test) which consists in applying and removing pressure-sensitive adhesive tape over 16 cross-hatched squares of 1x1 mm^2 made in the film (**Figures 4c and 4d**). That standard well-used test allows a direct comparison of the adhesion of films obtained under various conditions on similar substrates.

In both cases, these adhesion tests lead to qualitative and comparative results between various processes and threshold measurements.

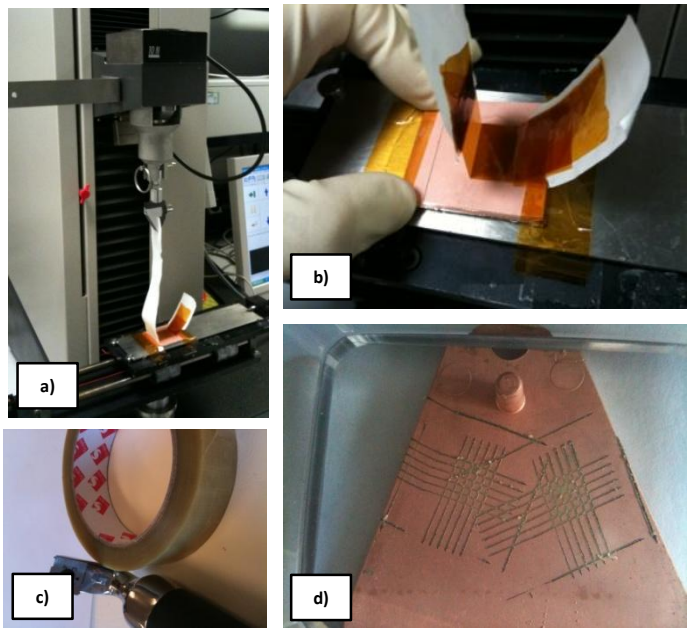

Figure 4: Images of the T-peel test (a, b) and of the scotch test (c, d)

To obtain the required adhesion (which strongly depends on the concerned application) of the metal layer onto the polymer substrates, there are three different kinds of pretreatments: mechanical, chemical and physical pretreatments.

1.1. Mechanical pretreatments

Mechanical pretreatments are mainly based on abrasive blasting and in particular sandblasting which is easily adjustable for various kinds of substrates and allows obtaining the expected roughness to get the best adhesion results.[25] However, it is quite expensive, it produces a lot of waste and it is not convenient for complex-shaped substrates. Hence, it tends to disappear from industrial processes.

1.2. Chemical pretreatments

Whereas mechanical pretreatments lead to the surface roughness increase without any surface oxidation, chemical pretreatments provide both surface roughness and oxidation. Depending on the chemical nature of the substrate, the chemical preatreatment can be different. As previously written, up to now, for ABS (Acrylonitrile-Butadiene-Styrene), ABS-PC (Acrylonitrile-Butadiene-Styrene-PolyCarbonate) and PA (PolyAmide) polymers which

represent more than 90 % of the polymers industrially metallized (**Figure 3**), the best (and most widely used) method is based on a chromic acid etching, which oxidizes the bulk polymer surface. These oxidation phenomena imply both chemical and mechanical adhesion respectively thanks to the chemical reactive groups formation and the superficial holes or cavities creation which increases the surface roughness. Besides, as an example, in the ABS and ABS-PC cases, chromic acid dissolves specifically the polybutadiene nodes in ABS and ABS-PC, which increases the surface roughness. **Figure 5** illustrates the chromic acid etching on ABS substrates.

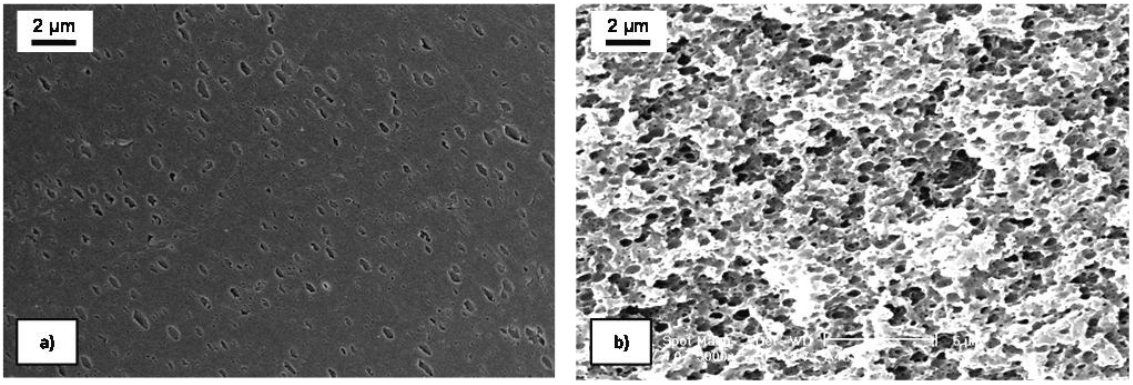

Figure 5 : SEM Images of a pristine ABS substrate (a) and an ABS substrate after a chromic acid etching (b)

Nevertheless, as explained above, that efficient process has to be replaced and numerous alternative pretreatments are described in the literature involving acid, basic, solvents etchings, their mixture or even several steps with an acid etching followed by a basic one [17, 18, 26-29]. None of them has yet shown as efficient as the chromic acid etching at the industrial scale. Likewise, it has to be said that some resistant polymers such as poly(ethylene) or poly(oxymethylene) are neither oxidized by the chromic acid etching nor by other available alternative pretreatments. These polymers are still considered as unplateable polymers.

Lastly, the chemical pretreatment step is always followed by a post-treatment involving a rinsing treatment and a neutralization step which allow removing all the waste and impurities (chromium derivatives, acids, etched polymer residues…) from the surface. A incomplete neutralization induces inhibition during the metal deposition step. Therefore, by taking each step into account, the chemical pretreatment produces high amounts of waste for reprocessing, which finally make most of the chemical treatments not valuable in the current environmental issue.

1.3. Physical treatments

To overcome the limitations previously exposed against the chromium use regarding the pollution aspect but also the limited substrates range, numerous dried techniques [8], such as ion-assisted laser treatment [30], plasma modification [31-34], excimer VUV laser irradiation [35] or dielectric barrier discharge [36] have been proposed. As the chromic-acid etching, dried treatments provide both surface oxidation and slight surface roughness increase but contrary to the chromic acid etching or all the other chemical treatments, no post-treatment is required. Nevertheless, most of dried treatments require drastic working conditions and vacuum chambers which are complicated to achieve on an industrial production line. Furthermore, dried treatments work only on planar-shaped substrates and are useless for complex-shaped substrates.

1.4. Conclusions

To date and as a conclusion for the surface conditioning step, even if many alternative treatments have been developed and are still being developed, the pollutant chromic acid etching is still the most efficient method to prepare the surface for the metal deposition at the industrial scale. However, because of the future European ban on hexavalent chromium use, this efficient process needs absolutely to be replaced.

2. Metallization/Metal plating of polymers

Once the surface conditioning is performed and optimized, the metal deposition can be carried out by different processes that are described in the following parts.

2.1. Solid and molten metal based deposition

The metal deposition can be made by applying a solid or molten metal based deposition. Solid based metal deposition is mainly made by hot stamping of a thin metal shit onto a polymer at 100-200°C [25]. This deposition method can be applied to various kinds of substrates (PS, PP, ABS) but it is restricted to planar surfaces which limits the applications. In

the case of molten metal based deposition, it consists in the simultaneous melting and projection by a thermal process onto the polymer surface [25]. The metallic droplets which are mainly made of zinc are projected to the surface and then, they coalesce on the surface upon cooling down and finally form a rough, conformal and massive metal layer. Nevertheless, for many applications such as the insets fabrication for injection molds, this process does not provide a good adhesion of the metal layer. Moreover, the glass transition temperature of most thermoplastics is lower than the working temperature of this process, which strongly limits the number of polymer substrates that can stand this method.

2.2. Gaseous phase based metal deposition (Dry process)

It consists in the thermal evaporation process followed by the metal condensation onto a substrate in a vacuum chamber. Various techniques coexist and are mainly divided into two main types: The chemical vapor depositions (CVD) and the physical vapor depositions (PVD).

2.2.1. Chemical vapor depositions (CVD)

Chemical Vapor Deposition (CVD) is a process in which the substrate is exposed to one or more volatile precursors, which react and/or decompose on the substrate surface to produce the desired thin metal layer. An alternative is Plasma-Enhanced Chemical Vapor Deposition (PECVD) which is a form of CVD that involves the creation of a plasma of the reacting gases and subsequent deposition onto a substrate. The plasma is generally created by a radio-frequency, direct-current or microwave discharge between two electrodes located in the space into which the reactive gases are introduced.

2.2.2. Physical vapor depositions (PVD)

PVD process encompasses a wide range of vapor-phase technologies, and is a general term used to describe any method to deposit thin solid films by the condensation of a vaporized form of the solid material onto various surfaces. PVD involves physical ejection of material as atoms or molecules and condensation and nucleation of these atoms onto a substrate. The more common PVD processes are evaporation and sputtering. Materials are physically created

in the vapor phase by energetic bombardment of a source (e.g. sputtering target) and subsequent ejection of material.

2.2.3. Conclusions

To conclude, even if vapor metal deposition is probably the cleanest method to obtain thin and homogeneous metal layer onto various kinds of substrates, vacuum chambers requires strict working conditions and high fabrication costs which are very restrictive for many industrial applications. Moreover, these techniques do not ensure the metallization of all-shaped substrates and rough pretreatments are needed to ensure the adhesion of the deposited metallic layer.

2.3. Solution based metal deposition: Electroless metal deposition (Wet process)

Electroless metal deposition is a process for chemical deposition of a metal from a solution containing a reducing agent and a derivative of the metal to be plated on a catalyzed surface. The process is generally inexpensive and can be performed in a manufacturing environment at or near room temperature under ambient and aqueous conditions. Electroless metal plating is the most used method to metallize insulating surfaces and more specifically polymers for the deposition of conformal metal films onto all-shaped substrates [6, 9, 37-39]. This electroless metal deposition step is followed by various electroplating steps to bring all the expected properties in terms of brightness, abrasion or corrosion resistance [24]. As a matter of fact, its main goal is to make the substrate conductive enough to allow a subsequent electroplating step.

Contrary to gaseous and solid based metal deposition, for which the surface conditioning was directly followed by the metal deposition itself, common electroless processes involve three main steps: (i) surface conditioning (See section II.1), (ii) surface activation or surface seeding with a catalyst, (iii) electroless deposition itself, which is the chemical deposition of a metal film from a solution containing a mild reducing agent and a derivative of the metal to be plated onto the seeded substrate [6, 9] (**Figure 6**). As described in Mallory's book [9], almost all metals of the Group VIII of the periodic table (Au, Pt, Ni, Cu, Co, Fe,…) can be plated and

exhibit autocatalytic behavior. Hence, the electroless metal deposition is not stopped once the catalyst is covered by the first metal deposit. All these active metals are also well-known as hydrogenation/dehydrogenation catalysts, which is a crucial point as explained later. Electroless deposition is actually a complex process involving multiple and simultaneous redox processes on the substrate surface which composition, structure and morphology are increasingly modified by the plating. Besides, mechanistic details of metal deposition still remain unclear. The mixed potential theory [9, 40] is the most used and experiment-based model for electroless metal deposition and consists of an initial spontaneous oxidation of the reducing agent at the catalytic surface, leading to electron charging of the substrate surface until its electrochemical potential becomes sufficiently negative to reduce the metallic derivative to metal. The mixed potential theory provides a correct description of the electroless plating mechanism when electron transfer between the reducing agent and the metallic ion is mediated by the activated surface and can be described by electrochemically controlled partial reaction currents [9, 40-42]. Further details on its mechanism will be given in the next parts.

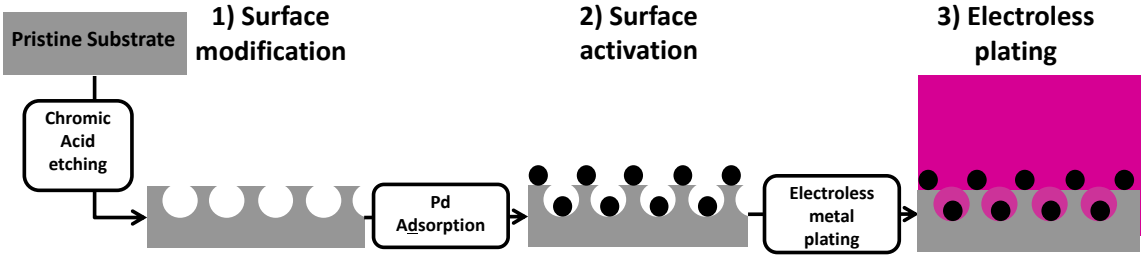

Figure 6 : Common industrial electroless plating process divided in three main steps (Adapted from Ref. [43])

2.3.1. Electroless plating step: Electrochemical-based mechanism

The electroless deposition mechanism is complex and can be explained using fundamentals of electrochemical deposition rules. As shown in **Figure 7a)**, an electrolytic cell for electrodeposition of metals from an aqueous solution needs, at least, to be composed of a power supply, two metal electrodes (metal cathode and metal anode) and water containing the dissolved ions of a metal salt MA (M^{z+}; A^{z-}). The equivalent electrolytic cell for electroless metal deposition is shown in **Figure 7b)** and a comparison of both cells shows that in

electroless deposition there is no power supply and the system has only "one metal electrode".

As well as for electrodeposition solution, the electroless solution composition is very complex and contains at least the following components: water, a metal salt MA (M^{z+}; A^{z-}), a reducing agent, pH buffer, bath stabilizers and complexing agents of the metal salt. Without any metal electrode, this solution remains stable such as in the case of the electrodeposition solution without any power applied.

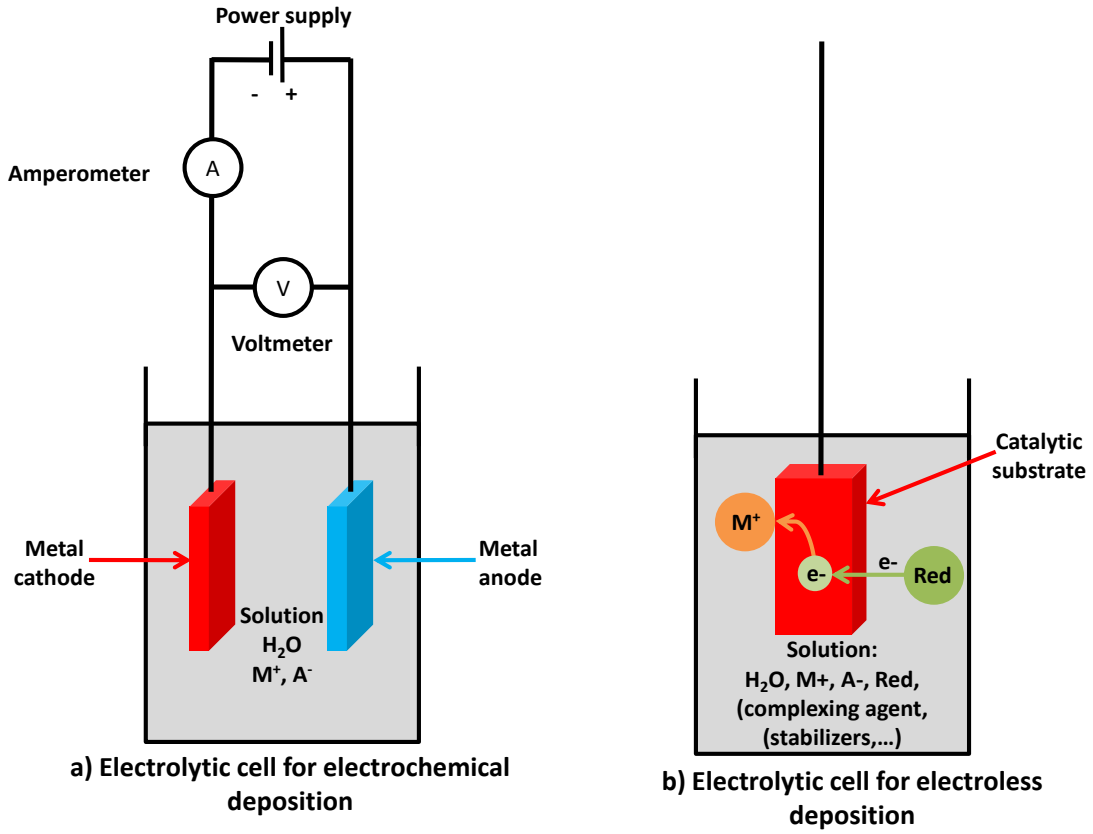

Figure 7: a) Electrolytic cell for electrodeposition of metal, M, from an aqueous solution of metal salt, MA and b) Electrolytic cell for electroless deposition of metal M from an aqueous solution of metal salt MA and a reducing agent Red.

The overall reactions of electrodeposition and electroless deposition may be used to compare these two processes. The process of electrodeposition of metal M is represented:

$$M^{z+}_{solution} + ze^- \xrightarrow{electrode} M_{lattice} \qquad \textbf{Eq. 1}$$

In this process z electrons are supplied by an external power supply. The overall reaction of electroless metal deposition is:

$$M^{z+}_{solution} + Red_{solution} \xrightarrow{\text{catalytic surface}} M_{lattice} + Ox_{solution} \qquad \textbf{Eq. 2}$$

Where Ox is the oxidation product of the reducing agent Red.

This reaction only occurs on the activated surface, also called catalytic surface and more specifically on appropriate metal previously adsorbed onto the surface such as Pd^0 particles. The reducing agent Red in the solution is the electron source and gives electrons to the catalytic surface and metal ions M^{z+} at the surface. The reaction represented by **Eq. 2** must be conducted in such a way that a homogeneous reaction between M^{z+} and Red, in the bulk of the solution, is inhibited. Indeed, in addition to the source of metal ion M^{z+} and its reducing agent Red, the electroless plating solution also contains suitable complexing agents and stabilizers. All these components create a whole solution which is in a metastable state at a constant pH.

Concerning the complexing agents, they perform three main functions in the electroless plating solution [9]. First, they exert a buffering action that prevents the pH of the solution from increasing or decreasing too fast. Then, they prevent the formation of metal hydroxides and reduce the concentration of free metal ions, which avoid the spontaneous reduction in solution and the subsequently decomposition of the electroless plating bath. In addition to these functions, complexing agents also affect the deposition reaction and hence the resultant metal deposit [9]. Indeed, the rate of metal deposition is proportional to the rate at which the metal complexing agent dissociates to form “free” metal ion. Thus, the plating rate is inversely related to the complexing agent stability constant, i.e., the higher the complexing agent stability constant, the lower the rate of complexing agent dissociation and concomitantly, the lower the rate of deposition. Lastly, in some cases, the nature of the metal complexing agent and its stability constant also affect the composition of the metal deposit. This will be described in the next parts.

As a result of its complex composition, electroless plating bath are actually metastable mixtures, which may decompose spontaneously at any time [9]. Bath decomposition is usually preceded by an increase of the volume of hydrogen gas evolved and the appearance of a

finely-divided black precipitate throughout the bulk of the solution. This precipitate consists of metal particles. Fortunately, chemical agents called stabilizers (or catalytic inhibitors, or poisons of the catalytic growth) are present to prevent the homogeneous reaction that triggers the subsequent random decomposition of the entire plating bath. Plating bath decomposition can be virtually eliminated by the addition of only trace amounts of stabilizer to the electroless plating solution. As described in Mallory's book, Gutzeit [9, 44-47] pointed out that most of these so-called "anti-catalysts" are identical to the materials that prevent hydrogenation/dehydrogenation catalysis.

Consequently, the chemical and physical properties of an electroless metal coating depend on its composition, which, in turn, depends on the formulation and operating conditions of the electroless metal plating bath.

As shown in **Figure 7a)**, electrochemical deposition involves two electrodes, a cathode and an anode, which induce two separate electron-transfer reactions that occur at two spatially separated electrode-electrolyte interfaces. At the cathode a reduction reaction occurs and at the anode an oxidation reaction occurs: for example,

$$M_{lattice} \xrightarrow{anode} M_{solution}^{z+} + ze^{-} \qquad \textbf{Eq. 3}$$

In electroless deposition the two electrochemical reactions, reduction of $M_{solution}^{z+}$ and oxidation of $Red_{solution}$, occur at the same electrode, at the same electrode–electrolyte interface (**Eq. 3 and Figure 7b)**). Thus, in electroless deposition there is a statistical division of the catalytic sites on the substrate into anodic and cathodic sites. Since these catalytic sites are part of the same piece of substrate, there is a flow of electrons between these sites [48].

In the following sections, the electrochemical model describing the electroless deposition mechanism will be discussed and coupled with the mechanistic approach.

Electrochemical model: Mixed-potential theory (MPT)

An electrochemical model for the electroless metal deposition was suggested by Paunovic and Saito on the basis of the Wagner–Traud mixed potential theory of corrosion processes [49-

51]. According to the mixed-potential theory (MPT) of electroless deposition, the overall reaction given by **Eq. 2** can be decomposed into one reduction reaction, the cathodic partial reaction,

$$M^{z+}_{solution} + ze^- \xrightarrow{\text{catalytic surface}} M_{lattice} \qquad \textbf{Eq. 4}$$

and one oxidation reaction, the anodic partial reaction,

$$Red_{solution} \xrightarrow{\text{catalytic surface}} Ox_{solution} + me^- \qquad \textbf{Eq. 5}$$

Thus, the overall reaction (**Eq. 2**) is the outcome of the combination of two different partial reactions (**Eq. 4 and Eq 5**). As mentioned above, these two partial reactions, however, occur at one electrode, the same metal–solution interphase. According to the electrochemistry laws, the equilibrium potential of the reducing agent, $E_{eq,Red}$ (**Eq. 5**) must be more negative than that of the metal electrode, $E_{eq,M}$ (**Eq. 4**), so that the reducing agent Red can function as an electron donor and M^{z+} as an electron acceptor.

According to the mixed-potential theory, the overall reaction of the electroless deposition ó**Eq. 2**ú can be described electrochemically in terms of current–potential curves thanks to the Evans diagram. In this method the sign of the current density is suppressed. **Figure 8** shows a general Evans diagram with current–potential functions i = f(E) for the individual electrode processes, **Eq. 4 and Eq. 5**. According to this presentation of the mixed-potential theory, the current–potential curves for individual processes, $i_c = i_M = f(E)$ and $i_a = i_{Red} = f(E)$, intersect. The coordinates of this intersection have the following meaning:

- The abscissa, the current density of the intersection, is the deposition current density i_{dep} (*i.e.*, log i_{dep}), that is, the rate of electroless deposition in terms of $mA.cm^{-2}$;
- The ordinate, the potential of the intersection, is the mixed potential, E_{mp}.

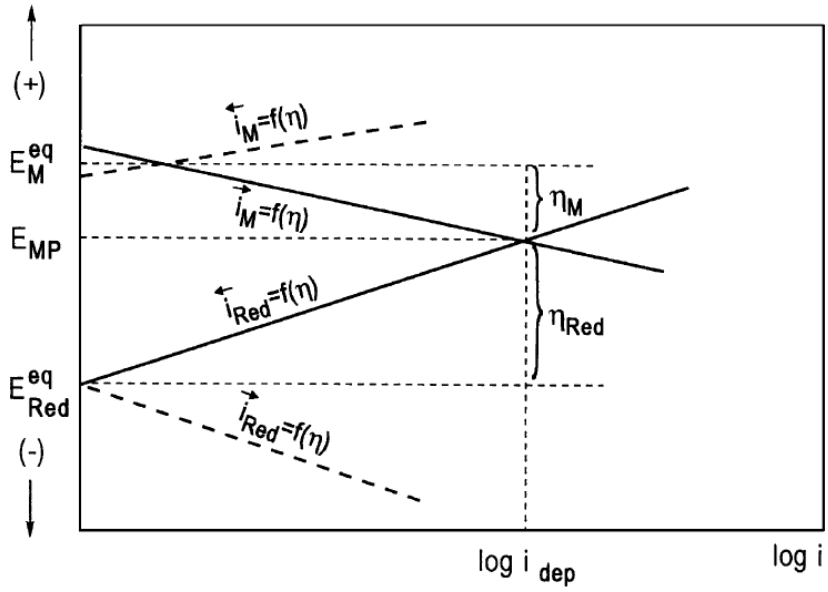

Figure 8 : Evans diagram of current–potential curves for a system with two different simultaneous electrochemical reactions corresponding to Eq. 4 and Eq. 5 (Extracted from Ref. [48])

When the catalytic surface is introduced into an aqueous solution containing M^{z+} ions and a reducing agent, the partial reduction reaction (**Eq. 4**) and the partial oxidation reaction (**Eq.5**) occur simultaneously. Each of these partial reactions strives to establish its own equilibrium, E_{eq}. The result of these processes is the creation of a steady state with a compromised potential called the steady-state mixed potential, E_{mp}. Consequently the potential of the redox couple Red/Ox (**Eq. 5**) is raised anodically from the reversible value $E_{eq,Red}$ (**Figure 8**), and the potential of the metal electrode M/M^{z+} (**Eq. 4**) decreased cathodically from its reversible value, $E_{eq,M}$, down to the mixed potential, E_{mp} (**Figure 8**). Thus, the basic four characteristics of the steady-state mixed potential are:

- Both redox systems are shifted from their own characteristic equilibrium potentials by the overpotential η:

$$\eta_M = E_{mp} - E_{eq,M} \qquad \textbf{Eq. 6}$$

$$\eta_{Red} = E_{mp} - E_{eq,Red} \qquad \textbf{Eq. 7}$$

- An electrochemical reaction occurs in each redox system since both reactions, **Eq. 4** and **Eq. 5**, are shifted from their equilibrium by introduction of the mixed potential.

- The criterion for a steady state is that the rate of reduction of M^{z+}, the cathodic current density i_M, is equal to the rate of oxidation of the reducing agent Red, the anodic current density i_{Red}:

$$i_{M,deposition} = i_{M,Emp} = i_{Red,Emp} \qquad \textbf{Eq. 8}$$

since no current can flow in an isolated system.

- A system at the steady-state mixed potential is not in equilibrium since an overall reaction does occur; therefore the free energy change is not equal to zero which corresponds to a system that is not in thermodynamic equilibrium.

This mixed-potential theory has been verified by experimental studies for electroless deposition of copper. Indeed, Paunovic [51] reported that an electroless copper solution containing ethylenediaminetetraacetic acid (EDTA) as complexing agent for copper ions, formaldehyde as reducing agent, with pH = 12.5, and operated at 25°C, behaves in agreement with MPT. The polarization curves for reduction of copper ions and oxidation of formaldehyde are shown in **Figure 9**. The intersection potential for these curves was found to be similar to the value of the equilibrium potential, or open circuit, of a copper electrode undergoing electroless deposition in the complete solution. Similarly, the estimated copper deposition rate at E_{mp} in **Figure 9** (2.2 $mg.h^{-1}.cm^{-2}$) was close to the value measured gravimetrically for an electrolessly-plated substrate, 1.8 ± 0.2 $mg.h^{-1}cm^{-2}$.

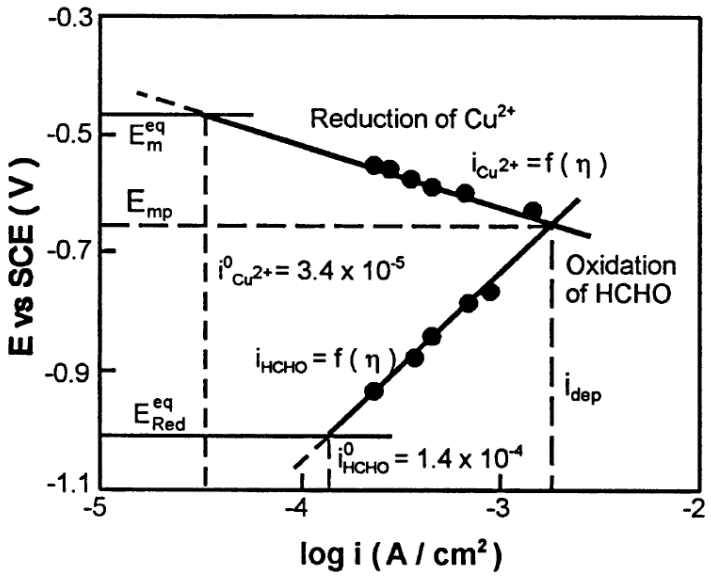

Figure 9 : Current-potential curves for reduction of copper ions and oxidation of formaldehyde. "$E_{eq,M}$" and "$E_{eq,Red}$" are the open circuit potentials for the copper ion reduction and formaldehyde oxidation reactions, respectively. The vertical lines represent the exchange current densities for the two half reactions, and the deposition current density for the complete electroless solution (Extracted from Ref. [48]).

Steady-state electroless metal deposition at mixed potential E_{mp} is preceded by a non-steady-state period, called the induction period. The induction period is defined as the time necessary to reach the mixed potential E_{mp} at which steady-state metal deposition occurs. It is determined in a simple experiment in which a piece of metal is immersed in a solution for electroless deposition of a metal and the potential of the metal is recorded from the time of immersion (or the time of addition of the reducing agent, *i.e.*, time zero) until the steady-state mixed potential is established. A typical recorded curve for the electroless deposition of copper on a copper substrate using HCHO as reducing agent is shown in **Figure 10**. Paunovic studied this induction period for the overall process, dividing it into dependence of the open-circuit potential (OCP) on the oxidation and reduction partial reactions, that is, into individual induction periods for each partial process [52]. The OCP of the Cu/Cu^{2+} system is reached instantaneously. From a comparison of these OCP curves, it has been concluded that the rate of setting of the OCP of the reducing agent, HCOOH, was the rate-determining partial reaction in the setting of the steady-state mixed potential.

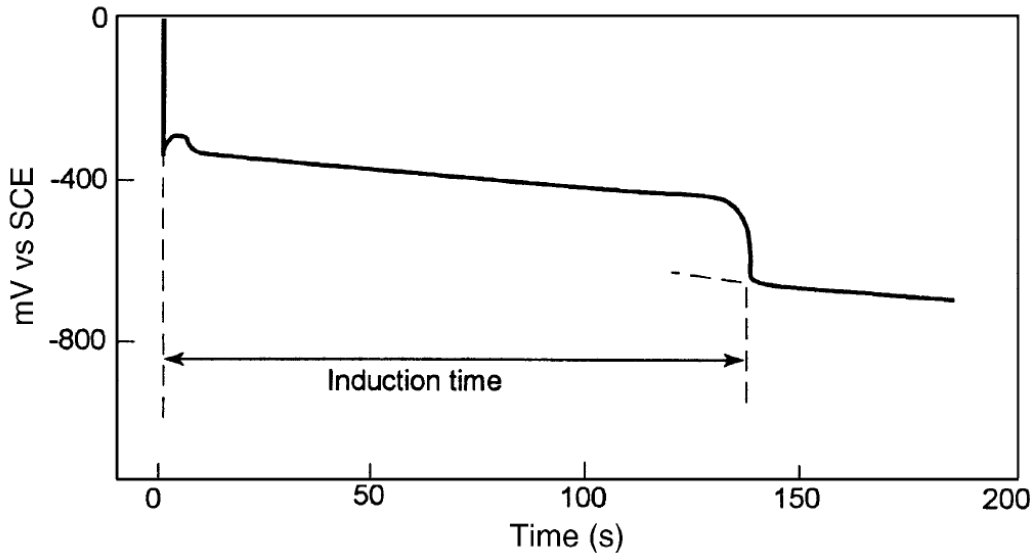

Figure 10 : Induction period for the solution containing EDTA (0.3 M), $CuSO_4$ (0.05 M), formaldehyde (2.5 g/L), Cu electrode, 25°C, pH=12.50, SCE reference electrode and argon atmosphere (Extracted from Ref. [52]).

The MPT has been tested and verified by experimental studies for other metals such as nickel or even gold associated with different reducing agents such formaldehyde or hypophosphite for electroless copper deposition [51, 53-56], dimethylamine borane for electroless nickel deposition [51] and potassium borohydride for electroless gold deposition [57].

The described MPT assumes that the two partial reactions are independent from each other, which is not always true. For example, Schoenberg [58] has shown that formaldehyde (used as reducing agent for electroless copper deposition) enters the first coordination sphere of the copper tartrate complex and thus influences the rate of the cathodic partial reaction. Ohno and Haruyama [59] showed the presence of interference in partial reactions for electroless deposition of Cu, Co, and Ni in terms of current–potential curves [57].

These latter details illustrate the complexity of electroless processes and the presence of a variety of factors that should be taken into account when applying the MPT to electroless processes. To better explain this electroless plating process, Mallory, Paunovic and Van Den Meerakker [9, 48, 60] described the mechanism of each (anodic and cathodic) partial reaction and the effects of all the variables of the electroless process; the next part will summarize that study:

Anodic partial reaction

The overall anodic partial reaction (**Eq. 5**), usually proceeds in at least two elementary steps (like the cathodic partial reaction): formation of electroactive species, and charge transfer. The formation of electroactive species (R) usually proceeds in two steps through an intermediate (Red_{interm}):

$$\mathrm{Red} \rightarrow \mathrm{Red_{interm}} \qquad \textbf{Eq. 9}$$

$$\mathrm{Red_{interm}} \rightarrow \mathrm{R} \qquad \textbf{Eq. 10}$$

Van den Meerakker [61, 62] proposed the following general mechanism for the formation of electroactive species R from the intermediate R_{interm}, now represented by R-H:

$$\mathrm{Red_{interm}} = \mathrm{R-H} \rightarrow \mathrm{R_{ads}} + \mathrm{H_{ads}} \qquad \textbf{Eq. 11}$$

Where R_{ads} is the electroactive species R adsorbed at the catalytic surface. According to this mechanism which corresponds exactly to the dehydrogenation mechanism (**Eq. 11**), the electroactive species R_{ads} is formed in the process of dissociative adsorption (dehydrogenation) of the intermediate R-H, which involves breaking the R-H bond.
The adsorbed hydrogen, H_{ads}, may desorb in the chemical reaction

$$2\,\mathrm{H_{ads}} \rightarrow \mathrm{H_2} \qquad \textbf{Eq. 12}$$

or in the electrochemical reaction

$$\mathrm{H_{ads}} \rightarrow \mathrm{H^+} + \mathrm{e^-} \qquad \textbf{Eq. 13}$$

For example, in electroless deposition of copper, when the reducing agent is formaldehyde and the substrate is Cu, H_{ads} desorbs in the chemical reaction (**Eq. 12**) [60]. If the substrate is Pd or Pt, hydrogen desorbs in the electrochemical reaction (**Eq. 13**) [60]. In electroless deposition of gold and silver, both electrochemical and chemical reactions are observed [60].

The most studied anodic partial reaction is the oxidation of formaldehyde, Red = HCOOH. The overall reaction of the electrochemical oxidation of formaldehyde at the copper electrode in an alkaline solution proceeds as

$$\mathrm{HCOH} + 2\mathrm{OH}^- \rightarrow \mathrm{HCOO}^- + \mathrm{H_2O} + {}^{1}\!/_{2}\mathrm{H_2} + \mathrm{e}^- \qquad \textbf{Eq. 14}$$

The mechanism of this reaction involves the following sequence of elementary steps [61-63]:

1. Formation of electroactive species R in three steps:

a. Hydrolysis of HCOOH and formation of methylene glycol:

$$\mathrm{HCHO} + \mathrm{H_2O} \leftrightarrow \mathrm{H_2C(OH)_2} \qquad \textbf{Eq. 15}$$

b. Dissociation of methylene glycol:

$$\mathrm{H_2C(OH)_2} + \mathrm{OH}^- \leftrightarrow \mathrm{H_2C(OH)O}^- + \mathrm{H_2O} \qquad \textbf{Eq. 16}$$

c. Dissociative adsorption of the intermediate, $\mathrm{H_2C(OH)O}^-$ (R-H), involving breaking the C-H bond in the R-H molecule:

$$\mathrm{H_2C(OH)O}^- \leftrightarrow [\mathrm{HC(OH)O}^-]_{\mathrm{ads}} + \mathrm{H_{ads}} \qquad \textbf{Eq. 17}$$

where $[\mathrm{H_2C(OH)O}^-]_{\mathrm{ads}}$ is $\mathrm{R_{ads}}$.

2. Charge transfer, the electrochemical oxidation (desorption) of electroactive species $\mathrm{R_{ads}}$:

$$[\mathrm{HC(OH)O}^-]_{\mathrm{ads}} + \mathrm{OH}^- \rightarrow \mathrm{HCOO}^- + \mathrm{H_2O} + \mathrm{e}^- \qquad \textbf{Eq. 18}$$

where HCOO^- is the oxidation product of $\mathrm{R_{ads}}$ (Ox).

Okinaka and Vandenmeerakker applied this kinetic scheme to other reducing agents, such as borohydride (Red = BH_4^-), hypophosphite ($H_2PO_2^-$), and hydrazine (NH_2NH_2) where the electroactive species RH are $[BH_2OH^-]_{ads}$, $[HPO_2^-]_{ads}$, and $[N_2H_3^-]_{ads}$, respectively [57, 61]. It was shown that parallel reactions occur with some reducing agents. For example, in the case of

oxidation of BH_4^- and $H_2PO_2^-$, the parallel reactions are probably cathodic reactions, resulting in incorporation of B and P into the metal deposit, respectively. These "codeposits" obviously modify the properties of the electroless metal layer. As an example, when electroless Ni is deposited from solutions containing BH_4^- as the reducing agent, a NiB layer is obtained and provides better diffusion barriers properties than usual Ni layer, whereas when the reducing agent is $H_2PO_2^-$, a NiP layer is obtained and provides better corrosion resistance.

Therefore, as introduced earlier, in that particular cases of BH_4^- and $H_2PO_2^-$ reducing agents, the nature of the metal complexing agent and its stability constant also affect the composition of the metal deposit. As an example for NiP deposit, when the fraction of catalytic sites onto which nickel ions have been adsorbed is large (small complex stability constant), the number of sites available for phosphorus reduction is small and the phosphorus content of the deposit is lowered. On the other hand, when the stability constant is relatively large, the free nickel ion concentration is low, and the fraction of sites covered by adsorbed nickel is small; hence, in the latter case, the number of sites available for phosphorus reduction is large and the phosphorus content of the coating is increased.

Finally, from the kinetic aspects, the major factors determining the rate of the anodic partial reaction are pH and additives. Since OH^- ions are reactants in the charge-transfer step (e.g., **Eq. 18**) the effect of pH is direct and significant [64]. Additives may have an inhibiting or an accelerating effect.

Cathodic partial reaction

Generally, metal ions in a solution for electroless metal deposition have to be complexed with a ligand. As previously explained, complexing agents are necessary to prevent formation of metal hydroxide, such as $Cu(OH)_2$, in electroless copper deposition. One of the fundamental problems in electrochemical deposition of metals from complexed ions is the presence of electroactive (charged) species. The electroactive species are in most cases, partially complexed metal ions and the kinetic scheme is that of charge transfer is preceded by partial or total dissociation of the complex.

The mechanism of the second case involves a sequence of at least two basic elementary steps:

- Formation of electroactive species followed by the charge transfer from the catalytic surface to the electroactive species. Electroactive species M^{z+} are formed in the first step by dissociation of the complex $[MLx]^{z+xp}$:

$$[ML_x]^{z+xp} \rightarrow M^{z+} + xL^{p} \qquad \textbf{Eq. 19}$$

where p is the charge state of the ligand L, z is the charge of the non-complexed metal ion, and z+xp is the charge of the complexed metal ion.

- The charge transfer

$$M^{z+} + ze^{-} \rightarrow M \qquad \textbf{Eq. 20}$$

proceeds in steps, usually with the first charge transfer (one-electron transfer) serving as the rate-determining step (RDS):

$$M^{z+} + e^{-} \xrightarrow{RDS} M_{lattice} \qquad \textbf{Eq.21}$$

Thus, from the kinetic aspects, the cathodic partial reaction is an electrochemical reaction (**Eq. 20**) that is preceded by a chemical reaction (**Eq. 21**). Paunovic demonstrated that the major factors determining the rate of the partial cathodic reaction are concentrations of metal ions and ligands, pH of the solution, and type and concentration of additives [52]. These factors determine the kinetics of partial cathodic reaction in a general way, as given by the fundamental electrochemical kinetic equations [48]. Therefore, Schoenberg, Paunovic and Arndt [58, 65-67] have shown that additives may have two opposing effects: acceleration and inhibition such as in the case of the anodic partial reaction.

Overall mechanism and alternative models

As mentioned earlier, the overall mechanism of the electroless deposition is governed by the electrochemical rules and more particularly the mixed potential theory. However, this theory has to be associated with the mechanistic approach of the reduction of metal salt and the oxidation of a reducing agent onto a metal electrode which are governed by the

heterogeneous catalysis rules. A scheme of the electroless mechanism describing the main steps of the process is suggested in **Figure 11**.

As suggested in **Figure 11**, in a first part, the reducing agent is adsorbed onto the metal surface leading to its R-H homolytic cleavage. In a second part, at this solid/solution interface, the coordination sphere of the complex salts is at least partially modified by a ligand adsorption onto the catalyst. This partial metal complex dissociation allows afterward obtaining the electron transfer between the adsorbed species of the reducing agent and the metal salt leading to its reduction onto the metal surface. Depending on the catalyst nature and the reactive baths, either the red or the blue pathway is promoted (**Figure 11**). Then, this process being autocatalytic, this mechanism is repeated as long as the activated surface is immersed into the electroless plating bath. It has to be said that for convenience reasons, the suggested mechanism in **Figure 11** does not describe the reduction of the reducing agent itself that occurs in the case of Boron or Phosphorous-containing reducing agents.

This chemical mechanism associated with the mixed potential theory finally provides a correct description of the electroless plating mechanism when electron transfer between the reducing agent and the metallic ion is mediated by the activated surface and can be described by electrochemically controlled partial reaction currents [9, 40-42]. Nevertheless, the mixed potential theory is not valid when an electron transfer can directly occur between the reducing agent and the metallic ion contained in the electroless plating bath, which is usually prevented by using stabilizers. More recently, improved electroless deposition models of the different mechanistic steps were published trying to take all the components of the electroless plating bath into account. At this stage, there are only based on theoretical calculations without any experimental data to confirm those models [68-71].

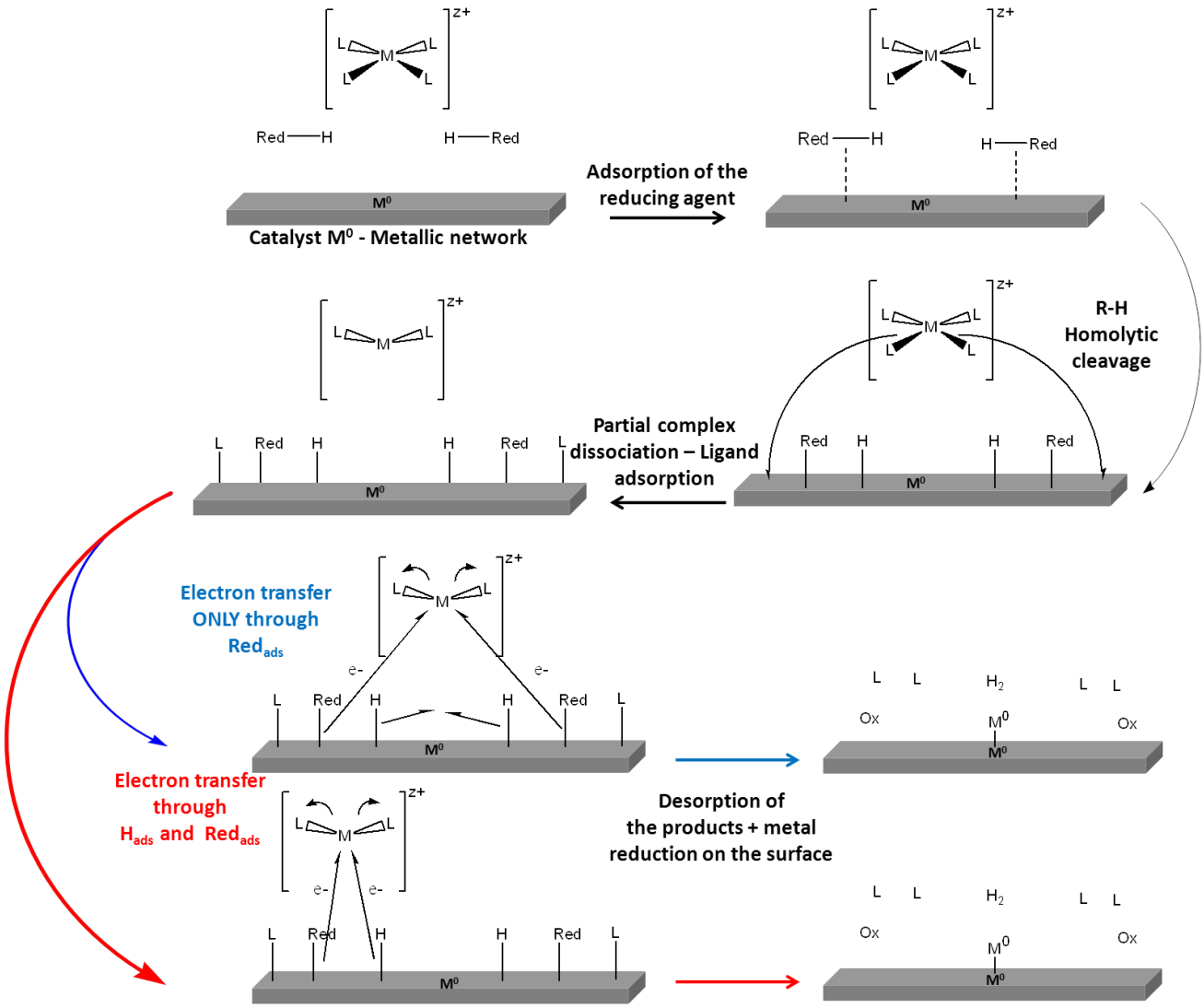

Figure 11 : Scheme of the electroless mechanism

2.3.2. Surface activation step through Pd-Sn catalyst

As previously introduced, electroless deposition starts only on a catalytic surface commonly based on Pd species. Indeed, this surface activation consists in the adsorption of a catalyst of the electroless plating growth onto the polymer surface. Palladium, in its zero oxidation state, is a “universal” catalyst used to initiate most electroless reactions involving various autocatalytic metals so that it plays a fundamental role in any electroless process [9]. The deposition of palladium seeds on the polymer surface is enough to initiate the redox reaction. The reaction goes further thanks to the autocatalytic property of the deposited metal species which is based on the capability of these metals to reduce their own ions, hence the term “autocatalytic” also used to describe the electroless plating process.

Historically, this seed layer was deposited by a two-step process consisting of substrate treatment by the successive immersion in stannous chloride ($SnCl_2$) and palladium chloride ($PdCl_2$) aqueous solutions [72-75]. The tin bath treatment is named "sensitization" and the palladium (or similar) second treatment is called "activation". The sensitization consists in the adsorption of Sn^{2+} ions onto the pretreated surface, followed by the activation which leads to the reduction of Pd ions by the adsorbed Sn^{2+} ions, according to **Eq. 22**:

$$\mathbf{Sn^{2+} + Pd^{2+} \rightarrow Sn^{4+} + Pd^{0}} \qquad \textbf{Eq. 22}$$

This two-step process was given up between 1975 and 1980 in favor of a one-step process using a mixed $SnCl_2$-$PdCl_2$ solution [5, 74, 76-78] with core-shell Pd-Sn colloidal species which exhibit complex compositions and chemistries [75]. As suggested by other groups [79], Cohen and West have shown by Mössbauer spectroscopy [75, 80] that Pd/Sn solutions consist of nano-colloids of around 2 nm. Indeed, Mössbauer spectroscopy gives access to chemical information, like the oxidation state of Pd and Sn, averaged over the whole ensemble of colloids in suspension. This work led to a discussion about the nature of the activator solution in the literature [81, 82]. The nano-colloids comprise a Pd-rich, zerovalent and crystalline Pd-Sn alloy, which functions as the catalytically component for electroless deposition [83-86]. Pd-Sn nano-colloids are surrounded by a stannic shell consisting primarily of μ-hydroxy-bridged Sn^{II} and Sn^{IV} which chemical composition and thickness depend on the working conditions (pH, solution composition, temperature, oxygen exposure) [77, 87, 88]. Before the electroless plating step, an acid “acceleration” treatment that dissolves a portion of the stannic shell to expose the catalytically active Pd-Sn core to the electroless plating is required. The adhesive properties of the stannic shell are obviously critically important for using the Pd-Sn colloid as an electroless catalyst. However, the stannic shell adsorption is only based on Van der Walls and other non-covalent interactions and generally leads to poor adhesion. Even if the adhesion of those Pd-Sn colloids is reinforced by the surface treatment, the use of covalent rather than non-covalent interactions to adhere the catalytic Pd core to the surface to be plated represent a straightforward and attractive means to enhance the electrolessly deposited metal layer adhesion.

2.3.3. Conclusions

Once the surface is activated by Pd^0 surface adsorption, different kinds of metal can be electrolessly deposited by immersion in the electroless plating bath and as previously explained, almost all the metals of the Group VIII of the periodic table (Au, Pd, Ni, Cu, Co,…) can be plated and exhibit autocatalytic behavior. In all cases, the electroless plating bath will be composed by a ionic complex of the metal to be plated, a reducing agent, a stabilizer which prevents spontaneous reduction in solution [9], but may delay or even hinder the initiation of the autocatalytic reaction through a kind of poisoning of the catalytic sites, hence resulting in an increase in the activation energy of the reaction [9]. Hence, the working conditions of the electroless plating bath, such as pH and temperature, are often controlled in situ on industrial setups. It is noteworthy that according to the plating bath composition, it is possible to induce different metal layer properties; for example, the incorporation of P or B into the metal layer respectively induces better corrosion resistance or better diffusion barriers layers than pure metal.

For most of the metal plated polymers, this wet process is the most efficient one and consequently the most used one by the polymers electroless plating industry. Accordingly, they are still industrial challenges to take up such as the replacement of the Pd-Sn activation step which involves weak interactions with substrates, and generates toxic waste due to the use of hazardous tin species and important costs in waste management.

In addition, the ability to develop a projection or transfer-based process instead of the described wet process involving many baths would ideally match the current industrial demands: Only the required matter would be used which consequently could minimize the waste production and would induce cost savings.

Lastly, a projection or transfer-based process would also enable the localization of the metal deposition and could be used for the fabrication of metal patterns for electronic applications.

2.4. Alternative method: Jet-Metal™ technology

Recently, an alternative to the wet and dried based metallization processes, combining spray deposition and electroless plating process has been proposed by the Jet Metal™ company [89]. As shown in Figure 12, metallization is obtained by spraying two solutions, at room

temperature, on the substrates. The mixture of these two aqueous solutions reacts through a redox reaction on the surface of the substrate, forms a homogenous and continuous metallic film with an excellent adhesion onto the substrate thanks to rough pretreatments carried out beforehand but without any surface activation step [89]. This technology takes advantages of the spontaneous reaction between a metal ion and a reducing agent (**Eq. 23**) without any stabilizing agents contrary to classical electroless plating solutions.

$$M^{z+}_{solution} + Red_{solution} \rightarrow M_{surface} + Ox_{surface} \qquad \textbf{Eq. 23}$$

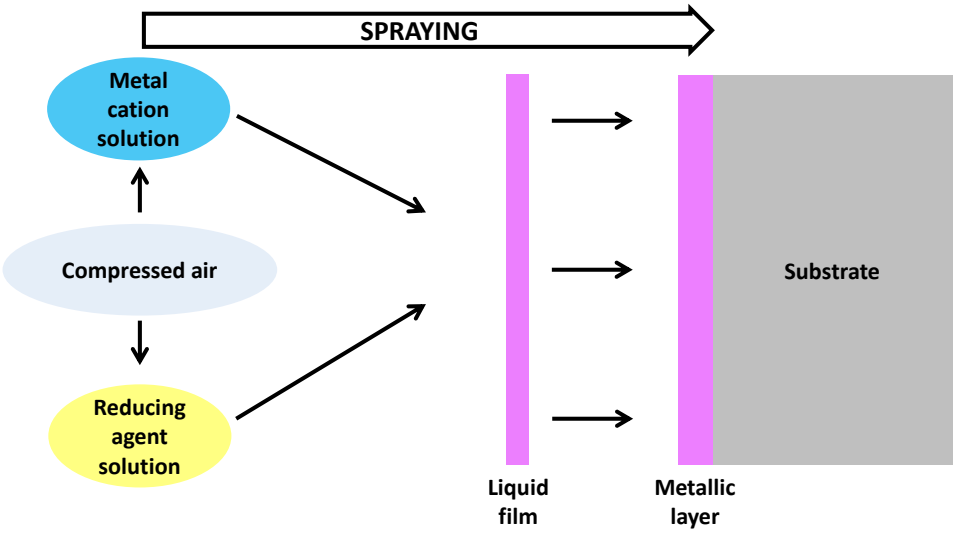

Figure 12 : Jet Metal™ technology

However, this technology does not ensure the metallization of all-shaped substrates and rough pretreatments are needed to ensure the adhesion of the deposited metallic layer.

3. *Electroless plating of Pd^{II}-Ligand modified polymers*

Alternative approaches to the common Pd-Sn catalysts adsorption onto Cr-oxidized substrates have been developed by various laboratories allowing the development of Sn-free activation processes and even in certain cases, a Cr-free conditioning process. It consists in the formation of an as-robust-as-possible interphase between the substrate surface and the deposited metallic layer which own two main properties:

First, during the activation step, this interphase needs to provide ligands capable of stabilizing the bond between the catalytically active Pd and the substrate surface. This

approach simplifies the composition of the catalyst and eliminates the use of the environmentally hazardous Sn species since the surface ligands are able to chelate (or complex) the Pd^{II} ions which, once reduced in Pd^{0} can act as the catalyst of the electroless metal plating. In addition, compared to the Pd-Sn colloids adsorption, it highly increases the binding strength of the metal/surface link and allows obtaining more selective and specific adsorption which induce the ability to achieve metal patterning on polymers by localized ligand coatings [90].

Second, in the best cases, this interphase is also intended to replace the rough interface which usually results from the chromic acid treatment [11, 91-93] by increasing the surface roughness and consequently bringing the expected mechanical adhesion of the electroless plated layer.

Even if a few substances naturally possess ligand functional groups as an integral part of their structure [94-96], it is mostly not the case of the materials used in the polymers metal plating industries. Consequently, ligand functional groups must be adsorbed on the surface. Unfortunately, working on non-conductive materials such as polymers based materials does not allow using electrochemical surface modifications processes such as vinylic monomer cathodic electrografting [97] or diazonium salts grafting by electrochemical reduction [98], which are very efficient onto conductive surfaces. Subsequently, the adsorption of ligand functional groups requires the use of alternative techniques and can be classified according to the type of ligation:

i. A 2D-ligation based on ligand functional groups only located on the top of the substrate surface. It finally leads to the **adsorption** of Pd species.

ii. A 3D-ligation based on various ligand functional groups located in the volume of the substrate. It finally leads to the **absorption** of various Pd species.

This ligand-based approach also allows direct patterning of the catalyst deposition and subsequent localized electroless metal plating growth, which will be related in the following sections.

3.1. Surface functionalization by SAM adsorption (2D-ligation)

The surface modification by adsorption of self-assembled monolayers (SAM) based on organosilicon derivatives is a well-known method to modify the physical and chemical surface

properties such as surface energy, adhesion, reactivity (**Figure 13**) [99]. Organosilicon derivatives such as organosilanes or organosiloxanes can easily be covalently grafted on hydroxylated surfaces such as glasses for various kinds of applications [100]. For non-polar substrates (as many polymers) important oxidation treatments (see Section II.1) have to be carried out in order to bring the necessary hydroxyls groups (OH) at the surface, such as in the case of fluoropolymers [101]. Then, on the hydroxylated surface, as shown in **Figure 13**, the hydrolysis of the alkoxysilane groups (which are defined at the head group) allows to create interfacial bonds (Substrate-O-Si) whereas terminal groups (alkyl, aromatic, amino, …), called functional groups, are at the extreme surface and are available to react with external chemical reagents.

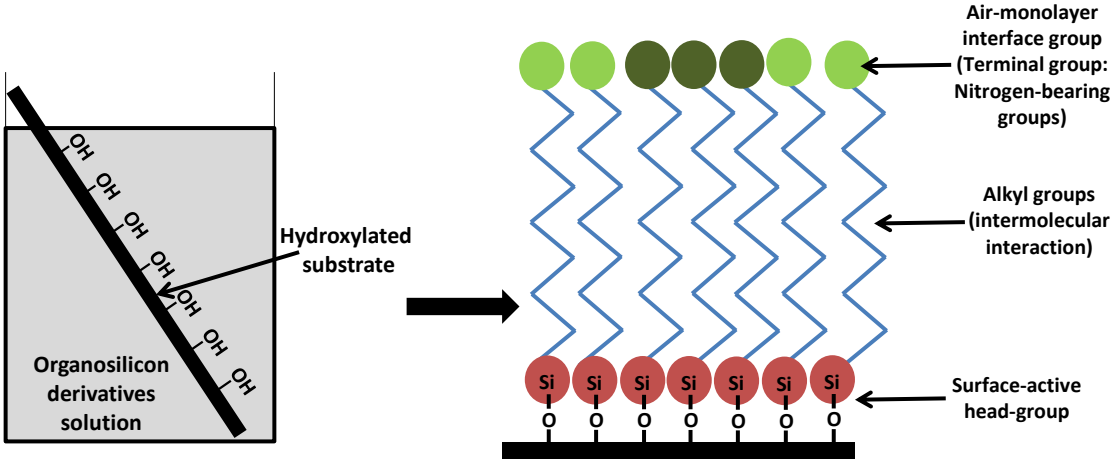

Figure 13 : Self-assembled monolayers are formed by simply immersing a substrate into a solution of the surface-active material. The driving force for the spontaneous formation of the 2D assembly includes chemical bond formation of molecules with the surface and intermolecular interactions [99].

In the early 90's, among various laboratories, Calvert and Dressick's group started to develop metal plating processes based on the surface functionalization by these organosilicon derivatives. Indeed, they used the strong chemical affinity of Pd^{II} species with nitrogen-bearing ligands by directly adsorbing self-assembled monolayers of an aminosilane which exhibit their amine groups in a terminal position [11, 37, 102-109]. Then, immersing the SAM-modified substrates into an appropriate Sn-free Pd^{II}-based solution [11] leads to the chemisorption of the Pd^{II} catalyst. This Pd affinity towards nitrogen-bearing ligands can be explained by the hard/soft acid/base theory [110]. Indeed, Pd is considered as a soft acid whereas the nitrogen-bearing ligands are soft bases, which finally leads to strong interactions. Then, once reduced by immersion into an appropriate reducing solution, Pd^{0} species act as catalyst of the selective electroless metal growth. This ligand based electroless plating approach allowed achieving

localized metallization and combining lithography with electroless plating (for more details on lithography techniques, see section II.4.). Therefore, by using a mask during the UV irradiation, they selectively irradiated the surface and selectively adsorbed Pd-Sn colloids on the mask-protected zone. Followed by an electroless metal growth, they demonstrated how to obtain metal patterns onto Si glasses. Nevertheless, these organosilane chromophores require high exposure doses that represent important industrial costs (350-400 $mJ.cm^{-2}$ for 193-nm UV exposures) [11]. Thus, based on the same approach, Calvert and Dressick's group also developed an alternative process which consists in the adsorption of (chloromethyl)phenylsilanes which are more sensitive to UV irradiations and consequently easily chemically modified to selectively obtain nitrogen functional groups as shown in **Figure 14** [102, 111, 112].

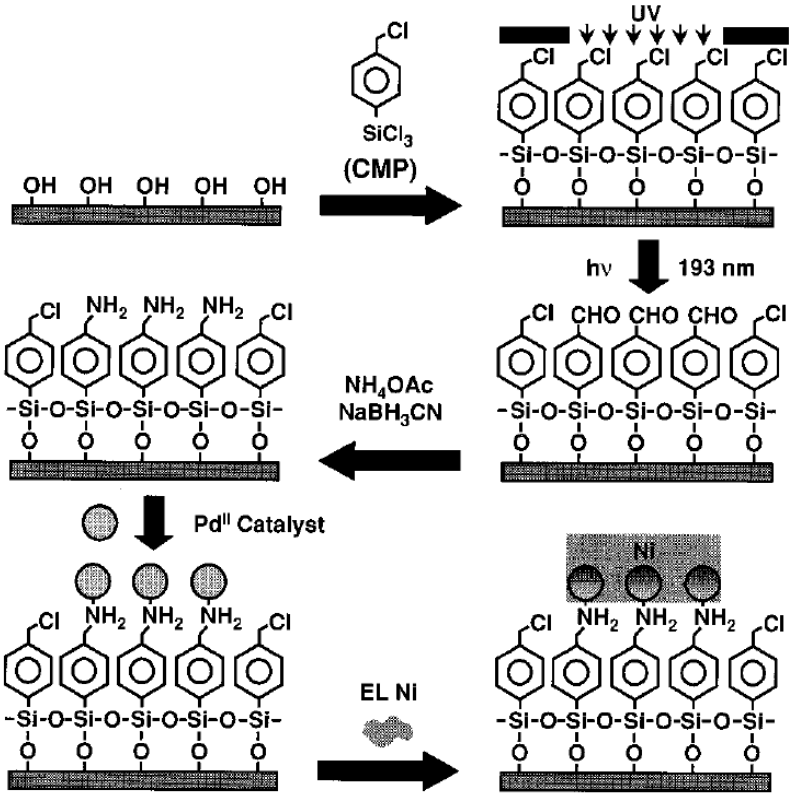

Figure 14 : Localized electroless nickel metallization of the ligand modified surfaces thanks to a process based on (chloromethyl)phenylsilane (Extracted from Ref. [102])

Nevertheless, even if these methods lead to the fabrication of sub-100-nm metallic features, several challenges remain before they can be implemented in the manufacturing environment. For example, the best available (chloromethyl)phenylsilanes SAMs used as imaging layers require exposure doses (*i.e.* ~50 $mJ.cm^{-2}$ for 193-nm UV exposures) that still

exceed those of conventional photoresists (e.g., < 10 $mJ.cm^{-2}$ for UV exposures), limiting clearly the industrial sample throughput [11]. In addition, the reproducible fabrication of uniform organosilane SAMs, especially due to the moisture sensitivity of the trichlorosilane molecules [113], presents a potential manufacturing problem. Lastly, all the previous processes were only applied onto Si substrates.

Most of these drawbacks have been erased by using photoresist-SAM composite films and it has been extended to polymer substrates as illustrated in **Figure 15** with the localized metallization of polyimide: An appropriate photoresist (for more details on lithography techniques, see section II.4.) is spin-coated onto a substrate bearing a chemisorbed organosilane ligand SAM. Exposure leads to chemical changes that increase (path A) or decrease (path B) photoresist solubility during a subsequent development step, which selectively uncovers the ligand SAM to define a pattern. Covalent binding of a colloidal Pd catalyst to the ligand selectively initiates electroless metallization within the pattern channels. Dissolution of the photoresist following plating leaves the desired negative-tone (path A) or positive-tone (path B) metal pattern.

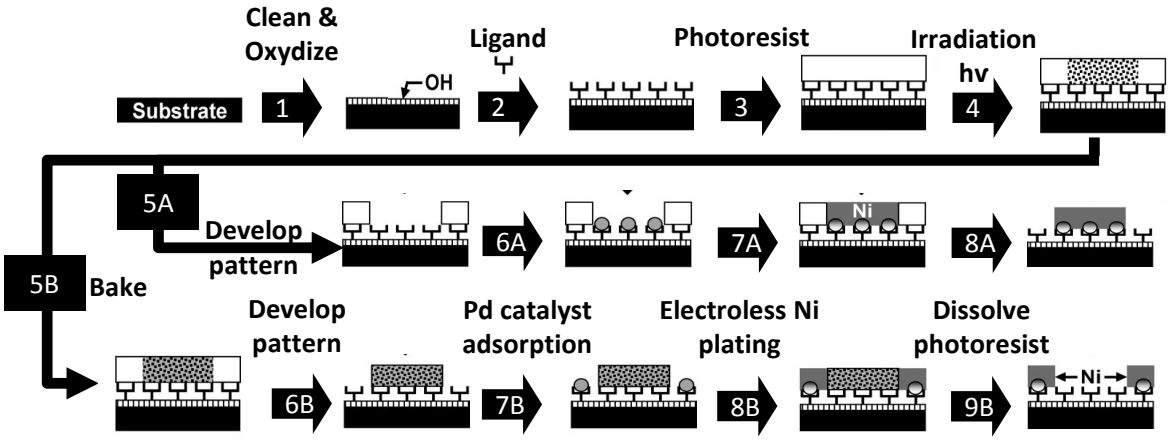

Figure 15 : Localized electroless nickel metallization onto surface-oxidized polyimide by the channel-constrained metallization process (CCM) with negative-tone metal feature (path A) and positive-tone metal feature (path B) [114].

As a conclusion, working with SAM organosilane-based interphases allows to selectively adsorb Pd species and then fabricate metal patterns. However, it works only on hydroxylated substrates which consequently limits the use of this process for the electroless plating of polymers or induce important surface pretreatment steps. Likewise, one of the major drawbacks working with organosilanes relies on the possible hydrolysis in basic or acidic

solution of the Substrate-O-Si bound created between the SAM layer and the substrate [115] which can especially occurs when the SAM cannot act as a barrier layer to these kind of solutions. Lastly, this 2D-ligation and SAM-based interphase between the metal layer and the substrate is highly restricted since there is only one metal/amine bond localized at the extreme surface of the SAM which is not sufficient to replace the rough interface which usually results from the chromic acid treatment by increasing the surface roughness and consequently bringing the expected mechanical adhesion of the electroless plated layer [11].

3.2. Surface functionalization by dried treatments (2D/3D-ligation)

Several dried pretreatments, "greener" than the chromic acid treatment, allow carrying out the surface conditioning while in the same time bringing enough nitrogen-bearing groups onto the surface to adsorb Pd^{II} species which are then commonly used as catalyst of the electroless metal layer.

Therefore, Charbonnier et al. [116] demonstrated an electroless metallization by a Sn-free process based on Pd^{II} species chemisorption on nitrogen-containing groups. The process presented in their work was divided in four main steps: (1) a specific surface treatment of the substrate aiming at grafting nitrogen-bearing groups, (2) a chemisorption of Pd^{II} species on this surface and (3) the necessary Pd^{II} reduction to Pd^{0} followed by the electroless plating (4).

They mainly used two different treatments for the surface treatment step (1):

- An RF plasma treatment under ammonia atmosphere which is fast (from a few seconds to 1 min) and very efficient since it allows to graft specific groups on the treated surface such as amine functionalities with NH_3 plasma treatment or nitrogen-based groups with N_2 plasma treatment [32, 116].
- A VUV irradiation treatment which is also fast (from 1 to 2 min), easy and as efficient as plasma treatments concerning the surface concentration of grafted amine functionalities [32, 35, 116]. It was performed under NH_3 atmosphere using the radiation emitted by the Xe_2 excimer lamp (172 nm, 7.2 eV) or under N_2 atmosphere using an Ar_2 excimer lamp (126 nm, 9.8 eV).

Charbonnier et al. [116] also developed a process based on plasma-assisted chemical vapor deposition (CVD) for the electroless plating of glasses using allylamine, an organic precursor containing nitrogen-based groups. Other works [117-119] also mentioned a graft polymerization of various precursors such as vinylimidazole and vinylpyridine after an Ar plasma treatment of a polymer surface as described in the next part: The so-modified surface brought into contact with the organic precursor slowly generates its polymerization with or without the help of a UV irradiation. These works that can be used for a large range of polymers (polyimide, polyethylene, polycarbonate, …)[116] aimed at improving the adhesion of a metal film deposited which is not sufficient in the other cases.

Despite the fact that these dried treatments-based interphases partially complete their expected role by adsorbing the Pd catalyst, most of them are not bringing the sufficient roughness to obtain enough adhesion of the subsequent electroless metal layer onto the substrate. Additionally, all these dried treatments are carried out in controlled atmosphere chamber which make them quite difficult to industrialize.

3.3. Surface functionalization by surface graft polymerizations (3D-ligation)

In a similar way than with SAM chemical adsorption or plasma-assisted chemical vapor deposition, Bittner and co-workers used microcontact-printing (μCP) to selectively and physically adsorb polyamide-amine (PAMAM) dendrimers, that are nitrogen-bearing ligands for Pd^{II} species, on bare Si wafers for selective electroless cobalt plating [120, 121]. Accordingly, after producing a passivation pattern with μCP of hydrophobic SAM organosilanes, dendrimers were physisorbed on the pristine zone of the wafers and Pd^{II} species were then selectively complexed on the adsorbed dendrimers and reduced to obtain Pd^{0} species (**Figure 16**). Electroless metal deposition finally occurred only on the areas covered with Pd^{0} species. Contrarily to the chemically adsorbed SAM-based processes where the interphase between the metal layer and the substrate was restricted to one metal/amine bond localized at the extreme surface of the SAM, the use of dendrimers allows creating a real interphase between the substrate and the electroless metal layer since dendrimers contain nitrogen-bearing ligands all along their chains. It finally leads to a 3D-ligation and increase the

adhesion of the electroless plated layer within the dendrimers by bringing mechanical and chemical adhesion at the molecular scale. Unfortunately, the main disadvantage of this process relies on the physisorption of the dendrimers which finally decreases the adhesive character of the whole process.

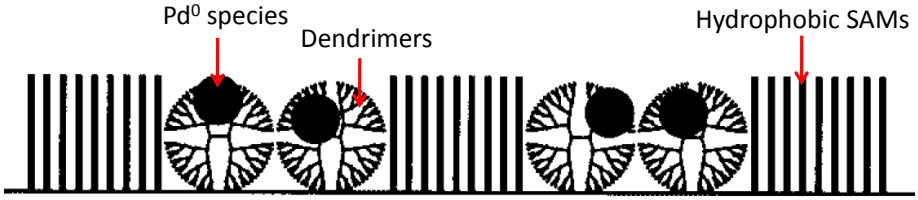

Figure 16 : Hydrophobic SAMs and Pd^0 species entrapped into adsorbed dendrimers on pristine zone (Extracted from Ref. [121])

To circumvent these weak adhesive properties, the fabrication of an active and complete adhesive 3D-structure has been suggested and is based on nitrogen-bearing polymer covalent grafting. It actually allows combining the covalent binding onto the surface provided by the SAM-based approach and the 3D interphase provided by the use of nitrogen-bearing dendrimers to specifically absorb Pd^{II} ions in the volume of the grafted polymer. Grafted polymer chains are then considered as a robust interphase between the substrate surface and the metal layer, which is intended to replace the rough interface which usually results from the chromic acid treatment. As previously mentioned that rough interface both promotes the transient deposition of catalytic particles, thanks to polar chemical groups formed upon the polymers surface oxidation, and also increases the final adhesion between the polymers and the final metal layer, by the interdigitation between the two materials. A bonded interphase should exhibit similar properties, due to specific affinity for the catalyst, robust anchoring on the polymers surface and deep interpenetration with the metal layer.

Besides, while the SAM-based approach was highly restricted by the substrate nature (by only working on hydroxylated surfaces), this approach allows increasing the substrate range.

Whereas in the previous approaches Pd catalysts were adsorbed in the form of Pd colloids (ranging from a few nm to several tens nm [11]) mainly onto nitrogen-bearing groups, in this case, monomeric Pd^{II} species such as $PdCl_4^{2-}$ are directly coordinated to the ligands at the molecular scale. Ligands are commonly strong σ-donor species such as ammonia, alkylamines, and also carboxylates, which bind Pd^{II} and stabilize the resulting monomeric complex.

Therefore, various types of ligand polymer brushes acting as host polymer films were used to immobilize Pd species from Pd salts acid aqueous solutions for the electroless copper plating [92, 94-96, 122-129]. Then, Pd^0 particles are formed via the reduction of bound Pd^{II} during a reduction step or directly during the electroless plating step (thanks to the reducing agent of the electroless plating bath itself) and act as catalyst for the electroless deposition. Various examples of graft polymerizations techniques have been investigated to complex Pd^{II} species and the best examples are exposed here:

- Oxidative graft polymerization of aniline on poly(tetrafluoroethylene) substrates substrates for the electroless plating of copper [130].
- UV-induced surface graft polymerizations of 4-vinylpyridine respectively on fluorinated polyimide for the electroless plating of copper (**Figure 17**) [118].
- Surface initiated atom-transfer radical polymerization of 4-vinylpyridine on polyimide substrates for the electroless plating of copper [92].

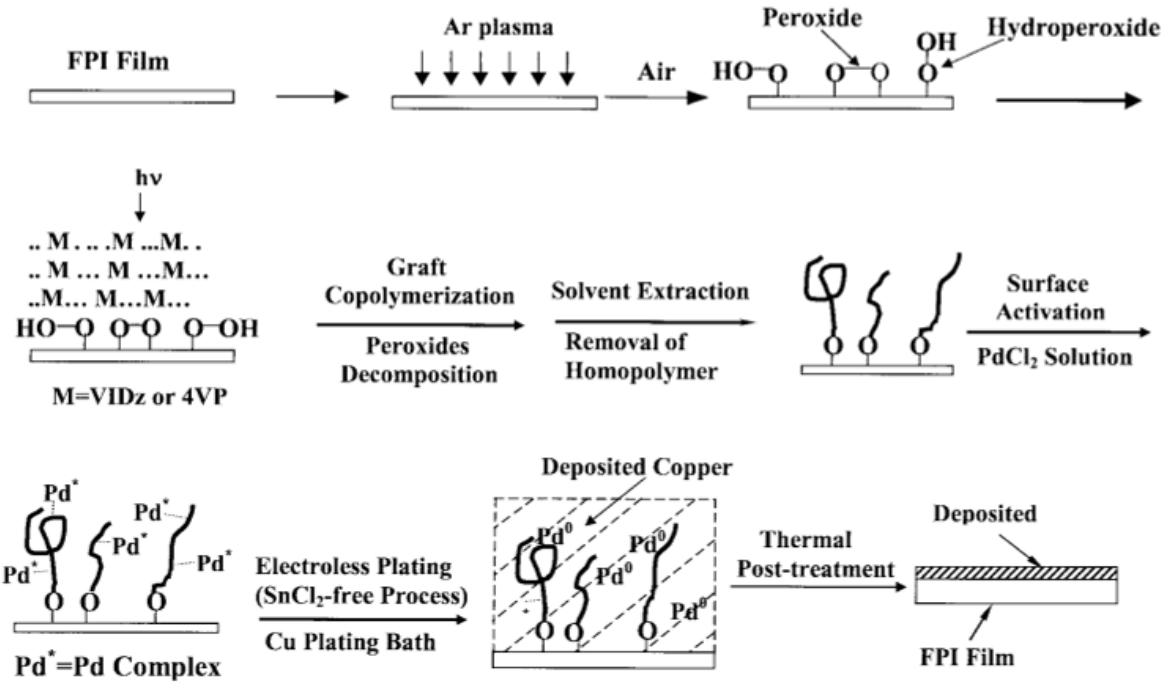

Figure 17: Schematic diagram illustrating the processes of Ar plasma pretreatment and UV-induced graft copolymerization of fluorinated polyimide (FPI) with 1-vinylimidazole (VIDz) to form the VIDz-grafted FPI surface and 4-vinylpyridine (4VP) to form a 4VP-grafted FPI surface, and the activation of the modified FPI surface via the Sn-free process for the subsequent electroless deposition of copper to form a copper/FPI assembly [118].

In a similar way, examples of this approach include the use of $Pd(NH_3)_4^{2+}$ complexes as catalysts for the electroless plating of charged phospholipid membranes [131] and physisorbed

polyacrylate multilayer films formed by Layer by Layer processing [132, 133]. More recently, as illustrated in **Figure 18**, Lancaster and coworkers described a method using block copolymers with one block designed to interpenetrate the substrate and the other one bearing chelating groups (such as polyacrylate) which were used to form a host polymer film for electroless plating on various polymer substrates [134]. That innovative method however requires the synthesis of a two-block copolymer in which one block is made of the same polymer as the substrate (or highly miscible with it), and another one bears chelating groups for the Pd^{II} species. It finally leads to a very complex and multi-step process.

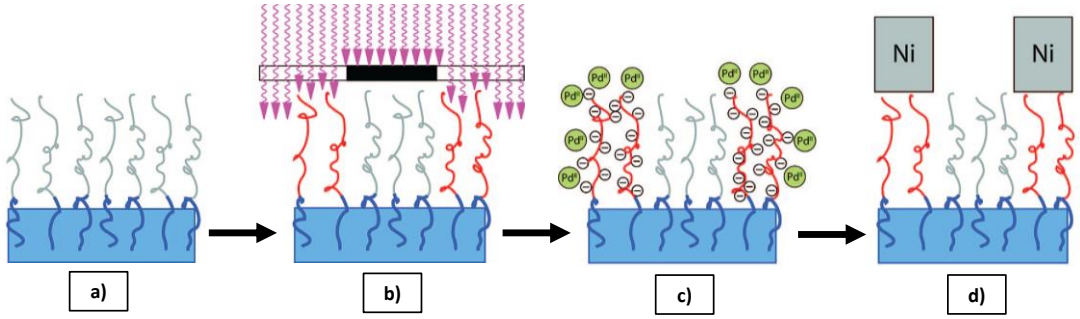

Figure 18 : Experimental scheme: a) Polystyrene substrate coated with Polystyrene-block-poly(tert-butyl acrylate) copolymer; b) UV irradiation of copolymer surface through contact mask; c) areas hydrolyzed to Poly(acrylic acid) (PAA) selectively adsorb the $[Pd(NH_3)_4]^{2+}$ catalyst; d) nickel selectively deposits onto areas of hydrolyzed PAA where the $[Pd(NH_3)_4]^{2+}$ catalyst had adsorbed (Adapted from Ref. [134])

3.4. Polymer surface swelling as host polymer film: The polyamide case

As mentioned earlier, several polymers to-be-plated bear in own their structure ligands capable of selectively adsorb Pd species to obtain the catalysis of the electroless plating growth. In that particular case, no pre-treatment is necessary before the activation step: The immersion of the polymer substrate into an appropriate solvent can lead to the polymer surface swelling which then constitutes an interphase acting as host polymer film for the catalyst precursor. In this regard, ATOTECH notably developed a process, called NOVIGANTH®, for the electroless plating of polyamide based on this approach and the adhesion of the electroless plating layer seems to lead to a competitive process but totally dependent on the nature substrate [135].

3.5. Pd-free Electroless plating of polymers

Using Sn-free catalysts simplifies the composition of the catalyst and reduces the hazardous Sn species waste in the process but taking into account that the cost of palladium has raised in recent years, the development of Pd-free catalysts has also attracted a lot of attention lately [136-140]. Besides, based on the autocatalytic behavior of the electroless plating growth for almost all the metals of the Group IB and VIII of the periodic table (Au, Pt, Ni, Cu, Co, Ag,…) [9], several authors have successfully used them directly as catalyst thanks their adsorption on ligand-bearing polymer surfaces such as amino or carboxylate groups. For example, silver has been adsorbed on polyimide, ABS or polycarbonate pretreated substrates for the electroless copper or gold plating [27, 141-144]. More recently, it has been demonstrated that copper and nickel [136, 139, 145-148] can also play this catalyst role on various polymer substrates (polyimide, ABS or glasses) and looking at their low prices, they look as the best industrial alternatives to palladium.

3.6. Conclusions

As a conclusion on the electroless plating of Pd^{II}-ligand modified polymers process, we have seen that they are a large number of different methods to adsorb polymers onto the surface of various substrates. Unfortunately, they are either very specific to one kind of substrate or very complicated to industrialize and it is clear that except for individual cases such as polyamide, the most used industrial electroless plating process is still based on Cr-etching and Pd-Sn activation.

4. Methods used for the localized metal deposition

The use of organic materials combined to metal deposition in the fabrication of microelectronics devices, bioelectronics devices and portable electronics has met a growing interest during the last few decades [10-16]. In recent years, increasing attention has been devoted for developing convenient and low-cost processing techniques to fabricate conductive features onto flexible substrates [149-151]. Consequently, the fabrication of metal patterns on polymer substrates becomes extremely important for the manufacturing processes of flexible

electronics. Therefore, localized metal deposition can be carried out by the association of a patterning technique and one of the previously described metallization process, when compatible. Among all the existing patterning techniques, this work will highlight the most used technique at the industrial scale which is photolithography but also printing processes which are appropriate low-cost techniques to obtain localized metal deposition.

4.1. Photolithography based process

Over the three past decades, photolithography has been the most used method for the surface patterning of polymers. As illustrated in **Figure 19**, in most cases, surface patterns are generated by selectively exposing a photo-resist-coated surface either to UV irradiation through a mask or to driven electron beam. Depending on the method, the irradiation step is then followed by the selective removal of the exposed (or non-exposed) areas by the dissolution in an appropriate solvent [152, 153]. Afterwards, the metallization of polymers is carried out by one of the previously described processes and followed by a lift-off step which selectively removes the remaining photoresist domains covered by the metal layer, leaving on the surface the metal domains where the photoresist was absent. Hence, a metallic pattern is obtained. It is noteworthy that this widely applied process clearly uses more metal than necessary, since the metal deposition step concerns the whole surface. Besides, disposal of the waste photoresist and unwanted metal adds to the process cost and induces environmental hazards. However, associating photolithography with a specific ligand deposition onto the pristine substrate area (after the photoresist development step) could be a way to avoid this metal waste. Accordingly, this localized ligand deposition would be then followed by the localized surface activation and finally with the electroless plating growth only on the activated area.

Although the photolithography method has been commonly adopted in the field of micro-fabrication, it is time-consuming, complicated and expensive.

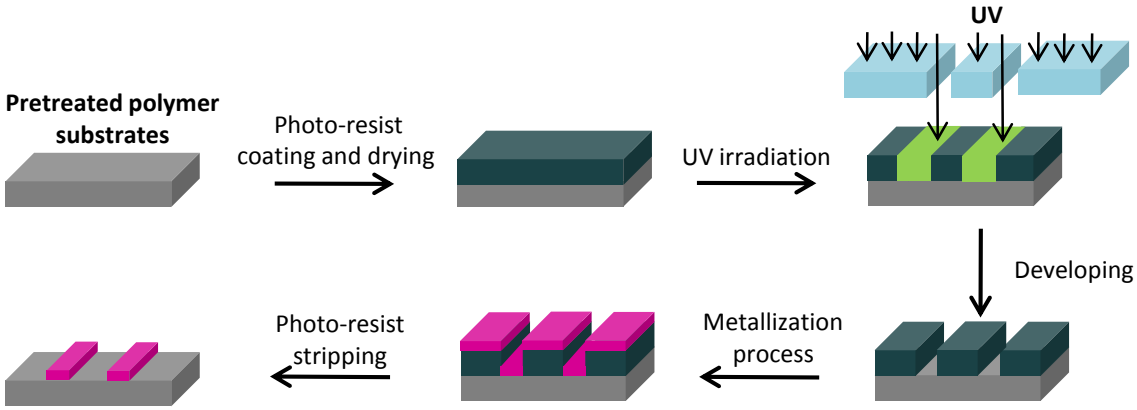

Figure 19 : Common localized metallization process based on the use of a photoresist

4.2. Printing techniques

Modern printing methods for polymer patterning include conventional printing techniques such as xerography and inkjet, screen and offset printing, and relatively new methods such as dip-pen lithography, nanoimprinting and microcontact printing. Printing methods can be classified into two groups: techniques involving the contact of a stamp or a writing head with a substrate, and the methods in which an 'ink' material is transferred to the substrate without direct contact with the surface.

Besides, compared to photolithography based processes, these printing techniques provides ecological benefits since only the amount of metal necessary to metallize the designed pattern will be used (contrary to classical lift off which discards a significant amount of metal deposited on top of the resist). In this report, we focus on two of the most described processes for the fabrication of micrometric metal patterns which are microcontact printing and inkjet printing.

4.2.1. Microcontact printing

Microcontact printing (µCP) is a mask-less and flexible method that provides the formation of patterned SAMs containing regions terminated by different chemical functionalities with submicron lateral dimensions [154]. The procedure is remarkably simple and is illustrated in **Figure 20**. An elastomeric stamp (mainly polydimethoxysilane PDMS) is used to transfer the ink to the surface of the substrate by contact. µCP was first demonstrated for SAMs of alkanethiolates on gold in 1993 by Whitesides [155]. Its success relies on the rapid reaction of

alkanethiols on gold and on the autophobicity of the resulting SAMs [154]. Then, microcontact printing has been extended to various substrates and molecules to be transferred. Besides, in 1996, Whitesides and coworkers developed the microcontact printing of Pd colloids for the electroless copper deposition onto aminosilane-functionnalized substrates [156]. As mentioned earlier, many other laboratories have been working on the direct microcontact printing of organosilane on various hydroxylated surfaces (glass, silicon wafers, oxidized poly(tetrafluoroethylene) or nitrogenated polyimide) to adsorb Pd^0 species which are able to catalyze the electroless plating growth [11, 34, 155, 157]. Notwithstanding, this process was limited to organosilane-functionnalized substrates. More recently, among the various examples founded in the literature, Miller et al. [158] described an interesting process based on the microcontact printing of an aluminum (III) porphyrin complex (tetraphenylporphyrinato) aluminum methoxide ((TPP)Al-OMe)) onto oxidized polymer substrates to obtain micrometric metal patterns after common electroless plating process (**Figure 20**).

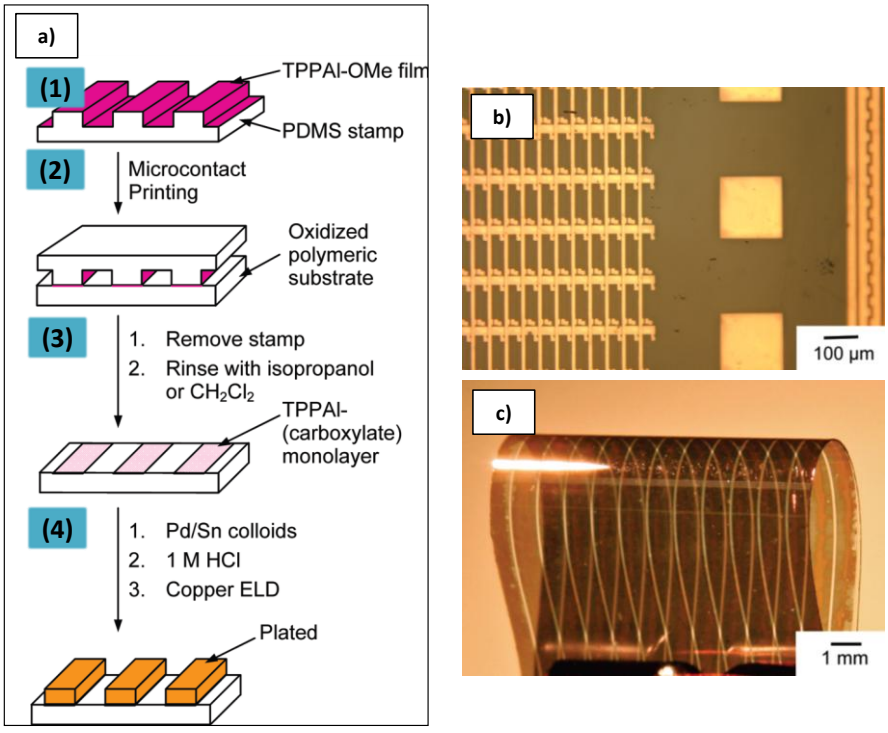

Figure 20 : (a) Schematic of the process steps used to fabricate patterned copper films on pretreated polymeric substrates and SEM (b) and optical (c) images of two examples of patterned coppers films obtained on pretreated Poly(ethylene terephthalate) (b) and Poy(ethylene naphtalate) sheets (c) (Extracted from Ref. [158])

4.2.2. Inkjet Printing

Inkjet printing can be defined as a mask-less digital process for the selective deposition of materials in liquid phase. As a matter of fact, printed patterns can be instantaneously modified through the digital technology which is very useful for small mass production or even personalized applications. Inkjet printing involves the controlled deposition of small droplets of liquid onto a substrate and offers a wide range of possibilities in micro-manufacturing. Indeed, the final inkjet printing solution depends on the inkjet printer and is usually around a few micrometers. **Figure 21** illustrates several routes by which inkjet printing can be used to obtain a metal coating. Any of these processes can be combined with one or more secondary electroless or electroplating steps to produce a thicker metallic deposit, which can even be of a different metal.

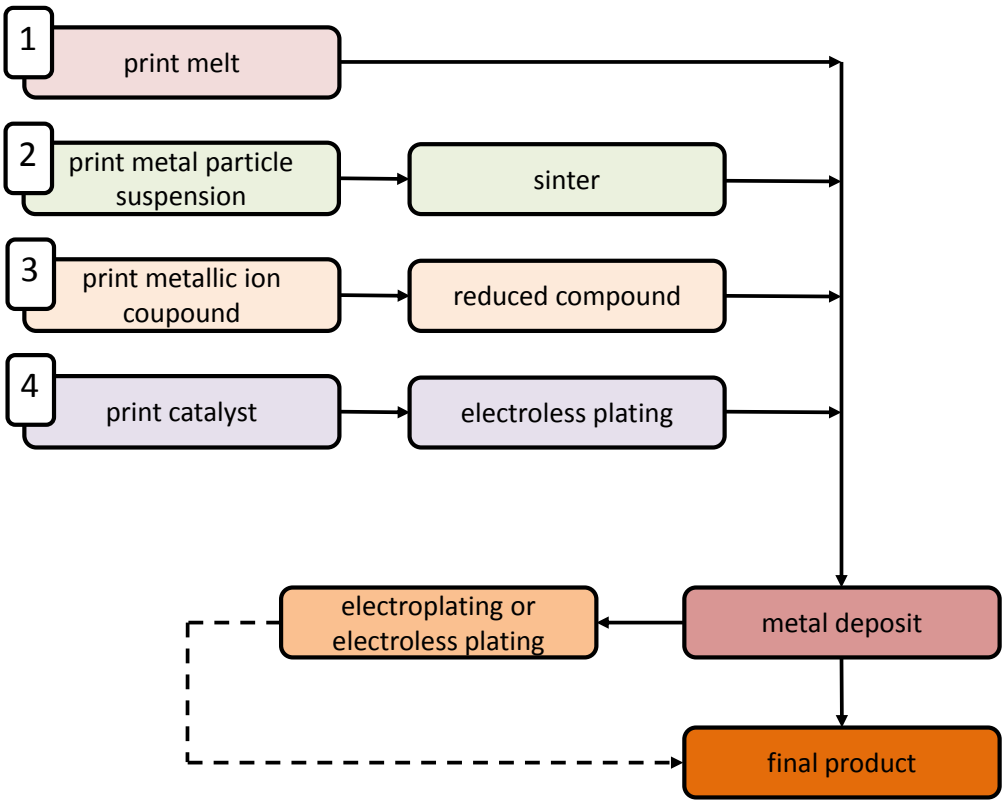

Figure 21 : Different routes for the inkjet deposition of metals

4.2.2.1. Direct printing from a melt

This is probably the simplest method to obtain metal patterns by inkjet printing since it consists in printing droplets of molten metal directly onto the substrate. Several groups have reported the printing of lead-tin solder alloys by both continuous (CIJ) and drop-on-demand (DOD) printing methods [159, 160]. Other metals with relatively low melting points such as indium, tin, lead and zinc have also been printed by CIJ and DOD [161, 162]. Nevertheless, deposition in an inert atmosphere is necessary to avoid oxidation of the molten droplets, and this requirement, associated with the complications introduced by operating the print head at high temperature, limits the attractiveness of the direct melt printing process for many metals. Lastly, this technique does not ensure good adhesion properties of the metals onto the printed substrate.

4.2.2.2. Printing a suspension of metallic particles which are then sintered

Metallic particles suspended in a suitable volatile solvent can be inkjet printed, and used for both structural and electrical applications. Small particles are generally favored as the suspensions are more stable, *i.e.* the particles do not sediment, and nozzle clogging is avoided. Particles smaller than 1/10, and preferably smaller than 1/50 of the nozzle diameter are required to avoid blockage. A further very important advantage of small particle size is that the high surface to volume ratio leads to a lowered sintering temperature. There is considerable interest in the development of nanoparticle inks with good electrical properties, oxidation resistance and low sintering temperatures for printable electrical conductors [163]. Inks based on silver nanoparticles, typically 5 – 50 nm in size for example, can be sintered to form deposits of high electrical conductivity at temperatures below 300°C, and even as low as 150°C, which allows them to be used with some polymer substrates [164-166]. **Figure 22 a)** is an example of the obtained silver conductive patterns inkjet printed on polyimide substrate. Likewise, gold or copper metallic particles have been successfully printed to obtain conductive patterns [150, 163, 167].

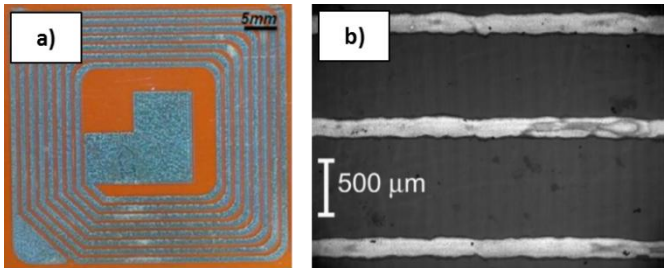

Figure 22: a) Photograph of silver conductive patterns inkjet printed onto polyimide substrate (Extracted from Ref. [164]) and b) SEM image of copper lines printed on polyimide film after surface treatment KOH(right) (Extracted from Ref. [168])

4.2.2.3. Printing a metal compound which is then chemically reduced to form the metal

The third method of achieving a metallic deposit by inkjet printing is to print a precursor: a solution of a compound of the metal, usually silver, which is then decomposed by heating at least at 150°C. For example, inks based on silver nitrate and on organic silver compounds have been successfully printed and sintered to yield conductive metallic deposits by CIJ [169] and DOD processes [170].

4.2.2.4. Printing a suitable catalyst followed by electroless plating to deposit the metal

The final approach, as shown in **Figure 21**, is to print a non-conductive but chemically active deposit which acts then as a catalyst of the electroless plating bath, typically to deposit copper or nickel [34, 168, 171]. The printing process produces a template for the subsequent plating, and defines the area to be coated as illustrated in **Figure 22 b)**. Excellent conductivity can be achieved by using this approach and the low processing temperature allows saving energy and represents a significant advantage for the metallization of polymers as described in the Chapter V.

4.3. Conclusions

Various lithographic and printing techniques have been developed to obtain localized metal deposition. The resolution and the chemical and physical properties of the metal pattern strongly depend on the technique. However, in the current socioeconomic and environmental

issue, ecological benefits brought by printing techniques become a crucial advantage at the industrial scale.

Combining the above-described patterning methods with the best available techniques to create a robust interphase between substrates and the metal layers is probably the best way to develop an industrial process competitive with the current Cr-based industrial process and to obtain localized metal deposition.

5. Diazonium induced anchoring process "DIAP" - Graftfast™ process

5.1. Graftfast™ origin

The grafting of polymers on surfaces is a major research topic of our laboratory and has thus been widely studied especially through the cathodic electrografting of vinylic monomers and, more recently, through a process called SEEP standing for Surface Electroinitiated Emulsion Polymerization. Indeed, the cathodic electrografting of vinylic monomers gives strongly adhesive polymer films on any conducting or semi-conducting surface from anhydrous solutions of vinylic monomers [97]. Overcoming the limitations of this process coming from the inherent mechanism of the reaction (anionic polymerization) has firstly led to work with diazonium salts in organic media and then to invent the SEEP process [98, 172, 173]. Indeed, this latter electroiniated radical polymerization process works in dispersed aqueous media and with a wide range of monomers. However, both processes, as electrochemical procedures, are limited to conducting substrates. To open the route towards the grafting of any type of surfaces from conductors to insulators, a method employing a reducing agent in solution was developed to activate the diazonium salts.

Such as its electrochemical counterpart process SEEP, this new procedure [174, 175], called "Diazonium Induced Anchoring Process" (DIAP) and registered under Graftfast™ brand, is a radical polymerization process based on the reduction in solution of diazonium salts generating radicals able to initiate the polymerization in solution of vinylic monomers. The nature of the films obtained ranges from poly(meth)acrylates (one of the only family of polymers synthesized by cathodic electrografting) to all polymers that can be synthesized by

radical polymerization. Graftfast™ leads to covalent grafted polymer films from a short one-step reaction occurring at atmospheric pressure, at room temperature, in water and requiring no external energy source.

To date, only a few processes comparable to Graftfast™ exist. The closest ones are a bioinspired method based on the self-polymerization of dopamine [176] and a cross-linked random copolymerization of styrene and methyl methacrylate [177] which can be followed by a classical polymerization. And unlike Graftfast™, the formation of polymer films on the surface of materials leads, *a priori*, to physisorbed films, requires a two-step (at least) reaction and involves long reaction times or high working temperature. Besides, among the previously described processes to functionalize materials by polymer films, the Graftfast™ process appears quite powerful since it has been successfully applied to a large variety of materials and, as demonstrated by previous works [175, 178-181], it enables to control the thickness of the films as well as the localization of the grafting. Besides, depending on the vinylic monomer, it is possible to control the surface properties.

5.2. Graftfast™ components and mechanism

As illustrated in **Figure 23**, carrying out a Graftfast™ experiment consists in choosing: an aryldiazonium salt, a reducing agent, a vinylic monomer, a substrate, possibly the solvent and adjusting the concentration of each reactant, the reaction time but also, if necessary, the temperature, the atmosphere, the bubbling of the solution with different gases, its stirring, its exposure to light ... Each parameter can influence the film grafting and has thus to be selected carefully according to the aim of the work. The main components of the Graftfast™ procedure are presented in the following sections.

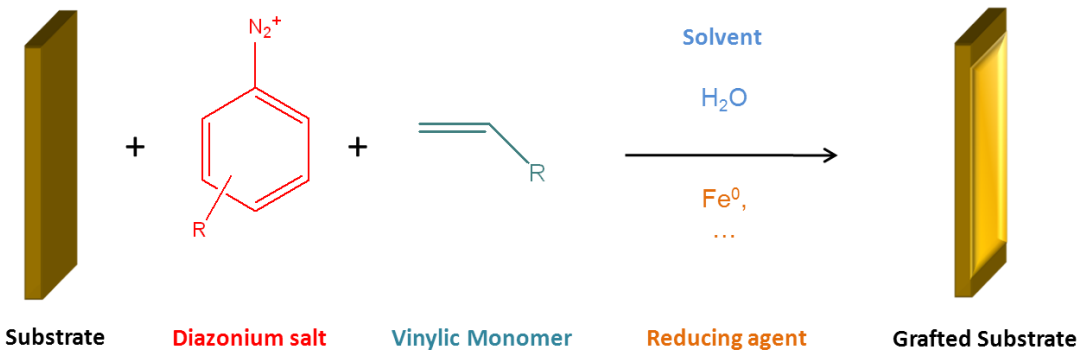

Figure 23: A typical Graftfast™ experiment.

5.2.1. Diazonium salts

A diazonium salt is an aliphatic, aromatic or heterocyclic compound in which a $-N_2$ group is attached to a carbon atom. In 1858, Peter Griess discovered aromatic diazonium compounds ($RN_2^+X^-$) [182]. Conjugation with the aromatic cycle π-electrons makes aryl diazonium ions much more stable [183] than their aliphatic counterparts which are potentially explosive when dry [184] and therefore rarely used in classical organic chemistry [185-187]. In contrast to all alkyl diazonium ions, aromatic diazonium salts are not Brønsted acids but Lewis acids [182]. The diazonium moiety (N_2^+) is reported to be the most electron-withdrawing substituent known [188]. Consequently, diazonium salts take part in a large variety of reactions [189-192] in particular nucleophilic additions on the β-nitrogen of the diazonium, nucleophilic substitutions [193] and azo coupling [194, 195]. Important industrial applications have arisen from those reactions including intermediates or end products such as azo dyes [182]. Likewise, electroreduction of aryldiazonium salts has been widely used for surface functionalization of conductive substrates such as glassy carbons, gold or platinum substrates [189, 196-198]. In those cases, aryldiazonium salts act as adhesion primer and coupling agent for binding various types of molecules [189, 199] such as conductive polymers [196] or metal nanoparticles [198] which finally also opens up a large variety of applications.

5.2.1.1. Diazotization reactions

A few para-substituted aromatic diazonium salts are commercially available among them 4-bromo, nitro or methoxy benzenediazonium tetrafluoroborate (BF_4^- is known to stabilize diazonium salts [182]). A range of di-substituted or complex aromatic diazonium salts can also be found. However, to synthesize and isolate aromatic diazonium compounds (diazotization reaction), a number of distinct methods are known [191]. The most common one consists in the reaction of sodium nitrite on an arylamine in acidic aqueous media (**Figure 24**) [182, 191]. Another synthesis way is based on the reaction of nitrosonium tetrafluoroborate with an arylamine in organic solvent media [180]. It is important to underline that these diazotization methods can be used to synthesize the aryldiazonium salt *in-situ i.e.* in the reactive solution consuming the aryldiazonium salt. This kind of method is known as *one-pot* reaction [200, 201].

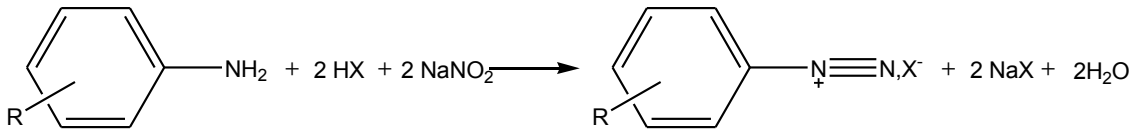

(X= Cl, Br, BF_4, ClO_4, ...)

Figure 24 : Typical diazotization reaction of an aryldiazonium salt.

5.2.1.2. Dediazotization reactions

Among the variety of reactions based on aryldiazonium salts, dediazotization reactions (referring to reactions involving the loss of dinitrogen) have attracted much interest. They may take place following either a heterolytic or a homolytic mechanism (**Figure 25**) [182, 190]. The heterolytic dediazotization pathway is the most likely mechanism in the degradation of aryldiazonium salts in solution as it forms a very stable product N_2 in addition to a metastable intermediate, the aryl cation leading to, for example, phenols [202]. Heterolytic cleavage of the C-N bond can also be involved in solvolytic or thermal reactions [203]. As known by organic chemists, carrying out a homolytic dediazotization requires an electron transfer which can be induced by, for instance, the solvent [190], a reduction at an electrode [190, 204] or by chemical reducing agents [205, 206] (metal cations [207], anions [182], H_3PO_2 [208, 209], ...). Lastly, UV photolysis of the diazonium salts in the presense of an electron donor leads also to an electron transfer and the aryl radical formation [210, 211]. However, according to the reaction conditions, a competition or coexistence of the two mechanisms is always possible.

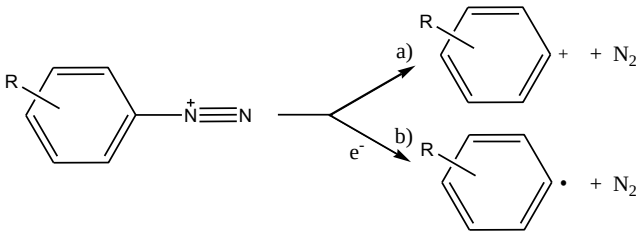

Figure 25 : Dediazotization through an a) heterolytic and b) homolytic mechanism of an aryldiazonium salt.

5.2.2. Chemical reducing agents

Unlike the electrochemical processes, in this anchoring method the electron transfer at the origin of the aryldiazonium salt reduction is not achieved by the application of an electrical potential but by an oxidation-reduction (redox) reaction. Therefore, it follows the same rules as any redox reaction. As a first approximation, all chemical reducing agents with a standard oxidation potential lower than the reduction potential of the aryldiazonium salt are estimated

to be suitable to operate the homolytic dediazotization reaction. Among the possible reducing agents, two different types can be distinguished: the reducer acting in heterogeneous phases (composed by a liquid and a solid) and those operating in homogeneous phase (liquid phase).

5.2.2.1. Heterogeneous phase

The reducing agents working in heterogeneous phase suitable for the anchoring process include all solid compounds fulfilling the requirements in terms of oxidation potential. Iron powder has been used as reducing agent in the original Graftfast™ experiments [175] and later for specific applications as the grafting of cation exchange membranes to improve their selectivity [212], for electro-switchable surfaces for heavy metal waste treatment and to create self-adhesive surfaces for the DNA or protein immobilization as described in the next parts [180, 213]. A lot of other compounds could also be suitable for instance all metals reductive enough (copper, nickel, zinc …). A large part of the work presented in this thesis was performed using iron as a reducing agent.

5.2.2.2. Homogeneous phase

The reduction of aryldiazonium salts into aryl radicals in homogeneous phases is a well-known reaction. It has been notably achieved with iodide [182, 190] and H_3PO_2 [214, 215]. It is only recently that this reaction has been considered as a way to functionalize the surface of materials. Up to now, hydroquinone [205], ferrocene (in organic media), L-ascorbic acid [181] and H_3PO_2 [216-220] have been used to reduce diazonium salts in order to graft organic layers.

5.2.3. Photochemical reduction

In aqueous solution, aryldiazonium salts show absorption maxima in the ultraviolet (UV) region. As an example, benzenediazonium has λ_{max} at 261 nm and 300 nm. Both absorption bands are shifted toward the visible region by electron-donating substituents [211]. Hence, the photolysis of aryldiazonium salts in the presence of an electron donor partially induces a homolytic dediazotization through an electron transfer and leads to the formation of an aryl radical [211]. The main bottleneck to use photochemical reduction relies on the low quantum yield for the photoelectron transfer and aryl radical formation towards the heterolytic cleavage and aryl cation formation especially in aqueous solution [211]. This quantum yield

can be highly increased by adding the ruthenium tris(bipyridine) complex $[Ru(bpy)_3]Cl_2$ which is well known for its electron transfer properties under visible irradiation provided by the metal-to-ligand charge transfer (MLCT) absorption band at 453 nm in the visible region [110, 221]. Therefore, an important part of the work presented in this thesis is based on the aryldiazonium photochemical reduction induced by the ruthenium complex.

5.2.4. Vinylic monomers

With the Graftfast™ process, all the vinylic monomers that can polymerize via a radical pathway are potentially usable. By analogy with the SEEP process, in the case of monomers with low solubility in water the anchoring method can be adapted by working in dispersed aqueous media (emulsion, mini-emulsion). We will only considered monomers soluble in water and in particular the work was focused on the polymerization of acrylic acid due to its ion exchange properties.

5.2.5. Substrate surface influence

Surface modification and more specifically covalent grafting onto a surface is, above all, an interfacial reactivity issue. Indeed, the first parameter in order to obtain the surface modification of a substrate is to allow the surface reactivity at the “substrate/reactive solution” interface. Consequently, surface wettability is a surface property that needs to be studied and controlled for each reactive solution/substrate to understand the difference in the grafting efficiency from one substrate to another. As an example, in the case of hydrophobic surfaces, the Graftfast™ process in aqueous solution will not be efficient since the wettability between the hydrophobic surface and the aqueous solution is not promoted. At this stage, two main solutions are available to improve the grafting efficiency and promote the interfacial reactivity:

i. To make an oxidative surface treatment to increase the surface hydrophilicity and subsequently surface wettability (such as the one developed in the surface conditioning section).
ii. To adapt the reagents choice such as the diazonium salt or the aqueous media (by adding surfactants) in order to increase the surface wettability toward the solution.

Likewise, the solubility of the grafted aryl groups (and therefore the aryldiazonium salt one) into the grafting solution is also essential since once the first aryl radical layer is grafted onto the surface, it leads to a new surface state precisely determined by the grafted aryl layer. As an example, in aqueous solution when the *para* position of the aryldiazonium salts is occupied by hydrophobic substituents such as bromide or alkyl groups, the grafted layer growth is not promoted whereas if bearing hydrophilic substituents such as ammonium or carboxylic groups, it will be the opposite.

To sum up, higher the surface reactivity, higher the grafting efficiency.

5.3. Graftfast™ versatility

Experiments demonstrated that Graftfast™ can suit various kinds of surface, insulators or conductors. The process has been widely applied on conducting or semi-conducting substrates such as, for example, on nickel, zinc, platinum, stainless steel (inox), titanium, gold, carbon fibres and aluminium as illustrated in **Figure 26** but also on nano-objects such as carpets of multiwalled carbon nanotubes [222]. Insulating materials from cellulose (wood, paper) to polymers or cotton have also been grafted by this process.

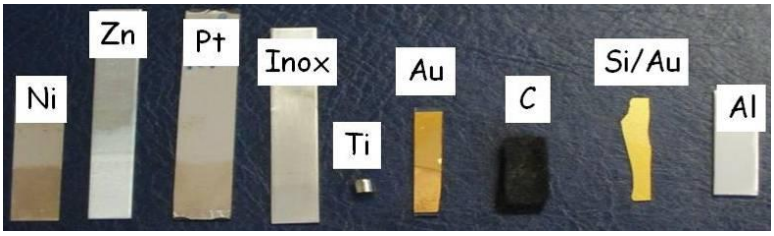

Figure 26 : Conducting or semi-conducting substrates successfully grafted by the Graftfast™ process [174, 175].

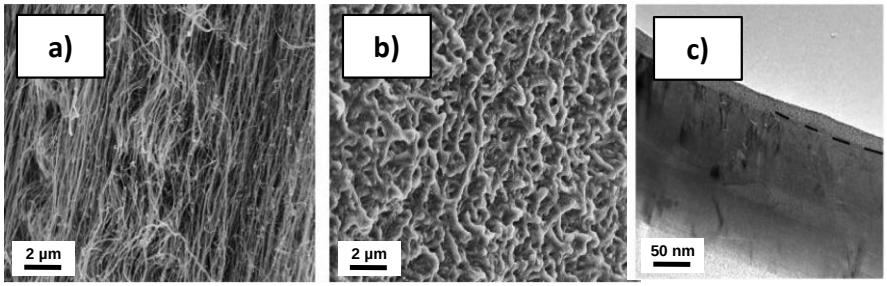

Figure 27 : SEM images a) before grafting and b) after grafting. TEM image of the grafted nanotubes in c). The dashed line corresponds to the interface polymer/nanotube [174, 175].

Therefore, various examples of applications using Graftfast™ were already developed and here are three different examples:

5.3.1. Surface patterning by microcontact printing

An important asset of this anchoring process lies in the control of the localization of the grafting. Indeed, as the radical moieties involved in the process are prone to graft on any surface, transient masking methods based on poorly adherent films can be used for preventing the covalent grafting in designated areas of the full substrate. First of all, in order to test the validity of lift-off processes, it was demonstrated the possibility of using a commercial ink simply drawn on a metallic substrate as a chemical mask to protect designated areas from the chemical grafting of polymers by Graftfast™. Then by using microcontact printed alkanethiols SAMs as sacrificial layers, gold surfaces were patterned by the Graftfast™ process as illustrated in Figure 28. Therefore, using common lift-off techniques in addition to the Graftfast™ process, the localization of polymer grafting was achieved which opens the route towards applications requiring patterned surfaces.

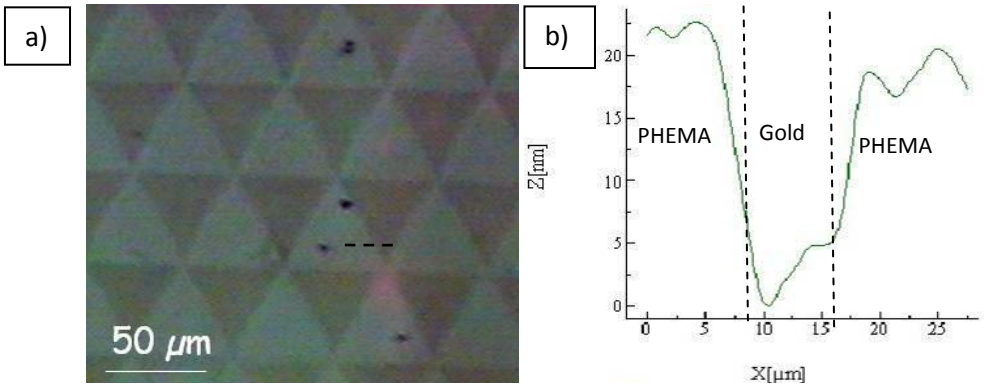

Figure 28 : The optical micrograph of a gold plate coated with a thiol mask with triangular patterns after treatment by Graftfast™ in the presence of HEMA and removal of a mask is shown in a). Dark zones correspond to the polymer while the clear ones correspond to non-covered gold. The graph (b) is the AFM profile obtained between covered and non-covered zones schematically represented in dashed line on a).

5.3.2. Self-adhesive surfaces

Through the Graftfast™process, covalent immobilization of various types of materials (carbon nanotubes, graphene, copper nanoparticles, polymers, …) was performed through a soft method [180]. This work was based on the *in situ* 4-aminophenyldiazonium salt synthesis

and grafting without any vinylic monomer which finally leads to the formation of a grafted polyaminophenylene layer. After diazotization of the amine groups contained on the polyaminophenylene grafted layer, this extremely simple and versatile process, applied on metallic and polymer materials, was eventually used as a self-adhesive primer for immobilizing different materials through a simple dipping step.

During this thesis, this self-adhesive primer was applied to biological applications through the fabrication of biochips. Indeed, self-adhesive primer has been patterned by cheap and easy methods as ink or UV masking. Then, biological model compounds such as low molecular weight DNA from salmon sperm and Glucose Oxidase (GOD) were locally covalently immobilized by this soft procedure as shown in **Figure 29** [213]. The complete article is presented in Appendix A.

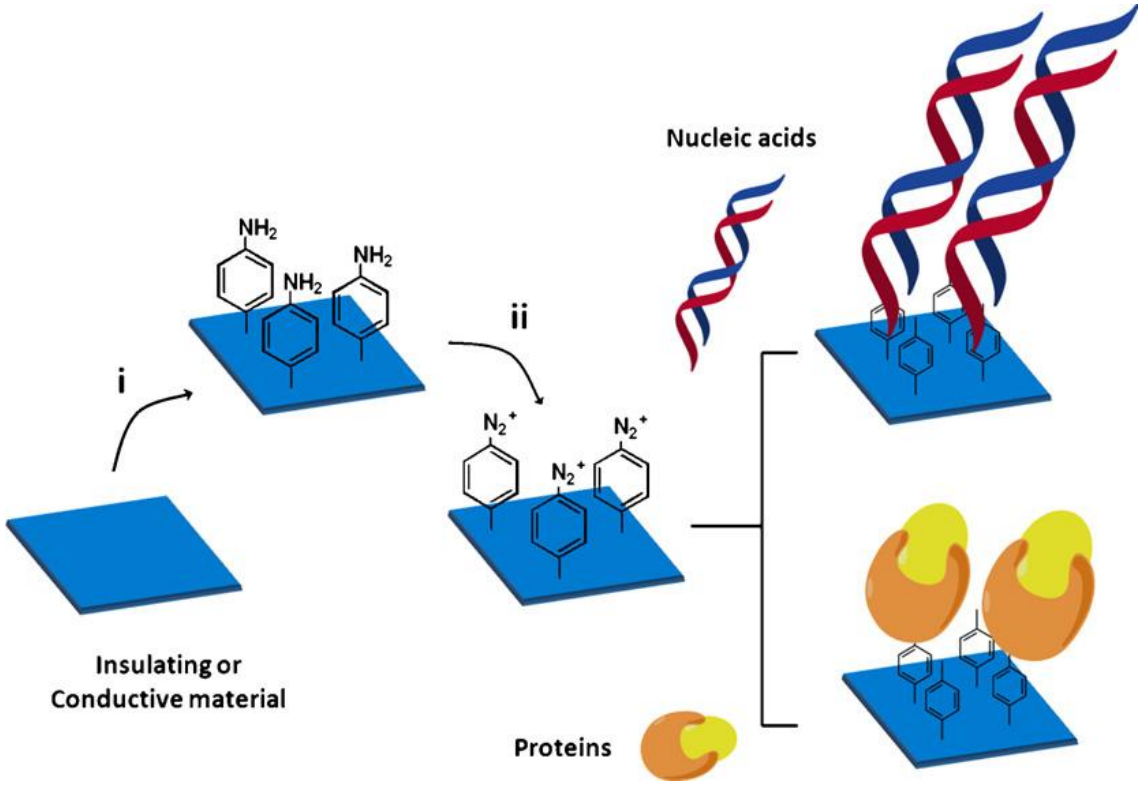

Figure 29 : Strategy for immobilizing nucleic acids or proteins on insulating or conductive materials with self-adhesive properties: i) and ii) preparation of self-adhesive surfaces as described in Figure 1, iii) direct and spontaneous grafting of biological materials put into contact with surfaces (Extracted from Ref. [213])

More recently, we have been able to demonstrate the application of these self adhesive surfaces to functionalize an Atomic Force Microscopy (AFM) scanning probe. Furthermore,

piezoelectric self-sensing scanning probe has been used to provide detailed information about interactions of small molecules with proteins. Specifically, the AFM spectroscopy can provide unique information on the magnitude of adhesion forces that can be used to guide the development of adhesion resistant materials, to analyze protein patterned biochips… In this sense, this work was considered to contribute to the development of a new kind of protein nanosensors with strong implications for molecular diagnosis or nanomedecine aims. The complete article is presented in Appendix B.

5.3.3. Electro-switchable surfaces for heavy metal waste treatment

In the current environmental issue previously exposed, the heavy metal ion waste treatment has logically grown in interest. Based on Graftfast™, a process to remove heavy metal ion waste by polymer-modified electrodes was developed [179, 223, 224]. The principle of heavy metal ion treatment by polymer films relies on the intrinsic chelating or ion exchange properties of the chosen polymers toward the metals ions. Poly(acrylic acid) brushes were grafted onto carbon felts thank to the Graftfast™process with the acrylic acid monomer (**Figure 30**). Thus, in a first step, due to its ion exchange properties, poly(acrylic acid) can capture heavy metal ions at very low concentration that cannot be reached with conventional electrodialysis using ion exchange membranes. And, in a second step, the release of the metal ions from the grafted polymer film can be obtained easily under electro-induced-acidification by applying an anodic potential at the felt electrode to promote localized water electrolysis. Besides, primary treatments of real industrial effluents were performed with a lab-made semi-pilot system and this electrochemical-pH-switchable PAA films can be considered within the field of aqueous effluent treatments in order to reach very low concentration in heavy metal ions.

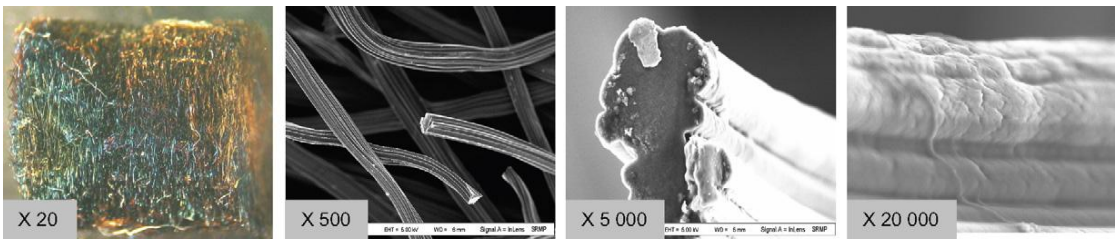

Figure 30: SEM images of Poly(acrylic acid)-grafted carbon felts at different scales [223].

5.4. Conclusions

The anchoring process based on the reduction of diazonium salts, also called Graftfast™ process, arised as an evolution of the electrografting process towards the grafting of all type of materials. On top of this remarkable property, the process has shown other very interesting advantages such as a control on the thickness of the films, on the surface properties or on the localization of the grafting. This anchoring process ranges from a simple reaction involving only the diazonium salt to more complex ones requiring a reducing agent as well as a vinylic monomer. However, to obtain an efficient grafting, the surface reactivity needs absolutely to be promoted which require to achieve a surface conditioning in certain cases.

REFERENCES

[1] K. Autumn, Y. A. Liang, S. T. Hsieh, W. Zesch, W. P. Chan, T. W. Kenny, R. Fearing, R. J. Full, *Nature* **2000**, *405*, 681.
[2] A. K. Geim, S. V. Dubonos, I. V. Grigorieva, K. S. Novoselov, A. A. Zhukov, S. Y. Shapoval, *Nat. Mater.* **2003**, *2*, 461.
[3] M. S. Prowse, M. Wilkinson, J. B. Puthoff, G. Mayer, K. Autumn, *Acta Biomater.* **2011**, *7*, 733.
[4] D. P. Long, J. M. Blackburn, J. J. Watkins, *Adv. Mater.* **2000**, *12*, 913.
[5] M. Charbonnier, M. Alami, M. Romand, *J. Electrochem. Soc.* **1996**, *143*, 472.
[6] E. Sacher, *Metallization of Polymers 2*, Plenum Publisher, New York **2002**.
[7] A. Vaskelis, H. J. Norkus, G. Rozovskis, H. J. Vinkevicius, *Trans. Inst. Met. Finish.* **1997**, *75*, 1.
[8] K. De Bruyn, M. Van Stappen, H. De Deurwaerder, L. Rouxhet, J. P. Celis, *Surf. Coat. Technol.* **2003**, *163*, 710.
[9] G. O. Mallory, J. B. Hajdu, *Electroless plating: Fundamentals and Applications*, The American Electroplaters and Surface Finishers Society, Washington, D.C. **1990**.
[10] T. Someya, T. Sekitani, S. Iba, Y. Kato, H. Kawaguchi, T. Sakurai, *Proc. Natl. Acad. Sci. U. S. A.* **2004**, *101*, 9966.
[11] D. Zabetakis, W. J. Dressick, *ACS Appl. Mater. Interfaces* **2009**, *1*, 4.
[12] B. L. Hassler, T. J. Amundsen, J. G. Zeikus, I. Lee, R. M. Worden, *Biosens. Bioelectron.* **2008**, *23*, 1481.
[13] N. Kohli, B. L. Hassler, L. Parthasarathy, R. J. Richardson, R. Y. Ofoli, R. M. Worden, I. Lee, *Biomacromolecules* **2006**, *7*, 3327.
[14] L. A. Bottomley, *Anal. Chem.* **1998**, *70*, 425R.
[15] X. Q. Liu, H. X. Chang, Y. Li, W. T. S. Huck, Z. J. Zheng, *ACS Appl. Mater. Interfaces* **2010**, *2*, 529.
[16] Y. N. Li, Y. L. Wu, B. S. Ong, *J. Am. Chem. Soc.* **2005**, *127*, 3266.
[17] EUROPEAN PARLIAMENT AND THE COUNCIL, 2002/95/EC, **2003**.
[18] EUROPEAN PARLIAMENT AND THE COUNCIL, 2005/90/EC, **2006**.
[19] P. Albericci, *United States Patent US4690736*, **1985**.
[20] W. C. Korbach, W. H. Mcmullen, *Worldwide Patent WO8805834*, **1987**.
[21] EUROPEAN PARLIAMENT AND THE COUNCIL, 1996/82/EC, **1996**.
[22] EUROPEAN PARLIAMENT AND THE COUNCIL, 1996/61/EC, **1996**.
[23] EUROPEAN PARLIAMENT AND THE COUNCIL, 2000/53/EC, **2000**.
[24] S. Dalbin, N. Pommier, *Métallisation des plastiques - Préparation par voie chimique*, Techniques de l'Ingénieur, Paris **2009**.
[25] F. Montfort-Windels, *Métallisation des plastiques*, Centre technique des industries mécaniques, Senlis **2005**.
[26] L. A. C. Teixeira, M. C. Santini, *J. Mater. Process. Tech.* **2005**, *170*, 37.
[27] N. Inagaki, H. Kimura, *J. Appl. Polym. Sci.* **2009**, *111*, 1034.
[28] G. N. Patel, D. Bolikal, H. Petel, *United States Patent US19900488256*, **1992**.
[29] E. G. Han, E. A. Kim, K. W. Oh, *Synth. Met.* **2001**, *123*, 469.
[30] H. Kupfer, G. Hecht, R. Ostwald, *Surf. Coat. Technol.* **1999**, *112*, 379.
[31] M. Charbonnier, M. Romand, E. Harry, M. Alami, *J. Appl. Electrochem.* **2001**, *31*, 57.
[32] M. Charbonnier, M. Romand, *Int. J. Adhes. Adhes.* **2003**, *23*, 277.

[33] H. W. Kim, J. H. Kim, D. J. Kim, N. E. Lee, *J. Electrochem. Soc.* **2009**, *156*, D525.
[34] F. Bessueille, S. Gout, S. Cotte, Y. Goepfert, D. Leonard, M. Romand, *J. Adhes.* **2009**, *85*, 690.
[35] M. Charbonnier, M. Romand, H. Esrom, R. Seebock, *J. Adhes.* **2001**, *75*, 381.
[36] H. Esrom, R. Seebock, M. Charbonnier, M. Romand, *Surf. Coat. Technol.* **2000**, *125*, 19.
[37] D. I. Ma, L. Shirey, D. McCarthy, A. Thompson, S. B. Qadri, W. J. Dressick, M. S. Chen, J. M. Calvert, R. Kapur, S. L. Brandow, *Chem. Mater.* **2002**, *14*, 4586.
[38] M. C. Demirel, M. Cetinkaya, A. Singh, W. J. Dressick, *Adv. Mater.* **2007**, *19*, 4495.
[39] R. R. Price, W. J. Dressick, A. Singh, *J. Am. Chem. Soc.* **2003**, *125*, 11259.
[40] I. Ohno, *Mater. Sci. Eng., A* **1991**, *146*, 33.
[41] A. Zouhou, H. Vergnes, P. Duverneuil, *Microelectron. Eng.* **2001**, *56*, 177.
[42] L. M. Abrantes, J. P. Correia, *J. Electrochem. Soc.* **1994**, *141*, 2356.
[43] A. Garcia, T. Berthelot, P. Viel, A. Mesnage, P. Jegou, F. Nekelson, S. Roussel, S. Palacin, *ACS Appl. Mater. Interfaces* **2010**, *2*, 1177.
[44] G. Gutzeit, *Plating* **1959**, *46*, 1158.
[45] G. Gutzeit, *Plating* **1959**, *46*, 1275.
[46] G. Gutzeit, *Plating* **1959**, *46*, 1377.
[47] G. Gutzeit, *Plating* **1959**, *47*, 63.
[48] M. Paunovic, M. Schlesinger, *Fundamentals of electrochemical deposition Second Edition*, Wiley Interscience, New York **2006**.
[49] C. Wagner, W. Traud, *Electrochemistry* **1938**, *44*, 391.
[50] M. Saito, *J. Met. Finish. Soc. Jpn.* **1966**, *17*, 14.
[51] M. Paunovic, *Plating* **1968**, *55*, 1161.
[52] M. Paunovic, *J. Electrochem. Soc.* **1977**, *124*, 349.
[53] F. M. Donahue, *J. Electrochem. Soc.* **1972**, *119*, 72.
[54] A. Molenaar, M. F. E. Holdrinet, L. K. H. van Beek, *Plating* **1974**, *61*, 238.
[55] S. M. Elraghy, A. A. Abosalama, *J. Electrochem. Soc.* **1979**, *126*, 171.
[56] A. Hung, I. Ohno, *J. Electrochem. Soc.* **1990**, *137*, 918.
[57] Y. Okinaka, *J. Electrochem. Soc.* **1973**, *120*, 739.
[58] L. N. Schoenberg, *J. Electrochem. Soc.* **1971**, *118*, 1571.
[59] I. Ohno, S. Haruyama, *Surface Technology* **1981**, *13*, 1.
[60] J. Vandenmeerakker, J. W. G. Debakker, *J. Appl. Electrochem.* **1990**, *20*, 85.
[61] J. Vandenmeerakker, *J. Appl. Electrochem.* **1981**, *11*, 395.
[62] J. Vandenmeerakker, *J. Appl. Electrochem.* **1981**, *11*, 387.
[63] R. P. Buck, L. R. Griffiths, *J. Electrochem. Soc.* **1962**, *109*, 1005.
[64] M. Paunovic, *J. Electrochem. Soc.* **1978**, *125*, 173.
[65] L. N. Schoenberg, *J. Electrochem. Soc.* **1972**, *119*, 1491.
[66] M. Paunovic, R. Arndt, *J. Electrochem. Soc.* **1983**, *130*, 794.
[67] D. Vitkavage, M. Paunovic, *Plating and Surface Finishing* **1983**, *70*, 48.
[68] Y. L. Chang, W. C. Ye, C. L. Ma, C. M. Wang, *J. Electrochem. Soc.* **2006**, *153*, C677.
[69] V. Dimitrov, L. Gorker, *Prog. React. Kinet. Mech.* **2006**, *31*, 45.
[70] T. Homma, A. Tamaki, H. Nakai, T. Osaka, *J. Electroanal. Chem.* **2003**, *559*, 131.
[71] T. Shimada, H. Nakai, T. Homma, *J. Electrochem. Soc.* **2007**, *154*, D273.
[72] S. L. Chow, Schlesin.M, J. Rezek, Hedgecoc.Ne, *J. Electrochem. Soc.* **1972**, *119*, 1013.
[73] J. Przyluski, M. Kasprzak, J. Bielinski, *Surf. Coat. Technol.* **1987**, *31*, 203.
[74] M. Schlesinger, J. Kisel, *J. Electrochem. Soc.* **1989**, *136*, 1658.
[75] R. L. Cohen, K. W. West, *J. Electrochem. Soc.* **1972**, *119*, 433.
[76] J. Shipley, R. Charles, *United States Patent US19590818554*, **1959**.

[77] M. C. Burrell, G. A. Smith, J. J. Chera, *Surf. Interface Anal.* **1988**, *11*, 160.
[78] M. Garcia-Gabaldon, V. Perez-Herranz, J. Garcia-Anton, J. L. Guinon, *J. Appl. Electrochem.* **2007**, *37*, 1145.
[79] A. Rantell, A. Holtzman, *Circuit World* **1976**, *2*, 30.
[80] R. L. Cohen, K. W. West, *Chem. Phys. Lett.* **1972**, *16*, 128.
[81] R. L. Meek, *J. Electrochem. Soc.* **1975**, *122*, 1177.
[82] R. L. Meek, *J. Electrochem. Soc.* **1975**, *122*, 1478.
[83] E. Matijevic, A. M. Poskanzer, P. Zuman, *Pating Surface Finishing* **1975**, *62*, 958.
[84] R. L. Cohen, K. W. West, *J. Electrochem. Soc.* **1973**, *120*, 502.
[85] G. Koziol, J. Bielinski, *Trans. Inst. Met. Finish.* **2003**, *81*, 110.
[86] O. Holderer, INSA Lyon, Lyon **2002**.
[87] M. Froment, E. Queau, J. R. Martin, G. Stremsdoerfer, *J. Electrochem. Soc.* **1995**, *142*, 3373.
[88] B. Pierson, K. W. Nebesny, Q. Fernando, T. Ogura, *Anal. Chem.* **1988**, *60*, 2661.
[89] S. Stremsdoerfer, *Worldwide Patent WO201012810*, **2010**.
[90] J. M. Calvert, G. S. Calabrese, J. F. Bohland, M. S. Chen, W. J. Dressick, C. S. Dulcey, J. H. Georger, J. Kosakowski, E. K. Pavelcheck, K. W. Rhee, L. M. Shirey, *J. Vac. Sci. Technol., B* **1994**, *12*, 3884.
[91] D. Aldakov, Y. Bonnassieux, B. Geffroy, S. Palacin, *ACS Appl. Mater. Interfaces* **2009**, *1*, 584.
[92] L. Li, G. P. Yan, J. Y. Wu, X. H. Yu, Q. Z. Guo, E. T. Kang, *Appl. Surf. Sci.* **2008**, *254*, 7331.
[93] W. C. Liaw, P. C. Huang, K. P. Chen, C. S. Chen, *Polym. J.* **2009**, *41*, 634.
[94] E. Renbutsu, S. Okabe, Y. Omura, F. Nakatsubo, S. Minami, H. Saimoto, Y. Shigemasa, *Carbohydr. Polym.* **2007**, *69*, 697.
[95] E. Renbutsu, S. Okabe, Y. Omura, F. Nakatsubo, S. Minami, Y. Shigemasa, H. Saimoto, *Int. J. Biol. Macromol.* **2008**, *43*, 62.
[96] Y. Omura, E. Renbutsu, M. Morimoto, H. Saimoto, Y. Shigemasa, *Polym. Adv. Technol.* **2003**, *14*, 35.
[97] S. Palacin, C. Bureau, J. Charlier, G. Deniau, B. Mouanda, P. Viel, *ChemPhysChem* **2004**, *5*, 1469.
[98] L. Tessier, G. Deniau, B. Charleux, S. Palacin, *Chem. Mater.* **2009**, *21*, 4261.
[99] A. Ulman, *Chem. Rev.* **1996**, *96*, 1533.
[100] K. L. Mittal, *Silanes and Other Coupling agents, Vol. 4*, VSP, Utrecht **2007**.
[101] T. G. Vargo, J. A. Gardella, J. M. Calvert, M. S. Chen, *Science* **1993**, *262*, 1711.
[102] S. L. Brandow, M. S. Chen, R. Aggarwal, C. S. Dulcey, J. M. Calvert, W. J. Dressick, *Langmuir* **1999**, *15*, 5429.
[103] S. L. Brandow, M. S. Chen, T. Wang, C. S. Dulcey, J. M. Calvert, J. F. Bohland, G. S. Calabrese, W. J. Dressick, *J. Electrochem. Soc.* **1997**, *144*, 3425.
[104] W. J. Dressick, L. M. Kondracki, M. S. Chen, S. L. Brandow, E. Matijevic, J. M. Calvert, *Colloids and Surfaces a-Physicochemical and Engineering Aspects* **1996**, *108*, 101.
[105] M. S. Chen, S. L. Brandow, C. S. Dulcey, W. J. Dressick, G. N. Taylor, J. F. Bohland, J. H. G. Georger, E. K. Pavelchek, J. M. Calvert, *J. Electrochem. Soc.* **1999**, *146*, 1421.
[106] D. L. Liu, Z. G. Yang, C. Zhang, *Mater. Sci. Eng., B* **2010**, *166*, 67.
[107] T. Osaka, N. Takano, T. Kurokawa, T. Kaneko, K. Ueno, *Surf. Coat. Technol.* **2003**, *169*, 124.
[108] T. Osaka, N. Takano, T. Kurokawa, T. Kaneko, K. Ueno, *J. Electrochem. Soc.* **2002**, *149*, C573.
[109] M. S. Chen, C. S. Dulcey, L. A. Chrisey, W. J. Dressick, *Adv. Funct. Mater.* **2006**, *16*, 774.

[110] J. E. Huheey, E. A. Keiter, R. L. Keiter, *Inorganic Chemistry*, De Boeck Université, Bruxelles **1998**.
[111] S. L. Brandow, M. S. Chen, S. J. Fertig, L. A. Chrisey, C. S. Dulcey, W. J. Dressick, *Chem. Eur. J.* **2001**, *7*, 4495.
[112] J. M. Calvert, T. S. Koloski, W. J. Dressick, C. S. Dulcey, M. C. Peckerar, F. Cerrina, J. W. Taylor, D. W. Suh, O. R. Wood, A. A. Macdowell, R. Dsouza, *Optical Engineering* **1993**, *32*, 2437.
[113] S. L. Brandow, M. S. Chen, C. S. Dulcey, W. J. Dressick, *Langmuir* **2008**, *24*, 3888.
[114] M.-S. Chen, S. L. Brandow, W. J. Dressick, *Thin Solid Films* **2000**, *379*, 203.
[115] C. Brinker, S. GW, *Sol-gel science*, Academic Press Inc., San Diego **1990**.
[116] M. Charbonnier, A. Romand, Y. Goepfert, D. Leonard, F. Bessueille, A. Bouadi, *Thin Solid Films* **2006**, *515*, 1623.
[117] C. S. Wong, H. P. Lem, B. T. Goh, C. W. Wong, *Jpn. J. Appl. Phys.* **2009**, *48*.
[118] W. C. Wang, R. H. Vora, E. T. Kang, K. G. Neoh, *Polym. Eng. Sci.* **2004**, *44*, 362.
[119] Y. Zhang, K. L. Tan, G. H. Yang, E. T. Kang, K. G. Neoh, *J. Electrochem. Soc.* **2001**, *148*, C574.
[120] X. C. Wu, A. M. Bittner, K. Kern, *Langmuir* **2002**, *18*, 4984.
[121] A. M. Bittner, X. C. Wu, K. Kern, *Adv. Funct. Mater.* **2002**, *12*, 432.
[122] V. W. L. Lim, E. T. Kang, K. G. Neoh, *Synth. Met.* **2001**, *123*, 107.
[123] W. C. Wang, E. T. Kang, K. G. Neoh, *Appl. Surf. Sci.* **2002**, *199*, 52.
[124] G. H. Yang, E. T. Kang, K. G. Neoh, *J. Polym. Sci., Part A: Polym. Chem.* **2000**, *38*, 3498.
[125] G. H. Yang, E. T. Kang, K. G. Neoh, Y. Zhang, K. L. Tan, *Langmuir* **2001**, *17*, 211.
[126] Z. H. Ma, K. L. Tan, A. D. Alian, E. T. Kang, K. G. Neoh, *J. Vac. Sci. Technol., A* **2001**, *19*, 2471.
[127] W. H. Yu, Y. Zhang, E. T. Kang, K. G. Neoh, S. Y. Wu, Y. F. Chow, *J. Electrochem. Soc.* **2002**, *149*, C521.
[128] W. H. Yu, Y. Zhang, E. T. Kang, K. G. Neoh, S. Y. Wu, Y. F. Chow, *J. Electrochem. Soc.* **2003**, *150*, F156.
[129] Y. Q. Zhu, E. T. Kang, K. G. Neoh, T. Osipowicz, L. Chan, *J. Electrochem. Soc.* **2005**, *152*, F107.
[130] Z. J. Yu, E. T. Kang, K. G. Neoh, *J. Electrochem. Soc.* **2002**, *149*, C10.
[131] M. A. Markowitz, G.-M. Chow, A. Singh, *Langmuir* **1994**, *10*, 4095.
[132] T. C. Wang, B. Chen, M. F. Rubner, R. E. Cohen, *Langmuir* **2001**, *17*, 6610.
[133] T. C. Wang, M. F. Rubner, R. E. Cohen, *Chem. Mater.* **2003**, *15*, 299.
[134] J. R. Lancaster, J. Jehani, G. T. Carroll, Y. Chen, N. J. Turro, J. T. Koberstein, *Chem. Mater.* **2008**, *20*, 6583.
[135] M. Hermann-Josef, L. Baosen, *Worlwide Patent WO200868049*, **2006**.
[136] M. Charbonnier, M. Romand, Y. Goepfert, *Surf. Coat. Technol.* **2006**, *200*, 5028.
[137] W. Dai, W. J. Wang, *Sens. Actuators, A* **2007**, *135*, 300.
[138] Y. S. Hsiao, W. T. Whang, S. C. Wu, K. R. Chuang, *Thin Solid Films* **2008**, *516*, 4258.
[139] Y. Matsumura, Y. Enomoto, M. Sugiyama, K. Akamatsu, H. Nawafune, *J. Mater. Chem.* **2008**, *18*, 5078.
[140] K. Miyoshi, Y. Aoki, T. Kunitake, S. Fujikawa, *Langmuir* **2008**, *24*, 4205.
[141] J. E. Graves, M. T. Goosey, D. Hirst, M. A. Poole, *Trans. Inst. Met. Finish.* **2001**, *79*, 90.
[142] C. Y. Kao, K. S. Chou, *Electrochem. Solid-State Lett.* **2007**, *10*, D32.
[143] J. H. G. Ng, M. P. Y. Desmulliez, K. A. Prior, D. P. Hand, *Micro. Nano. Lett.* **2008**, *3*, 82.
[144] Q. H. Zhou, H. W. Chen, Y. Wang, *Electrochim. Acta* **2010**, *55*, 2542.
[145] Y. Matsumura, Y. Enomoto, T. Tsuruoka, K. Akamatsu, H. Nawafune, *Langmuir* **2010**, *26*, 12448.

[146] N. Bicak, B. Karagoz, *Surf. Coat. Technol.* **2008**, *202*, 1581.
[147] X. J. Tang, C. L. Bi, C. X. Han, B. G. Zhang, *Mater. Lett.* **2009**, *63*, 840.
[148] M. Charbonnier, M. Romand, Y. Goepfert, D. Leonard, M. Bouadi, *Surf. Coat. Technol.* **2006**, *200*, 5478.
[149] B. J. de Gans, P. C. Duineveld, U. S. Schubert, *Adv. Mater.* **2004**, *16*, 203.
[150] D. Huang, F. Liao, S. Molesa, D. Redinger, V. Subramanian, *J. Electrochem. Soc.* **2003**, *150*, G412.
[151] Y. L. Wu, Y. N. Li, B. S. Ong, P. Liu, S. Gardner, B. Chiang, *Adv. Mater.* **2005**, *17*, 184.
[152] J. H. Moon, J. Ford, S. Yang, *Polym. Adv. Technol.* **2006**, *17*, 83.
[153] Z. H. Nie, E. Kumacheva, *Nat. Mater.* **2008**, *7*, 277.
[154] Y. N. Xia, G. M. Whitesides, *Annu. Rev. Mater. Sci.* **1998**, *28*, 153.
[155] S. C. Huang, T. C. Tsao, L. J. Chen, *J. Electrochem. Soc.* **2010**, *157*, D222.
[156] P. C. Hidber, W. Helbig, E. Kim, G. M. Whitesides, *Langmuir* **1996**, *12*, 1375.
[157] W. Prissanaroon, N. Brack, P. J. Pigram, P. Hale, P. Kappen, J. Liesegang, *Thin Solid Films* **2005**, *477*, 131.
[158] M. S. Miller, H. L. Filiatrault, G. J. E. Davidson, M. Luo, T. B. Carmichael, *J. Am. Chem. Soc.* **2010**, *132*, 765.
[159] M. Orme, J. Courter, Q. Liu, J. Zhu, R. Smith, *Materials Development for Direct Write Technologies* **2000**, *624*, 17.
[160] T. M. Lee, T. G. Kang, J. S. Yang, J. D. Jo, K. Y. Kim, B. O. Choi, D. S. Kim, *IEEE Trans. Electron. Packag. Manuf.* **2008**, *31*, 202.
[161] S. X. Cheng, T. G. Li, S. Chandra, *J. Mater. Process. Tech.* **2005**, *159*, 295.
[162] A. A. Tseng, M. H. Lee, B. Zhao, *J. Eng. Mater. and Tech. - T. ASME* **2001**, *123*, 74.
[163] B. K. Park, D. Kim, S. Jeong, J. Moon, J. S. Kim, *Thin Solid Films* **2007**, *515*, 7706.
[164] S. Jeong, H. C. Song, W. W. Lee, Y. Choi, B. H. Ryu, *J. Appl. Phys.* **2010**, *108*.
[165] V. Sanchez-Romaguera, M. B. Madec, S. G. Yeates, *React. Funct. Polym.* **2008**, *68*, 1052.
[166] J. Perelaer, C. E. Hendriks, A. W. M. de Laat, U. S. Schubert, *Nanotechnology* **2009**, *20*.
[167] S. Jeong, H. C. Song, W. W. Lee, S. S. Lee, Y. Choi, W. Son, E. D. Kim, C. H. Paik, S. H. Oh, B. H. Ryu, *Langmuir* **2011**, *27*, 3144.
[168] S. Busato, A. Belloli, P. Ermanni, *Sens Actuators, B* **2007**, *123*, 840.
[169] J. F. Mei, M. R. Lovell, M. H. Mickle, *IEEE Trans. Electron. Packag. Manuf.* **2005**, *28*, 265.
[170] P. J. Smith, D. Y. Shin, J. E. Stringer, B. Derby, N. Reis, *J. Mater. Sci.* **2006**, *41*, 4153.
[171] D. Zabetakis, P. Loschialpo, D. Smith, M. A. Dinderman, W. J. Dressick, *Langmuir* **2009**, *25*, 1785.
[172] G. Deniau, L. Azoulay, L. Bougerolles, S. Palacin, *Chem. Mater.* **2006**, *18*, 5421.
[173] L. Tessier, J. Chancolon, P. J. Alet, A. Trenggono, M. Mayne-L'Hermite, G. Deniau, P. Jegou, S. Palacin, *Phys. Status Solidi A* **2008**, *205*, 1412.
[174] V. Mévellec, S. Roussel, G. Deniau, *Worldwide Patent WO2008078052*, **2006**.
[175] V. Mevellec, S. Roussel, L. Tessier, J. Chancolon, M. Mayne-L'Hermite, G. Deniau, P. Viel, S. Palacin, *Chem. Mater.* **2007**, *19*, 6323.
[176] H. Lee, S. M. Dellatore, W. M. Miller, P. B. Messersmith, *Science* **2007**, *318*, 426.
[177] D. Y. Ryu, K. Shin, E. Drockenmuller, C. J. Hawker, T. P. Russell, *Science* **2005**, *308*, 236.
[178] T. Berthelot, A. Garcia, L. Xuan Tuan, J. El Morsli, P. Je gou, S. Palacin, P. Viel, *Appl. Surf. Sci.* **2011**, 3538.
[179] X. T. Le, P. Jegou, P. Viel, S. Palacin, *Electrochem. Commun.* **2008**, *10*, 699.
[180] P. Viel, X. T. Le, V. Huc, J. Bar, A. Benedetto, A. Le Goff, A. Filoramo, D. Alamarguy, S. Noel, L. Baraton, S. Palacin, *J. Mater. Chem.* **2008**, *18*, 5913.
[181] A. Mesnage, S. Esnouf, P. Jegou, G. Deniau, S. Palacin, *Chem. Mater.* **2010**, *22*, 6229.

[182] H. Zollinger, *Diazo chemistry I: Aromatic and Heteroaromatic coumponds*, VCH: Weinheim, New York **1994**.
[183] J. B. Moffat, *The Chemistry of Diazonium and Diazo Compounds*, John Wiley & Sons, New York **1978**.
[184] K. Forstinger, H. J. Metz, *Diazo Compounds and Diazo Reactions*, Wiley-VCH Weinheim **2000**.
[185] T. Breton, D. Belanger, *Langmuir* **2008**, *24*, 8711.
[186] F. Doctorovich, N. Escola, C. Trapani, D. A. Estrin, M. C. G. Lebrero, A. G. Turjanski, *Organometallics* **2000**, *19*, 3810.
[187] H. Zollinger, *Diazo chemistry II: Aliphatic, Inorganic ans Organometallic Compounds*, VCH: Weinheim, New York **1994**.
[188] E. S. Lewis, M. D. Johnson, *J. Am. Chem. Soc.* **1959**, *81*, 2070.
[189] S. Mahouche-Chergui, S. Gam-Derouich, C. Mangeney, M. M. Chehimi, *Chem. Soc. Rev.* **2011**.
[190] C. Galli, *Chem. Rev.* **1988**, *88*, 765.
[191] K. H. Saunders, *The Aromatic Diazo Compounds and their Technical Applications*, Edward Arnold, London **1949**.
[192] M. R. Heinrich, *Chem. Eur. J.* **2009**, *15*, 821.
[193] B. Andersson, B. Lamm, *Acta Chem. Scand.* **1969**, *23*, 2983.
[194] P. Guiriec, P. Hapiot, J. Moiroux, A. Neudeck, J. Pinson, C. Tavani, *J. Phys. Chem. A* **1999**, *103*, 5490.
[195] P. Doppelt, G. Hallais, J. Pinson, F. Podvorica, S. Verneyre, *Chem. Mater.* **2007**, *19*, 4570.
[196] V. Stockhausen, J. Ghilane, P. Martin, G. Trippe-Allard, H. Randriamahazaka, J. C. Lacroix, *J. Am. Chem. Soc.* **2009**, *131*, 14920.
[197] S. Gam-Derouich, B. Carbonnier, M. Turmine, P. Lang, M. Jouini, D. Ben Hassen-Chehimi, M. M. Chehimi, *Langmuir* **2010**, *26*, 11830.
[198] J. M. Noel, D. Zigah, J. Simonet, P. Hapiot, *Langmuir* **2010**, *26*, 7638.
[199] D. Belanger, J. Pinson, *Chem. Soc. Rev.* **2011**, *40*, 3995.
[200] B. Chen, A. K. Flatt, H. H. Jian, J. L. Hudson, J. M. Tour, *Chem. Mater.* **2005**, *17*, 4832.
[201] W. B. Lin, W. P. Lin, G. K. Wong, T. J. Marks, *J. Am. Chem. Soc.* **1996**, *118*, 8034.
[202] U. Costas-Costas, R. Pazo-Llorente, E. Gonzalez-Romero, C. Bravo-Diaz, *J. Chem. Educ.* **2000**, *77*, 384.
[203] C. G. Swain, J. E. Sheats, K. G. Harbison, *J. Am. Chem. Soc.* **1975**, *97*, 783.
[204] M. Delamar, R. Hitmi, J. Pinson, J. M. Saveant, *J. Am. Chem. Soc.* **1992**, *114*, 5883.
[205] K. C. Brown, M. P. Doyle, *J. Org. Chem.* **1988**, *53*, 3255.
[206] M. P. Doyle, J. K. Guy, K. C. Brown, S. N. Mahapatro, C. M. Vanzyl, J. R. Pladziewicz, *J. Am. Chem. Soc.* **1987**, *109*, 1536.
[207] J. K. Kochi, *J. Am. Chem. Soc.* **1957**, *79*, 2942.
[208] N. Kornblum, A. E. Kelley, G. D. Cooper, *J. Am. Chem. Soc.* **1952**, *74*, 3074.
[209] S. H. Korzeniowski, L. Blum, G. W. Gokel, *J. Org. Chem.* **1977**, *42*, 1469.
[210] W. Ando, *The Chemistry of Diazonium and Diazo Groups Part I*, John Wiley & Sons, New York **1978**.
[211] W. Horspool, F. Lenci, *CRC Handbook of Organic Photochemistry and Photobiology Second Edition*, CRC Press, Boca Raton **2004**.
[212] X. T. Le, P. Viel, P. Jegou, A. Garcia, T. Berthelot, T. H. Bui, S. Palacin, *J. Mater. Chem.* **2010**, *20*, 3750.
[213] T. Berthelot, A. Garcia, X. T. Le, J. El Morsli, P. Jegou, S. Palacin, P. Viel, *Appl. Surf. Sci.* **2011**, *257*, 3538.

[214] N. Kornblum, G. D. Cooper, J. E. Taylor, *J. Am. Chem. Soc.* **1950**, *72*, 3013.
[215] H. Zollinger, *Diazo Chemistry I: Aromatic and Heteroaromatic Compounds*, Wiley-VCH, Weinheim **1994**.
[216] M. Pandurangappa, T. Ramakrishnappa, *J. Solid State Electrochem.* **2008**, *12*, 1411.
[217] M. Pandurangappa, N. S. Lawrence, R. G. Compton, *Analyst* **2002**, *127*, 1568.
[218] A. T. Masheter, G. G. Wildgoose, A. Crossley, J. H. Jones, R. G. Compton, *J. Mater. Chem.* **2007**, *17*, 3008.
[219] G. G. Wildgoose, N. S. Lawrence, H. C. Leventis, L. Jiang, T. G. J. Jones, R. G. Compton, *J. Mater. Chem.* **2005**, *15*, 953.
[220] P. Abiman, G. G. Wildgoose, R. G. Compton, *J. Phys. Org. Chem.* **2008**, *21*, 433.
[221] B. Jousselme, G. Bidan, M. Billon, C. Goyer, Y. Kervella, S. Guillerez, E. Abou Hamad, C. Goze-Bac, J. Y. Mevellec, S. Lefrant, *J. Electroanal. Chem.* **2008**, *621*, 277.
[222] M. Pinault, V. Pichot, H. Khodja, P. Launois, C. Reynaud, M. Mayne-L'Hermite, *Nano Lett.* **2005**, *5*, 2394.
[223] X. T. Le, P. Viel, P. Jegou, A. Sorin, S. Palacin, *Sep. Purif. Technol.* **2009**, *69*, 135.
[224] X. T. Le, P. Viel, A. Sorin, P. Jegou, S. Palacin, *Electrochim. Acta* **2009**, *54*, 6089.
[225] C. I. Courduvelis, *Plating on plastics* Vol. Part B, Plastics Products Design Hand-book, New York **1983**.
[226] C. A. Harper, E. M. Petrie, *Plastics Materials and Processes: A Concise Encyclopedia*, Wiley-Interscience, Berlin **2003**.
[227] D. M. Kulich, *Kirk-Othmer Encyclopedia of Chemical Technology 4th. Ed.*, Vol. 9, John Wiley & Sons, New York **1994**.

All the results and discussions of this work will be now presented and based on five articles which are introduced in this “Quick guide":

III. Ligand Induced Electroless Plating (LIEP) via the Graftfast™ process

1. Introduction to the LIEP process

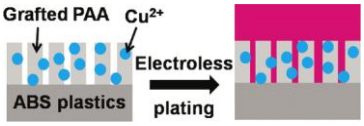

Article 1 ➡ ABS substrate

ACS Appl. Mater. Interfaces **2010**, *2*, 1177

2. Microscopic study of the LIEP process

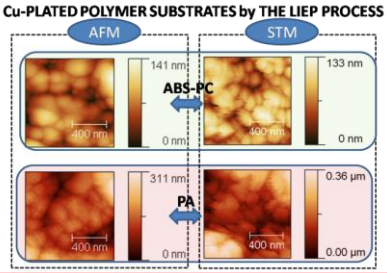

Article 2 ➡ ABS, ABS-PC, PA substrates

ACS Appl. Mater. Interfaces **2010**, *2*, 3043

IV. Localized LIEP process via lithographic based methods

Article 3 ➡ Cu patterns ➡ Flexible and transparent PET & PVDF sheets

Adv. Funct. Mater. **2011**, *21*, 2096

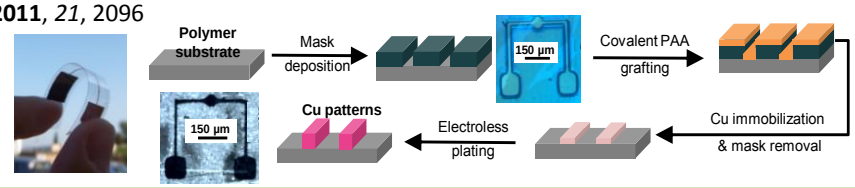

V. Localized LIEP via the Graftfast™ process by projection or transfer

Article 4 ➡ Cu patterns ➡ Flexible PET & PVC substrates + Gold substrates

Adv. Mater., **Submitted (11/07/05)**

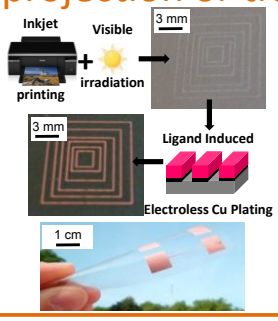

VI. Alternative process: Localized Amino-Induced Electroless Plating

Article 5 ➡ Ni & Cu patterns

ChemPhysChem, **Submitted (11/07/11)**

➡ Flexible and transparent PET sheets

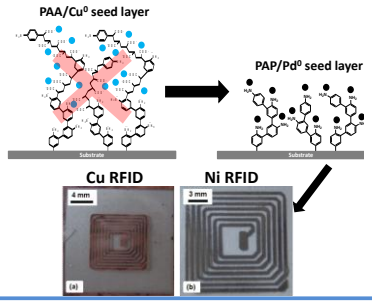

III. Ligand Induced Electroless Plating (LIEP) via the Graftast™ process

The use of polymeric materials combined to electroless metal deposition in the fabrication of microelectronics devices, bioelectronics devices and portable electronics has met a growing interest during the last few decades. For ABS, ABS-PC (Acrylonitrile-Butadiene-Styrene-PolyCarbonate) and PA (PolyAmide) polymers which represent more than 90 % of the polymers industrially metallized, the metal plating with an adherent metallic layer is only possible if an appropriate etchant system is previously employed for surface conditioning. Up to now, the industrial electroless metal plating process is still based on a chromic acid etching, which oxidizes the bulk polymer surface. However, as described in the introduction part of this report, that efficient process has to be replaced because of the future European ban on chromium waste.

In this context, whereas chemical and mechanical adhesion was brought by oxidation and creation of superficial holes or cavities in the case of chromium acid etching, in this work, adhesion is provided through the creation of a polymeric interphase between the metal layer and the polymer substrates covalently to the surface involving a 3D-ligation structure. This technological breakthrough is based on the Graftfast™ process and has its origin in the electro-switchable surfaces for heavy metal waste treatment which were based on the covalent grafting of polyacrylic acid using the Graftfast™process itself, as mentioned in Section II.5.. Indeed, if poly(acrylic acid) (PAA) grafted onto felt carbons is an available solution to capture heavy metal ion, it means that a metal ion can be entrapped into the PAA film and act as the catalyst of the electroless plating growth once reduced. We called our process the Ligand Induced Electroless Plating (LIEP) process and we started by applying this process to the acrylonitrile-butadiene-styrene (ABS) which is among the most widely used polymers in industry [225-227].

This process has been first patented with the following reference:

T. Berthelot, P. Viel, A. Garcia and S. Roussel, Processfor preparing a metallized substrate, said substrate and uses thereof Procédé de préparation d'un substrat métallisé, ledit substrat et ses utilisations, *FR20090052891*, 2009/04/30.

1. Introduction to the LIEP process – ABS electroless plating

A. Garcia, T. Berthelot, P. Viel, A. Mesnage, P. Jegou, F. Nekelson, S. Roussel, S. Palacin, ABS polymer electroless plating through a one-step poly(acrylic acid) covalent grafting, *ACS Appl. Mater. Interfaces* **2010**, *2*, 1177.

This work displays the efficient, palladium and chromium free process, known as "Ligand Induced Electroless Plating" (LIEP), for the electroless plating of acrylonitrile-butadiene-styrene (ABS) which is among the most widely used polymers in industry.

As previously introduced, the process is based on the ion exchange properties of polyacrylic acid (PAA) chemically grafted onto ABS via a simple and one-step method that prevents using classical surface conditioning. Hence, ABS electroless plating can be obtained in three steps, namely: (i) the grafting of PAA onto ABS, (ii) the copper Cu^0 seeding of the ABS surface, and (iii) the nickel or copper metallization using commercial-like electroless plating bath.

ABS Polymer Electroless Plating through a One-Step Poly(acrylic acid) Covalent Grafting

Alexandre Garcia,*,† Thomas Berthelot,† Pascal Viel,† Alice Mesnage,† Pascale Jégou,† Fabien Nekelson,‡ Sébastien Roussel,‡ and Serge Palacin†

CEA, IRAMIS, LSI Irradiated Polymers Grp (UMR 7642 CEA/CNRS/Ecole Polytechnique), F-91128 Palaiseau Cedex and CEA, IRAMIS, SPCSI Chemistry of Surfaces and Interfaces Grp, F-91191, Gif-sur-Yvette, France, and Pegastech, 86 rue de Paris, Bât. Erables, F-91400 Orsay, France

ABSTRACT A new, efficient, palladium- and chromium-free process for the electroless plating of acrylonitrile-butadiene-styrene (ABS) polymers has been developed. The process is based on the ion-exchange properties of poly(acrylic acid) (PAA) chemically grafted onto ABS via a simple and one-step method that prevents using classical surface conditioning. Hence, ABS electroless plating can be obtained in three steps, namely: (i) the grafting of PAA onto ABS, (ii) the copper Cu^0 seeding of the ABS surface, and (iii) the nickel or copper metallization using commercial-like electroless plating bath. IR, XPS, and SEM were used to characterize each step of the process, and the Cu loading was quantified by atomic absorption spectroscopy. This process successfully compares with the commercial one based on chromic acid etching and palladium-based seed layer, because the final metallic layer showed excellent adhesion with the ABS substrate.

KEYWORDS: electroless • poly(acrylic acid) grafting • ABS • copper seed layer • chromium and palladium free

1. INTRODUCTION

Metallization of plastics is widely used today in various technological applications ranging from the fabrication of printed circuits in microelectronics to decorative coatings in general manufacturing. Through metallization, the specific properties of plastics, such as light weight, design flexibility, and low cost of manufacturing, are enriched by the addition of properties usually associated with metals. These include reflectivity, abrasion resistance, electrical conductivity, and a variety of decorative effects. The processes that can be used for metallizing plastics (1, 2) can be either in gaseous phase such as physical (3) and chemical (4) vapor deposition or in solution as in wet-chemical metallization, i.e., plating (5). Plating can be subdivided into electroless plating and electroplating (6, 7).

Electroless metal plating is the most used method. Common process involves three main steps: (i) the surface preparation, (ii) the surface activation or surface seeding with the metal that is the catalyst of the next step, (iii) the electroless plating bath, which consists of a redox reaction between metallic ions (Ni^{2+} or Cu^{2+}) and a strong reducer both contained in the same solution. To activate the metal reduction onto the polymer, noble metal Pd is usually employed as catalyst to initiate the electroless plating (8−10). The development of Pd-free catalysts as a means of the cost and environment footprint of the plating process has been increased. Au or Ag nanoparticles are well-known electroless catalysts and can substitute for Pd in this role (11, 12). However, recently, the use of Cu and Ni species has spurred interest in the development of catalysts derived from less expensive metals (10, 13−19). Nevertheless, whatever the catalyst, the main difficulty of this process consists of chemisorbing the catalyst as metallic particles on the polymer surface. Several routes have been proposed in the literature for this purpose depending on the polymer and the targeted properties (13, 19−24). Indeed, various types of plastics can be plated, including acrylonitrile-butadiene-styrene (ABS) polymers, which are among the most widely used polymers in industry because of their excellent toughness, good dimensional stability, good processability, chemical resistance, and low cost (25−27). Plating ABS with an adherent metal layer is only possible if an appropriate etchant system is previously employed for surface conditioning in order to improve the adhesion and the surface seeding of the electroless catalyst. Up to now, the best method is based on a chromic acid etching, which aims to increase the surface energy and wettability of ABS plastics by oxidizing its surface (28). Moreover, chromic acid dissolves the polybutadiene nodes in ABS, which increases the surface roughness and significantly improves the mechanical adhesion. However, because of the future European ban on chromium wastes, that efficient process needs to be replaced (29, 30). Numerous chromium-free etchings in solution (15, 31) and dried techniques, such as ion-assisted laser treatment (32), plasma modification (33), and excimer UV laser (34) have been developed but they are neither as efficient as chromic acid etching for reaching sufficient adhesion, nor available on the industrial scale. Taking into account that the cost of palladium, as the catalyst of the second step of the process, has increased in recent years, the current electroless plating method is likely to become more and more expensive.

* Corresponding author. E-mail: alexandre.garcia@cea.fr. Phone: 00 33 1 69 08 12 80.

Received for review January 7, 2010 and accepted March 10, 2010

† CEA.

‡ Pegastech.

DOI: 10.1021/am1000163

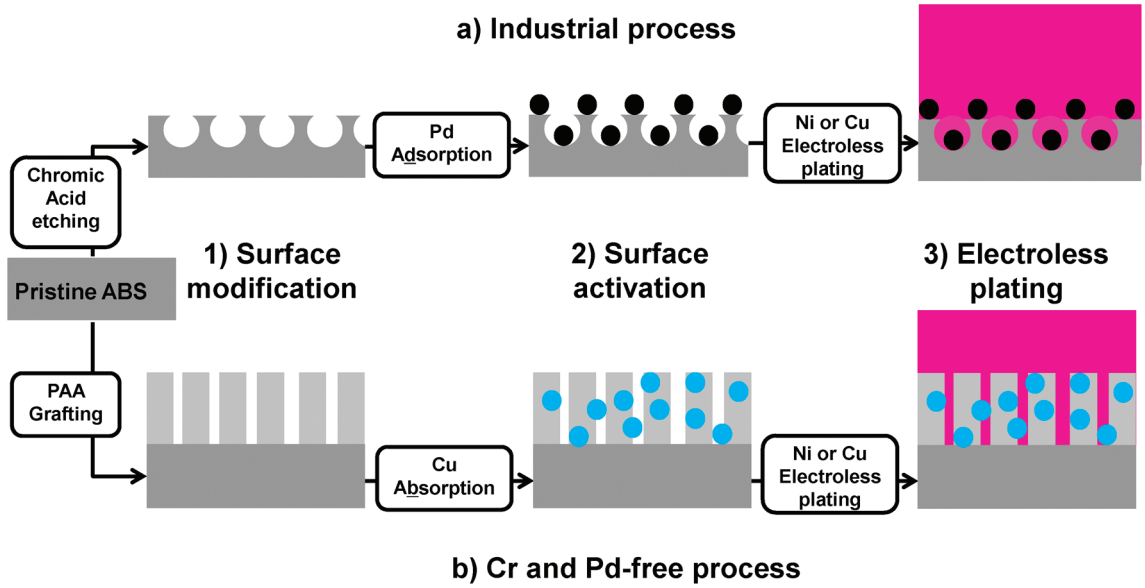

FIGURE 1. Surface preparation of ABS substrates for electroless metallization by (a) the usual industrial process and (b) our Cr- and Pd-free process.

To overcome these limitations, a chromium-free efficient process for electroless metallization on various polymers, also avoiding palladium as catalyst has been developed and is described in this paper. That new process is essentially based on the formation of a robust interphase between the plastics surface and the metal layer, which is intended to replace the rough interface that usually results from the chromic acid treatment. Indeed, that rough interface both promotes the transient deposition of catalytic particles, thanks to polar chemical groups formed upon the plastics oxidation, and increases the final adhesion between the plastics and the final metal layer, thanks to the interdigitation between the two materials. A bonded interphase should exhibit similar properties, thanks to specific affinity for the catalyst, robust anchoring on the plastics surface, and deep interpenetration with the metal layer. We will also evaluate the replacement of the classical palladium-based catalyst by copper nanoparticles formed in situ by reduction of copper(II) ions.

Recent works (10, 35−37) have demonstrated that the grafting of complexing groups on various substrates (gold, silica, polyimide) may allow satisfactory metallization, but these processes are inappropriate for ABS, the most widely electroless plated plastics. In our case, the interphase will be a thin polymer film (poly(acrylic acid), PAA) truly grafted on the ABS surface using a new grafting technology named GraftFast developed in the Laboratory of Chemistry of Surfaces and Interfaces (38, 39). It consists of a short one-step reaction occurring at atmospheric pressure, from aqueous solutions, which leads to stable, homogeneous and covalently coated PAA thin polymer film. Mevellec et al. (40) have thoroughly described the method, which proceeds via a "grafting to" mechanism with most vinylic monomers such as acrylic acid (AA) onto various substrates like metals (Au, Zn, Ti), glasses, carbon, or PTFE. In all cases, the first grafting layer and the initiation of radical polymerization are obtained via the redox activation of various aryl diazonium salts, synthesized in situ from the corresponding aryl amines. Thus, carboxylate groups contained in grafted PAA, at suitable pH, may act as complexing sites to immobilize Cu^{2+} ions. We demonstrate here that, once reduced by a suitable reducing agent, Cu^0 particles formed in situ from PAA-immobilized Cu^{2+} ions can be successfully used as metallization catalyst for the electroless metal deposition on ABS. Moreover, thanks to the metallic cations entanglement into grafted PAA acids chains, mechanical anchoring of the final metallic layer is also obtained by this process.

2. EXPERIMENTAL SECTION

Materials. ABS of technical quality was obtained from Pegastech as common test samples used in the industrial field. 1-4-Diaminophenylene dihydrochloride (Fluka, ≥99%), acrylic acid (Sigma Aldrich, ≥99%), sodium nitrite (Fluka, ≥99%) and iron powder (Prolabo VWR, 98%) were used for the poly(acrylic acid) grafting using the GraftFast technology. Cupric sulfate $CuSO_4 \cdot 5H_2O$ (Fluka, ≥99%), and sodium borohydride powder (Sigma Aldrich, ≥98.5%) were used for the copper chelation and reduction. Then, for the electroless metal deposition, two baths were used: The first one was an industrial nickel plating bath (NipositTM PM 988 supplied by Rohm and Hass) and the second plating bath was a homemade copper plating bath with a copper salt $CuSO_4,5H_2O$ (Fluka, ≥99%), formaldehyde (Sigma Aldrich, 37 wt % solution in water) and disodium tartrate $C_4H_4Na_2O_6 \cdot 2H_2O$ (Merck, ≥ 99.5%). The classical industrial conditioning step was reproduced using chromium(VI) oxide CrO_3 (Sigma Aldrich, ≥98%) for the chromium acid etching, stannous chloride $SnCl_2,2H_2O$ (Sigma Aldrich, ≥99.99%) for the sensitization solution and palladium chloride (Sigma Aldrich, ≥99.9%) for the activation solution. The electroless plating was carried out with the homemade copper plating bath previously described (41). Lastly, PAA spin-coating onto ABS substrates has been carried out using poly(acrylic acid) (Sigma Aldrich, average $M_w \approx 2000$).

Electroless Metal Deposition Process. The electroless plating process described in this work is divided into three main steps as shown in Figure 1.

Surface Modification Step: Covalent Grafting of Poly(acrylic acid) on ABS Surfaces. In a typical experiment, 1-4-

phenylenediammonium dihydrochloride was dissolved in a 0.5 M HCl solution to obtain 100 mL at 0.1 M (solution 1). Under stirring, 15 mL of $NaNO_2$ (0.1 M) was added stepwise to 15 mL of solution 1 in order to synthesize the aryldiazonium salt. Acrylic acid (15 mL) was then introduced into this solution. ABS substrates ($4 \times 1 \times 0.2$ cm^3) were introduced in the beaker, and iron powder (2.25 g) was added to the solution. After immersion for 2 h at 38 °C, ABS substrates were sonicated twice for 10 min in alkaline solution (NaOH, 1 M) and deionized water. The rinsing treatment allowed discarding most of the physisorbed matter.

Surface Activation Step: Chelation and Reduction of Metallic Cations. PAA-modified ABS substrates were immersed during 10 min into an alkaline (NH_3, 0.6 M) copper sulfate $CuSO_4 \cdot 5H_2O$ (0.1 M) solution at room temperature to induce an ion-exchange process. Afterward, samples were rinsed with deionized water. In order to reduce Cu^{2+} ions previously chelated by the carboxylate groups contained in grafted PAA films, modified ABS substrates were immersed into a sodium borohydride ($NaBH_4$)—NaOH (0.1 M) solution at 40 °C for 10 min.

Metallization Step: Electroless Metal Deposition Bath. The surface-activated ABS substrates were finally placed in the electroless metal plating baths. Two plating baths were tested. The first one was a proprietary nickel plating bath (NipositTM PM 988) of complex and unknown composition. Sodium hypophosphite NaH_2PO_2,H_2O was the reducing agent, optimum conditions were obtained with a nickel content of 4 g L^{-1}, a $NaH_2PO_2 \cdot H_2O$/Ni ratio of 3.75, and a pH equal to 9,4 and gave a final Ni coating containing 4—8% of phosphorus. ABS substrates were left in the bath for 10 min at 34 °C.

For the second case, a homemade electroless copper plating bath was used which contained $CuSO_4 \cdot 5H_2O$ as a source of Cu^{2+} ions (10 g L^{-1}), NaOH (12 g L^{-1}), disodium tartrate (18 g L^{-1}) as complexing agent, and formaldehyde (10 mL.L^{-1}) as a reducing agent, with a pH equal to 12.4. ABS substrates were left in the bath for 10 min at 40 °C (41).

"Industrial" Process: Chromic Acid Etching and Palladium Seed Layer Deposition. The industrial process was reproduced by mixing two different published works: First, the chromic acid etching step was based on a classical method described in Mallory's book (7). Second, the sensitization and activation step were based on the process described by Jiang et al. (8). Once activated by the palladium particles, the ABS substrates were plated with copper following the same method than in the case of the Cr- and Pd-free process.

3. CHARACTERIZATION

Spectroscopic Methods. Infrared spectra were recorded on a Bruker Vertex 70 spectrometer equipped with an Attenuated Total Reflection (ATR) Pike-Miracle accessory. The detector was a MCT working at liquid nitrogen temperature. The spectra were obtained after 256 scans at 2 cm^{-1} resolution.

XPS studies were performed with a KRATOS Axis Ultra DLD spectrometer, using the monochromatized Al Kα line at 1486.6 eV. The pass energy of the analyzer was kept constant at 20 eV for C_{1s} core level scans. The photoelectron takeoff angle was 90° with respect to the sample plane, which provides an integrated sampling probe depth of ca. 15 nm.

Atomic absorption spectroscopy was carried out on a Thermo Fisher Scientific Atomic Absorption Spectrometer (ICE 3000 Series) with a hollow cathode lamp for Co—Cu—Mn—Ni at a primary wavelenght of 324.8 nm and a bandpass of 0.5 nm using an air—acetylene flame at a gaz flow rate of 0.9 L/min and a 10 wt % HNO_3/deionized water matrix. The lamp current was 7.5 mA.

The scanning electron microscopy images were recorded by a Hitachi S4800 equipped with a field-emission gun (FEG-SEM) and coupled with an energy dispersive X-ray spectrometer (EDX).

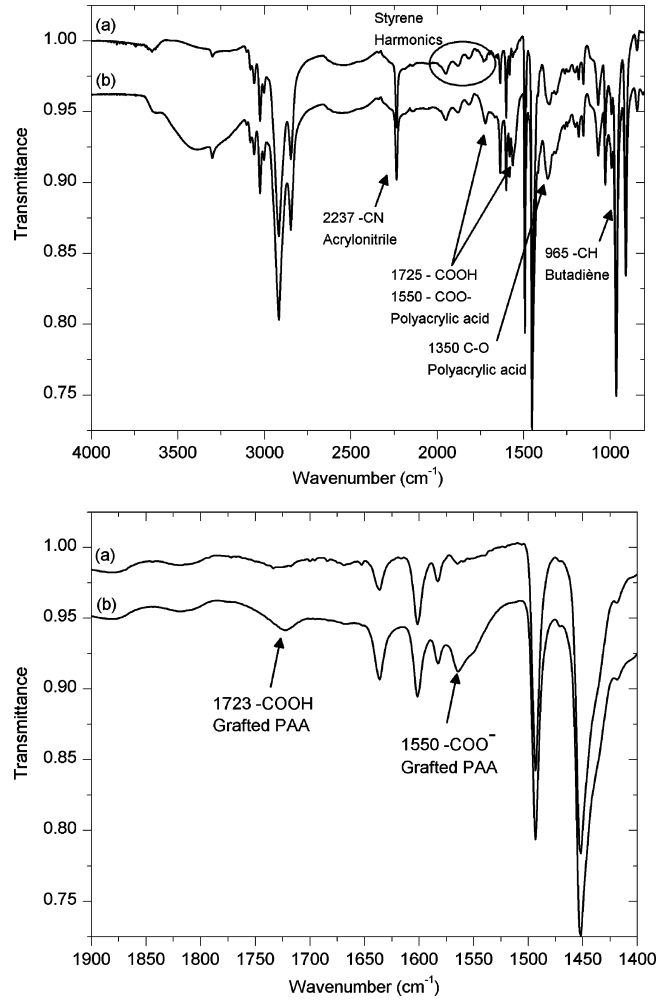

FIGURE 2. IR-ATR spectra of ABS substrate (a) before and (b) after PAA grafting with a close-up of the carboxylic acid characteristic bands (bottom).

Four-point probe (S302K-LRM, Lucas Lab) was used to measure the resistivity of the electrolessly deposited copper layers.

Mechanical Adhesion Test. The mechanical adhesion between the metallic layer and the ABS substrates was studied by a qualitative Scotch tape test inspired by the standard ASTM D3359 Scotch tape test (cross-cut tape test). It consists of sticking a high-performance transparent scotch-tape (Progress) onto the squared metallized ABS and then to remove it suddenly. Although qualitative, that well-used test allows for direct comparison of the adhesion of films obtained under various conditions on similar substrates.

4. RESULTS AND DISCUSSIONS

Covalent Grafting of Poly(acrylic acid) on ABS Surfaces. Poly(acrylic acid) has been grafted onto ABS substrates via the GraftFast technology, which is a concerted aryldiazonium reduction and AA polymerization (see the Supporting Information for details). Mevellec et al. (40) already pointed out the covalent grafting of PAA on various surfaces such as metals, glass, carbon nanotubes or PTFE by means of X-ray photoelectron and infrared spectroscopies. Here, we demonstrate that the process is also efficient on ABS.

First of all, in Figure 2, pristine ABS substrate was analyzed by ATR-FTIR and showed intense and characteristic absorption

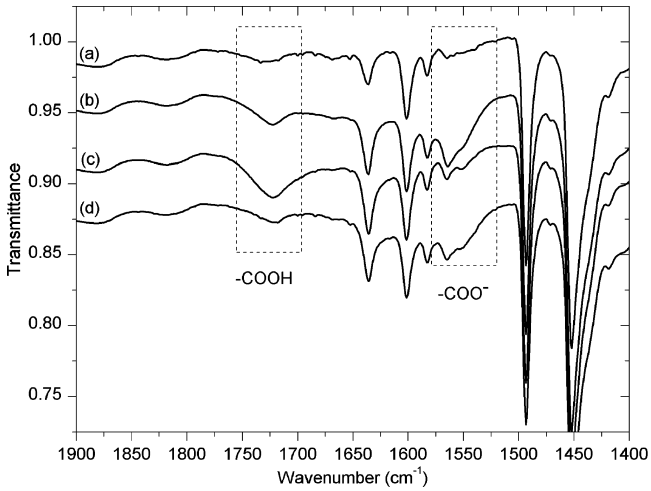

FIGURE 3. IR-ATR spectra of (a) pristine ABS, (b) after PAA grafting followed by rinsing with an alkaline solution (pH 13), (c) rinsing with an acidic solution (pH 1), and (d) after Cu^{2+} chelation.

bands at 2237, 1452, 1354, 1070, and 1028 cm^{-1} due to the acrylonitrile component of the copolymer, at 2920, 1637, 1450, 965, and 910 cm^{-1} due to the butadiene component, and at 2924, 2850, 1602, 1494, 1450, 910 cm^{-1} and all benzene harmonic absorption bands (2000−1600 cm^{-1}) due to the styrene component (42).

For PAA-grafted ABS, carboxylic group absorptions bands clearly appear either at 1723 cm^{-1} for the carboxylic acid form and/or at 1550 cm^{-1} for the carboxylate salts stretching vibrations and at 1350 cm^{-1} for the C−O stretching vibration (42). Because of the final rinsing step in deionized water (pH close to 5), the IR absorption spectra of PAA-grafted ABS generally exhibit both COOH and COO^- signals, indicating a mixed composition. Of course, the IR spectrum is dominated by the ABS absorption bands between 1500 and 1300 cm^{-1}. Figure 3 demonstrates that grafted carboxylic groups are accessible to external reagents; Indeed, immersing the PAA-grafted ABS sample successively in an alkaline and an acidic solution was followed by the expected increasing and decreasing of the carboxylate (COO^- at 1550 cm^{-1}) and carboxylic (COOH at 1725 cm^{-1}) bands, respectively.

To confirm the presence of the grafted PAA films, we studied the surfaces by XPS. Figure 4 displays XPS spectra on pristine ABS and PAA-grafted ABS surfaces. For pristine ABS, the C_{1s} core level showed one main peak centered at 285 eV, which mainly corresponds to CH and CH_2 aliphatic carbons contained in the polyacrylonitrile, polybutadiene, and polystyrene structure, and one peak at 286.8 eV, which corresponds to the CN nitrile group contained in the polyacrylonitrile component. Lastly, the polystyrene shakeup was observed around 292 eV (43). In the PAA-grafted case, in addition to the previous described peaks, a peak at 289 eV characteristic of a COOH carboxylic group was clearly observed. Moreover, according to the XPS analysis (Table 1), the CH/CN ratio increased after PAA grafting due to the contribution of CH bonds contained in the PAA film. In parallel, the O/C ratio increased 10 times and the N/C ratio decreased (5 times) after surface modification, which confirms the grafting of an oxygen-rich species. Because of the

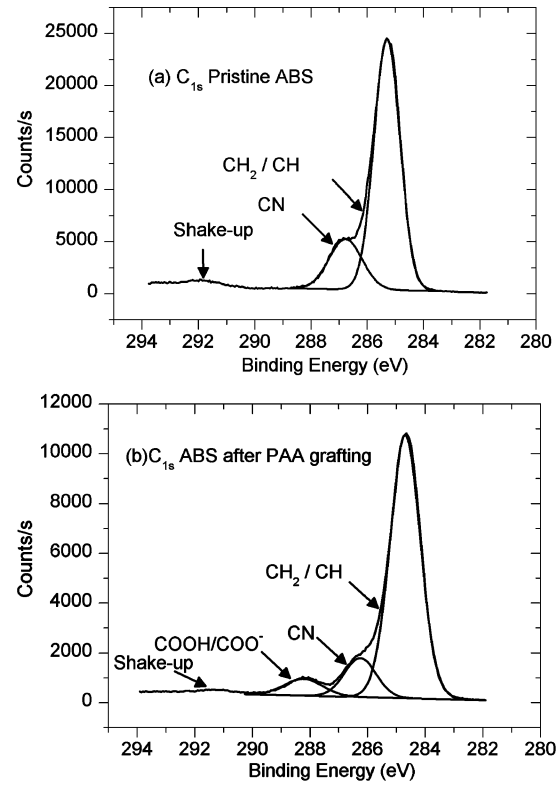

FIGURE 4. C_{1s} XPS Spectra of (a) pristine ABS and (b) PAA-grafted ABS.

Table 1. C_{1s} Normalized Atomic Ratio after PAA Grafting and Copper Complexation

	pristine ABS	ABS after PAA grafting	ABS after Cu^{2+} complexation
C1s	1.00	1.00	1.00
O1s	0.03	0.29	0.17
N1s	0.1	0.02	0.02

XPS photoelectronic mean free path ($\lambda \approx 5$ nm) for carbon, the related experimentally probed depth (a few λ), and the fact that ABS components are always observed in our spectra, we estimated that the grafted PAA film thickness was less than 15 nm.

Chelation and Reduction of Metallic Cations. When immersed in an alkaline solution containing ammonia (0.6 M) and $CuSO_4,5H_2O$ (0.1 M solution), PAA undergoes an ion exchange reaction. According to Mastumura et al. (19), the amount of loaded Cu^{2+} was found to depend on the pH solution used for ion exchange. In the absence of NH_3, the equilibrium exchange reaction was achieved after a few hours, whereas at basic pH, it was obtained after a few seconds. This was checked by flame atomic absorption spectroscopy. Indeed, after an immersion time of 30 s in the alkaline solution, the ion exchange equilibrium seemed to be achieved with an amount of Cu^{2+} around $\Gamma = 1.0\ \mu g\ cm^{-2}$, whereas after 10 min in the deionized water solution, the equilibrium was not achieved and the amount of Cu^{2+} was 10 times lower. As expected from the pH-switchable chelating properties of PAA, in both chelating media the copper ions were totally released from the polymer film by immersing the substrates in an acidic solution (pH 1) for 10

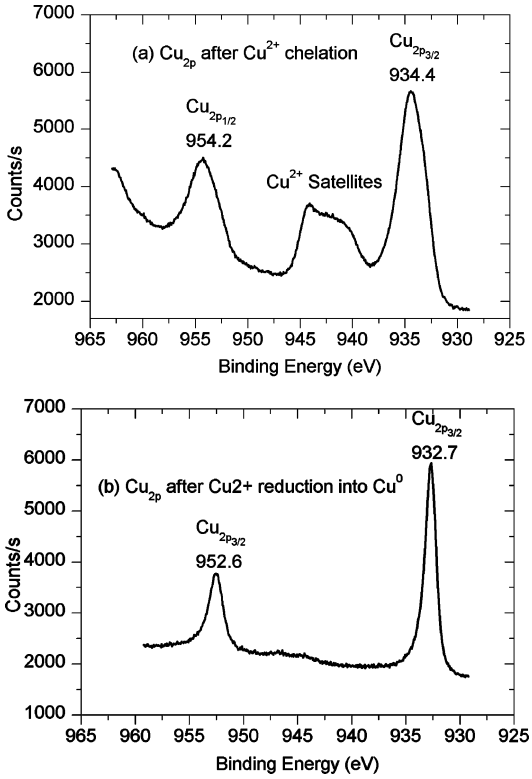

FIGURE 5. Cu_{2p} XPS spectra (a) after Cu^{2+} chelation and (b) after Cu^{2+} reduction.

min. Following the same process, various copper ions loading/unloading cycles were performed and the same amount of Cu^{2+} was obtained after each loading step, which demonstrates the full reversibility of the chelation.

The Cu^{2+} loading and the deprotonation of carboxylic acid of PAA-grafted ABS were also confirmed by infrared and XPS spectroscopies. As shown in Figure 3d, the carboxylic acid bands almost disappeared after the ion exchange, suggesting the formation of PAA−copper salts (42).

As shown in Figure 5, the Cu_{2p} spectra analysis confirmed the Cu^{2+} chelation by three peaks, respectively corresponding to $Cu_{2p3/2}$ (934.4 eV), Cu_{2p} satellites (from 938 to 945 eV), and $Cu_{2p1/2}$ (954.3 eV) core level binding energies. Besides, XPS analysis revealed a Cu/C ratio close to 2% (see the Supporting Information for details). Given that one metallic copper cation should normally be chelated by two carboxylate groups COO^- and according to the Cu_{2p}/COOH C_{1s} atomic ratio, 80% of the carboxylic groups were chelated by copper ions, which means that the PAA ion exchange properties are very efficient for copper seeding.

Reduction of Immobilized Metallic Cations. The reduction of Cu^{2+} ions immobilized by complexation in PAA-grafted ABS was then obtained by immersion of the Cu−PAA film in an alkaline solution of sodium borohydrure $NaBH_4$ and confirmed by XPS measurements with the study of the chemical state of copper. As shown in Figure 5, after immersion in $NaBH_4$, the peak of $Cu_{2p3/2}$ core level binding energy shifts partially toward lower energy and the characteristic Cu_{2p} satellites disappeared. Otherwise, the Cu/C ratio measured from XPS spectra remained constant (2%) after that reduction: all the formerly complexed copper ions were reduced within the film, without any release to the external solution.

Electroless Metal Deposition Bath. In both nickel and copper plating baths, the mechanism of the metallic ion reduction is complex and not totally understood yet (7, 44−48). However, it was shown that in the case of the nickel plating bath (Niposit TM PM 988), the Ni^{2+} reduction with hypophosphite induces some phosphorus incorporation in the metallic layer, whereas in the copper plating bath the metallic layer contains only copper.

It is noteworthy that the industrial Ni plating bath contains a stabilizer which prevents spontaneous reduction in solution (7), but may delay or even hinder the initiation of the autocatalytic reaction through a kind of poisoning of the Cu catalytic sites, hence resulting in an increase in the activation energy of the reaction (7). Thus, in the case of our copper homemade plating bath, no stabilizer was used.

Taking into account all the parameters, immersing the ABS substrate in the plating bath during 10 min allowed the formation of micrometer-thick films depending strongly on the kind of baths and the bath conditions.

The obtained metallic layers were characterized by XPS measurements and confirmed that Ni^0 and Cu^0 were successfully formed on the ABS substrates (see the Supporting Information for details).

Otherwise, based on the four-point probe method, the electrical resistivity of the as-plated copper was 3.2 $\mu\Omega$ cm, which is slightly higher than bulk copper, which is 1.67 $\mu\Omega$ cm (49). The presence of defects, hydrogen entrapment in the films, and film discontinuities are the major factors contributing to the observed increase in the resistivity of the plated films compared to that of bulk copper (50).

The metallized substrates were also observed by scanning electron microscopy and characterized by EDX measurements. As shown in Figure 6, in both cases, the metallic layer consists of 100 to 200 nm sized nanoparticles and the surface was not totally homogeneous at the microscopic scale; the metallic layer seems, however, to be more compact in the case of the copper plating bath. The electroless plating bath and more specifically the metallic growth are extremely difficult to control at the laboratory scale. Indeed, these electroless plating bath are developed for industrial production line and all the fluid mechanics involved in it. Nevertheless, the ABS section after Cu metallization showed a global homogeneous and planarized metallic top-layer and a good interfacial zone between the metal and the ABS. The metallic layer thickness is around 5−10 μm after 10 min. EDX spectra analysis revealed the presence of Cu^0 and Ni^0 and in the case of nickel deposition, phosphorus was also present and indicated a final composition of 92.5% nickel and 7.5% phosphorus ignoring carbon and oxygen residuals. EDX spectra are available on the Supporting Information.

Finally, preliminary adhesion tape tests gave very promising results: for both copper and nickel metallization, the metallic layer was fully undamaged after the tape test, as for the classical chromic acid-palladium seeding process. On

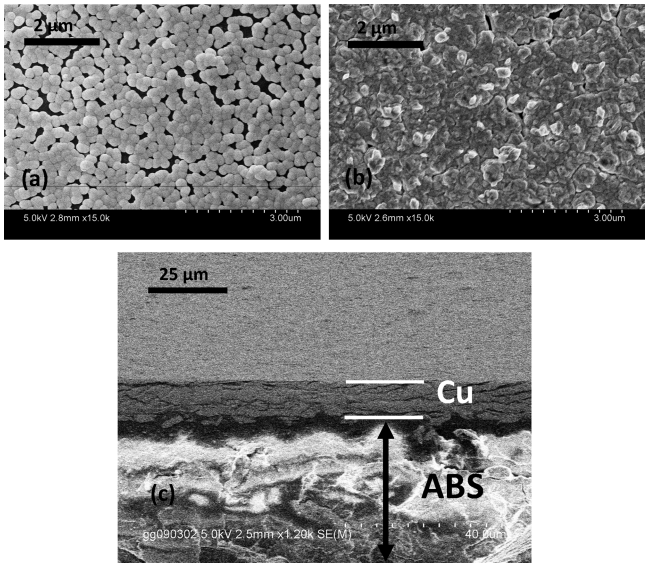

FIGURE 6. SEM images after electroless metal deposition: (a) nickel and (b) copper plating with a 2 μm scaled top view, and (c) copper plating with the 25 μm scaled ABS section with a tilt angle of 75°.

the contrary, when ABS was Cu-metallized either without any PAA grafting or after spin-coating PAA from a 0.5% w/w solution (51), the metallic layer was fully removed. That good adhesion may be attributed to the location of copper catalyst particles, which were formed in situ from complexed copper ions within the grafted PAA layer. Hence, the copper particles were buried within the PAA layer and obviously promote adhesion between the ABS substrate and the metal thin films through a nanometer-scale mechanical interlocking effect, which mimics the micrometer-scale interdigitation that occurs between the metal layer and the rough interface which results from the chromic acid treatment. Direct comparison between our process and the classical chromium-based method are currently under way in order to quantify the good mechanical adhesion reported above. Up to now, we can assume that our chromium-free process provides a promising alternative to usual chromium-based etching preparation step for the ABS electroless plating.

5. CONCLUSIONS

We have described a new and powerful method to metallize ABS plastics without the use of chromium (as etching agent) and palladium (as catalyst of the metallic layer growth). The pollutant etching step has been replaced by PAA chemical grafting using the GraftFast technology, which provides ecological benefits. Moreover, this process divided into 3 steps is cost-effective and showed a good adhesion between the final metallic layer and the ABS substrates. Further work aims at applying this process to other polymer substrates with different shapes and with quantitative adhesion tests between the metallic layer and the ABS substrates. Lastly, adaptation of this method to produce selective electroless metallization is currently under investigation.

Supporting Information Available: Chemical scheme showing mechanism of grafting; atomic absorption, XPS, and EDX data (PDF). This material is available free of charge via the Internet at http://pubs.acs.org.

REFERENCES AND NOTES

(1) Charbonnier, M.; Alami, M.; Romand, M. *J. Electrochem. Soc.* **1996**, *143*, 472–480.
(2) Sacher, E. *Metallization of Polymers 2*; Springer: New York, 2002.
(3) De Bruyn, K.; Van Stappen, M.; De Deurwaerder, H.; Rouxhet, L.; Celis, J. P. *Surf. Coat. Technol.* **2003**, *163*, 710–715.
(4) Long, D. P.; Blackburn, J. M.; Watkins, J. J. *Adv. Mater.* **2000**, *12*, 913–915.
(5) Vaskelis, A.; Norkus, H. J.; Rozovskis, G.; Vinkevicius, H. J. *Trans. Inst. Met. Finish.* **1997**, *75*, 1–3.
(6) Krulik, G. A.; Lauterer, K. R. *Modern Plastics Encyclopedia*; McGraw-Hill: New York, 1977.
(7) Mallory, G. O.; Hajdu, J. B. *ELECTROLESS PLATING: Fundamentals and Applications*; The American Electroplaters and Surface Finishers Society: Washington, D.C., 1990.
(8) Jiang, B. Q.; Xiao, L.; Hu, S. F.; Peng, J.; Zhang, H.; Wang, M. W. *Opt. Mater.* **2009**, *31*, 1532–1539.
(9) Nicolas-Debarnot, D.; Pascu, M.; Vasile, C.; Poncin-Epaillard, F. *Surf. Coating Tech.* **2006**, *200*, 4257–4265.
(10) Zabetakis, D.; Dressick, W. J. *ACS Appl. Mater. Interfaces* **2009**, *1*, 4–25.
(11) Dai, W.; Wang, W. J. *Sens. Actuators, A* **2007**, *135*, 300–307.
(12) Miyoshi, K.; Aoki, Y.; Kunitake, T.; Fujikawa, S. *Langmuir* **2008**, *24*, 4205–4208.
(13) Charbonnier, M.; Romand, A.; Goepfert, Y.; Leonard, D.; Bessueille, F.; Bouadi, A. *Thin Solid Films* **2006**, *515*, 1623–1633.
(14) Charbonnier, M.; Romand, M.; Goepfert, Y. *Surf. Coat. Technol.* **2006**, *200*, 5028–5036.
(15) Teixeira, L. A. C.; Santini, M. C. *J. Mater. Process. Technol.* **2005**, *170*, 37–41.
(16) Zhu, P. X.; Masuda, Y.; Koumoto, K. *J. Mater. Chem.* **2004**, *14*, 976–981.
(17) Hsiao, Y. S.; Whang, W. T.; Wu, S. C.; Chuang, K. R. *Thin Solid Films* **2008**, *516*, 4258–4266.
(18) Bicak, N.; Karagoz, B. *Surf. Coat. Technol.* **2008**, *202*, 1581–1587.
(19) Matsumura, Y.; Enomoto, Y.; Sugiyama, M.; Akamatsu, K.; Nawafune, H. *J. Mater. Chem.* **2008**, *18*, 5078–5082.
(20) Charbonnier, M.; Romand, M.; Goepfert, Y.; Leonard, D.; Bouadi, M. *Surf. Coating Technol.* **2006**, *200*, 5478–5486.
(21) Girginer, B.; Karagoz, B.; Urgen, M.; Bicak, N. *Surf. Coating Technol.* **2008**, *202*, 4176–4182.
(22) Rohan, J. R.; O'Riordan, G.; Boardman, J. *Appl. Surf. Sci.* **2002**, *185*, 289–297.
(23) Shibata, M.; Uda, T.; Yosomiya, T. *Thin Solid Films* **2003**, *440*, 123–128.
(24) Tang, X. J.; Bi, C. L.; Han, C. X.; Zhang, B. G. *Mater. Lett.* **2009**, *63*, 840–842.
(25) Courduvelis, C. I. *Plastics Products Design Handbook*; Marcel Dekker: New York, 1983; Vol. Part B.
(26) Harper, C. A.; Petrie, E. M. *Plastics Materials and Processes: A Concise Encyclopedia*; Wiley: Berlin, 2003.
(27) Kulich, D. M. *Kirk-Othmer Encyclopedia of Chemical Technology*, 4th ed.; Wiley: New York, 1993; Vol. 9.
(28) Wang, G. X.; Li, N.; Hu, H. L.; Yu, Y. C. *Appl. Surf. Sci.* **2006**, *253*, 480–484.
(29) EUROPEAN PARLIAMENT AND THE COUNCIL, 2002/95/EC, 2003.
(30) EUROPEAN PARLIAMENT AND THE COUNCIL, 2005/90/EC, 2006.
(31) Patel, G. N.; Bolikal, D.; Petel, H. U.S. Patent 5 160 600, 1992.
(32) Kupfer, H.; Hecht, G.; Ostwald, R. *Surf. Coat. Technol.* **1999**, *112*, 379–383.
(33) Charbonnier, M.; Romand, M. *Int. J. Adhes. Adhes.* **2003**, *23*, 277–285.
(34) Esrom, H.; Seebock, R.; Charbonnier, M.; Romand, M. *Surf. Coat. Technol.* **2000**, *125*, 19–24.
(35) Li, L.; Yan, G. P.; Wu, J. Y.; Yu, X. H.; Guo, Q. Z.; Kang, E. T. *Appl. Surf. Sci.* **2008**, *254*, 7331–7335.
(36) Liaw, W. C.; Huang, P. C.; Chen, K. P.; Chen, C. S. *Polym. J.* **2009**, *41*, 634–642.
(37) Aldakov, D.; Bonnassieux, Y.; Geffroy, B.; Palacin, S. *ACS Appl. Mater. Interfaces* **2009**, *1*, 584–589.

(38) Mévellec, V.; Roussel, S.; Tessier, L.; Chancolon, J.; Mayne-L'Hermite, M.; Deniau, G.; Viel, P.; Palacin, S. *Chem. Mater.* **2007**, *19*, 6323–6330.
(39) Mévellec, V.; Roussel, S.; Deniau, G. FR Patent 2 910 006, 2007.
(40) Mevellec, V.; Roussel, S.; Tessier, L.; Chancolon, J.; Mayne-L'Hermite, M.; Deniau, G.; Viel, P.; Palacin, S. *Chem. Mater.* **2007**, *19*, 6323–6330.
(41) Bercu, B.; Enculescu, I.; Spohr, R. *Nucl. Instrum. Methods Phys. Res., Sect. B* **2004**, *225*, 497–502.
(42) Socrates, G. *Infrared Characteristics Group Frequencies*; Wiley-Interscience: Chichester, U.K., 1994.
(43) Beamson, G.; Briggs, D. *High-Resolution XPS of Organic Polymers: The Scienta ESCA300* John Wiley & Sons: New York, 1992.
(44) Abrantes, L. M.; Correia, J. P. *J. Electrochem. Soc.* **1994**, *141*, 2356–2360.
(45) Ma, C. L.; Ye, W. C.; Shi, X. Z.; Chang, Y. L.; Chen, Y.; Wang, C. M. *Appl. Surf. Sci.* **2009**, *255*, 3713–3718.
(46) Wang, K.; Hong, L.; Liu, Z. L. *Ind. Eng. Chem. Res.* **2008**, *47*, 6517–6524.
(47) Wu, Z. J.; Ge, S. H.; Zhang, M. H.; Li, W.; Tao, K. Y. *J. Colloid Interface Sci.* **2009**, *330*, 359–366.
(48) Yin, X.; Hong, L.; Chen, B. H. *J. Phys. Chem. B* **2004**, *108*, 10919–10929.
(49) Weast, R. C. *CRC Handbook of Chemistry and Physics*; CRC Press: Boca Raton, FL, 1984.
(50) Aithal, R. K.; Yenamandra, S.; Gunasekaran, R. A.; Coane, P.; Varahramyan, K. *Mater. Chem. Phys.* **2006**, *98*, 95–102.
(51) Jackson, R. L., European Patent 0 250 867, 1988.

AM1000163

Supporting information

ABS polymer electroless plating through a one-step poly(acrylic acid) covalent grafting

Alexandre Garcia, Thomas Berthelot, Pascal Viel, Pascale Jégou, Fabien Nekelson, Sébastien Roussel and Serge Palacin

CEA, IRAMIS, LSI Irradiated Polymers Grp (UMR 7642 CEA/CNRS/Ecole Polytechnique), F-91128 Palaiseau Cedex and CEA, IRAMIS, SPCSI Chemistry of Surfaces and Interfaces Grp, F-91191, Gif-sur-Yvette, France

EMAIL ADDRESS: alexandre.garcia@cea.fr

- **PAA grafting mechanism according to the work published by Mévellec and al. (40)**

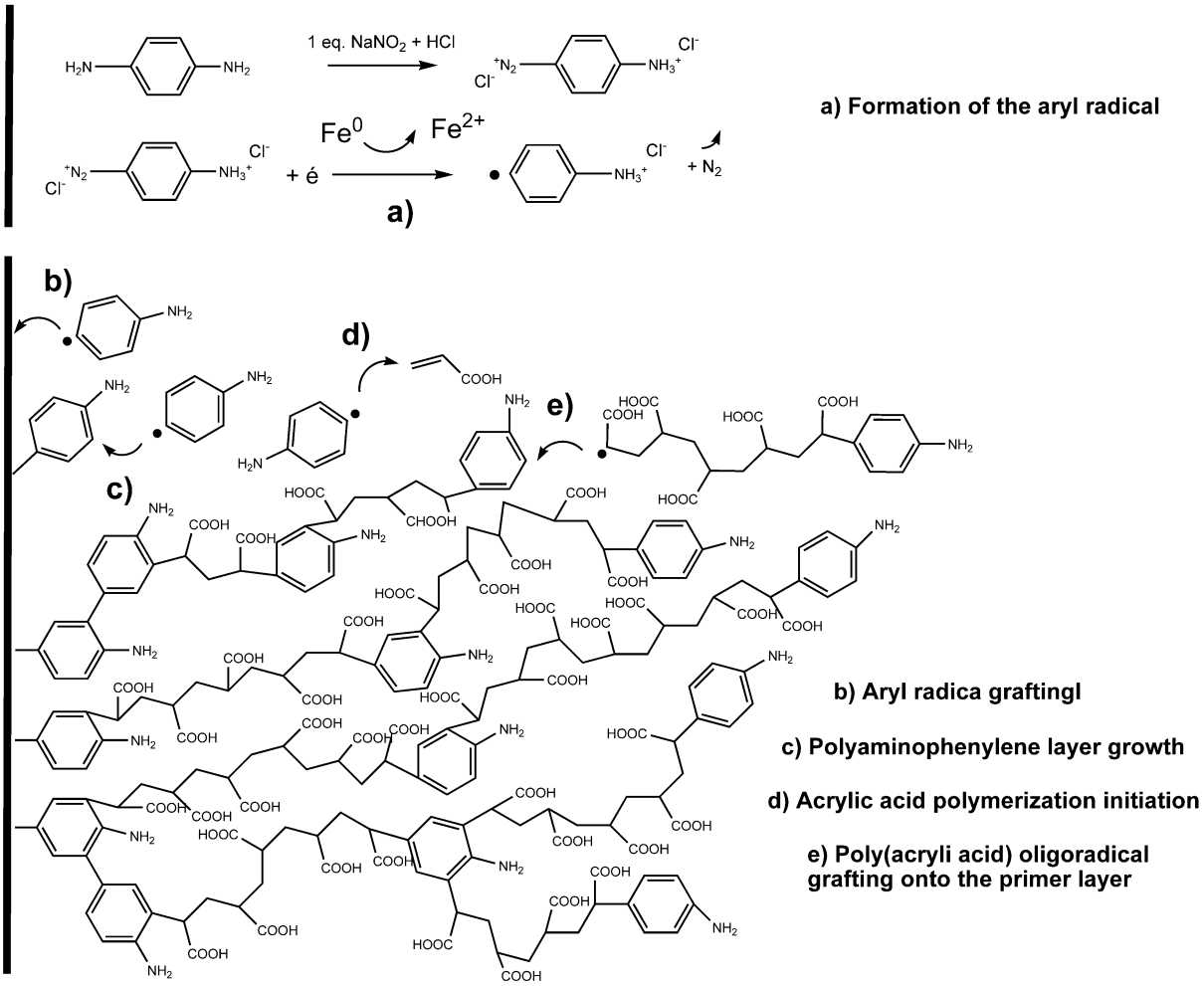

Figure S1: The GraftFast® mechanism: chemical route to produce grafted polyacrylic acid films: a) Formation of the aryl radical (b) Grafting of the resulting aryl radicals onto the surface and c) growth of the Polyaminophenylene multilayer, (d) Acrylic acid polymerization initiatied by the aryl radicals, (e) Polyacrylic acid oligoradicals grafting on the primer layer.

- **Surface coverage measured by atomic absorption spectroscopy after copper complexation**

When immersed in an alkaline solution containing ammonia (0.6 M) and $CuSO_4,5H_2O$ (0.1 M solution), PAA undergoes an ion exchange reaction. According to Mastumura et al(19), the amount of loaded Cu^{2+} was found to depend on the pH solution used for ion exchange. In the absence of NH_3, the equilibrium exchange reaction was achieved after a few hours while at basic pH, it was obtained after a few seconds. This was checked by flame atomic absorption spectroscopy. Indeed, after an immersion time of 30s in the alkaline solution, the ion exchange equilibrium seemed to be achieved with an amount of Cu^{2+} around Γ = 1.0 µg.cm^{-2} while after ten minutes in the deionised water solution, the equilibrium was not achieved and the amount of Cu^{2+} was 10 times lower.

Table S1: Cu^{2+} surface coverage at different pH and time immersion in $CuSO_4$, $5H_2O$ (0.1M)

	Γ(µg/cm^2)	**Γ(µg/cm^2)+ NH_3 (0.6 M)**
After 30s	0.05	1.00
After10 min	0.10	1.00

- **Cu2p and Ni2p XPS Analysis after each step of the plating process**

Table S2: C_{1s} normalized atomic ratio after each step of the nickel and copper plating processes

	ABS after Cu^{2+} complexation	ABS after Cu^{2+} reduction	ABS after plating	
			Ni	Cu
Cu_{2p}	2%	2%	0%	27%
Ni_{2p}	/	/	17%	/

- **XPS Analysis after plating bath**

The obtained metallic layers were characterized by XPS measurements. As shown in the Figure 2, the Ni_{2p} and the Cu_{2p} spectra, respectively corresponding to the nickel and the copper plating bath indicate that Ni^0 and Cu^0 were successfully formed on the ABS substrates. In addition, in both nickel and copper cases, oxygen and carbon elements are still present due to organic residuals coming from the plating bath and in particular from the complexing agent.

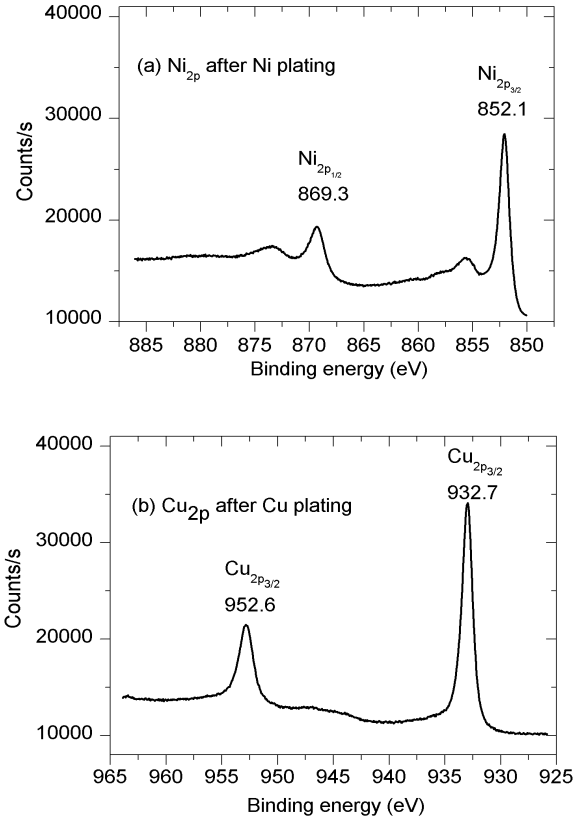

Figure S2: XPS Spectra after metallization: Ni2p (b) spectra after Ni metallization and Cu2p (d) spectra after Cu metallization

- **EDX analysis after plating bath**

EDX spectra analysis revealed the presence of Cu^0 and Ni^0 and in the case of nickel deposition, phosphorous was also present and indicated a final composition of 92.5 % nickel and 7.5% phosphorous ignoring carbon and oxygen residuals. EDX spectra are available on the supporting information.

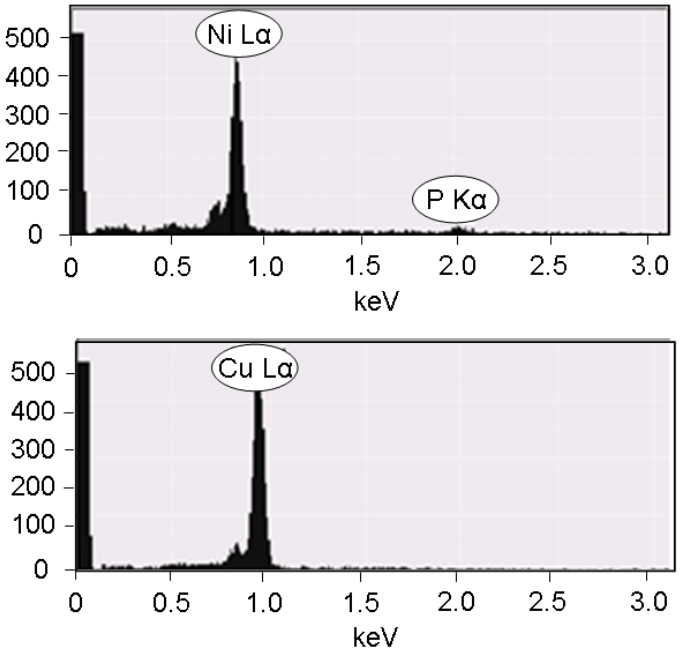

Figure S3: EDX spectra of nickel metallization on the top and copper metallization on the bottom

2. Microscopic study of the LIEP process through its application onto various substrates

A. Garcia, T. Berthelot, P. Viel, J. Polesel-Maris, S. Palacin, Microscopic study of a Ligand Induced Electroless Plating process onto polymers, *ACS Appl. Mater. Interfaces* **2010**, *2*, 3043.

Through the first article, the Ligand Induced Electroless Plating (LIEP) process was thoroughly demonstrated with one of the most used polymers for plating processes: ABS. Essentially based on ABS, ABS-PC (ABS-Polycarbonate) and PA (Polyamide) substrates, the present paper focuses on the role of the polymer substrate and the relationships between the macroscopic properties and microscopic characterizations such as IR, XPS, AFM and SEM.

Microscopic Study of a Ligand Induced Electroless Plating Process onto Polymers

Alexandre Garcia,*,†,‡ Thomas Berthelot,† Pascal Viel,‡ Jérôme Polesel-Maris,§ and Serge Palacin‡

LSI Irradiated Polymers Group (UMR 7642 CEA/CNRS/Ecole Polytechnique), CEA, IRAMIS, F-91128 Palaiseau Cedex, France, and SPCSI Chemistry of Surfaces and Interfaces Group and SPCSI Oxides Interfaces and Surfaces Group, CEA, IRAMIS, F-91191 Gif-sur-Yvette, France

ABSTRACT The ligand induced electroless plating (LIEP) process was recently developed and thoroughly demonstrated with one of the most used polymers for plating processes: acrylonitrile-butadiene-styrene (ABS). This generic process is based, thanks to the use of diazonium salts as precursors, on the covalent grafting of a thin layer of poly(acrylic acid) (PAA) acting as ligand for metallic salts onto pristine polymer surfaces. This strategy takes advantage of the PAA ion exchange properties. Indeed, carboxylate groups contained in PAA allow one to complex copper ions which are eventually reduced and used as catalysts of the metallic deposition. Essentially based on ABS, ABS-PC (ABS-polycarbonate) and PA (polyamide) substrates, the present paper focuses on the role of the polymer substrate and the relationships between the macroscopic properties and microscopic characterizations such as infrared (IR), X-ray photoelectron spectroscopy (XPS), atomic force microscopy (AFM), and scanning electron microscopy (SEM). The adhesion strength of the metallic layer deposited via that LIEP process with the bulk polymer substrates was successfully compared with the adhesion of similar copper films deposited by the usual process based on chromic acid etching and palladium-based seed layer, by measuring the T-peel adhesion strength, and by carrying out the common industrial scotch tape test. Lastly, the electrical properties of the deposited layer were studied thanks to a four-point probe and scanning tunneling microscopy (STM) measurements.

KEYWORDS: polymer electroless plating • metallization • electrical properties • adhesion • ABS • ABS-PC • polyamide and diazonium salts

1. INTRODUCTION

As materials interact with their environment via their surface, coating a metallic layer onto a polymer is a clever way to keep many properties brought by metals (conductivity, reflectivity, robustness versus mechanical stress) while reducing both the weight of the final objects and the costs associated with their manufacturing (transformation steps, polishing, transport). Electroless metal plating is the most used method to metallize insulating surfaces and more specifically polymers for the deposition of conformal metal films onto all-shaped substrates (1−5). Hence, nickel and electroless plating of polymers is of major importance in many fields including automotive, aerospace, microelectronics, decoration, and luxury packaging industries.

Common electroless processes involve three main steps: (i) surface preparation, (ii) surface activation or surface seeding with a catalyst, and (iii) the electroless deposition itself, which is the chemical deposition of a metal film from a solution containing a mild reducing agent and an ionic complex of the metal to be plated onto the seeded substrate (1, 2). Almost all the metals of the Group IB and VIII of the periodic table (Au, Pt, Ni, Cu, Co, Fe, etc.) can be plated and exhibit autocatalytic behavior. Hence, the electroless metal deposition is not stopped once the catalyst is covered by the first metal deposit (1, 2). Electroless deposition is actually a complex process involving multiple and simultaneous redox processes on the substrate surface in which composition, structure, and morphology are increasingly changing because of the plating. Besides, mechanistic details of metal deposition remain still unclear. The mixed potential theory (6) is perhaps the most used and experiment-based model for electroless metal deposition and consists of an initial spontaneous oxidation of the reducing agent at a catalytic surface, leading to electron charging of the substrate surface until its electrochemical potential becomes sufficiently negative to reduce the metallic complex to metal. The mixed potential theory provides a correct description of the electroless plating mechanism when electron transfer between the reducing agent and the metallic ion is mediated by the activated surface and can be described by diffusion controlled or electrochemically controlled partial reaction currents (6, 7). However, the mixed potential theory is not valid when an electron transfer can directly occur between the reducing agent and the metallic ion contained in the electroless plating bath, which is usually prevented by the use of a stabilizer. The latter prevents spontaneous reduction in solution (1). More recently, improved electroless deposition models on the different mechanistic steps were issued (8−11).

* Corresponding author. E-mail: alexandre.garcia@cea.fr. Phone: 00 33 1 69 08 12 80.

Received for review June 9, 2010 and accepted October 13, 2010

† LSI Irradiated Polymers Group (UMR 7642 CEA/CNRS/Ecole Polytechnique), CEA, IRAMIS.

‡ SPCSI Chemistry of Surfaces and Interfaces Group, CEA, IRAMIS.

§ SPCSI Oxides Interfaces and Surfaces Group, CEA, IRAMIS.

DOI: 10.1021/am100907j

In the electroless plating industry, noble metal Pd is commonly employed as catalyst to initiate the electroless deposition previously described (7, 12−14). Taking into account that the cost of palladium has been raised in recent years, the development of Pd-free catalysts has attracted a lot of attention lately (15−19), and copper has been proposed as an alternative catalyst (20−22).

For acrylonitrile-butadiene-styrene (ABS), ABS-PC (polycarbonate) and PA (polyamide) which represent more than 90% of the polymers industrially metallized, metal plating with an adherent metallic layer is only possible if an appropriate etchant system is previously employed for surface conditioning (23−33). The surface preparation step, thus, aims at (i) increasing the bulk polymer wettability by surface oxidation and (ii) increasing the bulk polymer roughness in order to improve the surface seeding of the electroless catalyst and the adhesion of the final metallic layer. Up to now, the best (and most widely used) method is based on a chromic acid etching, which oxidizes the bulk polymer surface (2, 23, 25, 26). These oxidation phenomena imply both chemical and mechanical adhesion, respectively, thanks to the chemical reactive group formation and the superficial hole or cavity creation which increases the surface roughness. However, because of the future European ban on chromium waste, that efficient process has to be replaced (34, 35). Recent works, based on a technological breakthrough, consist of the formation of a robust interphase between the substrate surface and the metallic layer which is intended to replace the rough interface which usually results from the chromic acid treatment (22, 36−39). For example, block copolymers with one block designed to interpenetrate the polymer substrate and the other one bearing chelating groups (such as poly(acrylic acid) (PAA)) were recently used to form a host polymer film for electroless plating on various polymer substrates (40). That innovative method, however, requires the synthesis of a two-block copolymer in which one block is made of the same polymer as the substrate (or highly miscible with it), and another one bears chelating groups for the catalyst precursor. As shown in Figure 1, the ligand induced electroless plating (LIEP) process is, on the contrary, based on the covalent grafting of a thin chelating polymer film from its monomer precursors onto a polymer substrate. In that case, the process does not require the synthesis of a designated reactant, and the resulting polymer film is covalently grafted to the substrate and able to complex copper ions which are then reduced and act as catalyst for the growth of the metallic phase which starts inside the host polymer. On these grounds, we recently reported the electroless plating of copper and nickel on ABS polymers based on the one-step covalent grafting of a poly(acrylic acid) (PAA) thin polymer film by the GraftFast process (22, 31, 41). Beyond the adhesive benefits describe above, the LIEP process can be applied to a wide range of polymers since the GraftFast process is a powerful toolset to graft covalent polymer films onto various substrates based on the chemical reduction of aryldiazonium salts (22, 31, 41).

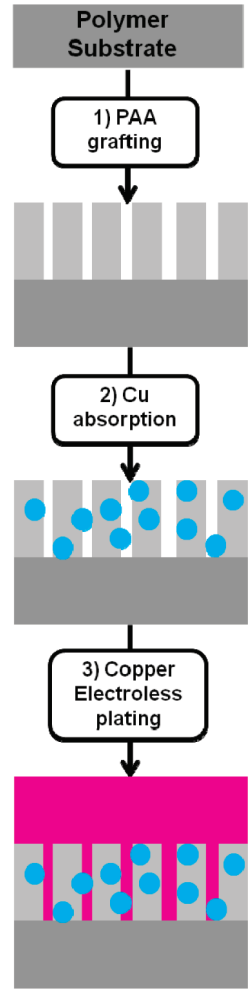

FIGURE 1. Schematic view of the LIEP process: (1) surface modification via the PAA grafting, (2) surface activation through the copper absorption (Cu chelation + reduction), and (3) growth of the Cu plated film thanks to the use of the electroless copper plating bath.

The present paper focuses on the influence of the chemical nature of the polymer substrate on the final metallic layer. We first studied the LIEP process onto the three individual components of the ABS copolymer (i.e., polyacrylontrile (PAN), polybutadiene (PB), and polystyrene (PS)). Then, we demonstrate that the LIEP process applies successfully to ABS-PC and PA, two polymers which are structurally very different. On both polymers, PAA grafting was demonstrated together with its effect on the metallic layer adhesion strength. Cu^{2+} ion complexation and reduction and copper electroless deposition steps were fully characterized. The electrical properties of the plated copper layer were studied by scanning tunneling microscopy (STM) measurements, and the plated copper resistivity was measured by a four-point probe. On the basis of these characterizations and the one carried out onto ABS substrates in our previous paper, we were able to decipher the role of the substrate chemical structure and its surface morphology on the PAA grafting and the plated copper layer.

2. EXPERIMENTAL SECTION

Materials. ABS, ABS-PC, and PA of technical quality were obtained from Pegastech S.A. as common test samples used in

the industrial field. An industrial detergent was used to clean the substrates: TFD4 (Franklab). 1-4-Diaminophenylene dihydrochloride (Fluka, ≥99%), acrylic acid (Sigma Aldrich, ≥99%), sodium nitrite (Fluka, ≥99%), and iron powder (Prolabo VWR, 98%) were used for the poly(acrylic acid) grafting using the GraftFast technology. Cupric sulfate $CuSO_4$, $5H_2O$ (Fluka, ≥ 99%), and sodium borohydride powder (Sigma Aldrich, ≥98.5%) were used for the catalytic copper chelation and reduction. Then, for the electroless metal deposition, an industrial copper plating bath (M Copper 85 supplied by MacDermid) was used.

Electroless Metal Deposition Process. As shown in Figure 1, the LIEP process is divided into three steps as discussed in the following three sections.

Covalent Grafting of Poly(acrylic Acid) on Polymer Substrates. All the polymer substrates were sonicated for 30 min into an industrial detergent (TFD4) and thoroughly rinsed in deionized water. Then, 1-4-phenylenediammonium dihydrochloride was dissolved in a 0.5 M HCl solution to obtain 100 mL at 0.1 M (Solution 1). Under stirring, 21 mL of $NaNO_2$ (0.1 M) was added stepwise to 35 mL of Solution 1 in order to synthesize the aryldiazonium salt. At this stage, the $NaNO_2$/1-4-phenylenediammonium molar ratio was equal to 0.6. Acrylic acid (10 mL) was then introduced into this solution. Polymer substrates (4 × 1 × 0.2 cm) were introduced in the beaker, and iron powder (5.25 g) was added to the solution. After 5, 10, 20, 30, and 40 min, 2 mL of $NaNO_2$ (0.1M) was added to the solution. At the end, the $NaNO_2$/1-4-phenylenediammonium dihydrochloride molar ratio reached ca. 0.9. That stepwise addition promoted a continuous aryldiazonium salt formation and subsequently a continuous phenyl radical formation; hence, both polyphenylene and poly(acrylic acid) polymerizations could be initiated all along the reaction. After immersion for 90 min at 38 °C, polymer substrates were sonicated twice for 10 min in alkaline solution (NaOH, 1 M) and deionized water. The rinsing treatment allowed one to discard most of the physisorbed matter, as evidenced by the subsequent stability of the infrared (IR) absorption bands of PAA upon further rinsing.

Chelation and Reduction of Metallic Cations. PAA-modified polymer substrates were immersed for 5 min into an alkaline (NH_3, 0.6 M) copper sulfate $CuSO_4 \cdot 5H_2O$ (0.1 M) solution at room temperature to induce an ion-exchange process. Afterward, samples were rinsed with deionized water. In order to reduce Cu^{2+} ions previously chelated by the carboxylate groups contained in grafted PAA films, modified substrates were immersed into a sodium borohydride ($NaBH_4$) (0.1M)—NaOH (0.1 M) solution at 40 °C for 10 min.

Electroless Copper Deposition. The surface-activated substrates were finally placed in the industrial copper electroless metal plating bath (M Copper 85). That commercial plating bath required the addition of a reducing agent just before the plating step. Formaldehyde HCHO was used as the reducing agent; optimum conditions were obtained with a copper content of 2 $g \cdot L^{-1}$, a mass ratio HCHO/Cu of 2, a pH at 13, a work temperature at 48 °C. The observed deposition rate was about 4 μm/h. Polymer substrates were left in the bath for 15 min.

3. CHARACTERIZATIONS

Characterization Methods. Infrared spectra were recorded on a Bruker Vertex 70 spectrometer equipped with an attenuated total reflection (ATR) Pike-Miracle accessory. The MCT detector:Hg-Cd-Te (MCT) detector working at liquid nitrogen temperature. The spectra were obtained after 256 scans at 2 cm^{-1} resolution.

X-ray photoelectron spectroscopy (XPS) studies were performed with a KRATOS Axis Ultra DLD spectrometer, using the monochromatized Al Kα line at 1486.6 eV. The pass energy of the analyzer was kept constant at 20 eV for C_{1s} core level scans. The photoelectron takeoff angle was 90° with respect to the sample plane, which provides an integrated sampling probe depth range going from 7 to 20 nm for our substrates.

Atomic absorption spectroscopy was carried out on a Thermo Fisher Scientific Atomic Absorption Spectrometer (ICE 3000 Series) with a hollow cathode lamp for Co—Cu—Mn—Ni at a primary wavelength of 324.8 nm and a bandpass of 0.5 nm using an air—acetylene flame at a gas flow rate of 0.9 L/min and a 10 wt % HNO_3/deionized water matrix. The lamp current was 7.5 mA.

Pristine polymer substrates were imaged by atomic force microscopy (AFM) in acoustic mode with a Molecular Imaging PicoSPMLe commercial AFM microscope (PicoScan 2100 controller, Scientec, France) using a commercial pyramidal Si tip (mounted on a 225 μm long single-beam cantilever with a resonance frequency of approximately 75 kHz and a spring constant of about 3 $N \cdot m^{-1}$). The scan rate was in the range of 0.25 Hz with a scanning density of 512 lines per frame. The AFM was mounted on a floating table to achieve vibration insulation during investigations. The root mean square (rms) roughness values of the scans were calculated using the Gwyddion 2.19 program covered by GNU General Public License.

Tunneling current spectroscopy characterization and high resolution AFM imaging of copper plated surfaces have been performed on a VT-AFM (Omicron GmbH) working in an ultra high vacuum environment at room temperature. This microscope has been modified to work with piezoelectric QPlus sensors (47) with etched Pt/It tip in order to combine AFM and STM imaging on the same conductive sample. To ensure the surface conductivity through the substrate, conductive silver ink was deposited between the studied surface and the conductive STM platform.

A four-point probe (S302K-LRM, Lucas Lab) was used to measure the resistivity of the plated metallic layers. The scanning electron microscopy images were recorded by a Hitachi S4800 equipped with a Field Emission Gun (FEG-scanning electron microscopy (SEM)) and coupled with an energy dispersive X-ray spectrometer (EDX).

Mechanical Adhesion Test. The adhesion between the plated metallic layer and the ABS-PC and PA substrates was studied by two different mechanical adhesion tests. The first method was a T-peel strength adhesion measurement, based on the standard test method for peel resistance of adhesives (T-peel test) ASTM D1876-08, measured thanks to the MTS Fundamental 90° Peel Fixtures Synergie 100 device. The second method was the standard ASTM D3359 Scotch tape test (cross-cut tape test) which consists of applying and removing pressure-sensitive adhesive tape over 16 cross-hatched squares of 1 × 1 mm^2 made in the film thanks to an Elcometer Cross Hatch cutter (Elcometer 107 X-Hatch ASTM Kit). That standard well-used test allows a direct comparison of the adhesion of films obtained under various conditions on similar substrates.

Table 1. O/C Ratio before and after PAA Grafting and Roughness on Pristine Polymers

	O/C ratio on pristine polymers	O/C ratio after PAA grafting + Cu^0	$roughness_{rms}$ (nm) for a 2 × 2 μm^2 area
ABS	0.03	0.17	38 ± 6
ABS-PC	0.28	0.34	28 ± 6
PA	0.14	0.35	112 ± 8
pure PAA	0.4		

4. RESULTS AND DISCUSSION

PAA Covalent Grafting and Cu^{2+} Chelation and Reduction. Like in the ABS case (22), poly(acrylic acid) has been covalently grafted onto all the substrates via the GraftFast process (31, 41) which relies on the redox activation of in situ synthesized aryldiazonium salts. Aryl radicals issued from the chemical reduction of aryldiazonium salts act both as initiators for the radical polymerization of acrylic acid and as direct source of a polyphenylene primer sublayer. In a previous paper (41), it has been proposed that, once the polyphenylene adhesion primer layer is covalently grafted to the polymer substrates, the interaction of growing oligoradical chains with the polyphenylene-like primer layer gives a grafted copolymer film. The growth of the poly(acrylic acid) film is then induced by the successive grafting of oligoradical chains and phenyl groups embedded in the already grafted chains. In order to initiate the poly(acrylic acid) radical polymerization, aryl radicals were produced all along the reaction by the successive additions of $NaNO_2$. $NaNO_2$ induces the aryldiazonium salt formation which is then reduced in aryl radical by the iron powder contained in solution. This PAA grafting was clearly observed by IR and XPS spectroscopy, and the same conclusions as in the case of the ABS substrates could be done (22). For details, see the Supporting Information.

The role of the polymer substrates on the PAA grafting was first evaluated by comparing the PAA grafted films obtained on PAN, PB, and PS, which are the three individual components of ABS (see Supporting Information). Thanks to contact angle measurements and IR and XPS analyses, PAA grafting was obviously promoted onto PAN substrate which is also more hydrophilic than PB and PS (42, 43). Those results give a first indication on the influence of the substrate properties (in particular its hydrophilic behavior) on the PAA grafting.

Then, PAA grafting was evaluated on ABS, ABS-PC, and PA. First, the PAA grafting efficiency was estimated thanks to the O/C ratio measured from the XPS spectra. Indeed, an increase of that ratio is expected upon the PAA grafting, since the O/C ratio is 0.4 for pure PAA, and only 0.03, 0.28, and 0.14 for pristine ABS, APS-PC, and PA, respectively. As indicated by Table 1, XPS spectra of the PAA-grafted polymers exhibit a significantly higher increase for the O/C ratio in the case of PA than for ABS and ABS-PC.

This result confirms the study of the PAA grafting onto PAN, PB, and PS: the PAA grafting appears promoted on hydrophilic substrates. This behavior is likely to arise from the better swelling of the surface of a hydrophilic substrate, with respect to a hydrophobic one such as PS or PB, by the aqueous reactive mixture which is used for the PAA grafting step. In the case of the ABS and ABS-PC which are both composite materials containing both hydrophilic (PAN, PC) and hydrophobic (PB, PS) polymers, we can assume local disparities in the PAA grafting efficiency, depending on the surface composition, since the PAA grafting is more efficient on PAN and polycarbonate which are more hydrophilic than on PS and PB.

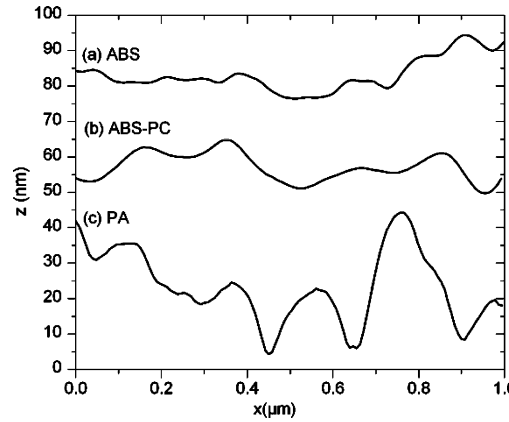

FIGURE 2. One micrometer profile extraction of pristine ABS (a), ABS-PC (b), and PA (c) substrates.

However, this higher O/C ratio for PA may also be attributed to the influence of surface roughness, measured thanks to AFM analysis, which is around three times higher for the PA substrate than for the ABS and ABS-PC ones at the micrometer scale, as shown in Table 1 and Figure 2. A higher roughness obviously induces the increase of the actual contact area with the reactive solution. Thereby, more PAA oligoradicals can be grafted onto the substrate surface for a given projected area probed by XPS or IR analysis.

Hence, we assume that both the morphology and the chemical composition of the surface of the pristine substrate play a key role in the density and homogeneity of the final grafted-PAA film.

This higher PAA grafting rate for PA substrates than for ABS and ABS-PC has a direct influence on the amount of loaded copper ions after immersion into an alkaline solution containing ammonia and $CuSO_4$. The copper ions surface concentration Γ ($\mu g \cdot cm^{-2}$) was measured by flame atomic absorption spectroscopy on 80 cm^2 substrates. After an immersion time of 5 min in the alkaline solution, the Cu^{2+} loaded substrates were immersed during 10 min into a 10 wt % HNO_3/deionized water solution. As expected from the pH-switchable chelating properties of PAA, the copper ions were totally released from the polymer film in the acidic bath. Flame atomic absorption spectroscopy on the acidic bath containing the copper species released from the films allows an accurate measurement of the pristine surface concentration of copper species within the grafted films at equivalent roughness. As shown in Table 2, for ABS and ABS-PC substrates, the final copper ions surface concentration Γ was measured at ca. 1 $\mu g \cdot cm^{-2}$ whereas for PA substrates, the amount of loaded Cu^{2+} was more than 10 times higher. Besides, the PA substrates blue color, visible with the naked eye, was a clear indication of the high amount of loaded

Table 2. Cu^{2+} Surface Coverage after Chelation and Cu Atomic Percentage after Chelation and Reduction

	Γ after chelation at equivalent roughness ($\mu g \cdot cm^{-2}$)	% Cu after chelation	% Cu after reduction
ABS	0.9 ± 0.2	2	2
ABS-PC	0.6 ± 0.2	1	0.8
PA	14.6 ± 2.8	7	4

Cu^{2+}. To a lesser extent, this high difference in the amount of loaded Cu^{2+} was also observed by Cu_{2p} XPS analysis since the Cu atomic percentage derived from the XPS spectra was 7% for PA substrates and only 2% and 1% for ABS and ABS-PC, respectively. Nevertheless, it is difficult to directly compare both evaluations (XPS and flame atomic absorption) in that case. Indeed, for flame atomic absorption which measures the copper species spontaneously adsorbed and then chemically released from the PAA grafted film, the analysis is unaffected by the surface morphology and the PAA actual thickness, whereas for XPS quantitative analysis, the average sampling probe depth is affected by the PAA layer morphology and the roughness. In other words, for the thicker PAA grafted films, a difference may be observed between XPS and flame absorption, because the sampling volume is not the same. Moreover, the analysis area differences (80 cm^2 for flame atomic absorption and less than 1 mm^2 for XPS analysis) can also be responsible for some differences in the copper evaluation, despite our XPS measurements were always averaged from two different analyses.

That higher copper loading also showed up after the reduction step. As shown in Figure 3, for both ABS-PC and PA substrates, after immersion into a $NaBH_4$ solution, the peaks of $Cu_{2p3/2}$ and $Cu_{2p1/2}$ core level binding energies confirmed the copper reduction (44). The catalytic-Cu^0 atomic ratio was measured at 2% for ABS, 0.8% for ABS-PC, and 4% for PA. It is noteworthy that the difference observed between PA and the two other substrates is lower after than before reduction. A significant part of the copper species absorbed within the PA/PAA substrates seems to be released in solution upon the reduction step. That may arise from the higher roughness of PA substrates (when compared to ABS and ABS-PC): Indeed, we assume that copper species (likely copper sulfate $CuSO_4$) are actually adsorbed but unchelated at the outer surface of the grafted PAA films. That phenomenon is obviously promoted by the high roughness for the PA/PAA surfaces, since adsorption is easier on complex geometries. A low amount of sulfur was indeed observed on the XPS spectra recorded after the chelation step on PA/PAA samples (data not shown), which clearly indicates that some unchelated copper species are present. Those "extra" copper species (with respect to the copper ions actually chelated by carboxylate anions within the PAA chains) explain the large difference between the copper loading after the chelation step between PA (high roughness) and ABS or ABS-PC (low roughness). After the reduction step, all copper species are reduced to Cu^0, since we did not observe any Cu^{II} signal in the XPS spectra. The Cu^0 species derived from previously chelated copper ions are physically trapped within the PAA chains, while the Cu^0 species arising from the copper salts only adsorbed on the outer parts of the films are only weakly linked and are likely to be more easily discarded by the rinsing steps. Hence, the high difference in copper loading observed after the chelation step between PA and ABS or ABS-PC decreases after the reduction step, as shown by Table 2.

Assuming that all chelated copper ions were retained in the polymer film during the reduction step, it was possible to estimate the carboxylate groups chelation rate by copper ions contained in the PAA films. On the basis of the Cu_{2p}/COOH C_{1s} atomic ratio evaluated by XPS analysis after reduction and given that one copper ion should normally be chelated by two carboxylate groups COO^-, between 70% and 80% of the carboxylate groups were occupied by copper ions whatever the substrate, which means that the PAA ion exchange properties are very efficient for copper seeding and the differences observed and previously described on the copper loading are thus directly linked to the higher PAA grafting on PA substrates.

Electroless Copper Deposition. Taking into account all the parameters described in the Experimental Section,

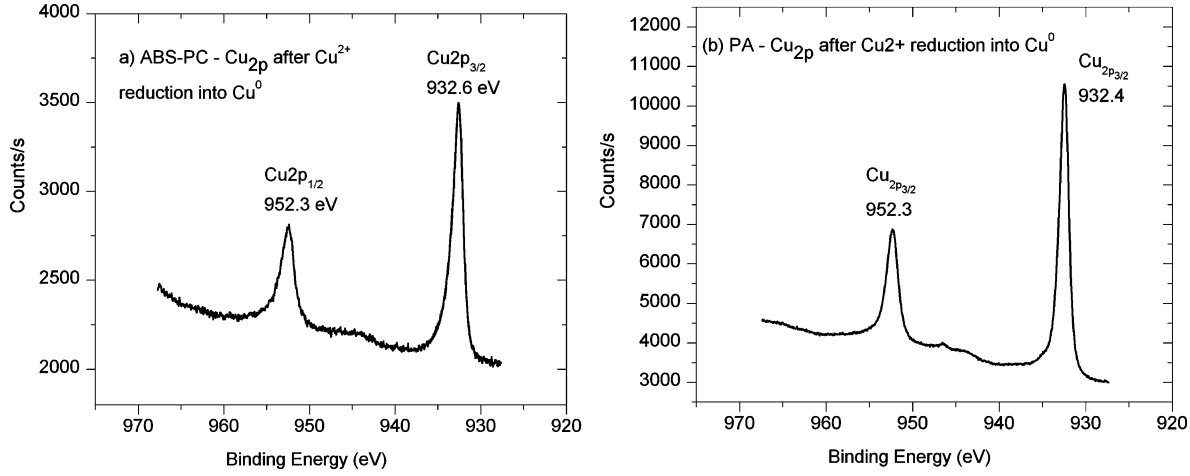

FIGURE 3. Cu_{2p} XPS spectra of ABS-PC (a) and PA (b) substrates after the reduction step.

immersing the Cu-activated substrates in the M Copper 85 industrial copper plating bath during 15 min allowed the formation of 1 μm-thick plated-copper films. It might be surprising that the plated-copper thickness was the same whatever the pristine substrates, since we demonstrated in the previous sections that more copper catalyst was formed on PA than on ABS or ABS-PC. Actually, as the electroless plating process is autocatalytic, the growth speed becomes constant once the first nanometers of plated copper are formed. The amount of catalytic copper does not seem to have any influence there (1, 45).

The obtained plated layers were characterized by XPS measurements. Again, as in the ABS case (22), Cu_{2p} spectra indicate that a plated Cu^0 layer was successfully formed on the ABS-PC and PA substrates (for details, see the Supporting Information). As expected, the Cu atomic percentage after the electroless plating was widely superior to the one obtained after reduction and around 30%. In both cases, oxygen and carbon elements were still present, due to organic residuals coming from the plating bath and in particular from the complexing agent, but they cannot be attributed to the underlying polymers because the plated copper layers were too thick to allow XPS to probe underlying species.

SEM images in Figure 4 showed that, for both ABS-PC and PA substrates, the metallic layer consists of a tight, dense, continuous, and void-free structure which is required for the following electroplated steps. Like in the ABS-PC case, the Cu-plated PA section showed a global homogeneous metallic top layer and a good interfacial zone between the plated metal and the substrate. Finally, whatever the substrate, the final metallic layer thickness was evaluated around 1 μm after a 15 min plating step.

EDX spectra analysis for Cu-plated PA substrates also revealed that the metallic layer surface is composed only of Cu^0 (for details, see the Supporting Information). Besides, the electrical resistivity of the as-plated copper measured by the four-point probe method was evaluated to be slightly higher than bulk copper (1.67 $\mu\Omega \cdot$ cm) (46): 3.2 $\mu\Omega \cdot$ cm for ABS, 2.54 $\mu\Omega \cdot$ cm for ABS-PC, and 2.15 $\mu\Omega \cdot$ cm for PA. The presence of defects and hydrogen entrapment in the films are the major factors contributing to the observed increase in the resistivity of the plated films, with respect to bulk pure copper (47). According to the obtained results, PA is the substrate which gave the best results from an electrical point of view. However, for both cases, STM and AFM images are really similar. Indeed, even if, in the PA case, the copper layer is more conductive, these STM images showed that on both PA and ABS-PC substrates the plated copper layers are conductive all over the substrate which is important for many applications. I−V tunneling current spectroscopy curves showed also a metallic behavior on both cases (for details, see Supporting Information).

As observed on the SEM images, AFM analysis showed that the plated copper particle size is almost three times lower in the case of PA substrate (ca. 40 nm) than in the ABS-PC case (Figure 5) (48). The grain size of the electroless plated layers is dependent on the catalyst one (1, 49). Indeed, the lower and more homogeneous the catalyst particles, the lower is the grain size of the electroless plated layer. In the PA case, the grain size of the electroless copper plated layers is three times lower than in the ABS-PC one, which suggests that the catalytic-Cu^0 particles size is lower

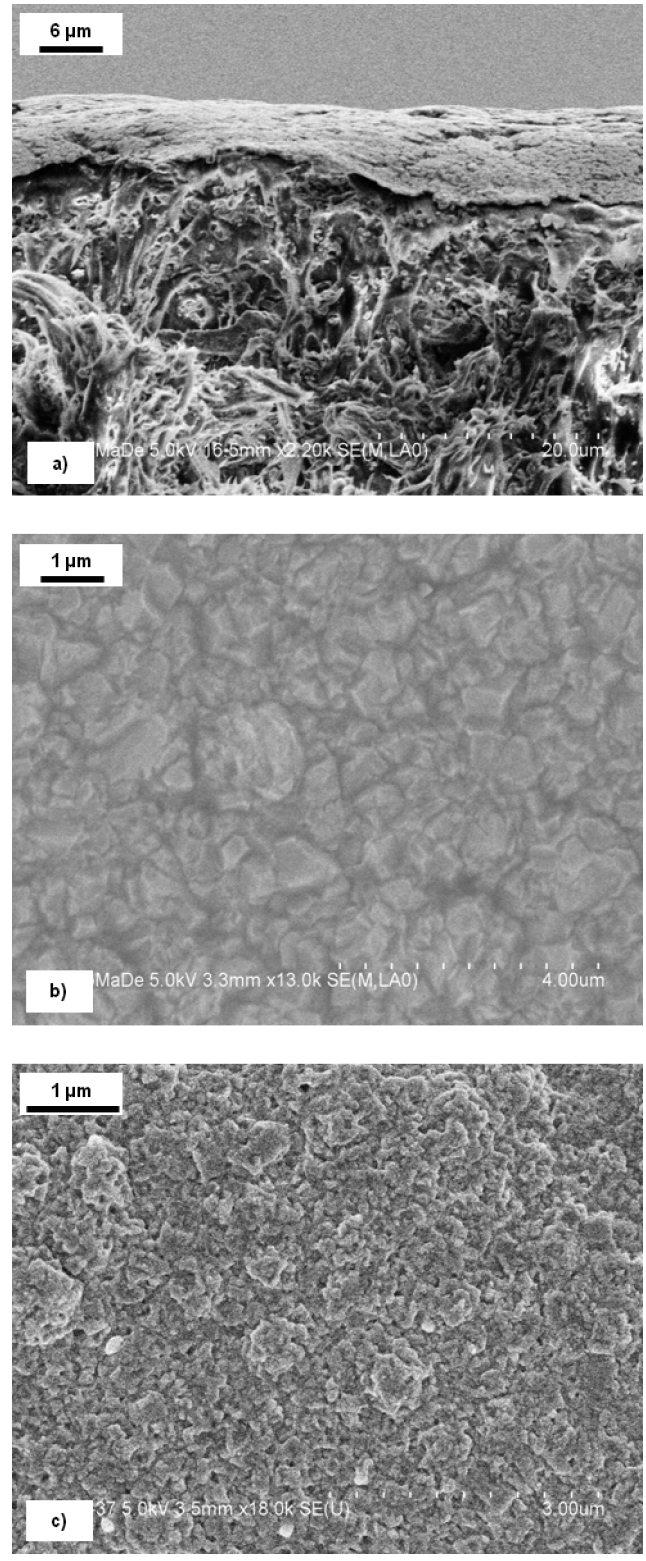

FIGURE 4. SEM images after electroless copper plating: PA section (a) and ABS-PC (b) and PA (c) top views. The scales are given on the images.

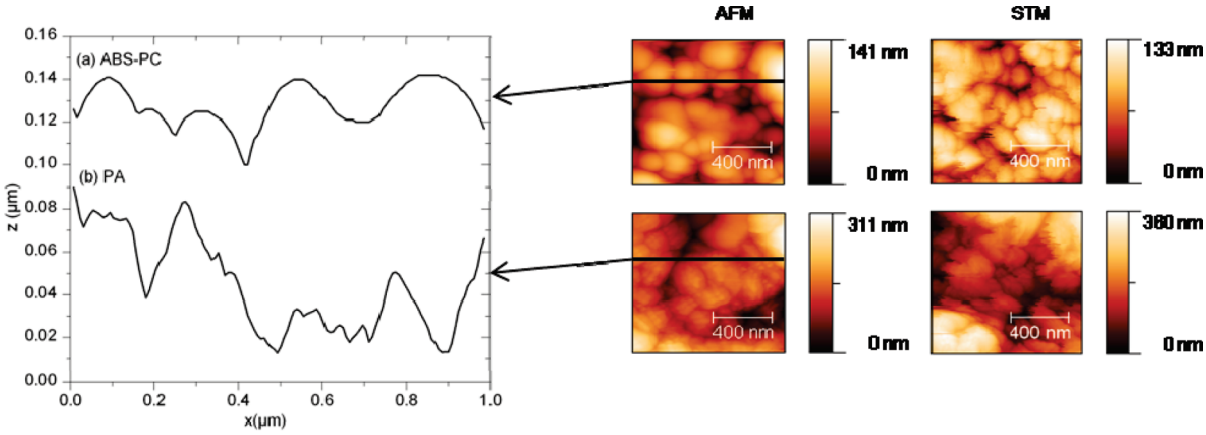

FIGURE 5. One × one micrometer AFM and STM images of Cu-plated ABS-PC (top) and PA (bottom) substrates with the corresponding profile extractions on the left.

and more homogeneous. This is supported by the fact that, in the PA case, the PAA layer is more homogeneous all over the substrate and more compact which allows one to obtain lower-size Cu-catalyst particles. The hydrophilic and rough surface of PA substrates promote the PAA grafting, and the obtained compact PAA chains involves the formation of lower and more homogeneous Cu-catalytic particles and lower Cu-plated grain size than for ABS-PC and ABS substrates. In the ABS-PC and ABS cases, according to all the characterizations, the grafted-PAA layer seems to be less compact and heterogeneous; there are less Cu-catalytic particles, and they are not homogeneous which lead to higher Cu-plated grain size.

Lastly, as expected, the 1 μm-thick plated metallic film is quite conformal to the pristine surface, whatever the pristine polymer. Hence, at the same scale than for the pristine substrates (2 μm^2), the roughness after plating was equal to 38 nm for ABS-PC and 109 nm for PA. According to the roughness of the pristine substrates previously described (Table 1), the PA/PAA/Cu roughness is still around three times higher than in the ABS-PC case.

Finally, the adhesion between the metallic layer and the polymer substrates was studied by two different methods. First, T-peel strength adhesion measurements were carried out and the results were excellent since in both cases; the metallic layer was not removed. No quantitative conclusion can be derived from those results, except that the adhesion strength of our plated-copper layers is largely enough for many applications, since the T-peel strength measurement is a classical corner stone of industrial qualification for metal plating processes.

Second, the adhesion strength has been studied by the most common industrial adhesion test which is also among the most demanding one: the standard ASTM D3359 Scotch tape test. When the classical chromic acid etching-based process was used on our ABS-PC and PA samples, none of the 16 cross-hatched squares was removed. For ABS-PC substrates plated following the LIEP process, we observed the removal of almost half of the squares, as it was observed for ABS substrates (see Supporting Information). On the contrary, Figure 6 shows, for PA samples, no squares were

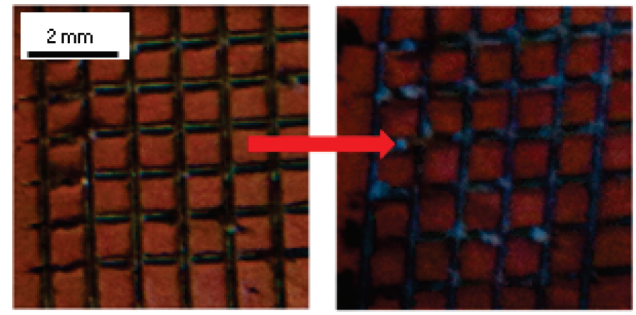

FIGURE 6. Images of a Cu-plated PA substrate before (left) and after (right) the scotch tape test.

removed, as for the classical chromium-based process. It is noteworthy that, when ABS-PC and PA were Cu-plated without any PAA-grafting or after spin-coating PAA from a 0.5% w/w solution (50), the same scotch test showed all the squares fully removed. These adhesion results can be attributed to the nanometer-scale mechanical interlocking effect, which mimics the micrometer-scale interdigitation that occurs between the metallic layer and the rough interface which results from the chromic acid treatment. The adhesion which is estimated by the Scotch tape test arises from two factors: (i) the strength of the interface between the PAA coating and the polymer substrate; (ii) the so-called "interlocking effect" between the copper metal film and its substrate.

As mentioned above, when PAA is spin-coated, most of the PAA layer is removed along with Cu after the scotch tape test. This is consistent with the absence of covalent bonding between the PAA coating and the substrate, taking into account the fact that, contrary to "classical electroless plating", the copper metal film grows within the PAA film and is thus only marginally in direct contact with the substrate. However, when comparing PAA films grafted on different polymers, that former factor should, at first sight, be considered as even. Actually, the roughness of the surface again plays a role here: As the scotch test consists of applying a constant force to peel out a given scotch tape test, the higher the roughness, the stronger is the actual strength of the polymer-to-PAA interface, because the actual number of covalent bonds between PAA and the substrate is higher on a rougher substrate for a given scotch area. That is a main

reason to explain why PAA on PA exhibits no damages after the scotch tape test, when compared to ABS or ABS-PC substrates which are less rough.

Regarding now the interlocking effect, the actual thickness of the PAA coating obviously enhances its role in the observed adhesion. However, as the observed higher amount is likely to arise from the higher roughness of PA, we cannot conclude on the role of the interlocking effect in the differences observed between PA, PC, and ABS-PC in the scotch tape test.

When compared to the strength adhesion measured after the chromic acid etching-based process, our results appear quite promising for PA substrates but still insufficient for ABS and ABS-PC, at least for all the applications which require a strong adhesion of the plated layer. Nevertheless, further works are currently carried out to improve the adhesion strength, using only soft and ecological methods in order to keep consistent with our primary goal, i.e., replace the chromic acid surface activation step by a more ecological one. However, for other applications such as flexible electronics where the copper layers are directly recovered and protected after the electroless plating, the adhesion strength observed for ABS and ABS-PC should be sufficient.

5. CONCLUSIONS

In this paper, we thoroughly compared three industrially relevant plastics as substrates for our recently described LIEP process. We demonstrated that initial roughness and surface composition significantly influence the chemical grafting of a PAA film, which eventually complexes copper ions as precursors for electroless plating catalysis. We have been able to link the macroscopic properties of the final metal plated layer, such as the strength adhesion and the electrical resistivity to the microscopic properties of its precursor steps, such as the amount of loaded catalyst precursors and the morphology and the chemical composition of the surface of the pristine substrate. Indeed, our results show that the higher PAA grafting rate, the higher is the amount of loaded catalytic copper, the lower is the particle size in the plated copper film, and the higher is its conductivity. This work highly strengthens the versatility of the LIEP process, which relies on available monomers and reactants and applies directly to any polymer surface, and increases its application fields. Further works are currently being carried out to take advantage of the GraftFast step to localize the electroless metal plating and to apply it to other polymers.

Acknowledgment. The authors would like to thank Dr Vincent Mévellec (Alchimer) for his help in the resistivity and T-peel strength adhesion measurements.

Supporting Information Available: Complementary IR, XPS, and EDX spectroscopies, I_T-V_b spectroscopy curves, and ABS-PC scotch tape test images. This material is available free of charge via the Internet at http://pubs.acs.org.

REFERENCES AND NOTES

(1) Mallory, G. O.; Hajdu, J. B. *Electroless Plating: Fundamentals and Applications*; The American Electroplaters and Surface Finishers Society, Washington, DC, 1990.
(2) Sacher, E. *Metallization of Polymers 2*. Plenum Publisher: New York, 2002.
(3) Demirel, M. C.; Cetinkaya, M.; Singh, A.; Dressick, W. J. *Adv. Mater.* **2007**, *19*, 4495–4499.
(4) Ma, D. I.; Shirey, L.; McCarthy, D.; Thompson, A.; Qadri, S. B.; Dressick, W. J.; Chen, M. S.; Calvert, J. M.; Kapur, R.; Brandow, S. L. *Chem. Mater.* **2002**, *14*, 4586–4594.
(5) Price, R. R.; Dressick, W. J.; Singh, A. *J. Am. Chem. Soc.* **2003**, *125*, 11259–11263.
(6) Ohno, I. *Mater. Sci. Eng., A* **1991**, *146*, 33–49.
(7) Zouhou, A.; Vergnes, H.; Duverneuil, P. *Microelectron. Eng.* **2001**, *56*, 177–180.
(8) Chang, Y. L.; Ye, W. C.; Ma, C. L.; Wang, C. M. *J. Electrochem. Soc.* **2006**, *153*, C677–C682.
(9) Dimitrov, V.; Gorker, L. *Prog. React. Kinet. Mech.* **2006**, *31*, 45–58.
(10) Homma, T.; Tamaki, A.; Nakai, H.; Osaka, T. *J. Electroanal. Chem.* **2003**, *559*, 131–136.
(11) Shimada, T.; Nakai, H.; Homma, T. *J. Electrochem. Soc.* **2007**, *154*, D273–D276.
(12) Jiang, B. Q.; Xiao, L.; Hu, S. F.; Peng, J.; Zhang, H.; Wang, M. W. *Opt. Mater.* **2009**, *31*, 1532–1539.
(13) Nicolas-Debarnot, D.; Pascu, M.; Vasile, C.; Poncin-Epaillard, F. *Surf. Coat. Technol.* **2006**, *200*, 4257–4265.
(14) Charbonnier, M.; Romand, A.; Goepfert, Y.; Leonard, D.; Bessueille, F.; Bouadi, A. *Thin Solid Films* **2006**, *515*, 1623–1633.
(15) Charbonnier, M.; Romand, M.; Goepfert, Y. *Surf. Coat. Technol.* **2006**, *200*, 5028–5036.
(16) Dai, W.; Wang, W. J. *Sens. Actuators, A* **2007**, *135*, 300–307.
(17) Hsiao, Y. S.; Whang, W. T.; Wu, S. C.; Chuang, K. R. *Thin Solid Films* **2008**, *516*, 4258–4266.
(18) Matsumura, Y.; Enomoto, Y.; Sugiyama, M.; Akamatsu, K.; Nawafune, H. *J. Mater. Chem.* **2008**, *18*, 5078–5082.
(19) Miyoshi, K.; Aoki, Y.; Kunitake, T.; Fujikawa, S. *Langmuir* **2008**, *24*, 4205–4208.
(20) Bicak, N.; Karagoz, B. *Surf. Coat. Technol.* **2008**, *202*, 1581−1587.
(21) Charbonnier, M.; Romand, M.; Goepfert, Y.; Leonard, D.; Bouadi, M. *Surf. Coat. Technol.* **2006**, *200*, 5478–5486.
(22) Garcia, A.; Berthelot, T.; Viel, P.; Mesnage, A.; Jegou, P.; Nekelson, F.; Roussel, S.; Palacin, S. *ACS Appl. Mater. Interfaces* **2010**, *2*, 1177–1183.
(23) Mance, A. M. *J. Electrochem. Soc.* **1992**, *139*, 724–728.
(24) Brandes, M.; Fels, C. C. *Met. Finish.* **2008**, *106*, 21–24.
(25) Wang, G. X.; Li, N.; Hu, H. L.; Yu, Y. C. *Appl. Surf. Sci.* **2006**, *253*, 480–484.
(26) Wang, G. X.; Li, N.; Li, D. Y. *J. Univ. Sci. Technol. Beijing* **2007**, *14*, 286–289.
(27) Charbonnier, M.; Romand, M. *Int. J. Adhes. Adhes.* **2003**, *23*, 277–285.
(28) Esrom, H.; Seebock, R.; Charbonnier, M.; Romand, M. *Surf. Coat. Technol.* **2000**, *125*, 19–24.
(29) Kupfer, H.; Hecht, G.; Ostwald, R. *Surf. Coat. Technol.* **1999**, *112*, 379–383.
(30) Dillard, D.; Maquire, E.; Donovan, L. U.S. Patent 4,335,164, 1982.
(31) Mévellec, V.; Roussel, S.; Deniau, G. FR Patent 2,910,006, 2007.
(32) Jacob, G. U.S. Patent 3,733,213, 1973.
(33) Hiroshi, N. EU Patent 1,148,153, 2001.
(34) European Parliament and the Council, 2002/95/EC, Brussels, 2003.
(35) European Parliament and the Council, 2005/90/EC, Brussels, 2006.
(36) Aldakov, D.; Bonnassieux, Y.; Geffroy, B.; Palacin, S. *ACS Appl. Mater. Interfaces* **2009**, *1*, 584–589.
(37) Li, L.; Yan, G. P.; Wu, J. Y.; Yu, X. H.; Guo, Q. Z.; Kang, E. T. *Appl. Surf. Sci.* **2008**, *254*, 7331–7335.
(38) Liaw, W. C.; Huang, P. C.; Chen, K. P.; Chen, C. S. *Polym. J.* **2009**, *41*, 634–642.
(39) Zabetakis, D.; Dressick, W. J. *ACS Appl. Mater. Interfaces* **2009**, *1*, 4–25.
(40) Lancaster, J. R.; Jehani, J.; Carroll, G. T.; Chen, Y.; Turro, N. J.; Koberstein, J. T. *Chem. Mater.* **2008**, *20*, 6583–6585.
(41) Mévellec, V.; Roussel, S.; Tessier, L.; Chancolon, J.; Mayne-L'Hermite, M.; Deniau, G.; Viel, P.; Palacin, S. *Chem. Mater.* **2007**, *19*, 6323–6330.
(42) Bayramoglu, G.; Metin, A. U.; Arica, M. Y. *Appl. Surf. Sci.* , *256*, 6710–6716.

(43) Wang, X. P.; Chen, Z. F.; Shen, Z. Q. *Sci. China, Ser. B: Chem.* **2005**, *48*, 553–559.
(44) Beamson, G.; Briggs, D. *High Resolution XPS of Organic Polymers: The Scienta ESCA300*; John Wiley & Sons: New York, 1992.
(45) Brandow, S. L.; Dressick, W. J.; Marrian, C. R. K.; Chow, G. M.; Calvert, J. M. *J. Electrochem. Soc.* **1995**, *142*, 2233–2243.
(46) Weast, R. C. *CRC Handbook of Chemistry and Physics*; CRC Press: Boca Raton, 1984.
(47) Aithal, R. K.; Yenamandra, S.; Gunasekaran, R. A.; Coane, P.; Varahramyan, K. *Mater. Chem. Phys.* **2006**, *98*, 95–102.
(48) Schaefers, S.; Rast, L.; Stanishevsky, A. *Mater. Lett.* **2006**, *60*, 706–709.
(49) Brandow, S. L.; Chen, M. S.; Wang, T.; Dulcey, C. S.; Calvert, J. M.; Bohland, J. F.; Calabrese, G. S.; Dressick, W. J. *J. Electrochem. Soc.* **1997**, *144*, 3425–3434.
(50) Jackson, R. L. EU Patent 0 250 867, 1988.

AM100907J

Supporting information

Microscopic study of a Ligand Induced Electroless Plating process onto polymers

Alexandre Garcia[*a,b], *Thomas Berthelot*[a], *Pascal Viel*[b], *Jérôme Polesel-Maris*[c], *and Serge Palacin*[b]

CEA, IRAMIS, LSI Irradiated Polymers Grp (UMR 7642 CEA/CNRS/Ecole Polytechnique), F-91128 Palaiseau Cedex and CEA, IRAMIS, SPCSI Chemistry of Surfaces and Interfaces Grp, F-91191, Gif-sur-Yvette, France

EMAIL ADDRESS: thomas.berthelot@cea.fr; alexandre.garcia@cea.fr

- **Contact angle measurements on Polyacrylonitrile, Polybutadiene and Polystyrene deposited by spin-coating on planar gold substrates**

Solutions of polyacrylonitrile (M_w=185000 g/mol, 2.5% in Dimethylformamide), polybutadiene (M_w=420000 g/mol, 0.5% in tetrahydrofuran) and polystyrene (M_w=192000 g/mol, 1% in tetrahydrofuran) were spin-coated onto planar gold substrates at 3000 rpm during 30 seconds. All the samples were then heated at 100°C during 5 min in order to dry the film. This heating treatment allowed to remove all the tetrahydrofuran solvent contained in the polybtuadiene (PB) and polystyrene (PS) films whereas all the DMF contained in the polyacrylonitrile (PAN) film was removed by a water rinsing under sonication. As shown in Table S1, the average roughness was measured for each substrate by mechanical prolilometry: all the substrates were found almost flat (i.e. Ra <= 5 nm). Then, all the samples were immersed in the same solutions than ABS, ABS-PC and PA substrates to graft PAA films.

As shown in Table 1, for equivalent roughness, contact angle measurements obtained from the droplet deposition of the solution used for the PAA grafting show that PAN is significantly more hydrophilic than PB and PS.

Table S1: Roughness average and contact angle measurements onto PAN, PB and PS substrates

Polymer substrate	Roughness average Ra (nm)	Contact angle (°)
Polyacrylonitrile	1.1 +/- 0.3	52.0 +/- 3
Polybutadiene	1.5 +/- 0.6	101 +/- 4
Polystyrene	5.3 +/- 2.1	93 +/- 1

- **IR and C1s XPS Characterizations after PAA grafting and Cu chelation and reduction on Polyacrylonitrile, Polybutadiene and Polystyrene deposited by spin-coating on planar gold substrates**

The PAN, PB and PS substrates were characterized by IR and XPS spectroscopies (Figure S1, Figure S2, Figure S3 and Figure S4).

Thanks to both analyses, as shown in Table S2, it is obvious that PAA grafting is promoted onto PAN substrate which is also the most hydrophilic substrate. On the contrary, on PB and PS substrates, the PAA grafting is less efficient.

Table S2: IR peak intensity of both COOH and COO^- bands and % C_{1s} COOH on total C1s XPS signal after PAA grafting of PAN, PB and PS substrates

Polymer substrate	IR band intensity (%)		% C_{1s} COOH on total C_{1s} XPS signal
	- COOH (after acidic rinsing)	- COO^- (after basic rinsing)	
Polyacrylonitrile	0.7	1.1	5.7
Polybutadiene	0.4	0.5	1.5
Polystyrene	0.3	0.3	0.7

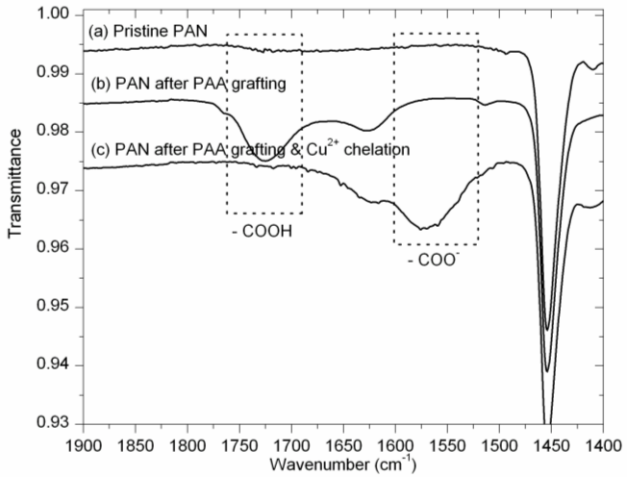

Figure S1: IR spectra of pristine PAN (a), after PAA grafting and Cu^{2+} chelation (b) and after PAA grafting and Cu^{2+} chelation (c)

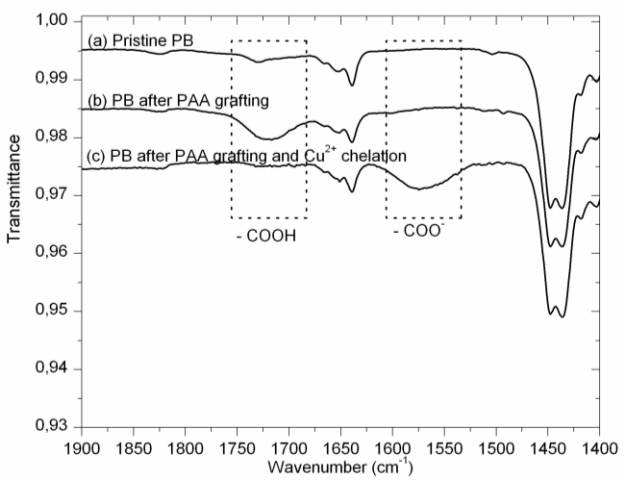

Figure S2: IR spectra of pristine PB (a), after PAA grafting and Cu^{2+} chelation (b) and after PAA grafting and Cu^{2+} chelation (c)

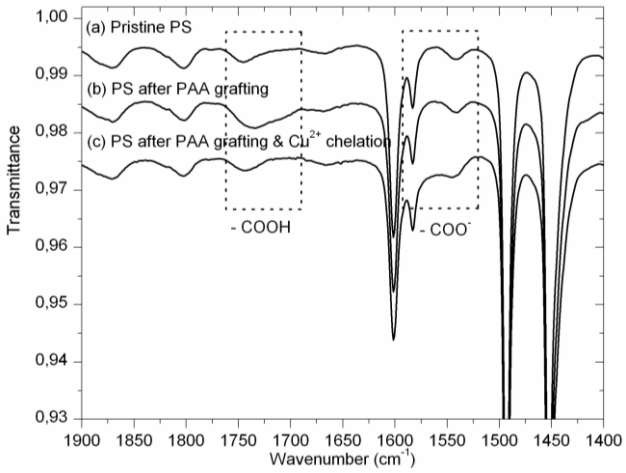

Figure S3: IR spectra of pristine PS (a), after PAA grafting and Cu^{2+} chelation (b) and after PAA grafting and Cu^{2+} chelation (c)

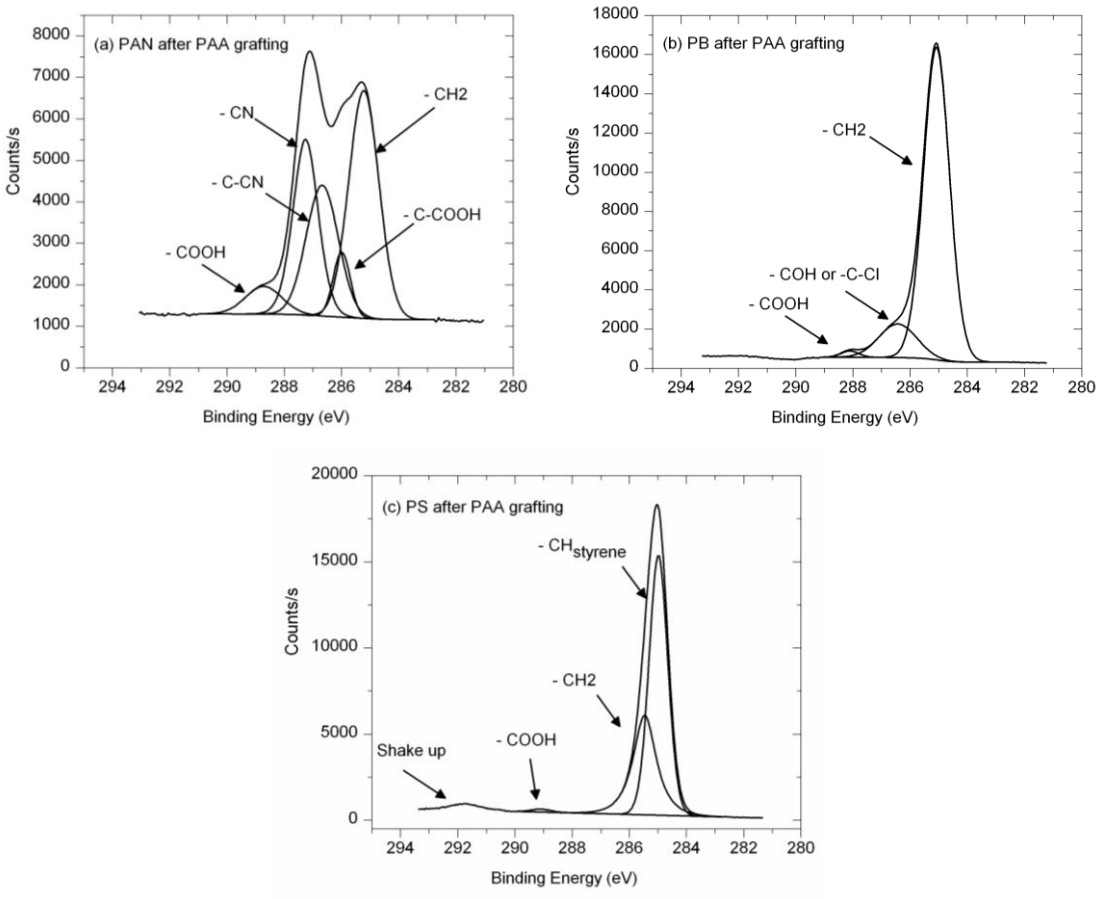

Figure S4: C1s XPS spectra of PANS (a), PB (b) and PS (c) after PAA grafting

- **IR and C1s XPS Characterizations after PAA grafting and Cu chelation and reduction on ABS-PC and PA substrates**

For ABS-PC substrates, the final rinsing step in deionized water (pH close to 5) exhibited both COOH and COO^- signals, respectively at 1720 cm^{-1} and 1558 cm^{-1}, indicating a mixed composition as shown in Figure S5. In the case of the PA substrates, the COOH band was observed around 1720 cm^{-1} whereas the COO^- one was hidden by the polyamide absorption band itself at 1539 cm^{-1}. Immersing the PAA-grafted samples into an alkaline solution was followed by the expected increase of the COO^- and decrease of the COOH bands, which confirmed the grafted carboxylate groups accessibility to external reagents. Besides, immersing these samples into an alkaline solution containing ammonia (0.6 M) and $CuSO_4$,$5H_2O$ (0.1 M solution) allowed to load the PAA grafting film with Cu^{2+} ions thanks to the PAA ion exchange properties. As expected, Figures S5 (1c) and S5 (2c) showed that in that case, the COOH absorption bands totally disappeared whereas COO^- one was observed (18, 22).

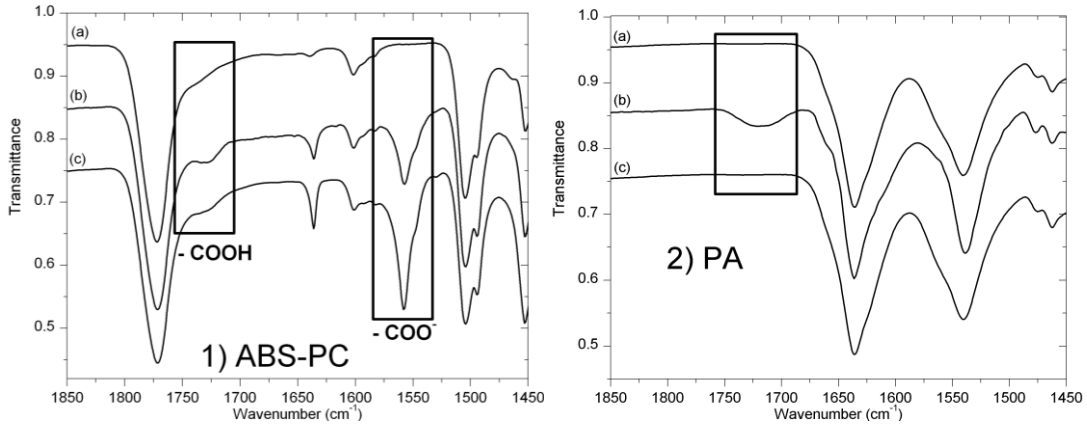

Figure S5: IR Spectra of pristine ABS-PC (1a), after PAA grafting followed by rinsing with an acidic solution (pH=1) (1b) and after Cu^{2+} chelation (1c); IR Spectra of pristine PA (2a), after PAA grafting followed by rinsing with an acidic solution (pH=1) (2b) and after Cu^{2+} chelation (2c)

XPS studies allowed ensuring the presence of the grafted PAA films onto the polymer substrates, as shown in Figure S6 with ABS-PC and PA C_{1s} XPS spectra on pristine polymers and after PAA grafting. For pristine ABS-PC, the C_{1s} core level showed one main peak centered at 284.9 eV, which mainly corresponds to CH and CH_2 aliphatic and phenyl carbons contained in the polycarbonate, polyacrylonitrile, polybutadiene and polystyrene structure and one peak at 286.5 eV, which corresponds to both CN nitrile group contained in the polyacrylonitrile

component and the two phenyl carbons bonded to an oxygen in the polycarbonate component. A third peak centered at 288.7 eV was observed and corresponded to the carbonyl carbons surrounded by three oxygen elements contained in the polycarbonate component. In the PAA-grafted case, in addition to the previous described peaks, a peak at 288.2 eV characteristic of a COOH group was clearly observed. Moreover, according to the XPS analysis, the CH/CN ratio increased after PAA grafting due to the contribution of CH bonds contained in the PAA film. In parallel, the O/C ratio increased and the N/C ratio decreased, which confirmed the grafting of an oxygen-rich species. In the case of the PA substrates, the same conclusions on the addition of a COOH group characteristic peak at 288.2 eV as well as the O/C ratio increased after PAA grafting could be done.

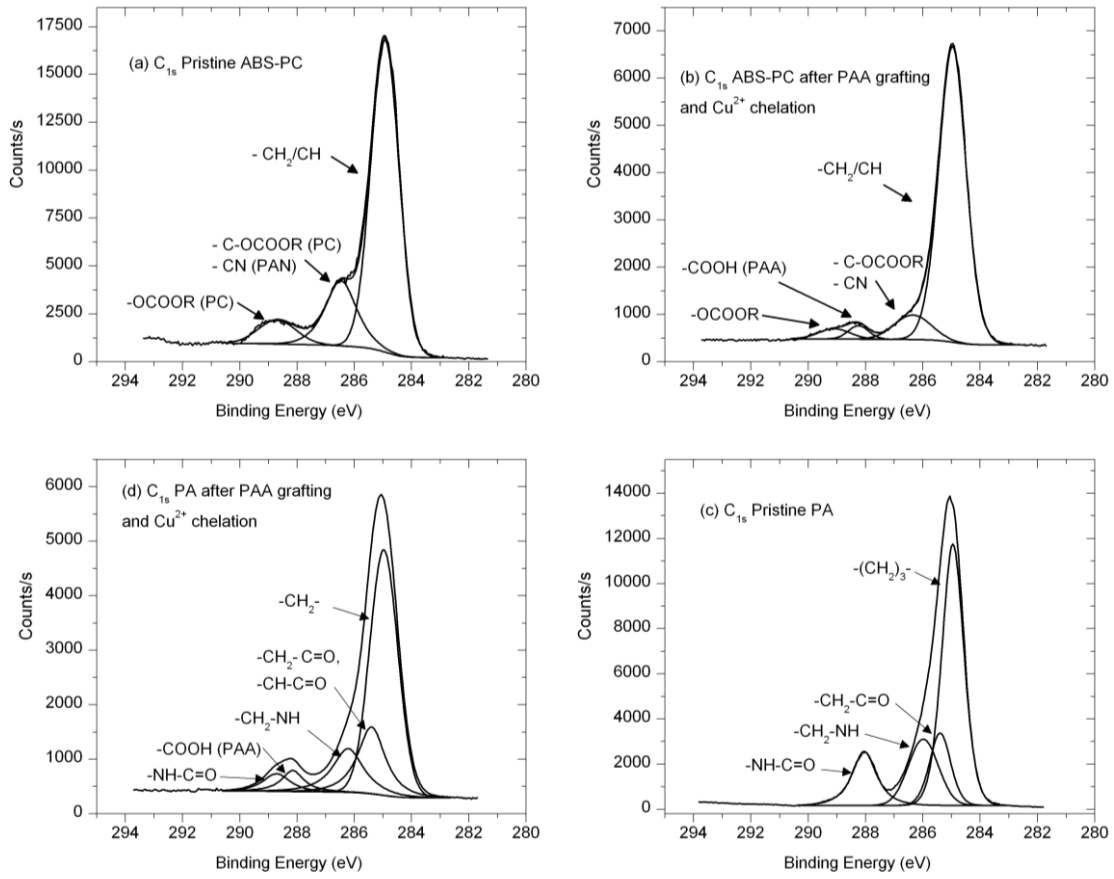

Figure S6: C_{1s} XPS spectra of pristine ABS-PC (a), after PAA grafting and Cu^{2+} chelation (b) and C1s XPS Spectra of pristine PA (c), after PAA grafting and Cu^{2+} chelation (d)

- **Cu2p XPS Spectra after Cu plating**

The plated metallic layers were characterized by XPS measurements. As shown in the Figure S7, the Cu_{2p} spectra indicated that a Cu^0 layer was successfully formed on the ABS-PC and PA substrates. In addition, at the extreme surface, oxygen and carbon elements were still present due to organic residuals coming from the plating bath and in particular from the complexing agent.

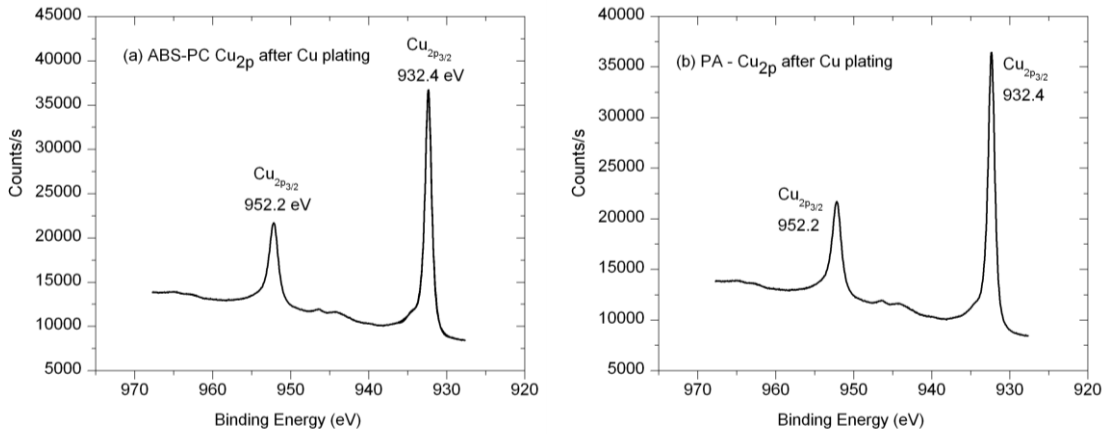

Figure S7: Cu_{2p} XPS spectra of ABS-PC (a) and PA (b) substrates after Cu plating

- **EDX Spectrum of Cu-plated PA substrates**

EDX spectrum analysis for Cu-plated PA substrates also revealed that the metal layer surface is composed only of copper metal.

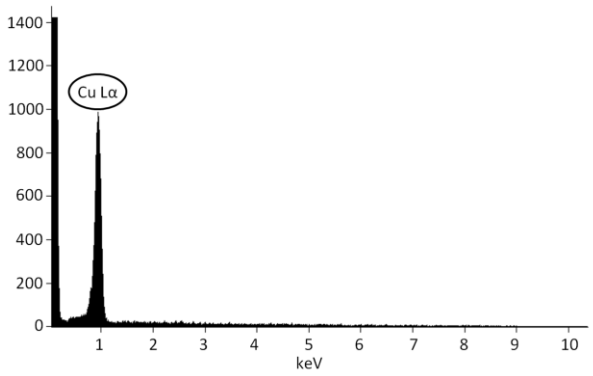

Figure S8: EDX Spectrum of Cu plating on the top of PA substrate

- **I_T-V_b spectrocopy curves**

STM measurements in Ultra High Vacuum environment were used to check the ohmic behavior for both ABS-PC and PA substrates. Several bias spectroscopy curves were acquired on different locations of the samples (covering an area of several hundreds of micrometers square) showing the same electrical behavior. The linear variation of tunneling current (I_T) with bias voltage (V_b) (Figure S9), i.e. the ohmic behavior of I-V characteristic of both plated copper layers showed that the density of states of the sample surfaces (ϕ_s) should be constant. This implies the metal-like behavior of the plated copper layers, both on ABS-PC and PA.

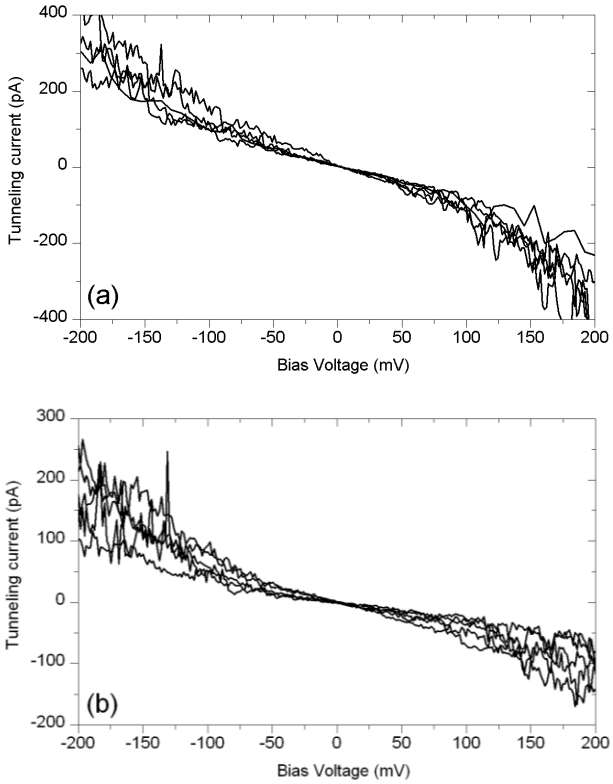

Figure S9: Tunneling current spectroscopy curves acquired on different locations of the samples as a function of the bias voltage for (a) ABS-PC and (b) PA substrates

- **ABS-PC Scotch tape test image**

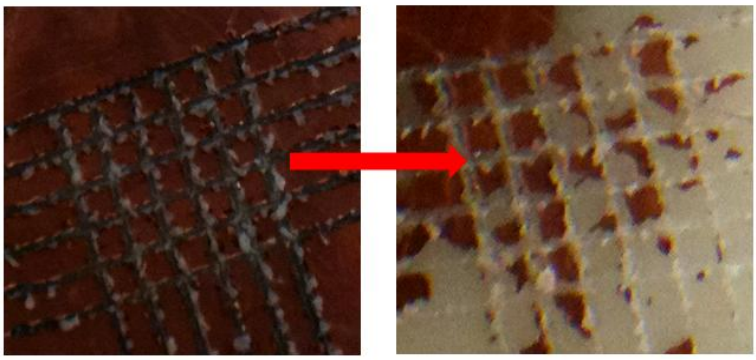

Figure S10. Images of ABS-PC substrates with Cu plating before (left) and after (right) the scotch tape test

3. Surface and interface Issues

In this article, we have demonstrated that initial roughness and surface composition significantly influence the chemical grafting of the aryl radical species and the resulting PAA layer. Besides, electrical properties of the electroless metal layer are directly linked to the PAA grafting deposition rate since higher the PAA grafting rate, higher the metal conductivity.

This article highlights surface and interfaces issues of the polymer grafting by Graftfast™ process and emphasizes the importance to promote the interfacial reaction of aryl radical species onto the substrate surface. Besides, through this article, at equivalent roughness, it is clear that the aryl radical grafting is promoted on hydrophilic substrates containing functional groups such as amine or carboxylic acids when working in aqueous solution. Indeed, this behavior is likely to arise from the better swelling of the surface of a hydrophilic substrate, with respect to a hydrophobic one, by the aqueous reactive mixture which is used for the PAA grafting step. On the contrary, we can imagine that on hydrophobic substrates, working in organic conditions or with wetting agent would promote the aryl radical grafting.

As a matter of fact, at equivalent roughness, wettability and swelling surface properties are the key parameters to understand the Graftfast™ process efficiency. Besides, these properties can be adjusted to improve Graftfast™ process efficiency by either preliminary surface treatment on the substrate surface or varying the surface tension of the reactive mixture.

Several surface preparation processes with the aim at the improvement of the Graftfast™ process efficiency have been patented with the following reference:

T. Berthelot, A. Garcia, S. Roussel and F. Nekelson, Method for preparing an organic film at the surface of a solid substrate with oxidizing processing, *WO2010125190*, 2010/11/04.

4. LIEP process for the metallization of a complex shaped object and made of different materials

As previously introduced, electroless plating is the best method for the metallization of polymers onto all-shaped substrates. As shown in **Figure 31**, the electroless copper plating through the LIEP process of a toy made of different materials perfectly illustrates it but also highlights the surface and interfaces issues previously exposed. Therefore, this toy, representing a lion made of poly(vinyl chloride) (PVC) wearing a cape and holding a racket both made of polyethylene (PE) (Blue parts) was partially plated after the LIEP process.

Indeed, this toy was firstly immersed into a KOH/EtOH solution (5N) during 3 min and sonicated for 5 min into an acidic solution HCl (0.5 N). This pretreatment allowed cleaning the toy but also slightly oxidizing the PVC areas without modifying the PE ones. Then, the LIEP process was applied and the copper plating growth was conformal to the surface but localized on the oxidized PVC area. Contrary to the hydrophilic PVC surfaces, PAA grafting was not promoted and the copper plating not observed on hydrophobic PE surfaces.

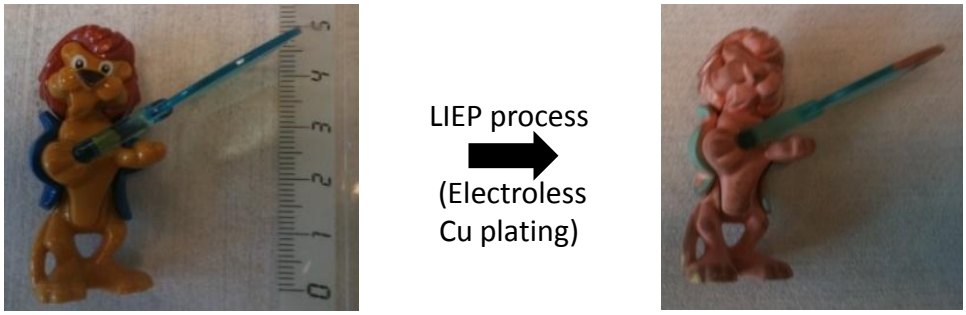

Figure 31 : Electroless copper plating of a toy via the LIEP process

IV. Localized LIEP via lithographic based methods

1. Introduction

Based on the same working conditions than for the electroless plating of ABS, ABS-PC and PA, we extended the LIEP process to flexible and transparent poly(ethylene terephtalate) (PET) and Poly(vinylidene fluoride) (PVDF) substrates sheets. Besides, as shown below, we have combined simple and lithographic methods with the LIEP process in order to obtain a selective polymer covalent grafting which induced the selective copper deposition. Indeed, localized modifications of material surfaces has grown in interest over the three past decades and are now used in many industries such as automotive, biotechnology, aerospace or electronics and the fabrication of metallic circuit patterns on polymer substrates becomes extremely important especially for the manufacturing processes of flexible electronics.

2. Fabrication of micrometric copper patterns onto PET and PVDF sheets

A. Garcia, J. Polesel-Maris, P. Viel, S. Palacin, T. Berthelot, Localized Ligand Induced Electroless Plating (LIEP) Process for the fabrication of copper patterns onto flexible polymer substrates, *Adv. Funct. Mater.* **2011**, *21*, 2096.

To prove the versatility of the LIEP process, localized metallization was obtained via two simple lithographic methods. The first one was based on classical photolithography using a positive photoresist as a mask to prevent the covalent grafting of PAA in designated areas of the polymer substrate. For the second one, the mask was provided by direct printing of the mask with a commercial laser printer. In both cases, the mask was lifted off before the copper electroless plating step. We demonstrated here the benefits of the localized LIEP process compared to physical vapor deposition (PVD) associated with conventional photolithography by reducing the steps number and by using only the amount of copper necessary to metalize the designed pattern (contrary to classical lift off which discards a significant amount of metal deposited on top of the resist) which provides ecological benefits.

ADVANCED FUNCTIONAL MATERIALS
www.afm-journal.de

Materials Views
www.MaterialsViews.com

Localized Ligand Induced Electroless Plating (LIEP) Process for the Fabrication of Copper Patterns Onto Flexible Polymer Substrates

*Alexandre Garcia, Jérôme Polesel-Maris, Pascal Viel, Serge Palacin, and Thomas Berthelot**

The "ligand induced electroless plating (LIEP) process" is a simple process to obtain localized metal plating onto flexible polymers such as poly(ethylene terephtalate) and polyvinylidene fluoride sheets. This generic and cost-effective process, efficient on any common polymer surface, is based on the covalent grafting by the GraftFast process of a thin chelating polymer film, such as poly(acrylic acid), which can complex copper ions. The entrapped copper ions are then chemically reduced in situ and the resulting Cu^0 species act as a seed layer for the electroless copper growth which, thus, starts inside the host polymer. The present work focuses on the application of the LIEP process to the patterning of localized metallic tracks via two simple lithographic methods. The first is based on a standard photolithography process using a positive photoresist masking to prevent the covalent grafting of PAA in designated areas of the polymer substrate. In the second, the patterning is performed by direct printing of the mask with a commercial laser printer. In both cases, the mask was lifted off before the copper electroless plating step, which provides ecological benefits, since only the amount of copper necessary for the metallic patterning is used.

1. Introduction

The use of organic materials combined with electroless metal deposition in the fabrication of microelectronics devices, bioelectronics devices, and portable electronics has generated growing interest during the last few decades.[1–7] Consequently, the fabrication of metallic circuit patterns on polymer substrates has become extremely important for the manufacturing processes of flexible electronics. Over the three past decades, photolithography has been the most used method for the surface patterning of polymers. In most cases, surface patterns are generated by selectively exposing a surface coated by a photosensitive resin to UV irradiation through a mask, or patterned by an electron beam. Depending on the method, the irradiation step is then followed by the removal of exposed areas in an adapted solvent.[8,9] Subsequently, physical vapor deposition (PVD) is used for the deposition of the target metal on the whole surface, followed by a lift-off step which selectively removes the remaining photoresist domains covered by the metal layer, leaving on the surface the metallic tracks defined on the free photoresist areas. Hence, a metallic pattern is obtained. It is noteworthy that this widely applied process clearly uses more metal than necessary, since the PVD step concerns the whole surface. Numerous alternative processes have been recently investigated such as ink-jet printing,[10–17] microcontact printing (μCP),[1,18–22] and screen printing[23–25] which all lead to less wastage of metal, but are not yet available at industrial scale.

In the present paper, a simple protocol to obtain selective metal plating deposition on polymers based on the ligand induced electroless plating (LIEP) process is described.[26–28] In contrast to the lift-off-based techniques previously described, this generic and cost-effective process does not use more metal than necessary for the metallic pattern itself. A thin chelating polymer film composed of poly(acrylic acid) (PAA), is first covalently grafted by the GraftFast process[26–30] onto polymer surfaces. Then, copper ions are chelated into the PAA layer and are then chemically reduced in situ to act as catalyst for the electroless metallic growth which starts inside the host polymer. The so-created interphase can be described as a composite where components are melted together at the atomic scale. Such an interphase provides similar mechanical adhesion compared to classical chromic acid treatment to the metal layer,[1,31–35] thanks to the interdigitation between the two materials. Moreover, the LIEP process is simple to implement and suitable for a wide range of polymer substrates,[26,29,30,36] while standard deposition methods are either specific to one kind of polymer or not available at industrial scale.

In this study, the LIEP process is adapted to provide micrometric copper patterns onto flexible polymer surfaces such as poly(ethylene terephtalate) (PET) and polyvinylidene fluoride (PVDF) sheets through a covalent grafted copper seed layer. Both polymers have been thoroughly investigated for their

A. Garcia, Dr. P. Viel, Dr. S. Palacin, Dr. T. Berthelot
SPCSI Chemistry of Oxides Surfaces and Interfaces Group
CEA, IRAMIS, Gif-Sur-Yvette, 91191, France
E-mail: thomas.berthelot@cea.fr
Dr. J. Polesel-Maris
SPCSI Oxides Interfaces and Surfaces Group
CEA, IRAMIS, Gif-Sur-Yvette, 91191, France

DOI: 10.1002/adfm.201100041

dielectric and specific properties (such as piezoelectricity in the PVDF case), and many papers have already reported PET and PVDF electroless plating for electromagnetic interference (EMI) applications or sensors applications avoiding conventional PVD. However, the reported processes are either extremely complicated to perform with numerous steps or without any robust bonding of the final metal layer, preventing a strong adhesion.[15,22,37–44]

To obtain metal patterns, two cost-effective lithographic methods have been combined with the LIEP process and are described in this work (**Figure 1**). The first method (Method A) uses a positive photoresist resin as a mask, allowing sub-micrometer patterning,[45–47] whereas the second (Method B) relies on a 1200 dpi laser printer for the direct printing of the mask on the flexible polymer sheets, allowing 20 µm-resolution features. The final features resolution also depends on the thickness of the electrolessly deposited layer. In both cases, the mask is lifted off before the copper plating, thus avoiding any metal waste. Combined with the LIEP process which reduces chemicals waste, these lithographic processes provide a selective copper growth which drastically reduces the effluent quantities and likewise the cost of copper material compared to conventional photolithography processing combined with PVD.

The copper patterns were characterized by optical and scanning electron (SEM) microscopy and by Cu_{2p} XPS mapping to check the conformity between the mask and the copper plated patterns. Copper resistivity was measured by a four-point probe. Finally, the electrical properties of the obtained flexible copper pattern in response to a controlled mechanical stress were studied.

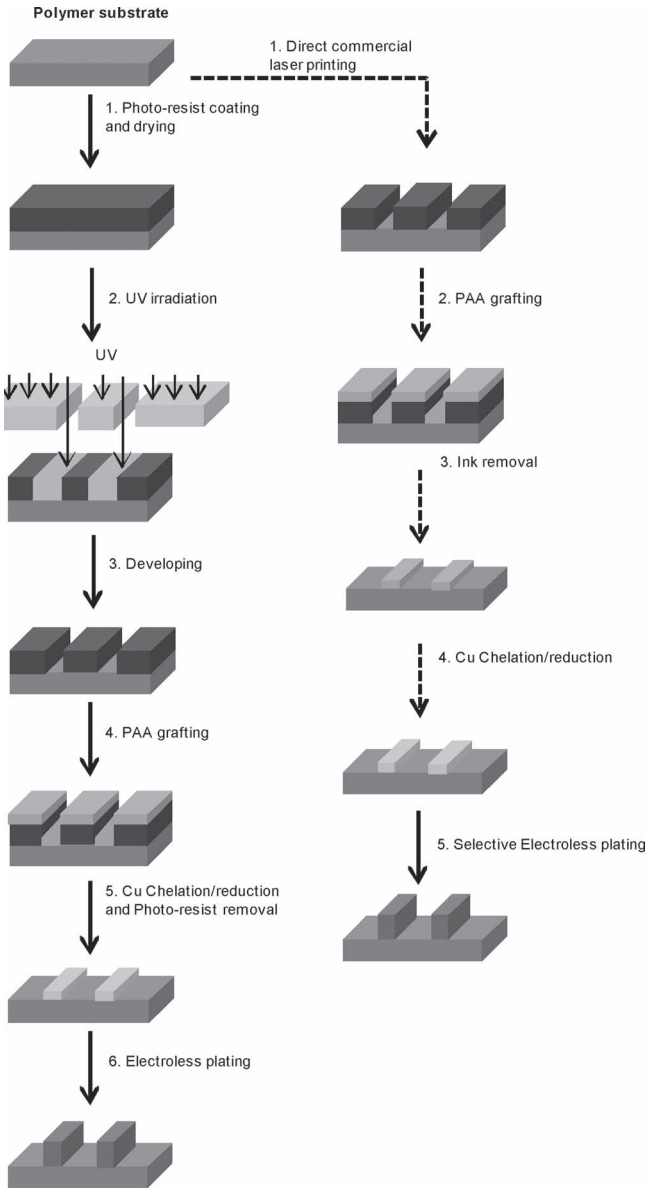

Figure 1. Localized LIEP process through two different lithographic methods: Photolithographic method (Method A, left path) and direct laser printing based method (Method B, right path).

2. Results and Discussions

Unless otherwise mentioned, all the results and discussions are based on Method A using the photoresist coating, as described in the Experimental Section.

2.1. Substrates Cleaning

Polymer surfaces are generally prone to organic pollution which could be detrimental to the LIEP process. Our PET sheets were thus submitted to a common industrial detergent cleaning (TFD_4) which is considered sufficient for removing most of the organic pollutants since we relied on a rinsing procedure commonly applied in industry before classical metallization. Similarly, in the case of the PVDF sheets, a KOH rinsing treatment was used for cleaning, but also for making the PVDF substrates more hydrophilic by surface oxidation. Indeed, the contact angle of PVDF decreased from 88 ± 6° to 65 ± 4° without any significant change in the substrate roughness (12.7 ± 0.2 nm before and 12.8 ± 0.3 nm after the KOH rinsing treatment for a 2 µm × 2 µm area). That decrease of the contact angle is important since a high wettability has been shown to promote the PAA grafting on other hydrophobic polymers.[27] In the PET case, the contact angle after detergent cleaning was equal to 80 ± 5° and sufficient to allow the PAA grafting.

2.2. Negative-Tone Metal Pattern Achievement Using the Positive Photoresist (Method A)

Method A is based on hard masking by applying the mask support on the surface coated by a positive photoresist. The minimal resolution depends of the mask feature resolution. With the chromium/glass mask, the final copper pattern resolution is about 2 µm[48] whereas, with the mask printed on a copier PET transparency film, the resolution of about 20 µm is determined by the laser printer. We mainly used that latter method to produce the flexible copper features (fine tracks terminated by connecting pads) adapted for measuring the electrical properties under mechanical deformation.

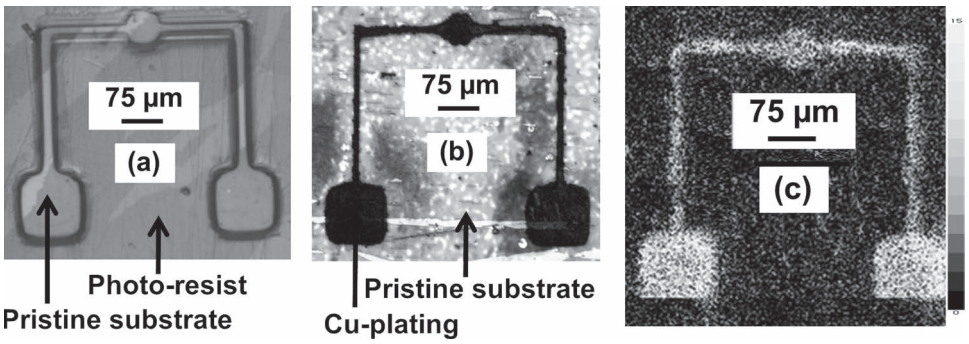

Figure 2. a) Optical images of a negative-tone metal pattern (after photoresist development), b) the corresponding metal pattern after copper plating, and c) the Cu_{2p} XPS mapping of the same copper pattern onto PET sheets.

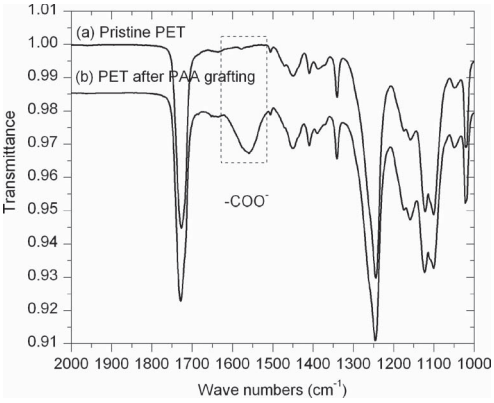

Figure 3. IR spectra of a) pristine PET and b) the same material after PAA grafting.

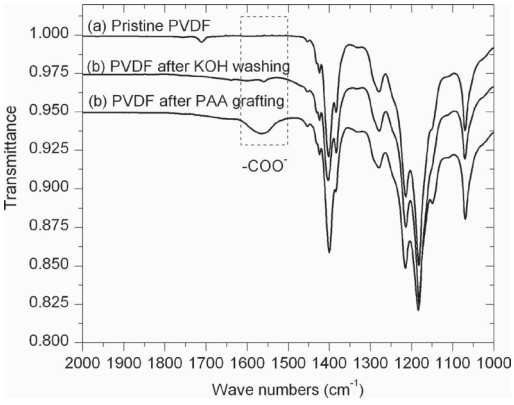

Figure 4. a) IR spectra of pristine PVDF and b) the same material after PAA grafting.

2.3. Characterization of PAA Covalent Grafting and Cu^{2+} Chelation and Reduction Onto Positive Photoresist Patterned PET and PVDF Sheets

Once the negative-tone metal pattern is obtained (**Figure 2**a), the first step of the LIEP process consists of the PAA grafting onto the modified PET and PVDF sheets, which were characterized by XPS and IR spectroscopy. At this stage, the PAA grafting is confirmed by IR spectroscopy on the pristine area, but is also expected on the photoresist-coated areas. We focused the analysis onto the pristine areas which constitute the negative-tone metal pattern.

Figure 3 and **Figure 4** show COO^- signals for both PET and PVDF substrates, at 1559 and 1563 cm^{-1}, respectively, indicating the PAA grafting. The presence of grafted PAA films onto the polymer surfaces was also demonstrated by XPS, on homogeneous samples. **Figure 5** displays XPS spectra on pristine PET and whole PAA-grafted PET sheets. For pristine PET the C_{1s} core level shows one main peak centered at 284.9 eV, which mainly corresponds to phenyl carbons contained in PET. A second peak centered at 286.4 eV corresponds to aliphatic carbons near the ester group and, finally, the third peak at 288.8 eV is characteristic of the PET ester groups.

For modified PET sheets, two additional peaks centered at 285.4 eV and 289.3 eV corresponding to the aliphatic carbon near the carboxylic group and the carboxylic group itself in PAA are observed and indicate the PAA grafting.[49] Those results are consistent with our previous studies on ABS, ABS-PC, or polyamide surfaces.[26,27] However, the whole experimental procedure was improved without any loss in the efficiency of the grafting: the acrylic acid monomer concentration was reduced by four fold, the reaction was carried out at room temperature instead of 38 °C, and the rinsing treatment time was 50% lower. All these process improvements allow important reductions in industrial costs. As shown in the Supporting Information, the Cu_{2p} spectra analysis confirmed the Cu^{2+} chelation obtained by

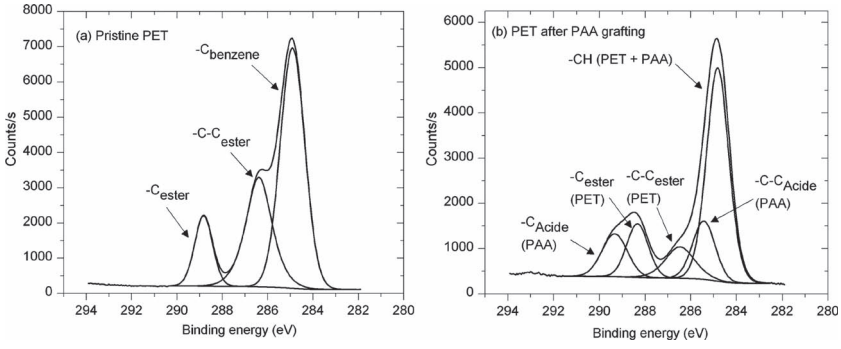

Figure 5. a) C_{1s} XPS spectra of pristine PET and b) the same material after PAA grafting.

immersion into an alkaline Cu^{2+}/NH_3 solution by three main peaks corresponding to $Cu_{2p3/2}$ (934.6 and 933 eV), Cu_{2p} satellites (from 938 to 947 eV) and $Cu_{2p1/2}$ (953.1 and 954.5 eV) core level binding energies. The two peaks observed for the $Cu_{2p3/2}$ and $Cu_{2p1/2}$ are probably due to different conformations of the PAA chains which induced differences in the Cu environment and its binding energy to the carboxylate groups. However, the presence of particles of copper oxides cannot be fully excluded.[50]

Reduction of Cu^{2+} ions was obtained by immersion of the Cu–PAA film in an alkaline solution of sodium borohydrure $NaBH_4$ and confirmed by XPS measurements. After immersion in $NaBH_4$, the peak of $Cu_{2p3/2}$ core level shifted partially toward lower energy and the Cu_{2p} satellites characteristic of Cu^{2+} ions disappeared (For details, see Supporting Information). As previously described, during the reduction step, the remaining photoresist was removed, generating a pattern of catalytic-Cu^0 particles. This pattern defines the seedbed of the copper metal pattern terminated by specific growth of the copper plated layer. We emphasize that the remaining photoresist has not been protected from the ambient light during the rinsing treatment after PAA grafting, chelation, and reduction steps of the LIEP process. This shows that the large broadband light (containing UV photons) exposure ensures solubility in those basic conditions. Hence, the reduction step, which was carried out in a sodium hydroxide solution at 70 °C for 10 min, allowed the entire dissolution of the ambient light exposed photoresist and led to the formation of the catalytic Cu^0 particles pattern.

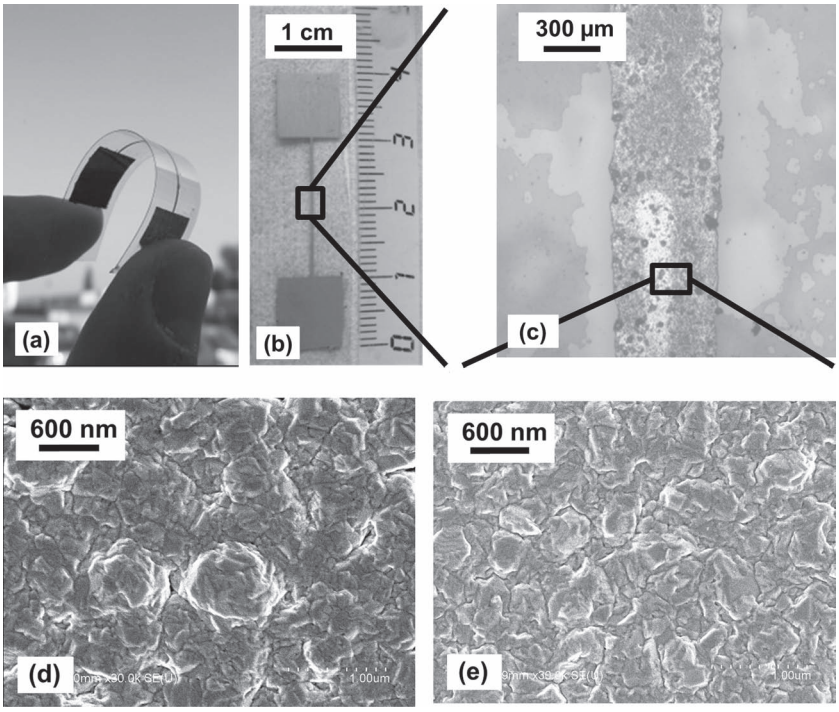

Figure 6. a–b) Pictures of Cu-patterned PET, c) Optical image of the same Cu-patterned PET. d–e) SEM images of the same Cu-patterns onto PET (d) and PVDF (e) substrates with a 600 nm scaled top view

2.4. Selective Copper Plating

Finally, the obtained metallic layers were characterized after Cu plating. The Cu_{2p} spectra indicate that Cu^0 was successfully formed on the polymeric substrates. As shown in **Figure 6**d and Figure 6e, the copper plated layer consists of dense and continuous tracks. AFM analysis showed that the plated copper particles size was between 10 and 30 nm for both substrates, which already proved enough to obtain good electrical properties (for more details see Supporting Information).[27]

As illustrated by optical images (Figure 2b) and Cu_{2p} XPS mapping (Figure 2c) of a metal pattern onto flexible PET sheets, the selective copper plating was conformal to the negative-tone metal pattern (Figure 2a). As shown in Figure 2c, Cu_{2p} XPS mapping at the micrometer scale demonstrated that copper was present only on the negative-tone metal pattern. Besides, Cu_{2p} XPS mapping (Figure 2c) confirmed that no copper is present outside of the copper patterns, avoiding electrical leakages between the metallized areas. A copper RFID coil is presented in Supporting Information as another example of the process conformity. Due to the isotropic nature of the electroless plating growth process[51] using the chromium/glass mask, the smallest features that can be obtained with this method were mainly limited by the thickness of the metal layer (1 µm here) and not by the fabrication mask step for this particular case. Although the copper pattern fabrication was not performed in cleanroom environment, the best resolution achieved about 2µm, whereas with a mask printed on a copier transparency film, the smallest features reached around 20 µm.

The adhesion between the copper plated layer and the polymer substrates was studied by the most demanding industrial adhesion test: the standard ASTM D3359 Scotch tape test. This measurement has been carried out on substrates with a 1 µm-thick homogeneous copper plated layer (measured by profilometry) in order to validate the adhesion results. For copper plated PET substrates, none of the squares was removed whereas for PVDF substrates 25% of the squares were removed (for details, see Supporting Information). As explained in a previous paper,[27] that slight adhesion difference can be attributed to a higher grafting density in the PET case which induces a higher mechanical interlocking effect between the copper metal film and its substrate and leads to a better adhesion.[26,27]

2.5. Electrical Properties Measurements on Flexible Sheets

Electrical properties were measured using specially designed samples exhibiting a linear 400 µm-wide track connected to two large pads for easier electrical contact (See Supporting Information). Those samples were prepared using Method A

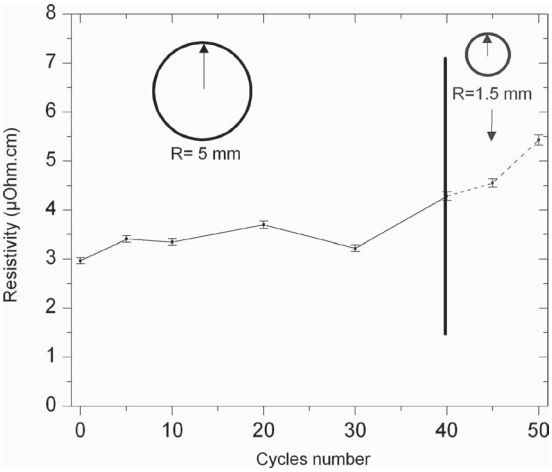

Figure 7. Resistivity measurements of Cu wires grafted on PET sheets and submitted to 40 cycles with the 5 mm-radius cylinder, followed by 10 cycles with the 1.5 mm-radius cylinder

with a laser printed transparency film mask and are shown in Figure 6a and Figure 6b. Without any mechanical stress, the electrical resistivity of the copper wire grafted onto the PET substrates was measured at 3.0 μΩ cm, i.e., within the range classically measured on electroless copper surfaces (2–3 μΩ cm).[27] The effect of the mechanical deformation on this resistivity was studied by bending the flexible copper tracks grafted onto the PET sheets around cylinders. Two different radii of curvature respectively equal to 5 and 1.5 mm were used. As shown in **Figure 7**, 30 cycles of repetitive strain around a 5 mm-radius cylinder did not induce any change in metal resistivity. A slight resistivity increase was, however, observed between 30 and 40 cycles, which was even more obvious when 10 cycles around the 1.5 mm-radius cylinder were added to the previous deformations. The resistivity increase is then promoted by high numbers of deformations cycles and low radii of curvature. Nevertheless, the copper patterns fabricated on flexible PET foils can withstand substantial mechanical deformation with weak conductivity change for cylinders with a radius superior or equal to 5 mm. The ability of copper tracks fabricated on flexible PET foils to tolerate tensile strain was attributed to the strong adhesion between the copper wire and the substrates and the copper particles nanometric size, as previously described.

2.6. Copper Wires Onto Flexible PET Substrates Fabricated Using Method B

The direct laser printing of an ink combined with LIEP proved as efficient as classical photolithography + LIEP to provide localized metallization of polymer substrates, except for the achieved resolution. Indeed, electrical properties were similar to the ones obtained with the photoresist based process (Method A). This very cost effective method, which also prevents unnecessary metal use and waste production, is significantly simpler to implement than the photolithographic route (Method A), with a minimum resolution of 20 μm of metal patterning. In Supporting Information, optical images illustrate the copper patterns obtained using direct laser printing of the mask. These results show the versatility of the LIEP process, which can be successfully combined with two distinct patterning methods for localized metallization.

3. Conclusions

We described two methods based on the LIEP process to obtain copper patterns onto flexible polymer substrates. It has been shown that, whatever the patterning technique, the LIEP process allows selective copper plating with good and stable electrical properties onto flexible polymer substrates. Hence, the LIEP process combined with any of those patterning methods could be an excellent alternative to classical processes for the cost-effective fabrication of large-area plastic electronics devices. Indeed, these simple and cost-effective methods work on smooth surfaces; copper growth is localized and conformal to the mask; electrical properties are stable and close to bulk values, and copper patterns fabricated on these flexible substrates withstand substantial mechanical deformation with slight loss in performance.

4. Experimental Section

Materials: 100 μm-thick Polyethyleneterephtalate (PET) sheets of technical quality were obtained from Tektronix as standard transparency films and used as polymer substrates for the localized plating. 25 μm-thick polyvinylidene fluoride (*β*-PVDF) sheets were obtained from Piezotech SA. An industrial detergent TFD_4 (Franklab) was used to clean the PET substrates. The liquid photoresist (POSITIV 20, CRC Industries Europe) was purchased from Radiospares and the photoresist irradiation has been carried out using a Sylvania UV-A lamp (315–400 nm, < 120 μW cm^{-2}). All chemicals were used as received. 1–4-diaminophenylene dihydrochloride (Fluka, ≥99%), acrylic acid (Sigma Aldrich, ≥99%), sodium nitrite (Fluka, ≥99%) and iron powder (Prolabo VWR, 98%) were used for the poly(acrylic acid) grafting using the GraftFast technology.[29,30] Cupric sulfate $CuSO_4{\cdot}5H_2O$ (Fluka, ≥99%), sodium borohydride powder (Sigma Aldrich, ≥98.5%) were used for the copper chelation and reduction. For the electroless metal deposition, an industrial copper plating bath (M Copper 85 supplied by MacDermid) was used.

Photolithographic Process Combined with the LIEP Process Onto Flexible Polymer Sheets (Method A): As shown in Figure 1, copper patterns were obtained by combining photolithography and the LIEP process. Photolithography was used to provide free areas on the substrate and promote the direct grafting of PAA in accordance with the mask. The copper features were then obtained by applying the LIEP process after lifting-off the remaining photoresist. Hence, the copper layer growth is observed only on the areas where PAA is directly grafted onto the polymer substrate. The process will be described step-by-step below.

All the polymer substrates were cleaned beforehand; PET substrates were sonicated for 15 min in an industrial detergent (TFD_4), and PVDF substrates were immersed into a KOH/EtOH solution (5N) for 15 min and sonicated for 10 min in an acidic solution of HCl (0.5 N). This rinsing treatment also allowed the slight oxidization of the PVDF surface without modifying its roughness.[52]

The photolithographic process is divided into three steps.

1) Photoresist coating and drying: All the polymer substrates were sprayed by the photoresist (POSITIV 20) from a distance of 20 cm, giving a typical coating thickness of 6–8 μm with a bluish color.

Then, the substrates were placed immediately in a dark oven and the drying temperature was increased slowly to 70 °C and maintained for 15 min. This step allowed homogenizing the thickness and the adhesion of the photoresist film.

2) Photoresist exposure and developing: The photoresist coating was then selectively irradiated by Sylvania UV-A lamps (120 μW cm^{-2}) through two different kinds of masks in direct contact with the photosensitive coating to provide different patterns resolution:[48,53] a) a rigid chromium/glass mask which offers, under the right conditions, sub-micrometric resolution mask features and b) a mask printed on a copier PET transparency film (same material as the working substrate) with resolution features defined by the laser printer resolution (1200 dpi = 20 μm). The irradiation time was 3 and 5 min respectively. The lamps were positioned at a distance of 5 cm from the masks.
3) Photoresist developing: The UV exposed areas of the photoresist coating were then dissolved by immersion in a sodium hydroxide bath (0.06 M) at ambient temperature under stirring for approximately 5 min. After developing, the polymer substrates were rinsed thoroughly with distilled water. Figure 2a displays the resulting positive photoresist coating.

The polymer substrates coated by a selective photoresist layer were submitted to the LIEP process which is divided into three steps:

1) Covalent grafting of poly(acrylic acid) on polymersubstrates: 1–4-phenylenediammonium dihydrochloride (1.81 g) was dissolved in a HCl solution (0.5 M, 100 mL) to obtain Solution 1. Under stirring, $NaNO_2$ (0.1 M, 200 mL) was added stepwise to the Solution 1 (100 mL) in order to synthesize the aryldiazonium salt. Acrylic acid (25 mL) was then introduced into this solution, followed by iron powder (15 g) as reducing agent of the aryldiazonium salts. Finally, different pieces of polymer sheets were introduced in the beaker. The final solution was dark brown. After immersion for 120 min at room temperature, the polymer substrates were removed from the reacting bath and sonicated twice for 10 min in alkaline solution (NaOH, 0.1 M) and deionized water. This rinsing treatment allowed discarding most of the physisorbed matter.[26,27]
2) Chelation/reduction of metallic cations and removal of the remaining photoresist: PAA-modified polymer substrates were then immersed for 10 min in an alkaline (NH_3, 0.6 M) copper sulphate $CuSO_4{\cdot}5H_2O$ (0.1 M) solution at room temperature to induce an ion-exchange process and provide copper carboxylates within the grafted film. Afterwards, samples were rinsed with alkaline solution (NaOH, 0.1 M) for 1 min. In order to reduce Cu^{2+} ions previously chelated by the carboxylates groups contained in grafted PAA films, the samples were immersed into a sodium borohydride ($NaBH_4$) (0.1 M)/ NaOH (0.1 M) solution at 70 °C for 10 min. During the reduction step, the removal of the remaining photoresist was achieved. Indeed, during the rinsing treatment after the PAA grafting, and during the chelation and reduction steps of the LIEP process, the remaining photoresist has been exposed to the ambient light. This shows that broadband light of the lab emits enough UV exposure to reach the required solubility in those basic conditions. Hence, this reduction step allowed obtaining a positive pattern of catalytic-Cu^0 particles which was then used for the electroless growth of the copper plated layer.
3) Electroless copper deposition: The patterned surface-activated substrates were finally placed in the industrial electroless copper plating bath (M Copper 85). Formaldehyde HCHO was the reducing agent, and optimum conditions were: copper content 2 g L^{-1}, HCHO/Cu mass ratio = 2, pH 13, working temperature 48 °C to get a deposition rate of ca 4 μm h^{-1}. The polymer substrates were left in the bath for various times. Figure 2b displays the resulting patterned copper films.

Direct Laser Printing of the Negative Tone Metal Pattern Combined with the LIEP Process Onto Flexible Polymer Sheets (Method B): As shown in Figure 1, this alternative method relied on the direct negative tone printing of the mask pattern by using a commercial laser printer (HP LaserJet P3005 PS) instead of photolithography. This extremely cost effective method is, however, limited by the laser printer resolution of about 20 μm (1200 dpi). The LIEP process was then applied to the polymer sheets which were selectively coated by the laser ink. In this case, the laser ink was removed after the PAA grafting by an ethanol rinsing treatment for 5 min, instead of during the reduction step like in the photolithographic method (Method A). After the copper chelation and reduction steps, the copper growth initiated by the catalytic-Cu^0 particles occurred selectively and the expected copper pattern was obtained.

Characterization: Surface characterization methods: Infrared spectra were recorded on a Bruker Vertex 70 spectrometer equipped with an attenuated total reflection (ATR) Pike–Miracle accessory. The detector was a MCT working at liquid nitrogen temperature. The spectra were obtained after 256 scans at 2 cm^{-1} resolution.

XPS and mapping XPS studies were performed with a KRATOS Axis Ultra DLD spectrometer, using the monochromatized Al Kα line at 1486.6 eV. The pass energy of the analyzer was kept constant at 20 eV for C1s core level scans. The photoelectron take-off angle was 90° with respect to the sample plane, which provides an integrated sampling probe depth range from 7 to 20 nm for our substrates.

Pristine and copper plated polymer substrates were imaged by AFM in contact mode with a Molecular Imaging PicoSPMLe commercial AFM microscope (PicoScan 2100 controller, Scientec, France) using a commercial pyramidal Si tip (mounted on a 225 μm long single-beam cantilever and having a spring constant of about 0.2 N m^{-1}). The scan rate was in the range of 1 Hz with a scanning density of 512 lines per frame. The AFM was mounted on a floating table to achieve vibration isolation during investigations. The roughness values of the scans were calculated using the Gwyddion 2.19 SPM software. The scanning electron microscopy images were recorded by a Hitachi S4800 equipped with a Field Emission Gun (FEG-SEM).

Mechanical Adhesion Test: The adhesion between the metallic layer and the polymer sheets was studied by the standard ASTM D3359 Scotch tape test (cross-cut tape test) which consists in applying and removing pressure-sensitive adhesive tape over 16 cross-hatched squares of 1 mm × 1 mm made in the film by an Elcometer Cross Hatch cutter (Elcometer 107 X-Hatch ASTM Kit). That well-used test allows direct comparison of the adhesion of films obtained under various conditions on similar substrates.

Electrical Properties Measurements: In every case, electrical properties were measured on tracks with the following dimensions: length = 2 cm, width = 400μm and height = 1μm measured by profilometry, and terminal pads of 1 cm^2 for electrical contact. An example of a track is illustrated on Figure 6. The resistivity of the wire was measured by means of a four-point probe set-up using a home-built constant current source as described in Keithley's handbook.[54] Electrical properties of the copper tracks were also studied under mechanical stress by measuring the electrical resistivity while bending the polymer sheets around cylinders with two radii of curvature equal to 5 and 1.5 mm respectively. The copper wires grafted on the polymer sheets were submitted to 50 cycles of repetitive strain around the cylinders (40 cycles with the 5 mm-radius cylinder, followed by 10 cycles with the 1.5 mm-radius cylinder).

Supporting Information

Supporting Information is available from the Wiley Online Library or from the author.

Received: January 6, 2011
Revised: February 7, 2011
Published online: April 12, 2011

[1] D. Zabetakis, W. J. Dressick, *ACS Appl. Mater. Interfaces* **2009**, *1*, 4.
[2] B. L. Hassler, T. J. Amundsen, J. G. Zeikus, I. Lee, R. M. Worden, *Biosens. Bioelectron.* **2008**, *23*, 1481.

[3] N. Kohli, B. L. Hassler, L. Parthasarathy, R. J. Richardson, R. Y. Ofoli, R. M. Worden, I. Lee, *Biomacromolecules* **2006**, *7*, 3327.
[4] L. A. Bottomley, *Anal. Chem.* **1998**, *70*, 425R.
[5] X. Q. Liu, H. X. Chang, Y. Li, W. T. S. Huck, Z. J. Zheng, *ACS Appl. Mater. Interfaces* **2010**, *2*, 529.
[6] Y. N. Li, Y. L. Wu, B. S. Ong, *J. Am. Chem. Soc.* **2005**, *127*, 3266.
[7] T. Someya, T. Sekitani, S. Iba, Y. Kato, H. Kawaguchi, T. Sakurai, *Proc. Natl. Acad. Sci. U. S. A.* **2004**, *101*, 9966.
[8] Z. H. Nie, E. Kumacheva, *Nat. Mater.* **2008**, *7*, 277.
[9] J. H. Moon, J. Ford, S. Yang, *Polym. Adv. Technol.* **2006**, *17*, 83.
[10] L. Yang, A. Rida, R. Vyas, M. M. Tentzeris, *IEEE Trans. Microwave Theory Tech* **2007**, *55*, 2894.
[11] F. Bessueille, S. Gout, S. Cotte, Y. Goepfert, D. Leonard, M. Romand, *J. Adhes.* **2009**, *85*, 690.
[12] S. Busato, A. Belloli, P. Ermanni, *Sens. Actuators, B* **2007**, *123*, 840.
[13] K. Cheng, M. H. Yang, W. W. W. Chiu, C. Y. Huang, J. Chang, T. F. Ying, Y. Yang, *Macromol. Rapid Commun.* **2005**, *26*, 247.
[14] B. J. de Gans, P. C. Duineveld, U. S. Schubert, *Adv. Mater.* **2004**, *16*, 203.
[15] D. P. Li, D. Sutton, A. Burgess, D. Graham, P. D. Calvert, *J. Mater. Chem.* **2009**, *19*, 3719.
[16] H. Sirringhaus, T. Kawase, R. H. Friend, T. Shimoda, M. Inbasekaran, W. Wu, E. P. Woo, *Science* **2000**, *290*, 2123.
[17] C. C. Tseng, C. P. Chang, Y. Sung, Y. C. Chen, M. D. Ger, *Colloids Surf., A* **2009**, *339*, 206.
[18] D. Aldakov, Y. Bonnassieux, B. Geffroy, S. Palacin, *ACS Appl. Mater. Interfaces* **2009**, *1*, 584.
[19] D. J. Garrett, J. Lehr, G. M. Miskelly, A. J. Downard, *J. Am. Chem. Soc.* **2007**, *129*, 15456.
[20] S. C. Huang, T. C. Tsao, L. J. Chen, *J. Electrochem. Soc.* **2010**, *157*, D222.
[21] W. Prissanaroon, N. Brack, P. J. Pigram, P. Hale, P. Kappen, J. Liesegang, *Thin Solid Films* **2005**, *477*, 131.
[22] M. S. Miller, H. L. Filiatrault, G. J. E. Davidson, M. Luo, T. B. Carmichael, *J. Am. Chem. Soc.* **2010**, *132*, 765.
[23] Y. N. Xia, G. M. Whitesides, *Annu. Rev. Mater. Sci.* **1998**, *28*, 153.
[24] D. Qin, Y. N. Xia, G. M. Whitesides, *Nat. Protoc.* **2010**, *5*, 491.
[25] F. C. Krebs, *Sol. Energy Mater. Sol. Cells* **2009**, *93*, 394.
[26] A. Garcia, T. Berthelot, P. Viel, A. Mesnage, P. Jegou, F. Nekelson, S. Roussel, S. Palacin, *ACS Appl. Mater. Interfaces* **2010**, *2*, 1177.
[27] A. Garcia, T. Berthelot, P. Viel, J. Polesel-Maris, S. Palacin, *ACS Appl. Mater. Interfaces* **2010**, *2*, 3043.
[28] T. Berthelot, A. Garcia, P. Viel, S. Roussel, *France Patent WO2010125189*, **2010**.
[29] V. Mévellec, S. Roussel, G. Deniau, *France Patent WO2008078052*, **2006**.
[30] V. Mévellec, S. Roussel, L. Tessier, J. Chancolon, M. Mayne-L'Hermite, G. Deniau, P. Viel, S. Palacin, *Chem. Mater.* **2007**, *19*, 6323.
[31] M. Brandes, C. C. Fels, *Metal Finishing* **2008**, *106*, 21.
[32] J. R. Lancaster, J. Jehani, G. T. Carroll, Y. Chen, N. J. Turro, J. T. Koberstein, *Chem. Mater.* **2008**, *20*, 6583.
[33] G. O. Mallory, J. B. Hajdu, *ELECTROLESS PLATING: Fundamentals and Applications*, The American Electroplaters and Surface Finishers Society, Washington, D.C. **1990**.
[34] A. M. Mance, *J. Electrochem. Soc.* **1992**, *139*, 724.
[35] G. X. Wang, N. Li, H. L. Hu, Y. C. Yu, *Appl. Surf. Sci.* **2006**, *253*, 480.
[36] T. Berthelot, A. Garcia, X. T. Le, J. El Morsli, P. Jégou, S. Palacin, P. Viel, *Appl. Surf. Sci.* **2010**, doi:10.1016/j.apsusc.2010.11.071.
[37] Y. X. Lu, *Appl. Surf. Sci.* **2010**, *256*, 3554.
[38] Y. X. Lu, S. H. Jiang, Y. M. Huang, *Surf. Coat. Technol.* **2010**, *204*, 2829.
[39] X. P. Gan, Y. T. Wu, L. Liu, B. Shen, W. B. Hu, *J. Alloys Compd.* **2008**, *455*, 308.
[40] S. L. Favaro, A. F. Rubira, E. C. Muniz, E. Radovanovic, *Polym. Degrad. Stab.* **2007**, *92*, 1219.
[41] E. G. Han, E. A. Kim, K. W. Oh, *Synth. Met.* **2001**, *123*, 469.
[42] S. C. Domenech, E. Lima, V. Drago, J. C. De Lima, N. G. Borges, A. O. V. Avila, V. Soldi, *Appl. Surf. Sci.* **2003**, *220*, 238.
[43] K. W. Oh, D. J. Kim, S. H. Kim, *J. Appl. Polym. Sci.* **2002**, *84*, 1369.
[44] M. Pascu, D. Debarnot, F. Poncin-Epaillard, G. G. Bumbu, S. Cimmino, C. Vasile, *J. Phys. D-Appl. Phys.* **2006**, *39*, 2224.
[45] M. D. Stewart, K. Patterson, M. H. Somervell, C. G. Willson, *J. Phys. Org. Chem.* **2000**, *13*, 767.
[46] D. P. Sanders, *Chem. Rev.* **2010**, *110*, 321.
[47] B. D. Gates, Q. B. Xu, M. Stewart, D. Ryan, C. G. Willson, G. M. Whitesides, *Chem. Rev.* **2005**, *105*, 1171.
[48] C. G. Willson, B. J. Roman, *ACS Nano* **2008**, *2*, 1323.
[49] G. Beamson, D. Briggs, *High Resolution XPS of Organic Polymers: The Scienta ESCA300*, John Wiley & Sons, New York **1992**.
[50] R. C. Weast, *CRC Handbook of Chemistry and Physics*, CRC Press, Boca Raton **1984**.
[51] S. L. Brandow, W. J. Dressick, C. R. K. Marrian, G. M. Chow, J. M. Calvert, *J. Electrochem. Soc.* **1995**, *142*, 2233.
[52] D. M. Brewis, I. Mathieson, I. Sutherland, R. A. Cayless, R. H. Dahm, *Int. J. Adhes. Adhes.* **1996**, *16*, 87.
[53] E. Menard, M. A. Meitl, Y. G. Sun, J. U. Park, D. J. L. Shir, Y. S. Nam, S. Jeon, J. A. Rogers, *Chem. Rev.* **2007**, *107*, 1117.
[54] Keithley, *Low Level Measurements Handbook*, Keithley Instruments, Cleveland **2007**.

Supporting information

Localized Ligand Induced Electroless Plating (LIEP) Process for the fabrication of copper patterns onto flexible polymer substrates

Alexandre Garcia[*a,b], *Thomas Berthelot*[a], *Pascal Viel*[b], *Jérôme Polesel-Maris*[c], *and Serge Palacin*[b]

CEA, IRAMIS, LSI Irradiated Polymers Grp (UMR 7642 CEA/CNRS/Ecole Polytechnique), F-91128 Palaiseau Cedex and CEA, IRAMIS, SPCSI Chemistry of Surfaces and Interfaces Grp, F-91191, Gif-sur-Yvette, France

EMAIL ADDRESS: thomas.berthelot@cea.fr

- **Cu_{2p} XPS Characterizations after Cu chelation and reduction and Cu plating onto PET sheets**

As shown in Figure SAa, the Cu_{2p} spectra analysis confirmed the Cu^{2+} chelation by three main peaks respectively corresponding to $Cu_{2p3/2}$ (934.6 and 933 eV), Cu_{2p} satellites (from 938 to 947 eV) and $Cu_{2p1/2}$ (953.1 and 954.5 eV) core level binding energies. The two peaks observed for the $Cu_{2p3/2}$ and $Cu_{2p1/2}$ are probably due to different conformations of the PAA chains which induced differences in the Cu environment and its binding energy to the carboxylate groups.

Reduction of Cu^{2+} ions immobilized by complexation in PAA-grafted ABS was obtained by immersion of the Cu-PAA film in an alkaline solution of sodium borohydrure $NaBH_4$ and confirmed by XPS measurements with the study of the chemical state of copper. After immersion in $NaBH_4$ (Figure S1b), the peak of $Cu_{2p3/2}$ core level binding energy shifts partially toward lower energy and the characteristic Cu_{2p} satellites disappeared.

Finally, the obtained metallic layers were characterized after Cu plating. As shown in the Figure S1c, the Cu_{2p} spectra indicate that Cu^0 was successfully formed on the PET sheets. In addition, oxygen and carbon elements are still present due to organic residuals coming from the plating bath and in particular from the complexing agent.

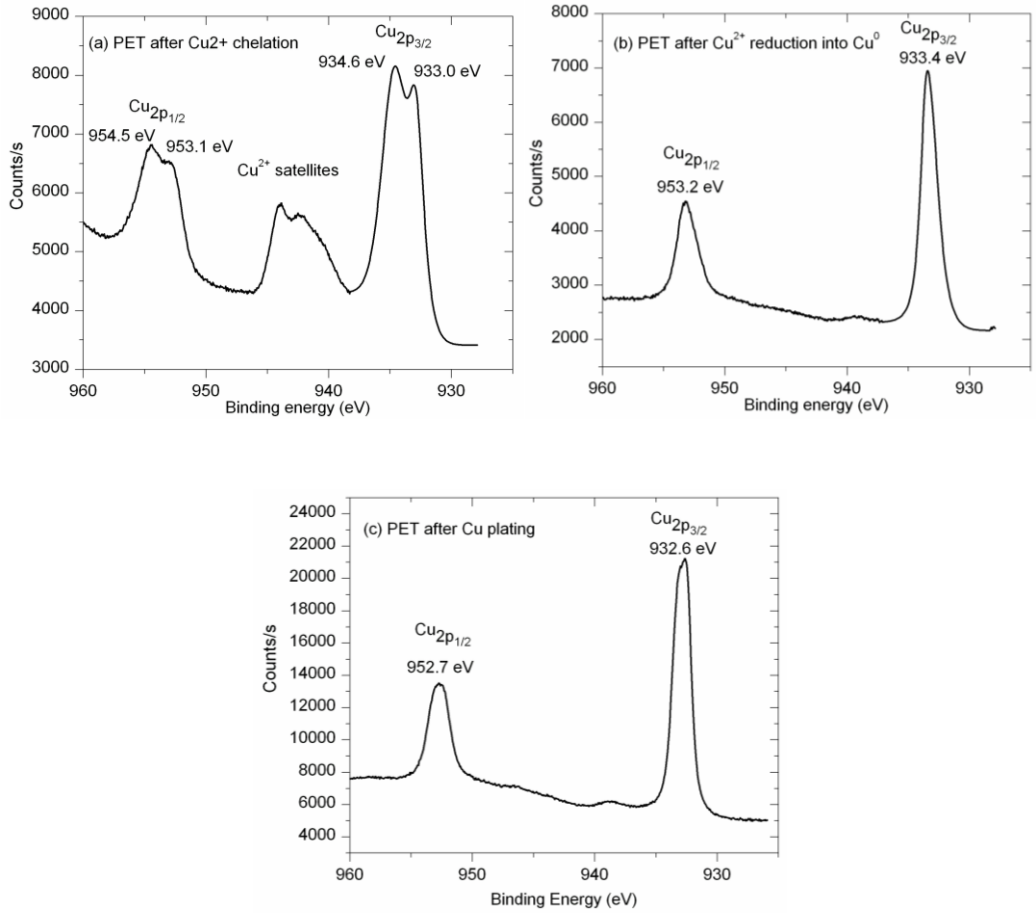

Figure S1: Cu_{2p} XPS spectra of PET after Cu chelation (a), Cu reduction (b) and after Cu plating

- **AFM analysis after localized Cu plating onto PET and PVDF sheets**

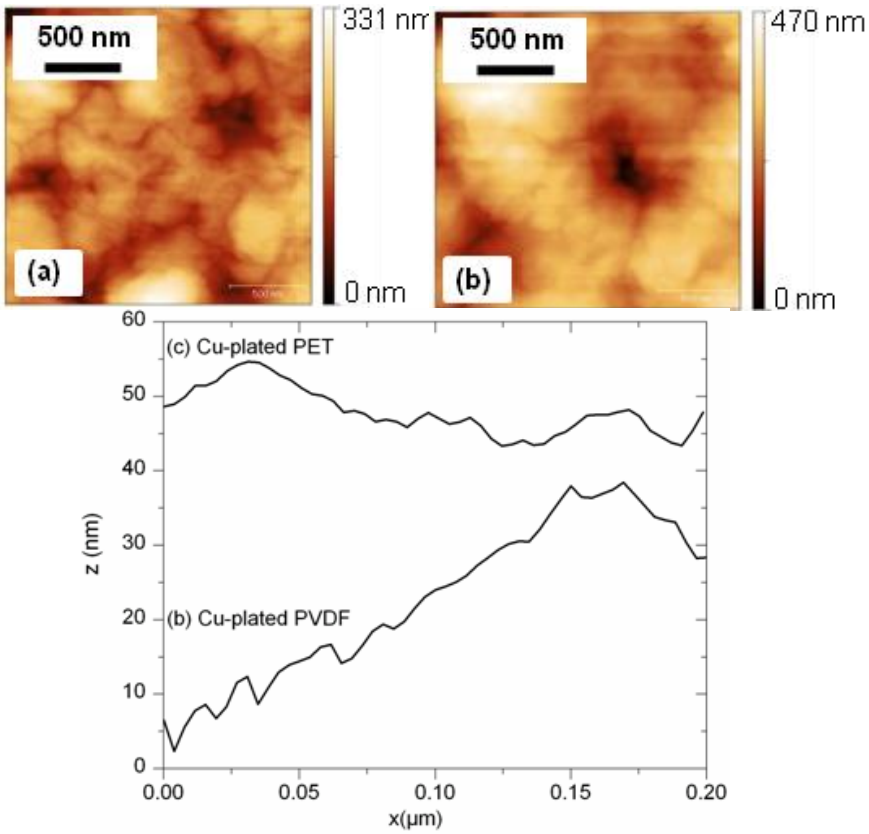

Figure S2: 2x2 µm AFM images of Cu-patterned PET (a) and PVDF (b) sheets with the corresponding profile extractions ((c) and (d))

- **Scotch tape test on Cu-plated PET and PVDF sheets**

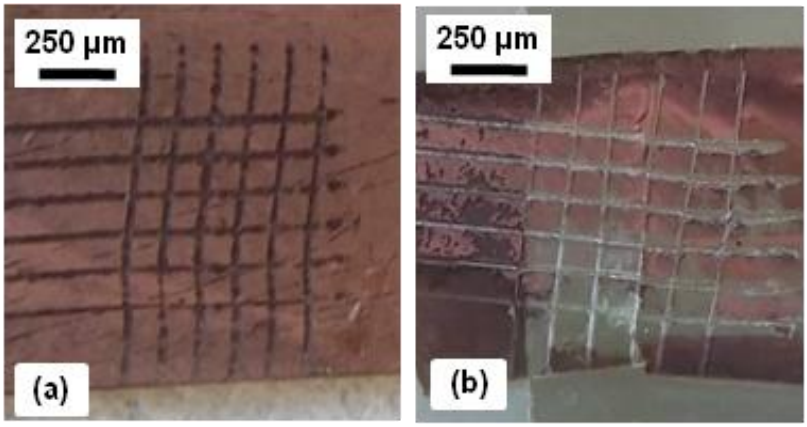

Figure S3: Images of Cu-plated PET and PVDF sheets with Cu plating after the scotch tape test

- **Copper RFID feature obtained by a photolithographic process combined with the LIEP process onto flexible polymer sheets the pattern on flexible PET sheets (1st method)**

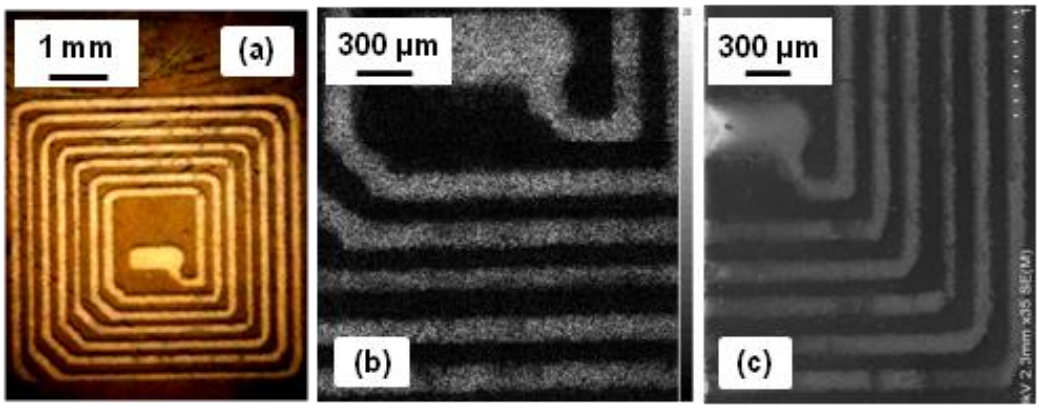

Figure S4: Optical image (a), Cu_{2p} XPS mapping (b) and SEM image (c) with a 30 µm scaled top view of an RFID feature

As shown in Figure S4, SEM images and Cu_{2p} XPS mapping of a RFID feature demonstrated at the micrometer scale that the copper was present only on the negative-tone metal pattern. Besides, Cu_{2p} XPS mapping (Figure S5b) confirmed that there was no copper pollutant between each line of the RFID copper wires avoiding short circuits.

- **Optical images of Cu patterns obtained by through direct laser printing of the negative tone of the pattern on flexible polymer sheets (2nd method)**

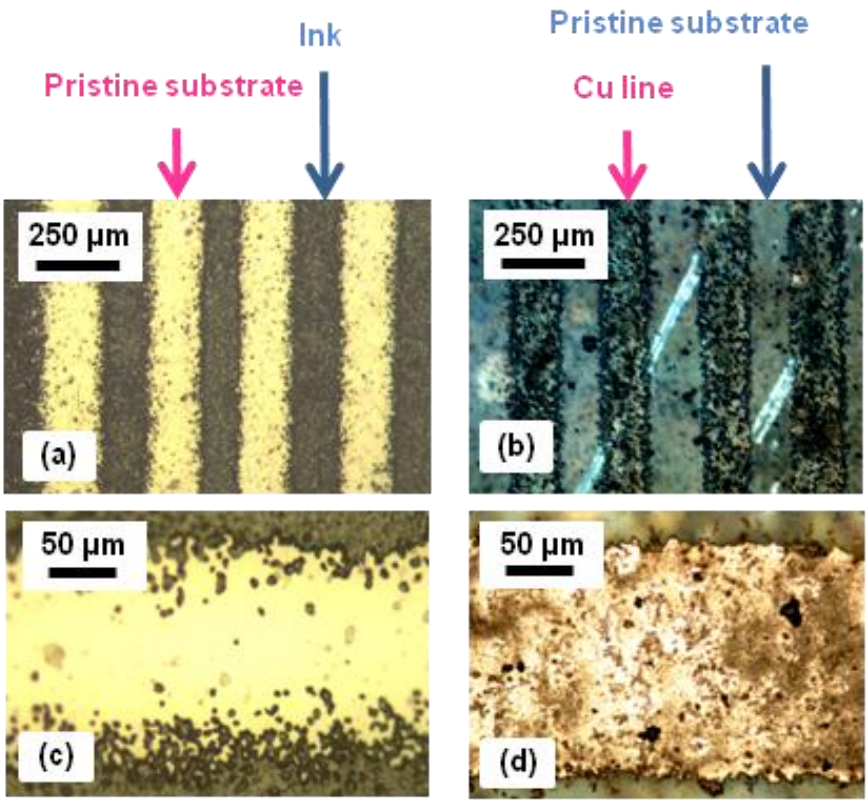

Figure S5: Optical images of a negative-tone metal pattern (after commercial laser printing) (a) and the corresponding metal pattern after copper plating (b) with a magnification x5 and the same feature with a magnification x10 (c) and (d) on flexible PET sheets.

V. Localized LIEP via the Graftfast™ process by projection or transfer

1. Introduction

As previously demonstrated (Article N°1 and N°2) for the metallization of polymers on whole surface, the LIEP process is based on successive immersions, which is perfectly suitable and competitive to be used on an industrial line to replace the current chromic acid based process, based on successive immersions itself. Such a LIEP process is especially tailored for the fabrication of decorative coatings in general manufacturing. Then, the wet LIEP process was easily combined with lithographic methods in order to obtain metal patterns onto flexible and transparent polymer surfaces (Article N°3) and to extend the use of the LIEP process to the fabrication of large-area plastic electronics devices.

All these process started with the versatile and "green" Graftfast™ technique which allows the covalent grafting of a PAA thin layer through the PAA polymerization in aqueous solution on various substrates. Unfortunately, this surface functionalization process obviously leads to the consumption of more reactive agents that needed since the polymerization reaction takes place in the entire solution. That consumption issue is even more relevant when the objective is to obtain localized grafting. Hence, the cost-effective lithographic methods used in this thesis involve additional steps inducing lots of chemical waste. Therefore, to move further on the development of a sustainable and versatile grafting process, this wet chemical process has been replaced by a transfer or projection process combining the versatility and adhesion properties of the Graftfast™ technique with a one-step polymer grafting which enables the direct production of selective patterns. This process has been patented with the following reference:

A. Garcia, T. Berthelot, P. Viel, N. Hanifi, Procédé de préparation d'un film organique à la surface d'un support solide par transfert ou par projection, *FR 11 52348*, 2011/03/22.

This approach aims at extending the use of the Graftfast™ process for local and one-step modification by transfer techniques such as stamping or by projection techniques such as inkjet printing or spraying. Ideally, through this localized Graftfast™ process, the purely chemical reducing agent used in the wet Graftfast™ process has been replaced with a photochemical one which has been post-activated after the transfer or projection step. As a matter of fact, the main goal here was to fit with the operating conditions of these projection

and transfer based processes. Hence, they require the use of a post-activated mixture avoiding the polymerization during the transfer or the projection process which would promptly leads to the damage of the device used for the transfer or the projection.

As an example, the inkjet printing of a post-activated Graftfast™ mixture and its application to the LIEP process for the fabrication of metal patterns will highlight this approach through the following article.

2. Localized LIEP via an inkjet-printed and photo-assisted Graftfast™ process

Alexandre Garcia, Nassim Hanifi, Thomas Berthelot, Pascal Viel*, Bruno Jousselme, Pascale Jégou and Serge Palacin, Photo-assisted and inkjet-printed polymer grafting and its application for flexible electronics, *Adv. Mater.* **2011**, submitted.

The present communication shows that Graftfast™ can be combined with the Drop-On-Demand (DOD) inkjet technology to provide localized covalent PAA grafting through a one-step method based on the photo-assisted radical polymerization of acrylic acid within a picoliter droplet. As the conventional Graftfast™ technology is based on the reduction of diazonium salts acting as polymerization initiators in solution, it is not *per se* compatible with DOD inkjet printing for obvious nozzle plugging reasons. Therefore, we replaced the purely chemical reducing agent in the cartridge for a photochemical one which is post-activated after the printing step. Accordingly, inkjet printing provides the localized deposition; visible light sets off the polymer covalent grafting from a stable “ink” located in the cartridge before printing. Likewise, this light based post-activation allows to circumvent the problems caused by carrying out free radical chemistry into oxygenated micro-reactors. Combined with the ligand induced electroless plating (LIEP) process, we applied this photo-assisted process for the fabrication of copper patterns onto two insulating and flexible substrates: poly(ethylene terephtalate) (PET) and polyvinylchloride (PVC) sheets commonly used as transparent substrates for flexible electronics and glossy paper substrates for (inkjet or laser) printing, respectively.

Photo-assisted and inkjet-printed polymer grafting and its application for flexible electronics

(COMMUNICATION Submitted to ADVANCED MATERIALS)

By *Alexandre Garcia, Nassim Hanifi, Thomas Berthelot, Pascal Viel*, Bruno Jousselme, Pascale Jégou* and *Serge Palacin*

Keywords: Light-induced covalent grafting, inkjet printing, electroless plating, and Drop-On-Demand

Localized modifications of material surfaces has grown in interest over the three past decades and are now used in many industries such as automotive, biotechnology, aerospace or electronics. Among all the patterning techniques, inkjet printing has lately become a reliable technique at micrometric scale especially for the development of flexible electronics applications. Hence, inkjet printing is a mask-less and one-step process digitally driven that allows localized deposition on demand with a low waste production and at lower cost [1-4] than most of the patterning techniques such as photolithography [5] and other printing techniques such as micro-contact printing [6-9] or screen printing [8, 10]. However, inkjet printing as most of the lithographic techniques rely on physisorbed coatings which involve weak interactions and possible loss of the expected mechanical properties with time.

Besides those processes, we recently developed a wet chemical technology based on diazonium salts chemistry, called GraftFast™, which provides covalently grafted polymer films exhibiting excellent adhesion and good mechanical properties [11-17]. GraftFast™ has already been applied to heavy metal waste treatment [13], chemical biosensing [14] carbon nanotubes [18] immobilization and for the electroless plating of polymers [15, 16].

The present communication shows that GraftFast™ can be combined with the Drop-On-Demand (DOD) inkjet technology to provide localized covalent polymer grafting through a one-step method based on the photo-assisted radical polymerization of a vinylic monomer within a picoliter droplet. As the conventional GraftFast™ technology is based on the reduction of diazonium salts acting as polymerization initiators in solution, it is not *per se* compatible with DOD inkjet printing for obvious nozzle plugging reasons. Therefore, we replaced the purely chemical reducing agent in the cartridge for a photochemical one which is post-activated after the printing step. Accordingly, inkjet printing provides the localized deposition; visible light sets off the polymer covalent grafting from a stable "ink" located in the cartridge before printing. As a matter of fact, each printed "micro-droplet" (a few picoliters) can be considered as a "single micro-reactor" in which the radical polymerization is observed at ambient atmosphere despite the presence of dioxygen which is well-known as radical polymerization inhibitor [19].

This innovative technique takes advantage of the versatile working conditions of the inkjet printing (ambient pressure and room temperature) and the excellent adhesion of GraftFast™ films [11, 12, 17]. Similar adhesion properties are usually only obtained by harsh dry (corona discharge, plasma) or wet (chromic acid etching) surface pretreatments. Moreover, this photo-assisted inkjet-printed polymer grafting process is almost waste and volatile organic compound-free. Hence, contrary to most of the lithographic methods previously exposed, this simple and cost-effective process is fully suited for "short-runs" and tailor-made patterning with short time reactions.

Lastly, combined with the ligand induced electroless plating (LIEP) process (**Figure 1**) [15, 16, 20]. we successfully applied this photo-assisted process for the fabrication of copper patterns on polymer substrates. Fabrication of narrow conductive tracks onto polymer substrates by inkjet printing was thoroughly investigated, but mostly requires a sintering step above 150°C, in order to improve conductive properties [1, 21, 22]. This is the main bottleneck of inkjet printing on polymers since the glass transition temperature of commonly used polymers, like poly(ethylene terephtalate) (PET) or polycarbonate (PC), is below 150°C.

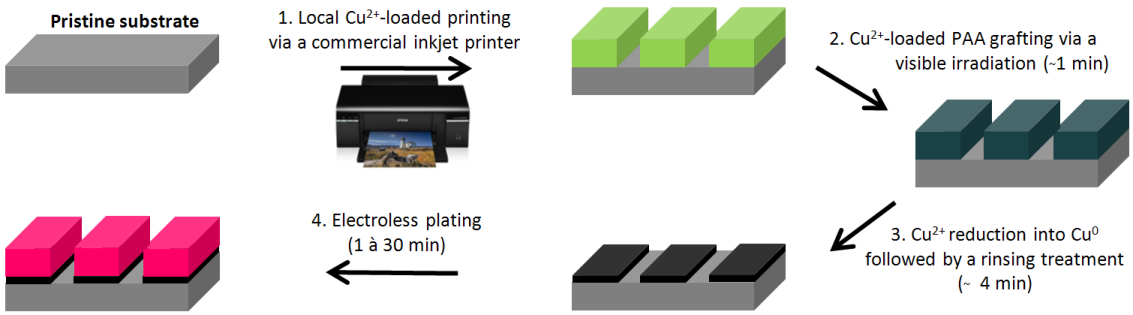

Figure 1: Ligand Induced Electroless Plating through the Cu^{2+}-loaded inkjet-printed and photo-assisted PAA grafting

The localized photo-assisted grafting was carried out with a commercial inkjet printer and an aqueous ink containing an aryldiazonium salt, a vinylic monomer (acrylic acid (AA) as an example), a ruthenium dye $[Ru(bpy)_3]Cl_2$ and triethylamine as sacrificial donor. A thickener (namely polyacrylic acid-co-maleic acid (PAA-co-PMA)) was added to the solution to increase its viscosity which leads to an improvement of the inkjet solution wettability onto the substrate and a better printing resolution. The absorbance spectrum of the resulting solution clearly shows the visible absorption range (400 to 500 nm) of the MLCT band of the ruthenium complex (**Figure S1**), while the other components absorb only in a UV range [23].

Three types of substrates were selectively printed: gold (used for IR and XPS characterizations) and two insulating and flexible substrates: poly(ethylene terephtalate) (PET) and polyvinylchloride (PVC) sheets commonly used as transparent substrates for flexible electronics and glossy paper substrates for inkjet or laser printing, respectively.

By adding copper sulfate ($CuSO_4$, $5H_2O$) to the previously described inkjet solution, a thin Cu^{2+}-loaded and covalently grafted poly(acrylic acid) (PAA) film was obtained after 1 min of visible light irradiation. The main advantage to introduce Cu^{2+} ions in this inkjet solution results in saving process steps and time compared to the common wet chemical process.[16] Subsequent reduction of the Cu^{2+} ions provides the catalyst for the electroless metal growth which starts inside the grafted host polymer.[16] Copper patterns were thus obtained on PET and PVC sheets.

Figure 2 illustrates the whole process on the example of a copper RFID coil onto flexible and transparent PET. Optical images of Cu^{2+}/PAA-grafted PET are given before and after the

electroless copper plating (respectively **Figures 2a,c and 2b,d**). They illustrate the process conformity at the micrometric scale since electroless plated copper is present only on the grafted-PAA pattern. As a matter of fact, the local Cu^{2+}/PAA coating can be considered as a latent image which is then developed when the entire substrate is introduced into the electroless plating bath. Additionally, as shown in **Figure 2g**, the 1 µm-thick plated-copper pattern showed quite homogeneous and uniform in thickness as analyzed by mechanical profilometry. Other examples of copper patterns obtained on PET and PVC sheets are given in **Supporting Information** (**Figures S7 and S8**).

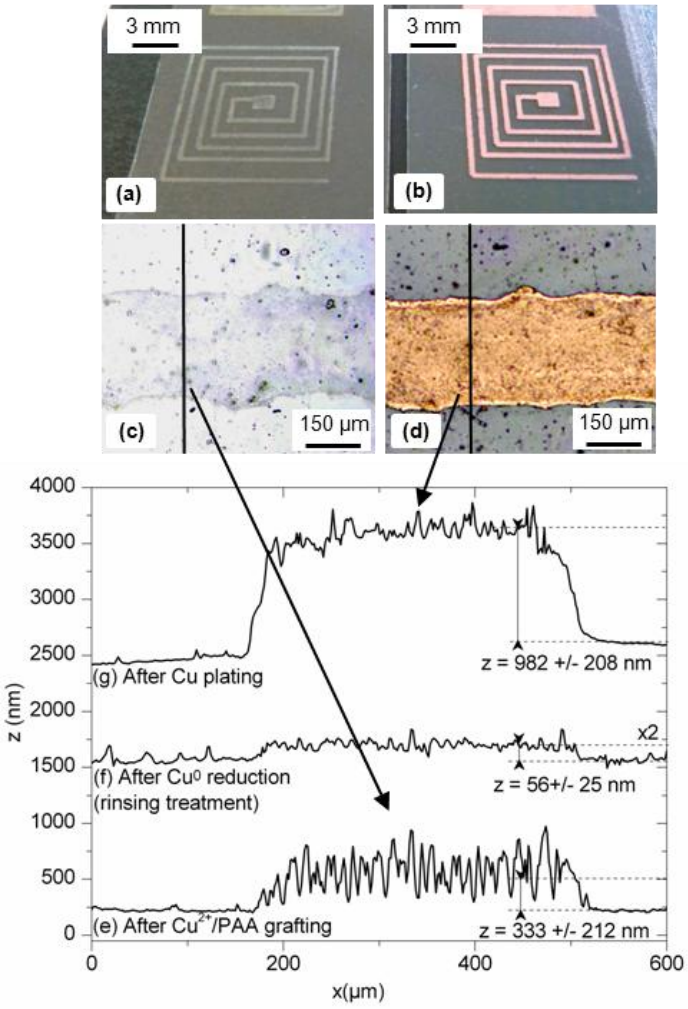

Figure 2: Optical images of Cu^{2+}/PAA-patterned PET sheets (a and c) and the corresponding Cu-patterned PET sheets (b and d) at different scales and the profile extracted at each step: after Cu^{2+}/PAA grafting (e), after Cu reduction (f) and Cu plating (g)

First, Cu-free light-induced PAA covalent grafting was confirmed by FTIR-ATR on gold substrates after rinsing treatments under sonication. To avoid interferences with grafted PAA

signals, those FTIR-ATR and XPS characterizations were carried out with a PAA-co-PMA thickener-free inkjet solution. Four main peaks at 1725, 1586, 1522 and 1350 cm^{-1} showed up in the IR spectrum after light-induced PAA grafting (**Figure 3**), which can be respectively attributed to the stretching vibrations of COOH and COO^- groups from PAA,[20] and nitrophenyl groups from diazonium salts derivatives.[12] As shown in **Supporting Information (Figures S2 and S3)**, the IR signature of carboxylic groups also appeared after PAA grafting on PET and PVC substrates.[15, 16, 20] The formation of grafted PAA films was also demonstrated by XPS onto gold surfaces (**Figure S4**).

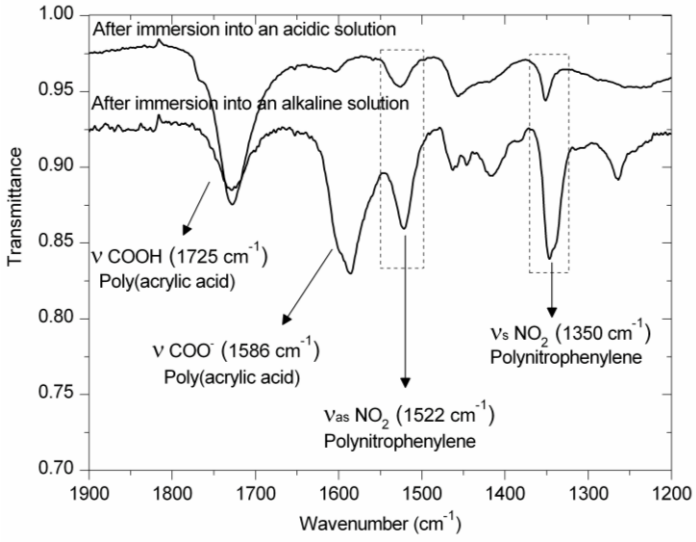

Figure 3: IR spectrum of gold substrates after Cu-free photo-assisted PAA grafting

Second, Cu^{2+}-loaded PAA covalent grafting was also confirmed by IR analysis. Hence, PAA grafting did not seem to be disturbed by the presence of Cu^{2+} ions which are not concerned by the photoreduction process (**Figure S5**).[24] Cu^{2+}-loaded printed substrates obviously derive from complexation by the carboxylate groups contained all along the grafted PAA chains and the entrapped PAA-co-PMA thickener. After immersion into a sodium borohydride solution, the Cu^{2+} reduction was confirmed by XPS measurements (**Figure S6**). The resulting thickness of the catalytic Cu^0-grafted layer was approximately evaluated by mechanical profilometry at *ca.* 50 nm, which is around six times less than before reduction (**Figures 2c and 2d**). It was indeed shown that this reduction step allowed discarding most of the physically adsorbed matter and thus acted as a rinsing treatment. Finally, the obtained metallic layers were characterized after Cu electroless plating catalyzed by that catalytic Cu^0-grafted layer.[25] Excellent adhesion

between the copper plated layer and the polymer substrates was obtained and copper wires grafted onto PET and PVC substrates revealed promising electrical properties under tensile strains (For details, see **Supporting Information** and especially **Figures S9 to S11**).

In respect to these results and our previous works [11-17], a complete grafting mechanism is suggested in **Figure 4,** where the chemical reducing agent commonly used for the Graftfast™ process is replaced by a photo-assisted one. The ruthenium tris(bipyridine) complex is well known for its electron transfer properties under visible irradiation thanks to the metal-to-ligand charge transfer (MLCT) absorption band at 453 nm.[23, 26] (**Figure S1**). Thus, under visible irradiation, a photo-induced electron transfer between the ruthenium dye and the aryldiazonium salt induces the formation of an aryl radical (**Figure 4a**).[27] The following steps are similar to the ones already proposed for the GraftFast™ process (**Figures 4b**, **4c and 4d**).[11, 12, 15] The oxidized ruthenium dye was eventually reduced by the triethylamine present in the mixture to restart the photo-catalytic process. As indicated by XPS analysis of the Cu_{2p} signal after the irradiation (**Figure S5**), no direct electron transfer occurs between the ruthenium tris(bipyridine) complex and Cu^{2+} ions. As a matter of fact, each printed "micro-droplet" consists of a "single micro-reactor" in which the AA radical polymerization occurs despite the presence of dioxygen which is a radical polymerization inhibitor. We consider that once the irradiation begins, there is a fast and a complete depletion of the dioxygen concentration contained in the "micro-reactor" which is entrapped by the first formed aryl radicals and/or by the acrylic acid oligoradicals. Then, before the oxygen concentration rises again by spontaneous diffusion, the acrylic acid polymerization proceeds following the mechanism described in **Figure 4**. It is worth to mention that without any aryldiazonium salt, no PAA grafting was found. Likewise, without any photosensitizer, the PAA polymerization and grafting only occurred after longer irradiation times (15 min at least) and with larger droplets. Indeed, it demonstrates the electron provider role of the ruthenium complex under visible irradiation which highly increases the aryl radical concentration allowing the PAA grafting within those "micro-droplets". This innovative, versatile and one-step method provides a selective and COV-free modification of the substrate properties with a covalent link to the surface.

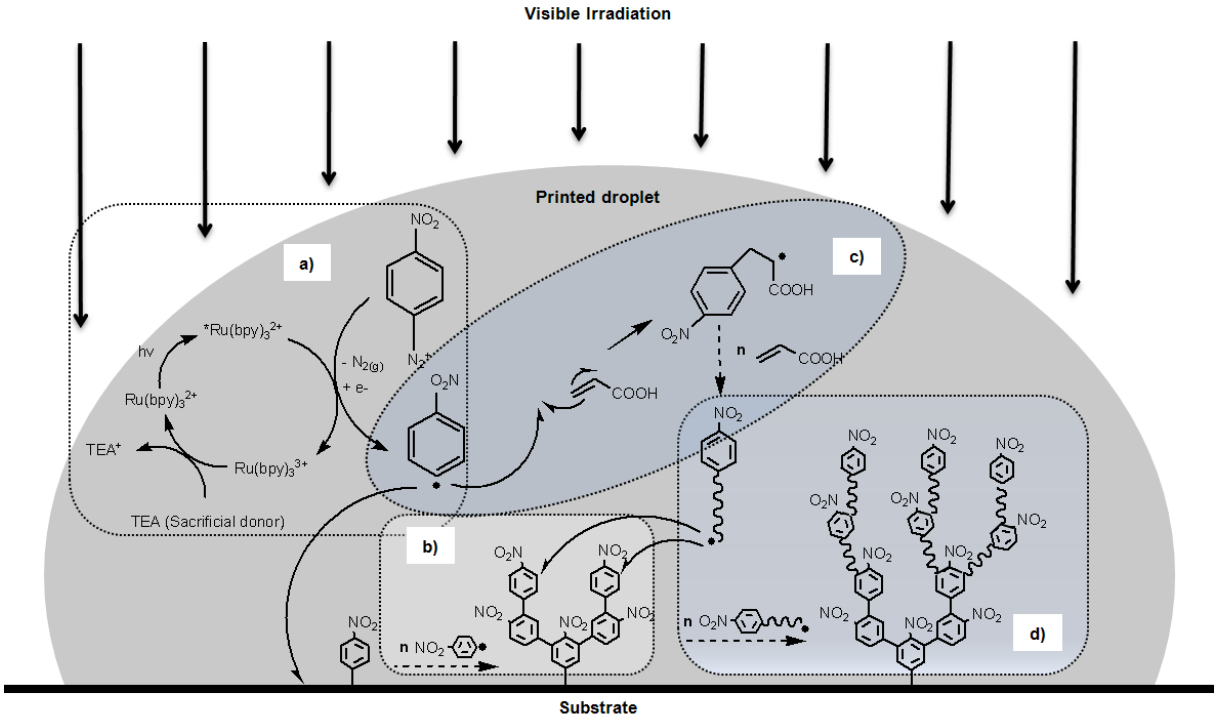

Figure 4: Proposed mechanism divided into four main steps based on the GraftFast™ process:[12, 14] (a) Photo-assisted reduction of the aryldiazonium compound (b) Grafting of the resulting aryl radicals onto the surface and growth of the polynitrophenylene multilayer, (c) Acrylic acid polymerization initiated by the aryl radicals, (d) Polyacrylic acid oligoradicals grafting on the primer layer.

In summary, we present a robust and almost waste-free patterning process suitable for a large range of substrates by direct covalent grafting of PAA by inkjet printing. This visible light-induced process was demonstrated on gold, PET and PVC substrates. This process combined with the PAA-based LIEP process was also used for the fabrication of micrometric metal patterns with excellent adhesion results of the metal layer onto the substrate and very promising electrical properties. Lastly, in the near future, this process will be extended to various dyes absorbing at different wave numbers and to other substrates in order to extend the industrial applications of this photo-assisted inkjet-printed process.

Experimental

***Photo-Assisted Polymer Covalent Grafting by Inkjet Printing*:** Inkjet printing was carried out with a commercial inkjet printer (EPSON Stylus P50) equipped with a piezoelectric drop-on-demand technology (Epson Micro Piezo™) using an 5760 x 1440 optimized dpi resolution (~ 3.5 µm) and a minimum ink droplet size about 1.5 pL on three different types of substrates: Flexible and 100 µm-thick poly(ethylene terephtalate) (PET) sheets of technical quality

obtained from Tektronix® as standard transparency films, flexible and 500 µm thick polyvinylchloride (PVC) papers of technical quality from MGI and gold substrates made by successive metallic evaporation of chromium underlayer (5 nm) and gold as top coat (200 nm) on microscopic glass slides (BALZERS BAK600). The inkjet solutions were always made first by mixing the 4-nitrobenzenediazonium tetrafluoroborate (200 mg) to aqueous solutions of $[Ru(bypy)_3]Cl_2$ (4 mL, 5.10^{-4} M) and triethylamine (2 mL, 0.1 M). Then, acrylic acid (2 mL) and polyacrylic acid-co-maleic acid sodium salt (200 mg, average M_w = 50 000 $g.mol^{-1}$) were added to the previous solution. After printing, the patterned surfaces were irradiated through a visible halogen desk lamp (OSRAM, 100 W) for 1 min (For details on its emission spectrum, see **Supporting Information**). The grafted substrates were immersed for 3 min in alkaline solution (NaOH, 1 M - which is the best solvent for the PAA hydrosoluble polymer) at 50°C and then sonicated for 1 min in deionized water. That treatment was shown by IR analysis sufficient to discard most of the physisorbed matter and equivalent to the usual surface treatment.[15, 16, 20]

***Ligand Induced Electroless Plating*:** In order to obtain metal patterns based on the LIEP process on polymers substrates, copper sulfate ($CuSO_4$, $5H_2O$, 100 mg) was added to the inkjet solution and allowed to obtain Cu^{2+}-loaded PAA grafting after irradiation, following the same procedure described above for Cu-free mixtures. The Cu^{2+} ions chelated by the carboxylate groups contained in the grafted PAA films were then reduced through the substrate immersion into a sodium borohydride ($NaBH_4$) (0.1M) – NaOH (0.1 M) solution at 50°C for 3 min followed by a rinsing treatment in deionized water. Both immersions have shown to allow discarding most of the physisorbed matter. Finally, the patterned surface-activated substrates were placed in the industrial electroless copper plating bath (M Copper 85) using formaldehyde (HCHO) as the reducing agent, and optimum conditions were: copper content 2 $g.L^{-1}$, HCHO/Cu mass ratio = 2, pH 13, working temperature 48°C to get a deposition rate of ca 4 $\mu m.h^{-1}$. The polymer substrates were left in the bath for 30 min.

***Characterizations*:** Infrared spectra were recorded on a Bruker Vertex 70 spectrometer equipped with an Attenuated Total Reflection (ATR) Pike-Miracle accessory.

REFERENCES

[1] J. Perelaer, C. E. Hendriks, A. W. M. de Laat, U. S. Schubert, *Nanotechnology* **2009**, *20*.
[2] M. Singh, H. M. Haverinen, P. Dhagat, G. E. Jabbour, *Adv. Mater.* **2010**, *22*, 673.
[3] J. W. Song, J. Kim, Y. H. Yoon, B. S. Choi, J. H. Kim, C. S. Han, *Nanotechnology* **2008**, *19*.

[4] T. H. J. van Osch, J. Perelaer, A. W. M. de Laat, U. S. Schubert, *Adv. Mater.* **2008**, *20*, 343.
[5] B. D. Gates, Q. B. Xu, M. Stewart, D. Ryan, C. G. Willson, G. M. Whitesides, *Chem. Rev.* **2005**, *105*, 1171.
[6] D. Aldakov, Y. Bonnassieux, B. Geffroy, S. Palacin, *ACS Appl. Mater. Interfaces* **2009**, *1*, 584.
[7] M. S. Miller, H. L. Filiatrault, G. J. E. Davidson, M. Luo, T. B. Carmichael, *J. Am. Chem. Soc.* **2010**, *132*, 765.
[8] D. Qin, Y. N. Xia, G. M. Whitesides, *Nat. Protoc.* **2010**, *5*, 491.
[9] E. C. Hagberg, J. C. Scott, J. A. Shaw, T. A. von Werne, J. A. Maegerlein, K. R. Carter, *Small* **2007**, *3*, 1703.
[10] F. C. Krebs, *Sol. Energy Mater. Sol. Cells* **2009**, *93*, 394.
[11] V. Mevellec, S. Roussel, L. Tessier, J. Chancolon, M. Mayne-L'Hermite, G. Deniau, P. Viel, S. Palacin, *Chem. Mater.* **2007**, *19*, 6323.
[12] A. Mesnage, S. Esnouf, P. Jegou, G. Deniau, S. Palacin, *Chem. Mater.* **2010**, *22*, 6229.
[13] X. T. Le, P. Viel, A. Sorin, P. Jegou, S. Palacin, *Electrochim. Acta* **2009**, *54*, 6089.
[14] T. Berthelot, A. Garcia, X. T. Le, J. El Morsli, P. Jegou, S. Palacin, P. Viel, *Appl. Surf. Sci.* **2011**, *257*, 3538.
[15] A. Garcia, T. Berthelot, P. Viel, J. Polesel-Maris, S. Palacin, *ACS Appl. Mater. Interfaces* **2010**, *2*, 3043.
[16] A. Garcia, J. Polesel-Maris, P. Viel, S. Palacin, T. Berthelot, *Adv. Funct. Mater.* **2011**, *21*, 2096.
[17] V. Mévellec, S. Roussel, G. Deniau, *Worldwide Patent WO2008078052*, **2006**.
[18] P. Viel, X. T. Le, V. Huc, J. Bar, A. Benedetto, A. Le Goff, A. Filoramo, D. Alamarguy, S. Noel, L. Baraton, S. Palacin, *J. Mater. Chem.* **2008**, *18*, 5913.
[19] J. Brandrup, E. H. Immergut, E. A. Grulke, A. Abe, D. R. Bloch, *Polymer Handbook (4th Edition)*, John Wiley & Sons, Chichester **2005**.
[20] A. Garcia, T. Berthelot, P. Viel, A. Mesnage, P. Jegou, F. Nekelson, S. Roussel, S. Palacin, *ACS Appl. Mater. Interfaces* **2010**, *2*, 1177.
[21] S. Jeong, H. C. Song, W. W. Lee, S. S. Lee, Y. Choi, W. Son, E. D. Kim, C. H. Paik, S. H. Oh, B. H. Ryu, *Langmuir* **2011**, *27*, 3144.
[22] D. Q. Vo, E. W. Shin, J. S. Kim, S. Kim, *Langmuir* **2010**, *26*, 17435.
[23] J. E. Huheey, E. A. Keiter, R. L. Keiter, *Inorganic Chemistry*, De Boeck Université, Bruxelles **1998**.
[24] G. Beamson, D. Briggs, *High Resolution XPS of Organic Polymers: The Scienta ESCA300*, John Wiley & Sons, Chichester **1992**.
[25] G. O. Mallory, J. B. Hajdu, *Electroless plating: Fundamentals and Applications*, The American Electroplaters and Surface Finishers Society, Washington, D.C. **1990**.
[26] B. Jousselme, G. Bidan, M. Billon, C. Goyer, Y. Kervella, S. Guillerez, E. Abou Hamad, C. Goze-Bac, J. Y. Mevellec, S. Lefrant, *J. Electroanal. Chem.* **2008**, *621*, 277.
[27] W. Horspool, F. Lenci, *CRC Handbook of Organic Photochemistry and Photobiology Second Edition*, CRC Press, Boca Raton **2004**.
[28] Keithley, *Low Level Measurements Handbook*, Keithley Instruments, Cleveland **2007**.
[29] R. C. Weast, *CRC Handbook of Chemistry and Physics*, CRC Press, Boca Raton **1984**.

Supporting information

Photo-assisted and inkjet-printed polymer grafting and its application for flexible electronics

Alexandre Garcia, Nassim Hanifi, Thomas Berthelot, Pascal Viel, Bruno Jousselme, Pascale Jégou* and *Serge Palacin*

CEA, IRAMIS, SPCSI Chemistry of Surfaces and Interfaces Grp, F-91191, Gif-sur-Yvette, France

EMAIL ADDRESS: pascal.viel@cea.fr

- **Characterizations**

Infrared spectra were recorded on a Bruker Vertex 70 spectrometer equipped with an Attenuated Total Reflection (ATR) Pike-Miracle accessory. The detector was a MCT working at liquid nitrogen temperature. The spectra were obtained after 256 scans at 2 cm^{-1} resolution.

XPS studies were performed with a KRATOS Axis Ultra DLD spectrometer, using the monochromatized Al Kα line at 1486.6 eV. The pass energy of the analyzer was kept constant at 20 eV for C1s core level scans. The photoelectron take-off angle was 90° with respect to the sample plane, which provides an integrated sampling probe depth range going from 7 to 20 nm for our substrates.

The adhesion between the metallic layer and the polymer sheets was studied by the standard ASTM D3359 Scotch® tape test (cross-cut tape test) which consists in applying and removing pressure-sensitive adhesive tape over 16 cross-hatched squares of 1x1 mm^2 made in the film by an Elcometer Cross Hatch cutter (Elcometer 107 X-Hatch ASTM Kit). That well-used test allows direct comparison of the adhesion of films obtained under various conditions on similar substrates.

Electrical properties were measured on tracks with the following dimensions: length = 2 cm, width = 300µm and height = 500 nm measured by profilometry, and terminal pads of 1 cm^2 for electrical contact. The resistivity of the wire was measured thanks to a four-point probe set-up using a home-built constant current source as described in Keithley's handbook.[1]

- **Cu-free and photo-assisted PAA grafting**

1) Absorbance spectrum of the inkjet printed solution

Localized surface modification was carried out through the inkjet printing with a commercial printer of an organic-solvent-free ink composed of an aqueous mixture containing a vinylic monomer (acrylic acid AA), the 4-nitrobenzenediazonium tetrafluoroborate acting as acrylic acid polymer initiator and adhesion primer, a thickener namely polyacrylic acid-co-maleic acid (PAA-co-PMA), a ruthenium dye $[Ru(bpy)_3]Cl_2$ acting as photosensitizer and its sacrificial donor compound which is triethylamine (TEA). As mentioned in the text, the absorbance spectrum of the resulting solution clearly shows the visible absorption range (400 to 500 nm) of the MLCT band of the [Ru] complex (**Figure S1**). The other compounds present in the mixture absorb only in a UV range.[2]

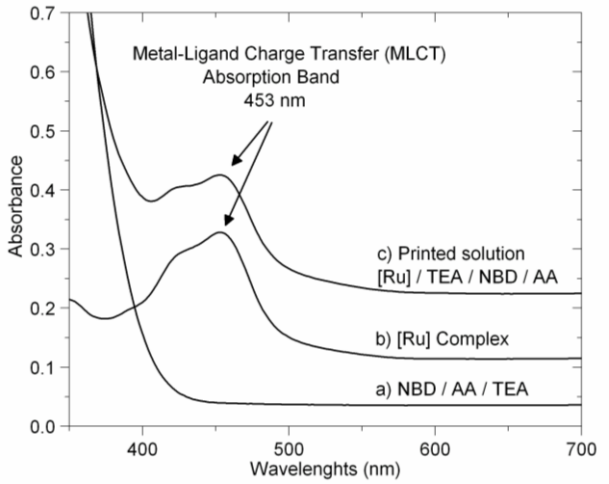

Figure S1: Absorbance of aqueous solutions of NBD salt, AA and TEA (a), of the [Ru] complex (b) and of the printed solution containing all the components (c)

2) Details on the halogen desk lamp for inkjet solution irradiation

After printing, the patterned surfaces were irradiated with a visible halogen desk lamp (OSRAM, 100 W) for 1 min. The major part of the emitted energy (up to 85 %) lies in the infrared and near-infrared regions of the spectrum, 15-20 % in the visible range (400 to 700 nm), and less than 1 % in the ultraviolet range (below 400 nm). Some experiments were carried out using a UV filter on pipette-deposited droplets, in order to assess the actual role of

UV light on the photo-assisted grafting: no differences were observed with respect to filter-free irradiations.

3) IR-ATR spectroscopy after PAA grafting onto PET and PVC substrates

PAA grafting has been confirmed by IR-ATR onto PET and PVC substrates after the same rinsing treatment than the one mentioned in the text: An immersion for 3 min in alkaline solution (NaOH, 1 M) at 50°C followed by an immersion for 1 min in deionized water under sonication. As shown in **Figures S2 and S3**, the IR absorption band characteristic of the carboxylate groups also appeared after PAA grafting on PET and PVC substrates.

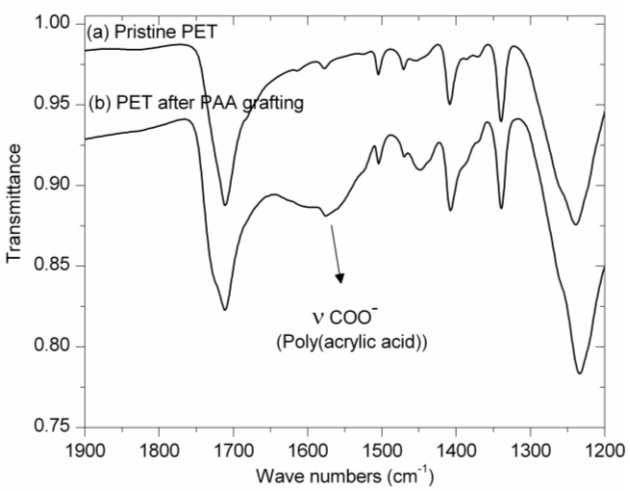

Figure S2: IR spectra of pristine PET (a), and the same after photo-assisted PAA grafting (b)

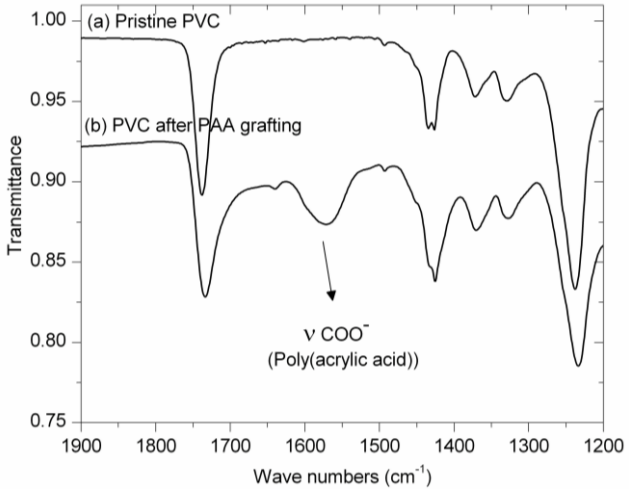

Figure S3: IR spectra of pristine PVC (a), and the same after photo-assisted PAA grafting (b)

4) XPS Spectroscopy after PAA grafting onto gold substrates

PAA grafting has been confirmed by XPS spectroscopy on gold substrates after the rinsing treatment mentioned in the text. As illustrated in **Figure S4**, a typical C_{1s} core level spectrum is composed of four main peaks. Two peaks centered at 284.4 eV and 286.8 eV respectively correspond to the phenyl carbons C-H and the phenyl carbons bounded to the nitro groups C-NO_2, which confirm the presence of the nitrophenyl groups. Two other peaks centered at 285.2 eV and 289.0 eV are respectively assigned to CH_2 and COO^- moieties, confirming the grafting of PAA on the gold substrates.[3]

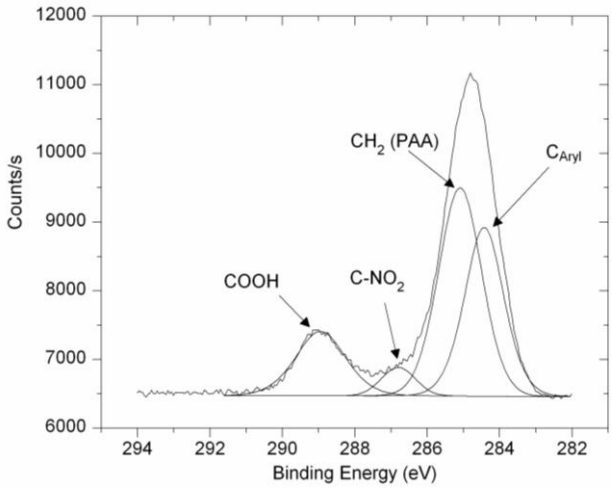

Figure S4: C1s XPS spectrum after photo-assisted PAA grafting onto gold substrates

5) Comment on the inability to obtain the PAA grafting without any diazonium salt

As mentioned in the text, no PAA grafting was observed using a diazonium salt free inkjet solution after an irradiation of 1 min. After longer irradiation time (at least 15 min), it was however possible to polymerize AA. We assume that polymerization is actually thermally-assisted, arising from the heat generated by the infrared energy emitted by the halogen desk lamp. But the resulting PAA was totally discarded from the substrate by the rinsing procedure, confirming that no grafting occurred.

- **Cu^{2+}-loaded and photo-assisted PAA grafting**

1) IR-ATR spectroscopy after Cu^{2+}-loaded PAA photo-assisted grafting onto gold, PET and PVC substrates

The effect of copper salts in the inkjet solution on PAA grafting was studied onto gold, PET and PVC substrates by IR after the same rinsing treatment than for Cu^{2+}-free PAA grafting: IR signals were found identical in both cases.

2) Cu_{2p} XPS spectrum after Cu^{2+}-loaded PAA photo-assisted grafting onto PET substrates

As shown in **Figure S5**, the Cu2p spectra analysis confirmed the Cu^{2+} chelation by three main peaks respectively corresponding to Cu2p3/2 (933.2, 935.3 and 937.1 eV), Cu2p satellites (from 938 to 947 eV) and Cu2p1/2 (953.2 and 954.8 eV) core level binding energies.[3] The different peaks observed for Cu2p3/2 and Cu2p1/2 are probably due to different conformations of the PAA or PAA-co-PMA chains which induced differences in the Cu environment and its binding energy to the carboxylate groups.

That XPS analysis confirmed that no electron transfer occurred between the ruthenium tris(bipyridine) complex and Cu^{2+} ions upon irradiation, since no Cu^{0} or Cu^{I} signals were observed.

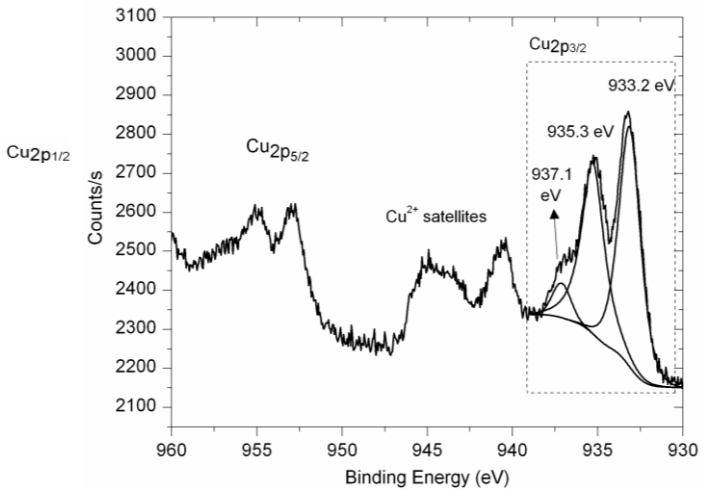

Figure S5: Cu_{2p} XPS spectrum after Cu^{2+}-loaded photo-assisted PAA grafting onto PET substrates

- **Cu^{2+} reduction within the photo-grafted PAA layer**

Reduction of Cu^{2+} ions was obtained by immersion of the Cu-PAA film in an alkaline solution of sodium borohydride $NaBH_4$ and confirmed in **Figure S6** through the Cu_{2p} XPS spectrum by two main peaks corresponding to $Cu_{2p3/2}$ (932.5 eV) and $Cu_{2p1/2}$ (952.4 eV) core level binding energies.[3]

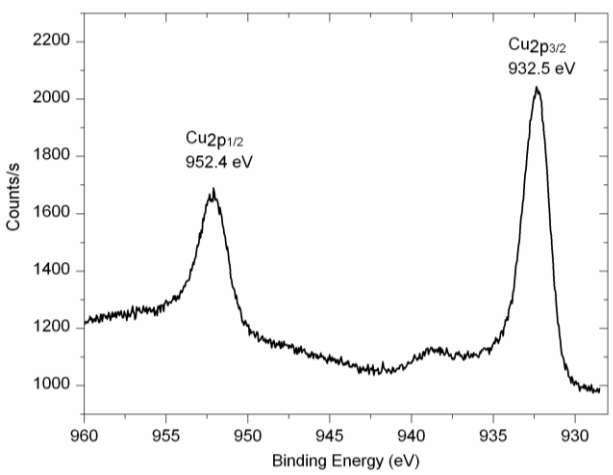

Figure S6: Cu_{2p} XPS spectrum after Cu reduction onto PET substrates

- **Cu patterns after electroless copper plating**

1) Examples of PAA-patterned PET sheets and the corresponding Cu-patterned PET sheets and Cu-patterned PVC sheets

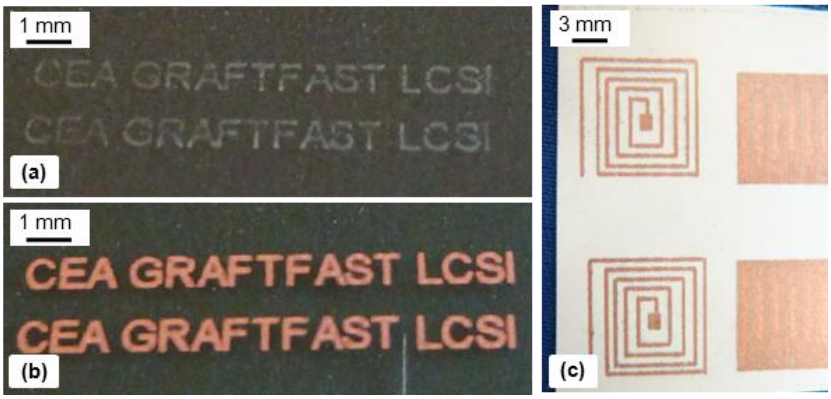

Figure S7: Pictures of after PAA-patterned PET sheets (a) and the corresponding Cu-patterned PET sheets (b) and Cu-patterned PVC sheets (c)

2) Other examples of Cu-patterned PET sheets

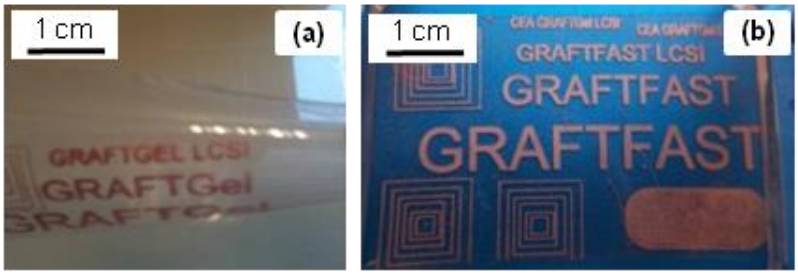

Figure S8: Pictures of Cu-patterned PET sheets (a) and (b)

3) Adhesion tests of the Cu-plated layers onto PET and PVS sheets

The adhesion of the plated copper films was checked with the classical cross-cut tape test. For both 1 µm-thick copper plated PET and PVC substrates, none of the cross-hatched squares was removed. Such as in the case of our previous works,[4,5] these excellent adhesion results can be attributed to the mechanical interlocking effect between the copper metal film and the photografted polymer, which mimics the micron-scale interdigitation that occurs between the metal layer and the rough interface which results from the common and toxic chromic acid treatment used in the electroplating of polymer industry.

4) Electrical properties through resistivity measurements of copper wires grafted on polymer substrates

The resistivity of copper wire (**Figure S9 and S10**) photo-grafted onto the PET and PVC substrates was measured at 3.0 µΩ.cm without any mechanical stress, i.e. within the range classically observed on electroless copper surfaces (2-3 µΩ.cm). We also got similar results when using wet chemistry based method (3 µΩ.cm).[4,5]

Electrical properties of the copper tracks were also studied under mechanical stress by measuring the electrical resistivity while bending the polymer sheets around cylinders with two radii of curvature equal to 5 and 1.5 mm respectively. The copper wires grafted on the polymer sheets were submitted to 150 cycles of repetitive strain around the cylinders (100 cycles with the 5 mm-radius cylinder, followed by 50 cycles with the 1.5-mm cylinder).

As shown in **Figure S11**, 100 cycles of repetitive strain around the 5 mm-radius cylinder induced a slight increase in metal resistivity. An important resistivity increase was however observed after 50 cycles around the 1.5 mm-radius cylinder added to the previous deformations. The resistivity increase is thus promoted by high numbers of deformations cycles and low radii of curvature. Nevertheless, the copper patterns fabricated on flexible PET foils withstand substantial mechanical deformation with weak conductivity change for cylinder with a radius superior or equal to 5 mm. The ability of copper tracks fabricated on flexible PET foils to tolerate tensile strain was attributed to the strong adhesion between the copper wire and the substrates and the copper particles nanometric size as previously described.[4,5]

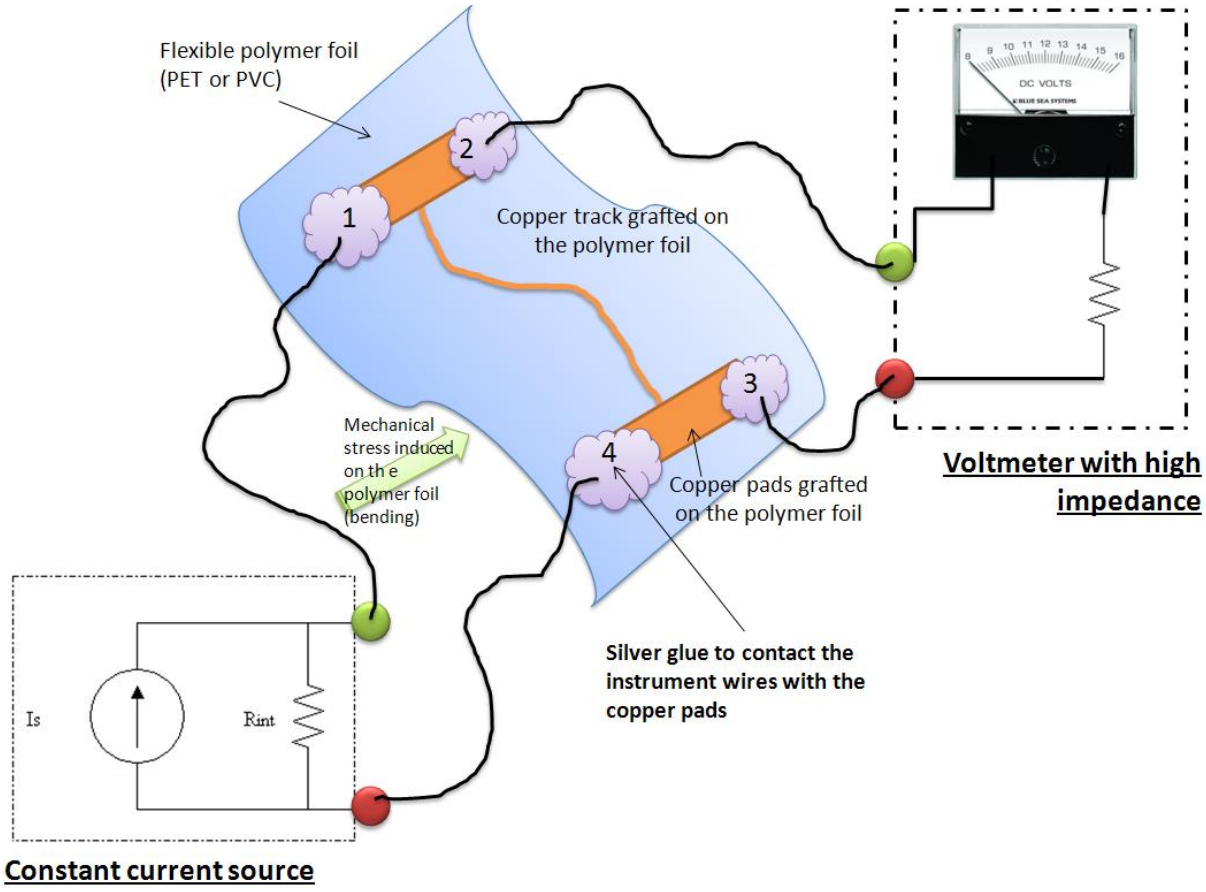

Figure S9: Schematic of the electrical measurement device and the associated special copper feature

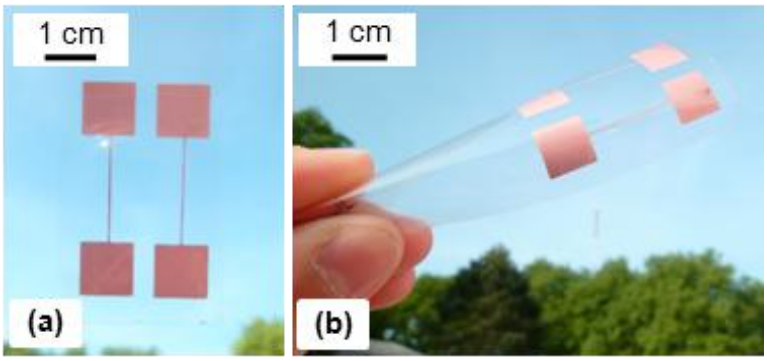

Figure S10: Pictures of Cu-patterned PET sheets used for resistivity measurements

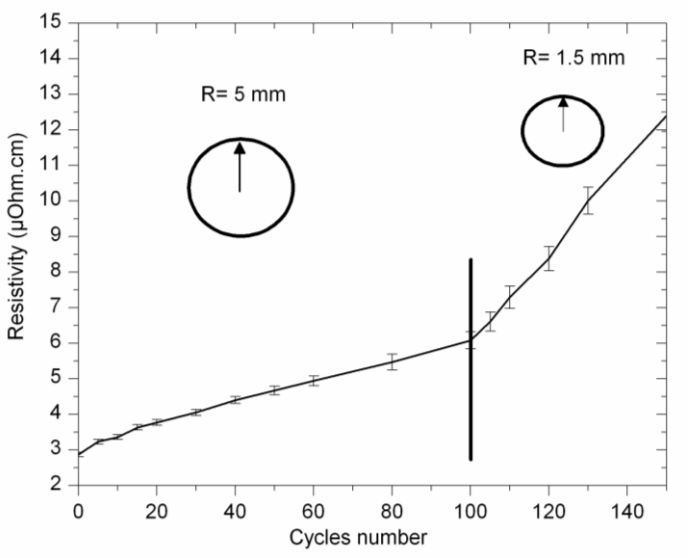

Figure S11: Resistivity measurements of Cu wires grafted on PET sheets and submitted to 100 cycles of repetitive strain around a cylinder with radius with the 5 mm-radius cylinder, followed by 50 cycles with the 1.5 mm-radius cylinder

REFERENCES

[1] Keithley, *Low Level Measurements Handbook*, Keithley Instruments, Cleveland **2007**.
[2] J. E. Huheey, E. A. Keiter, R. L. Keiter, *Inorganic Chemistry*, De Boeck Université, Bruxelles **1998**.
[3] G. Beamson, D. Briggs, High *Resolution XPS of Organic Polymers: The Scienta ESCA300*, John Wiley & Sons, Chichester **1992**.
[4] A. Garcia, T. Berthelot, P. Viel, J. Polesel-Maris, S. Palacin, *ACS Appl. Mater. Interfaces* **2010**, *2*, 3043.
[5] A. Garcia, J. Polesel-Maris, P. Viel, S. Palacin, T. Berthelot, *Adv. Funct. Mater.* **2011**, *21*, 2096.

VI. Alternative process: Localized Amino-Induced Electroless Plating

1. Introduction

Our previous works were mainly based on the association of an aryldiazonium with a vinylic monomer such as acrylic acid to create a PAA thin film layer acting as an interphase between the substrate and the electrolessly metal layer. That LIEP process was based on the ion exchange properties of poly(acrylic acid) (PAA) to complex Cu^{II} species. Meanwhile, we have seen that many laboratories and plating industries based their processes on the Pd^{II} complexation thanks to nitro-bearing ligands immobilized onto the substrate surface. In this context, we suggest here a simplified alternative of our LIEP process by applying the same diazonium anchoring process but without any acrylic acid monomer. Hence, it leads to the formation of a polyaminophenylene (PAP) layer which is usually used as an adhesion primer for the Graftfast™ process. This more common approach based on Pd catalyst is even easier to be scaled up and insert this Amino Induced Electroless plating (AIEP) process on industrial production lines. In the meanwhile, this process is also potentially adjustable to the projection or transfer based Graftfast™ process for the direct and local grafting.

The Pd/PAP activated polymer layer acts both as a seed layer for electroless metal growth and as an interdigital layer to enhance adhesion properties of the metallic patterns. In the case of PAA-based LIEP process, the excellent adhesion of electrolessly plated layer on the polymer substrates was basically attributed to the covalent bound between the surface and the grafted PAA brushes as well as to the nanometer-scale mechanical interlocking of the growing electrolessly plated layer within the PAA brushes which are provided by the polymer viscoelastic and high swelling intrinsic properties. In this alternative approach, the strong interface bound of the PAP layer onto the surface is still present but the inelastic property of the PAP layer composed of aromatic rings induce obviously less mechanical interlocking effects which could potentially weaken the mechanical and durability properties of the metal layer with time.

2. Localized Amino-Induced Electroless Plating process

A. Garcia, T. Berthelot*, P. Viel, P. Jégou and S. Palacin, Localized Amino-Induced Electroless Plating: A powerful toolset for localized metallization onto polymers substrates, *ChemPhysChem* **2011**, submitted

In the present work, we combined the Pd^{II} chemical affinity for amine ligands with the Graftfast™ process by grafting a polyaminophenylene (PAP) layer onto the polymer substrates to be metalized. Then, palladium Pd^{II} species were strongly complexed all along the grafted polyaminophenylene chains. Finally, the entrapped palladium species were chemically reduced *in situ* during the electroless plating and the resulting Pd^{0}-containing film acted as a seed layer for the electroless metal growth which thus started inside the host polymer.

This “Amino-induced electroless plating (AIEP) process” is an easy and cost-effective way to produce metallic patterns onto flexible polymer substrates with a micrometric resolution and based on the direct printing of the mask with a commercial printer.

3D-Amino-Induced Electroless Plating Process: a Powerful Toolset for Localized Metallization onto Polymers Substrates

(ARTICLE Submitted to ChemPhysChem)

Alexandre Garcia, Thomas Berthelot, Pascal Viel, Pascale Jégou and Serge Palacin*

CEA, IRAMIS, SPCSI Chemistry of Surfaces and Interfaces Grp, F-91191, Gif-sur-Yvette, France

EMAIL ADDRESS: Thomas.berthelot@cea.fr

KEYWORDS: polymer covalent grafting, 3D-ligation, palladium seed layer, electroless plating, lithography

ABSTRACT

The "3D-amino-induced electroless plating (3D-AIEP) process" is an easy and cost-effective way to produce metallic patterns onto flexible polymer substrates with a micrometric resolution and based on the direct printing of the mask with a commercial printer. Its effectiveness is based on the covalent grafting onto substrates of a 3D-polymer layer which presents the ability to entrap Pd species. Therefore, this activated Pd-loaded and 3D-polymer layer acts both as a seed layer for electroless metal growth and as an interdigital layer for enhance mechanical properties of the metallic patterns. Consequently, flexible and

transparent PET sheets were selectively metalized with nickel or copper patterns. Electrical properties of the obtained metallic patterns were also studied.

INTRODUCTION

The localized metal deposition process onto polymer substrates is of major importance for use in lightweight plastics electronics devices. Coating polymer substrates with localized metal plating enables the transmission of electrical signals on advanced technologies such as organic thin-film transistors (OTFT) [1, 2], microelectro-mechanical systems (MEMS) [3] and radio frequency identity (RFID) tags [4]. Over the three past decades, localized metal deposition has been the mostly obtained by combining photolithography with physical vapor deposition (PVD). It is noteworthy that this widely applied process is very expensive and clearly uses more metal than necessary, since the PVD step concerns the whole surface. Fabrication of narrow conductive tracks onto polymer substrates by printing techniques such as metal nanoparticles inkjet printing was also thoroughly investigated and drastically reduced the effluent quantities and by the same reduces the cost of metal compared to conventional photolithography processing combined with PVD. However, those printing techniques mostly requires a sintering step around 250 - 300°C, in order to improve conductive properties [5-7] and represent an important bottleneck since the glass transition temperature of commonly used polymers, like poly(ethylene terephtalate) (PET) is below 150°C. In this context, localized electroless metal plating appears to be the most suitable method to metallize insulating surfaces and more specifically polymers for the deposition of conformal metal films onto all-shaped substrates but also for the fabrication of metal patterns [8-16]. Common electroless processes involve three main steps: (i) surface preparation, (ii) surface activation or surface seeding with an appropriate metal catalyst and (iii) the electroless deposition itself, which is the chemical deposition of a metal film from a solution containing a mild reducing agent and an ionic complex of the metal to be plated onto the seeded substrate [8, 9].

To obtain electrolessly deposited metal patterns onto polymers, the surface activation is commonly based on palladium species and more specifically on a mixed $SnCl_2$-$PdCl_2$ solution containing core-shell Pd-Sn colloidal species that are adsorbed onto oxygenated surfaces resulting from oxidative and pollutant surface preparations commonly applied to polymer

surfaces [14-16]. Alternative approaches have been recently developed and are based on a thin layer which contains designated ligands which are able to entrap Sn-free Pd catalyst onto the substrate. Compared to the Sn-Pd colloids adsorption described above, the use of appropriate ligands, such as primary amine groups or carboxylic acids, is expected to be more selective and more robust, a key asset for the subsequent reduction step which provides the actual catalyst [14]. Among all the available techniques to complex Pd^{II} species, organosilane adsorption with nitrogen-bearing terminal groups was probably the most studied technique and it was based on a single Pd/NH_2 2D-interface[14]. Unfortunately, this approach presents some drawbacks: i) it can be applied only on hydroxylated substrate and ii) the weak SiO-C interface bound created between the organosilane and the substrate is easily hydrolyzed in basic or acidic solution [17].

Another wet approach consists in the covalent grafting of polymer-based materials which contains chelating groups to create a 3D-ligation system [18-21]. Therefore, this 3D-structure based on covalently grafted polymer chains is then considered as a robust interphase between the polymers surface and the metal layer, which is intended to replace the rough interface. The majors drawbacks of these advanced processes are: i) their specificity towards one kind of polymer and ii) their impossibility to use them at the industrial scale due to their excessive complexity [18-21].

As in the case of wet processes, several dried treatments (radio-frequency plasma treatment or VUV irradiation) were developed to modify the surface with nitrogen-bearing groups in order to adsorb Pd^{II} species [22]. However, even if those treatments (leading to a 2D or 3D-ligation structure depending on the pretreatment working conditions) are leading to good adhesion properties of the metal layer onto the substrates, they are carried out in controlled atmosphere chamber which make them very expensive and extremely difficult to industrialize.

On these grounds, we demonstrate in the present work a powerful and one-step toolset to graft a nitrogen-bearing polymer thin layer. This 3D-ligation structure is obtained by the reduction of amino-aryldiazonium salts in solution. The resulting layer consists in a polyaminophenylene (PAP) has been already used in our laboratory as an intermediate to graft covalently carbon nanotubes, graphene flakes or biomolecules on different kind of substrates [23, 24].

As illustrated in **Figure 1**, metal patterns onto polymer sheets were obtained with 20 µm-maximum resolution features by combining the direct mask printing based on a 1200 dpi laser printer and this diazonium induced anchoring process allowing the formation of positive-tone metal pattern made of the PAP layer. Hence, this localized and covalently grafted and 3D-ligation structure is used to immobilize Pd^{II} precursor salts thanks to the strong Pd^{II} affinity towards NH_2 ligands [25] (**Figure 2**). That immobilization is stable enough for subsequent reduction into the PAP layer of immobilized Pd^0 species which eventually proved efficient for selective electroless metal plating onto flexible and transparent poly(ethylene terephtalate) (PET) sheets. Each step of this 3D-Amino-Induced Electroless Plating (3D-AIEP) process was characterized by IR and XPS spectroscopy. The metal patterns were characterized by optical microscopy to check the conformity between the mask and the metal plated patterns and by mechanical profilometry to study the thickness conformity. Adhesion properties of the metal patterns onto the flexible PET substrates were studied by carrying out the common industrial scotch tape test. Finally, the evolution of the electrical resistivity of the obtained flexible copper pattern submitted to a controlled mechanical stress was studied.

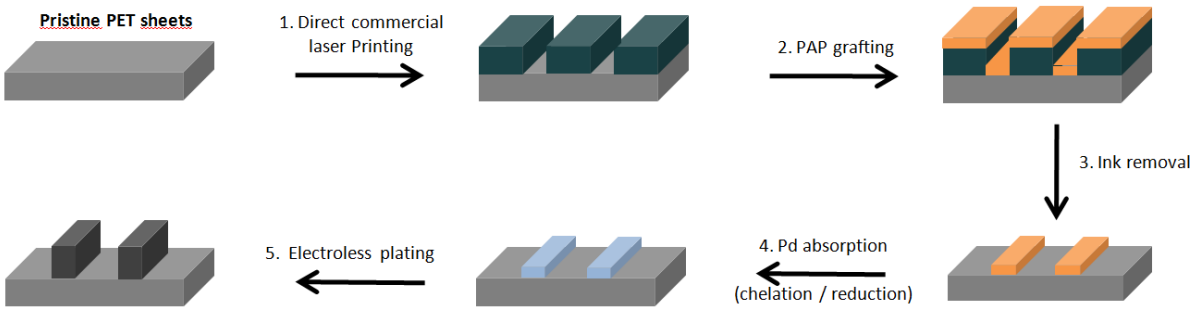

Figure 1: Localized 3D-AIEP process through the direct laser printing of a mask

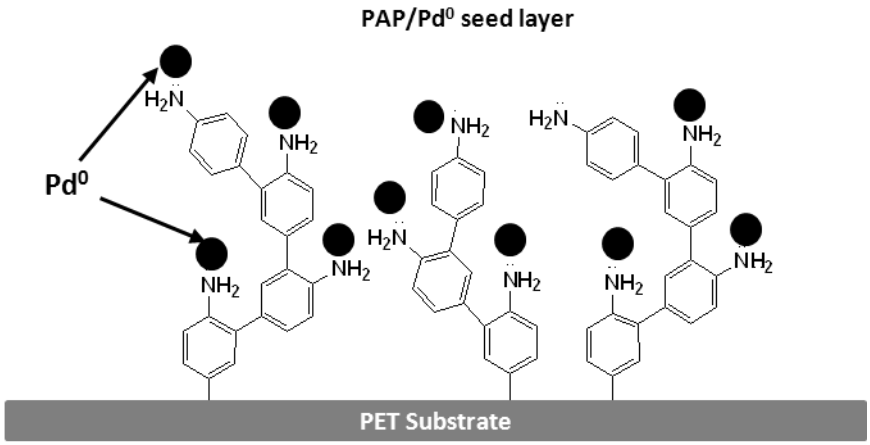

Figure 2: Structure of the PAP/Pd0 seed layer grafted onto PET substrate

EXPERIMENTAL SECTION

Materials

100µm-thick and flexible PET sheets of technical quality were obtained from 3M® as standard transparency films and used as polymer substrates for the localized plating. An industrial detergent was used to clean the substrates: TFD_4 (Franklab). 1-4-diaminophenylene dihydrochloride (Fluka, ≥ 99%), sodium nitrite (Fluka, ≥ 99%) and iron powder (Prolabo VWR, 98%) were used for the polyaminophenylene grafting using the diazonium induced anchoring process. Palladium chloride (Sigma Aldrich, ≥ 99,9%) and sodium hypophosphite (Sigma Aldrich, ≥ 98.5%) were used for the Pd absorption. For the electroless metal deposition, two industrial plating baths were used: a nickel plating bath (Niposit™ PM 988 supplied by Rohm and Haas) and a copper plating bath (M Copper 85 supplied by MacDermid).

Selective 3D-AEIP Process

Polymer surfaces are generally prone to organic pollution which could be detrimental to our 3D-AIEP process. Therefore, PET substrates were submitted to a common industrial detergent cleaning (TFD_4) which is industrially used for removing most of the organic pollutants before metallization.

The 3D-AEIP process is then divided into four main steps:

Mask impression by ink-jet procedure. The direct negative tone printing of the mask pattern is performed with a commercial laser printer (HP LaserJet P3005 PS) onto the pristine PET sheets. This extremely cost effective method is however limited by the laser printer resolution of about 20 µm (1200 dpi).

Polyaminophenlylene (PAP) layer covalent grafting. 1-4-phenylenediammonium dihydrochloride (1.81 g) was dissolved in a HCl solution (0.5 M, 100 mL). Under stirring, $NaNO_2$ (0.1 M, 100 mL) were added stepwise to the previous solution in order to synthesize the aryldiazonium salt. Iron powder (15 g) was then introduced into this solution, as reducing agent of the aryldiazonium salts. Finally, modified PET sheets and references substrates (pristine PET sheets and gold substrates) were introduced in the beaker. After immersion for 30 min at room temperature, the substrates were removed from the reacting bath and sonicated twice for 10 min in deionized water and 1 min in ethanol. That rinsing treatment was shown to allow discarding most of the physisorbed matter. The laser ink was removed by an acetone rinsing treatment for 30 sec under sonication.

Pd absorption. PAP-modified substrates were then immersed for 2 min into an acidic (HCl, 0.12 M) palladium chloride $PdCl_2$ (3.10^{-3} M) solution at room temperature to complex Pd^{II} species within the grafted film thanks to the formation of a dative covalent bond between the amine groups and Pd^{II} species. Afterwards, samples were rinsed with distilled water for 5 min under sonication. In order to reduce Pd^{II} species previously entrapped and complexed within the grafted PAP films, the samples were immersed into a sodium hypophosphite (H_2PO_2Na, xH_2O) (1M) solution at 40°C for 2 min and were rinsed with distilled water for 5 min under sonication. Hence, this reduction step allowed obtaining catalytic-Pd^0 particles entrapped into the PAP layer which were then used for the electroless growth of the metal plated layer.

Growth of the metal plated layer. Surface-activated substrates were finally placed in the electroless metal plating baths. Two commercial plating baths were tested. The first one was a nickel plating bath (Niposit™ PM 988). Sodium hypophosphite NaH_2PO_2,H_2O was the reducing agent, optimum conditions were obtained with a nickel content of $4g.L^{-1}$, a ratio NaH_2PO_2,H_2O/Ni of 3.75 and a pH equals to 9,4, working at 34°C to get a deposition rate of ca 1.33 $\mu m.h^{-1}$ and a final Ni coating containing 4-8% of phosphorus. The second one was a copper plating bath (M Copper 85). Formaldehyde HCHO was used as the reducing agent; optimum conditions were obtained with a copper content of $2g.L^{-1}$, a mass ratio HCHO/Cu of 2, a pH at

13, a work temperature at 48°C; the observed deposition rate was about 4µm.h^{-1}. The duration of the plating was adjusted with respect to the sought thickness.

Characterization methods

Infrared spectra were recorded on a Bruker Vertex 70 spectrometer equipped with an Attenuated Total Reflection (ATR) Pike-Miracle accessory. The detector was a MCT working at liquid nitrogen temperature. The spectra were obtained after 256 scans at 2 cm^{-1} resolution.
XPS studies were performed with a KRATOS Axis Ultra DLD spectrometer, using the monochromatized Al Kα line at 1486.6 eV. The pass energy of the analyser was kept constant at 20 eV for C_{1s} core level scans. The photoelectron take-off angle was 90° with respect to the sample plane, which provides an integrated sampling probe depth range going from 7 to 20 nm for our substrates.

The scanning electron microscopy images were recorded by a Hitachi S4800 equipped with a Field Emission Gun (FEG-SEM) and coupled with an energy dispersive X-ray spectrometer (EDX).

The adhesion between the metallic layer and the polymer sheets was studied by the standard ASTM D3359 Scotch® tape test (cross-cut tape test) which consists in applying and removing pressure-sensitive adhesive tape over 16 cross-hatched squares of 1x1 mm^2 made in the film by an Elcometer Cross Hatch cutter (Elcometer 107 X-Hatch ASTM Kit). That well-used test allows direct comparison of the adhesion of films obtained under various conditions on similar substrates.

In any cases, electrical properties were measured thanks to the formation of wires with the following dimensions: length = 2 cm, width = 300µm and height = 500 nm measured by profilometry and pads of 1 cm^2 at the end of the wire for electrical contact. The resistance of the wire was measured thanks to a four-point probe set-up using a home-built constant current source as described in Keithley's handbook [26]. Copper wires electrical properties were studied under mechanical stress by measuring the electrical resistivity while bending the polymer sheets around cylinders with two radii of curvature equal to 3 and 1 mm respectively. The metal wires grafted on the polymer sheets were submitted to 60 cycles of repetitive strain around the cylinders (40 cycles with the 3 mm-radius cylinder + 20 cycles with the 1 mm-cylinder).

RESULTS AND DISCUSSIONS

PAP grafting

The surface chemistry process used in this report was based on the reduction in solution of an aryl diazonium salt [23]. The corresponding amine layer was obtained by the in situ diazotization reaction of commercial 1-4-phenylenediammonium dihydrochloride followed by it reduction in solution. Polyaminophenylene (PAP) layers have been already used in our laboratory as an intermediate to graft covalently carbon nanotubes, graphene flakes or biomolecules on different kind of substrates [23, 24].

The presence of grafted PAP films onto the polymer surfaces was mainly demonstrated by IR and XPS spectroscopies, on homogeneous samples (without any patterns).

Therefore, PAP-grafted PET substrates were analyzed by ATR-FTIR and **Figure 3** displays IR spectra on pristine PET, PAP-grafted PET sheets and PAP-grafted on gold as a reference. After PAP grafting (**Figure 3b**), two novel bands at 1515 and 1617 cm^{-1} respectively attributed to phenyl ring vibrations and NH_2 deformation are observed and are identical to the one obtained on the PAP-grafted gold substrate with the same process and used as a reference.

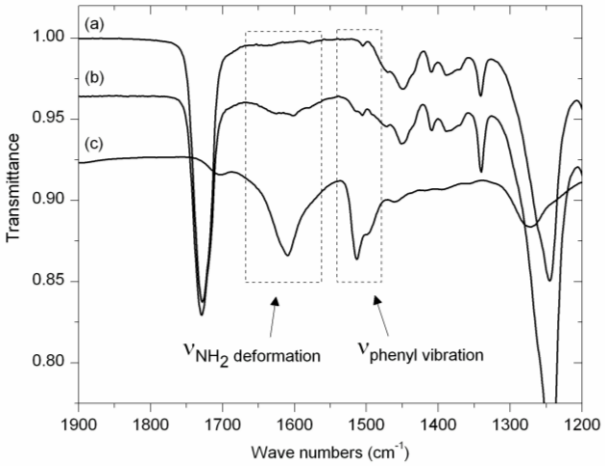

Figure 3: IR-ATR spectra of (a) pristine PET, (b) after PAP grafting on PET and after PAP grafting on gold as a reference (c)

To confirm the presence of the grafted PAP films, the surfaces were studied by XPS. **Figure 4** displays XPS spectra on pristine PET (**Fig 4a**) and PAP-grafted PET sheets (**Fig 4b**). For pristine PET the C_{1s} core level shows one main peak centered at 284.9 eV, which mainly corresponds to

phenyl carbons contained in PET. A second peak centered at 286.4 eV corresponds to aliphatic carbons near the ester group and finally the third peak at 288.8 eV is characteristic of the PET ester groups. For modified PET sheets, two novel peaks centered at 286.9 eV and 285.3 eV corresponding to the phenyl carbon near the amine group and all the phenyl carbons contained in the PAP layer are observed.

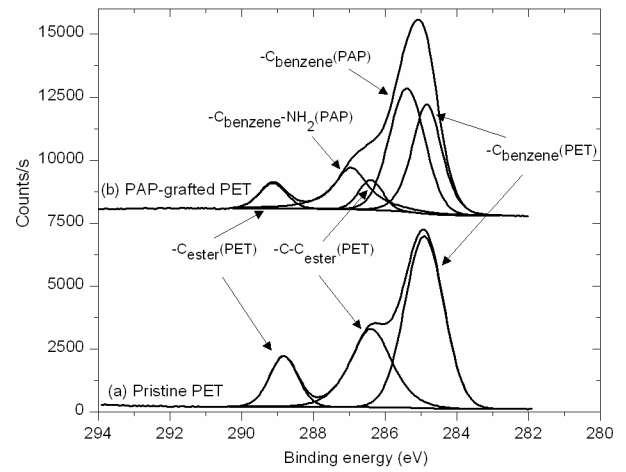

Figure 4: C_{1s} XPS spectra of pristine PET (a) and after PAP grafting (b)

Pd absorption (chelation / reduction)

As shown in **Figure 5a**, the Pd_{3p} spectra analysis confirmed the Pd^{II} chelation obtained by immersion into an acidic HCl/Pd solution by two main peaks corresponding to $Pd_{2p5/2}$ (338.1 eV), and $Pd_{3p3/2}$ (343.2 eV) core level binding energies [27]. As demonstrated by Dressick et al. [14], Pd^{II} chelation in those conditions, i.e. with hydrochloric solution and palladium chloride, results in complexed Pd^{II} monomeric species on nitrogen-bearing groups despite the low pH value, probably via the minority amino groups, which can be constantly replaced through the acido-basic equilibrium. As a result, we assume that in our case, Pd^{II} monomeric species are complexed within the covalent grafting PAP layer. *In situ* reduction of Pd^{II} species was obtained by immersion of the Pd^{II}-PAP film in a sodium hypophosphite solution and confirmed by XPS measurements. After immersion in H_2PO_2Na, both $Pd_{3p5/2}$ and $Pd_{3p3/2}$ core level peaks shifted toward lower energy (336.0 and 341.2 eV) (**Fig. 5b**) as expected for Pd^0 species [27]. However, two shoulders corresponding to non-reduced Pd^{II} species could still be observed. As shown later, that partial Pd reduction has no consequence on the electroless plating step.

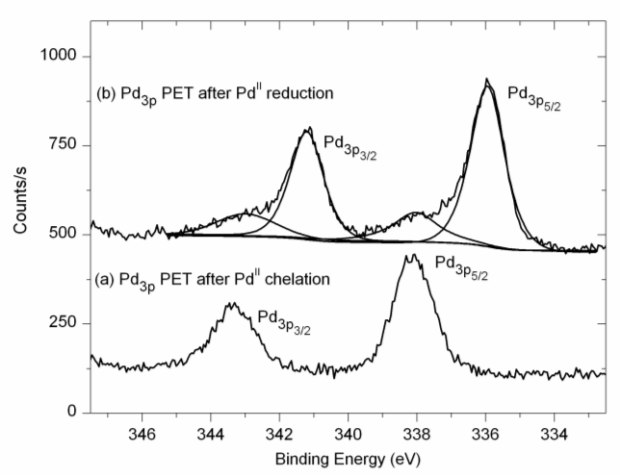

Figure 5: Pd_{3p} XPS spectra of PAP-grafted PET sheets after the chelation (a) and the reduction (b) steps

Electroless metal plating

Taking into account all the parameters described in the experimental section, immersing the Pd-activated substrates in either the industrial nickel plating bath (Niposit™ PM 988) or the industrial copper plating bath copper (M Copper 85) plating baths during 40 and 15 min respectively allowed the formation of 1 µm-thick plated-metal films. In both cases, the metallic layer growth started within a few seconds at the Pd^0-activated surface. The absence of time-lag indicates that the low proportion of remaining immobilized Pd^{II} species, shown above, does not delay the plating process. Indeed, Charbonnier et al. [22] demonstrated that a partial Pd reduction can still initiate the reaction, but after a time-lag which allows the Pd^{II} reduction to be completed by the plating bath reducer. Our results show that we did not have enough remaining Pd^{II} species to allow any time-lag to be detectable.

The obtained metallic layers were characterized by SEM and EDX spectroscopy. As shown in **Figure 6**, the metal plated layer consists of a tight, dense, continuous and void-free film and the metal plated layer is quite conformal to the pristine surface. Cu-plated films exhibit the same properties.

Then, as expected, in the case of the nickel plating layer, EDX spectra analysis revealed the presence of nickel and phosphorous with a final composition of 92 % nickel and 8% phosphorus whereas the copper plating layer contains only copper. Besides, in the case of the nickel plating layer, oxygen was also observed due to an important and spontaneous nickel oxidation at ambient atmosphere.

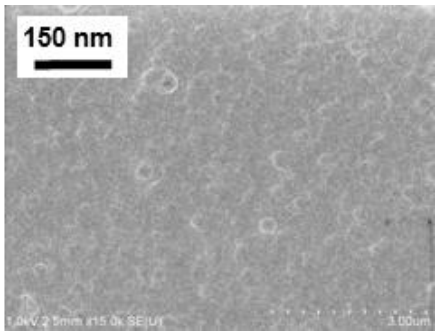

Figure 6: SEM images after electroless nickel deposition onto flexible PET sheets with a 150 nm scaled top view

The adhesion between the metal plated layer and the polymer substrates was studied by the most common industrial adhesion test which is also among the most demanding one: The standard ASTM D3359 Scotch tape test. This measurement has been carried out on substrates with a 1 µm-thick homogeneous nickel and copper plated layers in order to validate the adhesion results. As shown in **Figure 7**, for nickel plated PET substrates, none of the squares was removed. The same results were obtained with copper plated substrates. These excellent adhesion results are quiet surprising since the PAP layer made of aromatic chains is a quite inelastic structure. Hence, it was demonstrated that ligand-bearing brush-like polymers allowed obtaining excellent adhesion of the electrolessly plated layer onto the surface. In those cases, it was basically attributed to the covalent bound between the surface and the grafted polymer brushes as well as to the nanometer-scale mechanical interlocking of the growing electrolessly plated layer within the brushes which was provided by the polymer viscoelastic and high swelling intrinsic properties [28]. In our case, the strong interface bound of the PAP layer onto the surface is obviously kept but the inelastic PAP layer induces less mechanical interlocking effects. According to the adhesion results, it was however sufficient to bring good adhesion results onto the substrates.

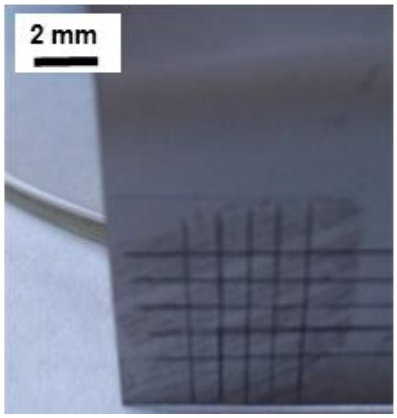

Figure 7: Images of Ni-plated PET substrates with Ni plating after the scotch tape test

Figure 8a and **8b** displays nickel and copper RFID-like features of different sizes obtained onto flexible PET sheets. As illustrated by optical images (Fig. **8d)** of this corresponding nickel pattern, the selective nickel plating was conformal to the negative-tone metal pattern **(Fig. 8c)**. Besides, as shown in **Figure 8e**, the 0.5 µm-thick plated-nickel pattern was analyzed by mechanical profilometry and showed that the nickel layer was quite homogeneous and uniform in thickness except for classical edge-effects.

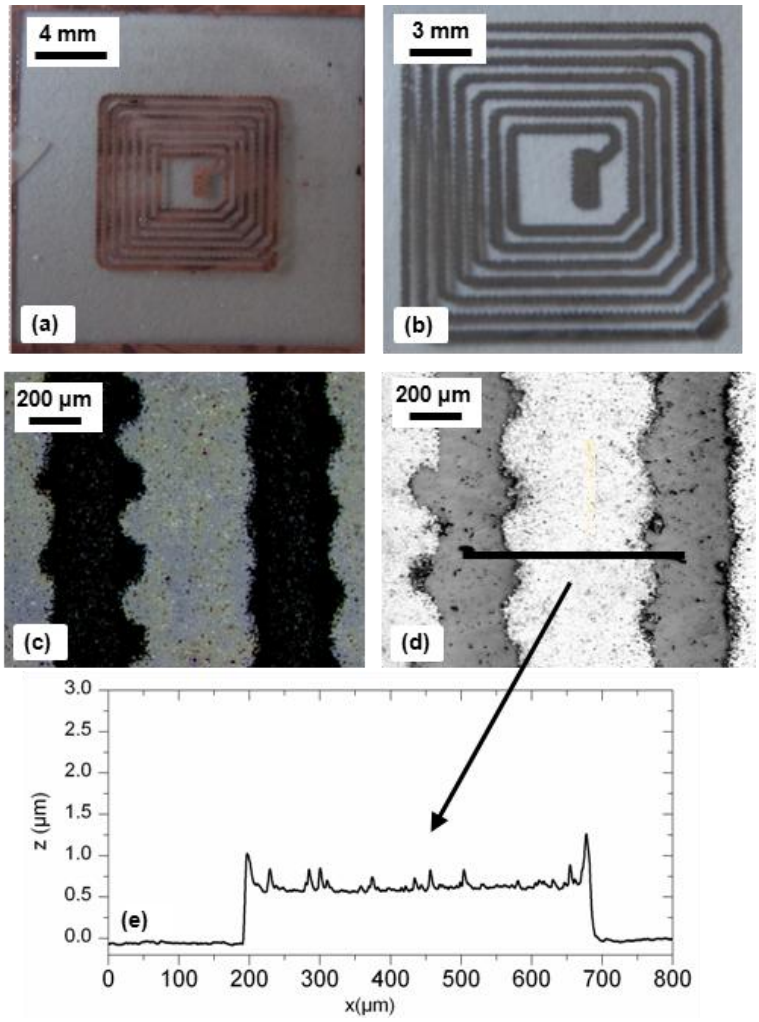

Figure 8: Images of a 1 cm-size copper RFID feature on flexible PET sheet (a), a 1.5 cm-size nickel RFID feature on flexible PET sheet (b) and optical images of the corresponding negative-tone nickel pattern (after inkjet printing of the mask) (c) and the resulting metal pattern after nickel plating (d) with the corresponding profile extractions after nickel plating (e)

Finally electrical properties were measured thanks to specially designed samples exhibiting a linear 300 µm-wide track connected to two large pads for easier electrical contact. As expected, the electrical resistivity of the nickel wire was found infinite due to the well-known spontaneous nickel surface oxidation [29]. On the contrary, the resistivity of copper wire grafted onto the PET substrates was measured at 4.0 µΩ.cm without any mechanical stress, i.e. within the range classically observed on electroless copper surfaces (2-3 µΩ.cm) [28]. Thereafter, in this work, we focused on the electrical properties of the copper wire and the effect of the mechanical deformation on this resistivity was studied by bending the flexible copper tracks grafted onto the PET sheets around cylinders. Two different radii of curvature

respectively equal to 5 and 1.5 mm were used. As shown in **Figure 9**, 40 cycles of repetitive strain around a 5 mm-radius cylinder did not induce any change in metal resistivity. An important resistivity increase was however observed between 40 and 60 cycles around the 1.5 mm-radius cylinder added to the previous deformations. The resistivity increase is then promoted by high numbers of deformations cycles and low radii of curvature. Nevertheless, the copper patterns fabricated on flexible PET sheets withstand substantial mechanical deformation with weak conductivity change for cylinder with a radius superior or equal to 5 mm. The ability of copper tracks fabricated on flexible PET sheets to tolerate tensile strain was attributed to the strong adhesion between the copper wire and the substrates and the copper particles nanometric size [28].

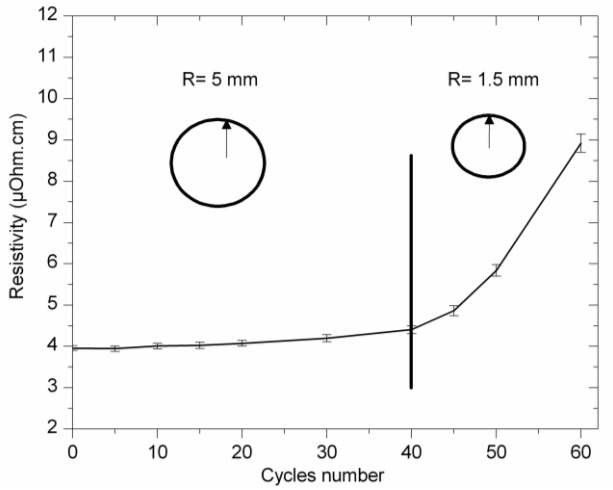

Figure 9: Resistivity measurements of Cu wires grafted on PET sheets and submitted to 40 cycles of repetitive strain around a cylinder with radius with the 5 mm-radius cylinder, followed by 20 cycles with the 1.5 mm-radius cylinder

CONCLUSIONS

We have described an alternative and powerful method to selectively metallize polymer substrates using PET sheets as an example. Based on the one-step chemical grafting of a 3D-ligation structure able to strongly entrap catalysts of the electroless plating growth, it provides excellent adhesion results of the final metal layer onto the substrates. Therefore, this extremely simple 3D-Amino Induced Electroless Plating combined with a direct patterning method allows producing selective metal patterns with good electrical and mechanical properties onto those flexible and transparent PET sheets. Such a process could be an

excellent alternative to usual processes for the cost-effective fabrication of large-area plastic electronics devices

REFERENCES

[1] Y. Wen, Y. Liu, Y. Guo, G. Yu, W. Hu, *Chem. Rev.* **2011**, *111*, 3358.
[2] J. Doggart, Y. L. Wu, P. Liu, S. P. Zhu, *ACS Appl. Mater. Interfaces* **2010**, *2*, 2189.
[3] Y. Shacham-Diamand, A. Inberg, Y. Sverdlov, V. Bogush, N. Croitoru, H. Moscovich, A. Freeman, *Electrochim. Acta* **2003**, *48*, 2987.
[4] R. Oberle, *US Patent 20090128417*, **2009**.
[5] S. Jeong, H. C. Song, W. W. Lee, S. S. Lee, Y. Choi, W. Son, E. D. Kim, C. H. Paik, S. H. Oh, B. H. Ryu, *Langmuir* **2011**, *27*, 3144.
[6] J. Perelaer, C. E. Hendriks, A. W. M. de Laat, U. S. Schubert, *Nanotechnology* **2009**, *20*.
[7] D. Q. Vo, E. W. Shin, J. S. Kim, S. Kim, *Langmuir* **2010**, *26*, 17435.
[8] G. O. Mallory, J. B. Hajdu, *Electroless plating: Fundamentals and Applications*, The American Electroplaters and Surface Finishers Society, Washington, D.C. **1990**.
[9] E. Sacher, *Metallization of Polymers 2*, Plenum Publisher, New York **2002**.
[10] M. C. Demirel, M. Cetinkaya, A. Singh, W. J. Dressick, *Adv. Mater.* **2007**, *19*, 4495.
[11] D. I. Ma, L. Shirey, D. McCarthy, A. Thompson, S. B. Qadri, W. J. Dressick, M. S. Chen, J. M. Calvert, R. Kapur, S. L. Brandow, *Chem. Mater.* **2002**, *14*, 4586.
[12] R. R. Price, W. J. Dressick, A. Singh, *J. Am. Chem. Soc.* **2003**, *125*, 11259.
[13] G. O. Mallory, J. B. Hadju, *Electroless plating: Fundamentals and Applications*, The American Electroplaters and Surface Finishers Society, Washington, D.C. **1990**.
[14] D. Zabetakis, W. J. Dressick, *ACS Appl. Mater. Interfaces* **2009**, *1*, 4.
[15] F. Bessueille, S. Gout, S. Cotte, Y. Goepfert, D. Leonard, M. Romand, *J. Adhes.* **2009**, *85*, 690.
[16] M. S. Miller, H. L. Filiatrault, G. J. E. Davidson, M. Luo, T. B. Carmichael, *J. Am. Chem. Soc.* **2010**, *132*, 765.
[17] C. Brinker, S. GW, *Sol-gel science*, Academic Press Inc., San Diego **1990**.
[18] Z. H. Ma, K. L. Tan, A. D. Alian, E. T. Kang, K. G. Neoh, *J. Vac. Sci. Technol., A* **2001**, *19*, 2471.
[19] W. C. Wang, R. H. Vora, E. T. Kang, K. G. Neoh, *Polym. Eng. Sci.* **2004**, *44*, 362.
[20] Y. Q. Zhu, E. T. Kang, K. G. Neoh, T. Osipowicz, L. Chan, *J. Electrochem. Soc.* **2005**, *152*, F107.
[21] J. R. Lancaster, J. Jehani, G. T. Carroll, Y. Chen, N. J. Turro, J. T. Koberstein, *Chem. Mater.* **2008**, *20*, 6583.
[22] M. Charbonnier, A. Romand, Y. Goepfert, D. Leonard, F. Bessueille, A. Bouadi, *Thin Solid Films* **2006**, *515*, 1623.
[23] P. Viel, X. T. Le, V. Huc, J. Bar, A. Benedetto, A. Le Goff, A. Filoramo, D. Alamarguy, S. Noel, L. Baraton, S. Palacin, *J. Mater. Chem.* **2008**, *18*, 5913.
[24] T. Berthelot, A. Garcia, X. T. Le, J. El Morsli, P. Jegou, S. Palacin, P. Viel, *Appl. Surf. Sci.* **2011**, *257*, 3538.
[25] J. E. Huheey, E. A. Keiter, R. L. Keiter, *Inorganic Chemistry*, De Boeck Université, Bruxelles **1998**.
[26] Keithley, *Low Level Measurements Handbook*, Keithley Instruments, Cleveland **2007**.

[27] G. Beamson, D. Briggs, *High Resolution XPS of Organic Polymers: The Scienta ESCA300*, John Wiley & Sons, Chichester **1992**.
[28] A. Garcia, T. Berthelot, P. Viel, J. Polesel-Maris, S. Palacin, *ACS Appl. Mater. Interfaces* **2010**, *2*, 3043.
[29] *In the industrial electroplating of polymers, the electroless nickel plating is preferred to the electroless copper plating because the latter requires a pollutant reducing agent (Formaldehyde). To overcome the spontaneous nickel layer oxidation, the electroless nickel plating bath is immediately (i.e. within a few seconds to limit the nickel layer passivation) followed by a copper electroplating step which provides the required conductivity for the following steps [6].*

VII. General conclusion and outlooks

Initially, this work was motivated by the development of a sustainable and efficient process for the electroless metal plating of polymers within the current environmental and socio-economic context. The main objective aimed precisely at the replacement of the pollutant industrial process based on a chromium-acid etching by a competitive and versatile process, called Ligand Induced Electroless Plating (LIEP), based on a new adhesion approach of the metal layer onto the polymer substrates. Hence, the LIEP process was based on the covalent grafting of a thin chelating polymer films (which acts as the interphase) through the "Diazonium Induced Anchoring Process" (DIAP) registered under Graftfast™ brand. In this work, chemical and mechanical adhesion was provided by the creation of an interdigitated interphase between the covalently grafted polymer film and the metal layer, whereas, at the industrial scale, adhesion is brought by the creation of superficial holes or cavities onto the surface thanks to an oxidative chromic-acid etching.

We focused on the electroless plating of acrylonitrile-butadiene-styrene (ABS) which is among the most widely used polymers in industry. Hence, ABS ligand induced electroless plating was obtained in three steps, namely: (i) the Poly(acrylic acid) grafting through the Graftfast™ process onto ABS acting as an 3D interphase between the surface and the metal, (ii) the copper Cu^0 seeding of the ABS surface within the PAA-grafted brushes, and (iii) the nickel or copper metallization using commercial-like electroless plating bath which starts on the Cu^0 catalyst particles.

Then, we thoroughly compared three industrially relevant plastics (ABS, ABS-PC and PA) as substrates for our LIEP process. We have been able to link the macroscopic properties of the final metal plated layer, such as the strength adhesion and the electrical resistivity, to the microscopic properties of its precursor steps, such as the amount of loaded catalyst precursors and the morphology and the chemical composition of the surface of the pristine substrate. Indeed, we demonstrated that the higher the PAA grafting rate, the higher the amount of loaded catalytic copper, the lower the particle size in the plated copper film, and the higher its conductivity. Moreover, this work highly strengthens the versatility of the LIEP process and increases its application fields.

As a result, this wet LIEP process based on successive immersions is potentially suitable and competitive to be used on an industrial line to replace the current chromic acid based process. Hence, this significant technological breakthrough is ready to be transferred at the industrial scale for general manufacturing since it does not need any particular requirements

either upstream or downstream from the LIEP process. In a similar way, each step of the LIEP process is also COV-free and based on mild working conditions.

Regarding the future prospects for this “wet LIEP process”, it would be a key asset for plating industries to extend it to polymers with specific bulk properties which are currently “unplateable” polymer substrates at the industrial scale (such as poly(oxymethylene) or poly(tetrafluoroethylene)) by an optimization of the Graftfast™ process working conditions.

Subsequently, we logically combined the LIEP process with two cost-effective patterning techniques to obtain copper patterns onto flexible PET and PVDF substrates. It has been shown that, whatever the patterning technique, the LIEP process allowed to produce selective copper plating with good and stable electrical properties onto flexible polymer substrates. Hence, the LIEP process combined with any of those patterning methods could be an excellent alternative to classical processes for the cost-effective fabrication of large-area plastic electronics devices. Indeed, these simple and cost-effective methods work on smooth surfaces; copper growth is localized and conformal to the mask; electrical properties are close to bulk values and stable and copper patterns fabricated on these flexible substrates withstand substantial mechanical deformation with only slight loss in performance.

Then, we were able to transpose this wet LIEP process to a robust and waste-free patterning process suitable for a large range of substrates by direct photo-assisted covalent grafting of PAA by inkjet printing. This visible light-induced process was demonstrated with gold, PET and PVC substrates. Hence, GraftFast™ has been combined with the trendy Drop-On-Demand (DOD) inkjet technology to provide localized covalent polymer grafting through a one-step method based on the photo-assisted radical polymerization of a vinylic monomer within a picoliter droplet. The purely chemical reducing agent in the cartridge has been replaced for a photochemical one which is post-activated after the printing step. Then, combined with the PAA-based LIEP process, we were able to produce micrometric metal patterns with excellent mechanical and electrical properties while saving time, matter and energy compared to all the processes described in the literature.

Lastly, in order to improve the versatility of the wet LIEP process, we have described an alternative and simplified method to metallize PET substrates with neither the use of

chromium (as etching agent) nor PAA grafting. Hence, by just using the same grafting solution than for the Graftfast™ process without any acrylic acid, a polyaminophenylene (PAP) layer which is usually used as an adhesion primer for the Graftfast™ process has been covalently grafted. As in the case of PAA grafting, this activated 3D-polymer layer acts both as a seed layer for electroless metal growth and as an interdigital layer to enhance mechanical properties of the metallic patterns. Whereas our previous work was based on Cu species strongly immobilized by carboxylate groups contained all along the PAA chains, this process takes advantage of the Pd strong affinity towards amino ligands contained all along the PAP chains. Besides, this alternative approach was guided by most of the electroless plating process which are based on Pd seed layer thanks to nitrogen-bearing groups. Combined with a cost-effective lithographic method, this Amino-Induced Electroless plating (AIEP) process allowed to produce metal patterns with identical electrical and adhesion properties than with the PAA-based LIEP process. However, due to their better elasticity and swelling properties, metal patterns fabricated on flexible PET sheets by the PAA-based LIEP process seem to withstand mechanical deformation better. Further studies on the structure of the grafted and ligand-bearing Graftfast™ layer behavior towards mechanical deformation are needed to better understand the real impact on the mechanical properties of the electroless plated layer.

Based on these results, the future evolution of this project will have to focus on the possibility to adapt this AIEP process to the photo-assisted and inkjet-printed LIEP process. Indeed, it could allow reducing again the production costs and could be an excellent alternative to our own PAA-based LIEP process for applications where the mechanical property is not a requirement.

In the near future, the development of an all-printing process also including the catalyst seeding and the electroless plating growth steps could definitively be the main challenge to take up and it would allow the LIEP process to be directly inserted on a printing industrial line. It would represent a huge advantage for its applications in flexible electronics.

Finally, even this research project was focused on metallization of polymers especially through the development of two ligand induced electroless plating processes, it also led to extend the Graftast™ technology to various kinds of substrates and applications based on local surface functionalization such as biochips or microfluidics chips and represent a chemical and direct-write technology.

APPENDIXES

Appendix A: Versatile toolset" for DNA or protein immobilization: Toward a single-step chemistry

T. Berthelot, A. Garcia, X. T. Le, J. El Morsli, P. Jegou, S. Palacin, P. Viel, "Versatile toolset" for DNA or protein immobilization: Toward a single-step chemistry, *Appl. Surf. Sci.* 2011, *257*, 3538.

Applied Surface Science 257 (2011) 3538–3546

Contents lists available at ScienceDirect

Applied Surface Science

journal homepage: www.elsevier.com/locate/apsusc

"Versatile toolset" for DNA or protein immobilization: Toward a single-step chemistry

Thomas Berthelot[a], Alexandre Garcia[a,b], Xuan Tuan Le[b], Jenna El Morsli[b], Pascale Jégou[b], Serge Palacin[b], Pascal Viel[b,*]

[a] Laboratoire des Solides Irradiés UMR 7642 CEA/CNRS/Ecole Polytechnique, CEA-DSM/IRAMIS LSI, Ecole Polytechnique, F-91128 Palaiseau Cedex, France
[b] Chemistry of Surfaces and Interfaces, CEA Saclay, DSM/IRAMIS/SPCSI, F-91191 Gif-sur-Yvette Cedex, France

ARTICLE INFO

Article history:
Received 27 August 2010
Received in revised form
10 November 2010
Accepted 10 November 2010
Available online 20 November 2010

Keywords:
Biosensor
DNA
Protein
Covalent immobilization of biomolecule
Diazonium salt
Surface chemistry

ABSTRACT

Covalent immobilization of non-modified biological materials as proteins or nucleic acids has been performed through a single and soft method. Based on diazonium salt chemistry, this protocol leads to an ultrathin grafted film, on metallic or polymer materials, which can eventually be used as a self-adhesive primer for immobilizing biological materials from aqueous solutions through a simple dipping step. Moreover, this self-adhesive primer may be patterned by cheap and easy methods as ink or UV masking. Biological models as low molecular weight DNA from salmon sperm and glucose oxidase (GOD) were covalently immobilized by this soft procedure. In order to evaluate the consequences of this non-specific covalent immobilization method on biological activity, enzymatic activity of GOD was monitored by electrochemical detection of hydrogen peroxide (H_2O_2). We thus demonstrate that such a self-adhesive primer represents a new and alternative process offering a versatile toolset for immobilizing biological material for biosensor development on conductive and non-conductive materials.

1. Introduction

Biology as the electronic is following a path of miniaturization and large-scale integration process that will revolutionize biotechnology [1]. These ongoing processes are compiled in devices known as biosensors and/or biochips, including microarrays and lab-on-a-chip microfluidic devices [2–4]. In biosensors the recognition species are either proteins (enzymes, receptors, antibodies, peptides, etc.) [1,5] or nucleic acids (DNA, RNA, etc.) [6,7]. Two key parameters appear to govern the overall performance of biosensors are both the surface chemistry and the method used for biomolecule immobilization.

Nowadays, the microarray material and the type of biomolecules often determine the method used for immobilization. Moreover, the detection method to visualize biological event is conditioned itself by the nature of microarray material [1,5–7]. In order to overcome all these conventional drawbacks, a versatile surface chemistry capable of selective functionalization of raw conductive, semiconductive and insulating materials, with surface density control, and compatible with chemical and biological element immobilization is highly desirable. An obvious need exists to develop a flexible immobilization process or "versatile toolset" to provide strong, stable, and accessible binding of the sensing element (DNA, proteins and peptides) with the same chemistry, thus leading to sensitive and reproducible biosensor performances.

Methods used for biomolecule immobilization are classified into two categories: (i) non covalent attachment which includes sol–gel encapsulation, polymer entrapment and physical adsorption (electrostatic and hydrophobic adhesion) and (ii) covalent attachment [8,9]. Concerning the first category it is noteworthy that three-dimensional supports are generally plagued by problems relating to mass transport effects and high background signals, resulting in false kinetic rate constants. The question of which strategy can be considered as the best one is still open [1,5–7]. Concerning the second category many chemical routes have been explored, the first one consists to only prepare the surface to react with biological materials the second one consists to modify randomly the biological materials in order to react with the surface. The formation of irreversible covalent bonds between biomolecules and reactive groups on the support is one of the most widely investigated methods [8,10]. However, the disadvantages of most covalent attachment schemes are: (i) the surface activation methods may be incompatible with biological

* Corresponding author. Tel.: +33 01 69 08 41 47; fax: +33 01 69 33 64 62.
E-mail address: pascal.viel@cea.fr (P. Viel).

0169-4332/$ – see front matter © 2010 Elsevier B.V. All rights reserved.
doi:10.1016/j.apsusc.2010.11.071

medium, (ii) the coupling procedures may require harsh conditions or release byproducts which can produce artefacts and (iii) the covalent attachment may be detrimental for the biological activity. The formation of surface functional groups (carboxyl, amino, etc) through various chemistries such as silane on glass or silicon [11,12], alkanethiol monolayers on Au [13] and conducting polymers [14,15] such as modified polypyrrole and polyaniline have been employed to improve surface functionalization and to immobilize biomolecules onto surfaces. Recently a method proposed by Bailey's group use benzophenone-modified substrates to photochemically control covalent coupling of solution-phase biomolecules [16,17].

In this context, using aryldiazonium salts, which substituent may be selected at will, appears attractive because the grafted polyaryl layers obtained from aryldiazonium salts exhibit a very high stability, in particular at high temperature, in harsh solvent conditions, under sonication, limitation of non-specific protein adsorption and may be stored without any damage over several months in air [18,19]. Indeed, diazonium chemistry was already used to attach a variety of biomolecules including DNA, proteins and peptides on conductive or semiconductive materials [8,18,20–24].

There are actually two generic methods used to attach biomolecules with diazonium chemistry. The first one is the chemical modification of the biomolecule with a diazonium group. The modified biomolecule is then used to functionalize surfaces by electrografting a conductive material. This process has two drawbacks: (i) the chemical modification of biomolecules can damage their biological activity and is time-consuming (purification, etc.) and (ii) this process is only limited to conductive materials. The second one is a multistep process which consists to electrograft onto surfaces a diazonium layer bearing a functional group (for example an amino group). Afterwards, the chemical ligation between the biomolecules and this layer can be performed with generic coupling agents such as carbodiimide or aldehyde for example. This process also presents some drawbacks: (i) this process is also limited to conductive materials and (ii) some side products can be generated which can affect the activity of the biomolecule or create artefacts.

Recently, we have shown that redox grafting of diazonium salt provide a very simple way to modify any surface (metallic, semiconductor or insulating) of any complex geometry with robust polyphenylene-like films [25,26]. Chemical reactivity of these layers is used to graft polymers, metallic nanoparticles and MWCNT in one step immobilization procedure [27,28]. Concurrently, an electrochemical process has been reported for the immobilization of Horseradish peroxidase on gold electrode surface [29]. Nevertheless, this protocol presents some drawbacks: (i) the electrochemical reduction of diazonium salt for layer synthesis and (ii) the electrochemical conversion of the nitro to amine groups reduce the support used for biosensor synthesis to conductive or semiconductive materials.

Herein, we present, for our knowledge, the first "versatile toolset" for biosensor synthesis. Based on a purely chemical reduction of diazonium salts, it can be applied for the surface modification of both conductive and insulating materials with a simple, robust, "green" and soft procedure. Afterwards, aryldiazonium layers can react with a multitude of biomolecule functions which lead to covalent bonds between the surface and proteins or nucleic acids. Results based on the use of these self-adhesive surfaces and the grafting procedure concerning different biomolecules as protein (glucose oxidase) and DNA strands are reported, together with preliminary results on the formation of patterned self-adhesive surfaces. In order to confirm the potential of that immobilizing method for biosensing, the biological activity of the immobilized enzyme was also checked.

2. Experimental

2.1. Chemicals

All standard chemicals and solvent were of research grade, purchased from Sigma–Aldrich and used as received. Iron particles were purchased from VWR (98%, mean particle size 45–100 mm). Glucose oxidase from *Aspergillus niger* and DNA from salmon sperm were purchased from Sigma–Aldrich and used as received. Glucose solution BioUltra grade, 20% in H_2O for molecular biology and PBS were purchased from Sigma–Aldrich and used as received. Gold substrates were obtained by successive metallic evaporation of 5 nm of chromium underlayer and 200 nm of gold as top coat on microscopic glass slides. PP (polypropylene) films were purchased from Goodfellow and cleaned before use with water and ethanol under ultrasonic treatment for 10 min.

2.2. Self-adhesive surfaces preparation

The synthesis of self-adhesive surfaces was performed in open air in a simple flask. The grafting of polyaminophenylene (PAP) onto gold and PP surfaces was realized according to the process summarized here and detailed in a previous paper [25]. After addition of sodium nitrite (Eq. (1)) to an acidic solution (HCl 0.25 N, pH 0.3) of *p*-phenylenediamine, iron powder was added to reduce the aryldiazonium salt in solution and start the overall grafting and growing chemical process. Then gold or polymeric substrates were introduced and left in the solution for 15 min to 2 h at 38 °C. Note that the film thickness increased with the reaction time whereas the film properties are the same whatever the film thickness [25,27]. The film thickness was appreciated with the highest IR band intensity as presented in Section 2.5. Afterwards, samples were rinsed with deionized water and acetone in an ultrasonic bath for 5 min. The resulting PAP film on gold was analyzed by FTIR-ATR (Fig. 1b). The diazotisation of the grafted PAP layer on substrates could be performed either in aqueous or in organic medium. In aqueous medium, the PAP layer was soaked 60 s with acidic nitrite sodium solution in the same way that the first diazotisation, rinsed with dry acetone or acetonitrile then finally dried with a flow of nitrogen. In organic medium, the PAP layer was soaked 60 s in acetonitrile with $NOBF_4$.

2.3. Patterning strategies

2.3.1. Ink patterning

Small squares representing the future spots of grafting were drawn by using a simple indelible commercial marker (Stabilo OHPen universal). After the PAP grafting step, ink was eliminated by a rinsing in acetone. Then, after the surface drying, the diazotisation step was carried out.

2.3.2. UV patterning

After the conversion of PAP layer into PDP reactive thin layer, samples were exposed to UV (Spectra Physics, 200 W mercury–xenon lamp with a 380 nm cut off filter) through a mask for 10 min. Afterwards, UV protected areas were used to graft biomolecules.

2.4. Spontaneous grafting and rinsing

The spontaneous grafting of organic and bio-organic molecules onto self-adhesive (PDP) surfaces was performed by a simple droplets deposition. After 10 min, the substrates were sonicated for 10 min in an appropriate solvent. This rinsing treatment allowed discarding all the physisorbed matter without preserving the biological activity. Glucose oxidase (1 mg) was dissolved in 3 mL of

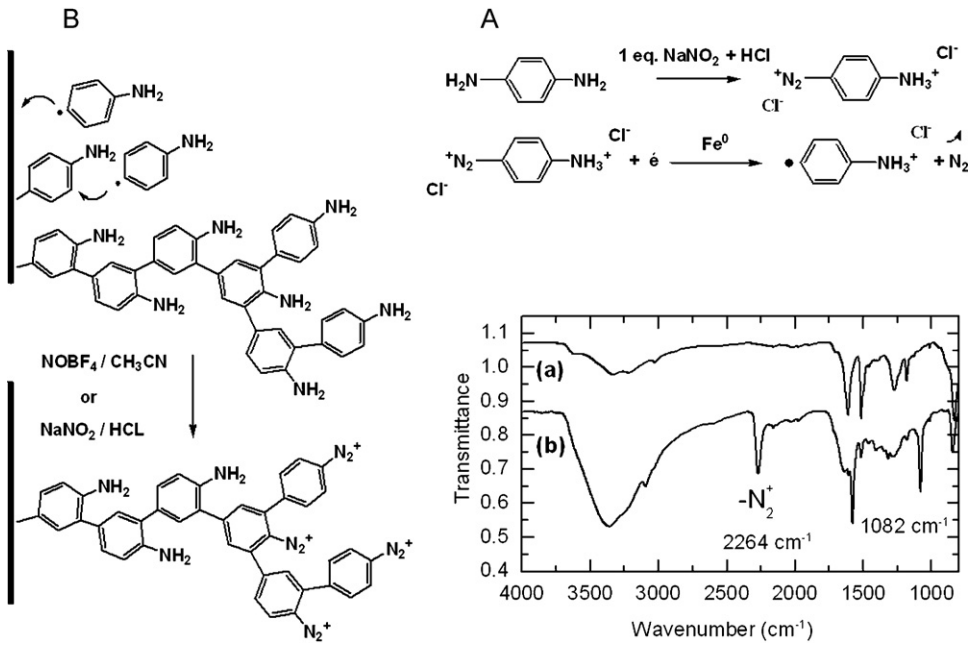

Fig. 1. Chemical route to produce self-adhesive surfaces for biological materials: for the sake of simplicity amine moieties are quoted as neutral on step (b) and (c). Left part: (a) production of reactive species, (b) grafting of amino phenylene moieties, (c) growing of polyaminophenylene (PAP) layer, (d) chemical conversion through amine diazotisation to produce polydiazophenylene (PDP) acting as self-adhesive surface. Right-part: IR-ATR spectrum of (c) polyaminophenylene (PAP) layer and of (d) polydiazophenylene (PDP) layer acting as self-adhesive surface (SAS).

MilliQ water under soft agitation before deposition onto the PDP surface. DNA (1 mg) was dissolved in 5 mL of MilliQ water under soft agitation and applied on the PDP surface. The latter protocols were also applied to non-diazotised (PAP) surfaces in order to check biomolecule unspecific adsorption onto a PAP layer.

2.5. IR spectroscopy

Infrared spectra were recorded on a Bruker Vertex 70 spectrometer controlled by OPUS software. ATR mono-reflexion Pike-Miracle and Hyperion 2000 microscope accessories were implemented. The detector was for both accessories MCT working at liquid nitrogen temperature. For ATR spectra acquisitions were obtained at 2 cm^{-1} resolution after 8 scans for neat products and after 256 scans for films. Mapping was performed on Hyperion 2000 controlled by OPUS video 3D software using a motorized moving stage, grazing angle objective accessory and polarized light. Optical field of 50 μm was defined by glass slide. Spectra acquisitions were obtained at 6 cm^{-1} resolution after 64 scans. IR spectra were employed mainly to determine the chemical structure of films but also to determine film thicknesses through the absorption band intensities. Regarding this latter point thicknesses were obtained only after having made a calibration procedure between IR and direct profilometric measurements.

2.6. XPS spectroscopy

XPS studies were performed with a KRATOS Axis Ultra DLD spectrometer, using the monochromatized Al Kα line at 1486.6 eV. The pass energy of the analyzer was kept constant at 20 eV for C_{1s} core level scans. The photoelectron take-off angle was 90° with respect to the sample plane, which provides an integrated sampling probe depth of ca. 15 nm.

2.7. Electrochemistry

Cyclic voltammetry was recorded with a potentiostat EGG model 273. For GOD activity measurement, a gold electrode was modified with a PDP layer of thickness ca. 20 nm. A diluted glucose oxidase solution (3 μg/mL) was deposited on this activated surface. After 10 min, this modified electrode was washed three times with PBS solution without ultrasonic treatment to preserve biological activity. The electrodes and the solution were placed in a typical three-electrode electrochemical cell: a working electrode bearing grafted glucose oxidase, an auxiliary electrode (graphitic plate) and a saturated calomel electrode as reference electrode. The electrolyte was pH 7 phosphate buffer solution. A solution of D-glucose at 7.69×10^{-3} M was added to the electrochemical cell. Cyclic voltammetry was then used to measure glucose oxidase activity.

3. Results and discussion

3.1. Self-adhesive surfaces synthesis

The self-adhesive surfaces were obtained by the following two-diazotisation steps protocol based on *p*-phenylenediamine. The first step dealt with the synthesis of polyaminophenylene (PAP) layer on the desired substrates according to a chemical route in aqueous medium as presented in Fig. 1. As previously demonstrated, the resulting PAP films are stable in ambient conditions [23]. Fig. 1a shows the suggested chemical mechanism for conversion of the grafted amine groups to grafted aryldiazonium salts (PDP). The resulting polydiazophenylene (PDP) films on gold substrate were analyzed by FTIR-ATR (Fig. 1). Vibrational bands at 2270 and 1082 cm^{-1} are respectively attributed to the so-formed aryldiazonium salt and its BF_4^- counter ion. The decrease of the NH_2 (1617 cm^{-1}) band also confirms the diazotisation process. However persistence of lower intensity bands at 1511, 1171 and 1177 cm^{-1} belonging to the previous PAP form attests that the conversion of PAP into PDP is not complete (Fig. 1). We assume that the conversion is probably more efficient on the top part of the grafted PAP film than in the bulk of the film.

This conversion should be done just before "using" the self-adhesive surfaces to minimize spontaneous decomposition of the grafted aryldiazonium salts. Global XPS spectrum of PAP layer

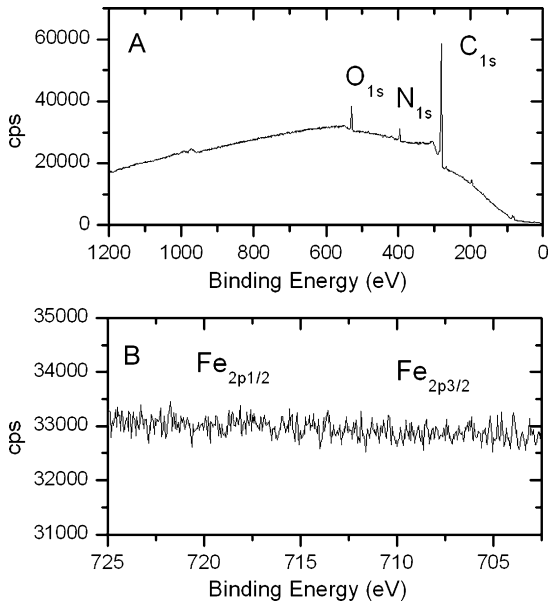

Fig. 2. X-ray photoelectron spectroscopy analysis. (a) Survey XPS spectrum of PAP layer. (b) Close view in the iron XPS energy range showing that iron atoms were absent.

(Fig. 2) highlights that self adhesive surfaces obtained by this process are free of heavy metallic ions which may inhibit biological activity of the immobilized enzyme.

3.2. Patterning results on PAP and PDP layers

A microarray is defined as a collection of miniaturized spots, arranged on a solid substrate. Patterning appears as one of the key points for the synthesis of microarrays as protein or DNA chip. To demonstrate the feasibility to produce array format with self-adhesive surfaces, two different approaches were used based on (i) ink mask process and on (ii) UV irradiation through a mask.

The first method was carried out by drawing a mask on the desired surface with ink. For this purpose, the selected ink must be insoluble in the solvent used for the PAP film synthesis. This process led to draw four small un-inked gold squares representing the future activated spots of the biosensors. The grafting of the PAP layer occurred all over the surface, either inked or not. After the ink dissolution with acetone, the PAP grafted on top of the inked areas was lifted-off and the four small squares of PAP directly grafted on the free gold zones appeared (Fig. 3). Then the diazotisation process was carried out selectively on the PAP-grafted squares. Fig. 3A shows, IR spectra outside (a) and inside (b) one square and a 3D IR mapping view based on the 1617 cm^{-1} absorption band (NH_2 bending from grafted PAP) (Fig. 3B). This very simple and handmade patterning method was only carried out to illustrate that any lift-off process is compatible with the formation of the PAP grafted film. Hence, any usual photolithographic method may be used to reach smaller patterns.

The second patterning approach was based on the well-known photochemical decomposition of diazonium salts (Fig. 4). Commonly, diazonium salts are decomposed under UV irradiation and converted to phenyl cations which are generally transformed into phenol groups [30]. Hence the grafted PDP film could be used as a locally sacrificial layer for patterning. After the grafted PDP film synthesis, the modified substrate was submitted to UV radiation (320–500 nm) through a mask for 10 min. The mask consisted of fused silica slide partially covered with metallic zones. Thus, the diazonium salts located under the covered zones were successfully protected from the photochemical decomposition and still self-adhesive whereas the diazonium salt areas which experienced the UV irradiation were disclosed. Indeed, the aryldiazonium stretching band (2270 cm^{-1}) disappeared from the UV-irradiated areas (Fig. 4). No significant loss of matter was observed after the UV-irradiation process. These results enhanced that self-adhesive surface process could be used to produce any array format by easy and cheap methods.

3.3. Diazonium stability in water

Commonly aqueous medium is recognized to destabilize diazonium salts. However working with biological compounds requires to overcome this problem. In fact, the chemistry of diazonium salts as a function of pH appears complex [31,32]. It is widely accepted that aryldiazonium salts are more stable at acidic pH than at neutral or basic pH, which induce spontaneous hydrolysis reactions

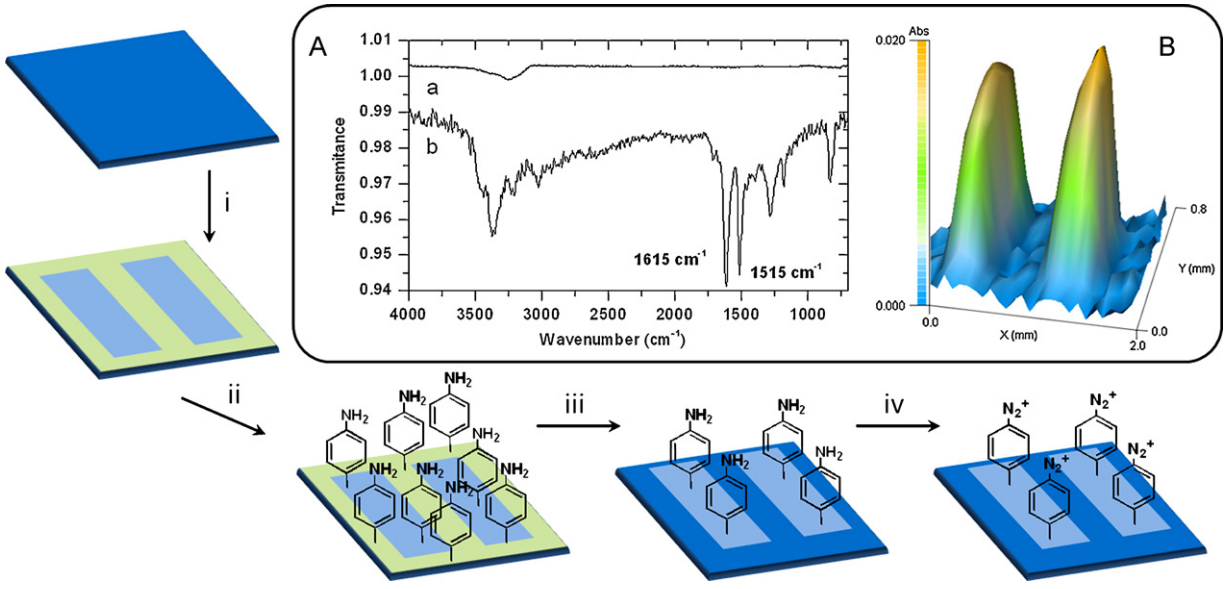

Fig. 3. Ink-patterning strategy: (i) drawing a mask with ink, (ii) polyaminophenylene layer grafting, (iii) ink dissolution with appropriate solvent, (iv) rediazotisation of polyaminophenylene layer. (A) IR spectra outside (a) and inside the squares (b). (B) 3D view acquired on mapping IR mode obtained by integration of the 1615 cm^{-1} peak on a patterned-PDP layer.

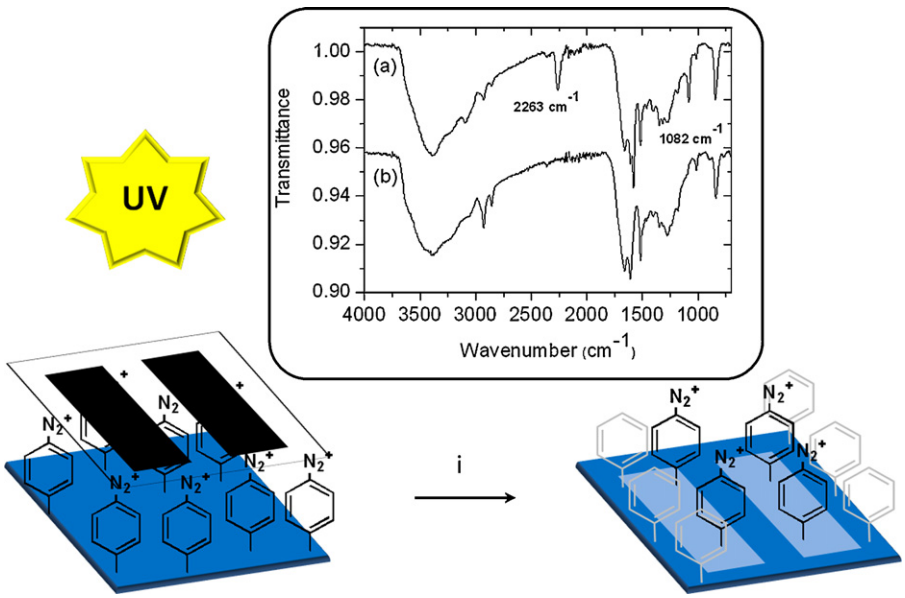

Fig. 4. Photochemical decomposition patterning strategy: (i) UV irradiation process through a mask to obtain self-adhesive patterned surface. IR microscopy analysis of protected (a) and exposed (b) areas of a grafted PDP layer after UV irradiation for 10 min through a mask.

and produce phenol derivatives, although those decomposition reactions take place only after several minutes and coupling reactions between diazonium salts and proteins or amino acids at pH between 5 and 9 were reported [33]. Nevertheless neutral or basic pHs were shown to reduce the grafting efficiency and stability of diazonium salt solutions, contrarily to acidic medium [34]. In order to study the aqueous stability of our self-adhesive surfaces and their compatibility with admissible biological conditions (pH 7 ± 1), PDP films were immersed in MilliQ water (pH 6–7) and the intensity of the aryldiazonium stretching band at 2270 cm^{-1} was normalized and expressed as a function of time. A complete loss of the diazonium signature was reported after 20 min in water at pH 6–7 (Fig. 5). This result is compatible with the use of PDP films to immobilize DNA or proteins in biological conditions since shorter reaction times will be shown to be enough to get covalent grafting.

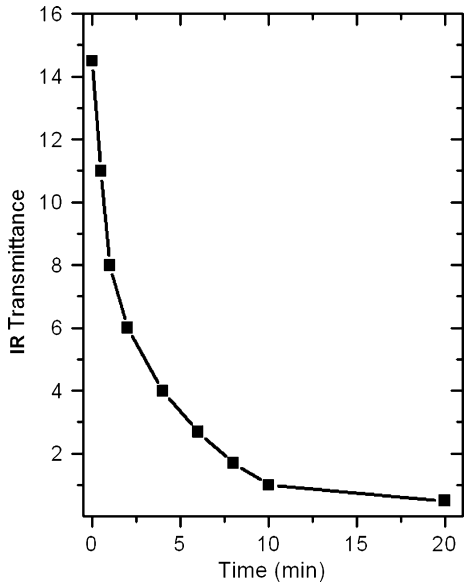

Fig. 5. Stability of the PDP layer immersed in aqueous pH 6–7 medium. Points represent IR transmittance diazonium band intensity variation with immersed time. Samples were blowed with N_2 before measuring.

3.4. Diazonium reactivity toward biological molecules

Diazonium salts are known to react easily with nucleophilic groups like thiols, amines or even aromatic compounds [35–38]. Biological molecules as nucleic acids and proteins are natural polymers of nucleotides or amino acids, respectively, which present different chemical groups as aromatics, thiols, phenol rings, phosphates, primary amines, imidazole rings, guanidine functions [33,39,40]. Some direct reactions of selected biomolecules and diazonium salts in solution have already been demonstrated, with the formation of azo linkages for example. Table 1 lists some of those reported evidences, from which it can be assumed that any biological molecule should be able to react spontaneously with diazonium salts. We will take advantage of that to immobilize biomolecules onto our PDP surfaces.

Hence the reactivity of grafted diazonium groups toward biomolecules was evaluated through two biological models: low molecular weight DNA from salmon sperm and glucose oxidase (GOD) (Fig. 6). Biological immobilizations were analyzed by FTIR experiments after abundant rinsing and ultrasonic treatment in the suitable solvent to discard any adsorbed material without any consideration of biological activity. To demonstrate the covalent grafting on PDP layer, all deposit experiments were realized and analyzed both on untreated surfaces (PAP) and on self-adhesive (PDP) surfaces.

Table 1
Confirmed biological groups which can react with diazonium moieties.

Chemical function	Molecule	Kind of biomolecules
Imidazol	Histidine [37,41]	Proteins
Aromatic ring	Tyrosine [36,41], Phenylalanine, Tryptophane	Proteins
Primary amine	Lysine [36]	Proteins
Thiol	Cystein [36]	Proteins
Guanidine	Arginine [36]	Proteins
Amide	Asparagine, glutamine	Proteins
Alcohol	Serine [36], threonine	Proteins
Purine ring	Adenine or guanine [38,39]	DNA or RNA

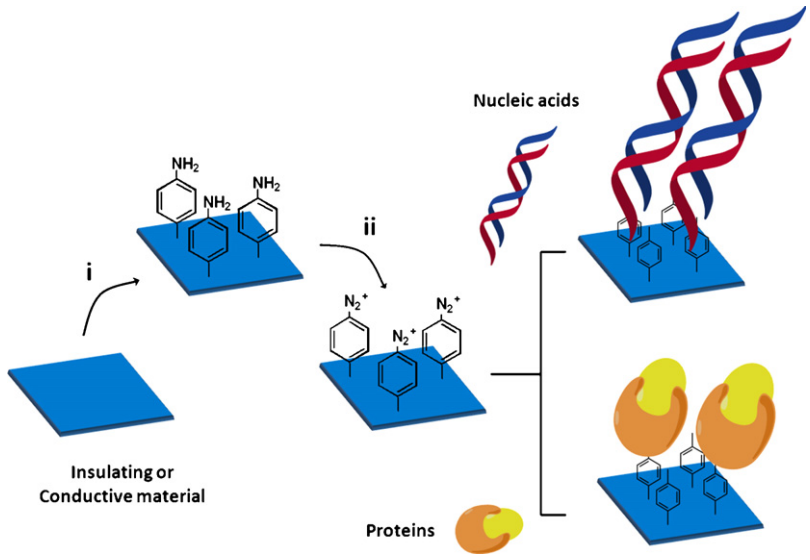

Fig. 6. Strategy for immobilizing nucleic acids or proteins on insulating or conductive materials with self-adhesive properties: (i) and (ii) preparation of self-adhesive surfaces as described in Fig. 1, (iii) direct and spontaneous grafting of biological materials putted into contact with surfaces.

After dissolving DNA on MilliQ water, a gold surface with PDP film was added to this solution for 10 min. After abundant rinsing with water and ultrasonic treatment, the characteristic IR bands of phosphate backbone at 1226 cm^{-1} for the asymmetric PO_2^- stretching mode, 1080 cm^{-1} for symmetric PO_2^- stretching mode and broad band at 1700–1630 cm^{-1} from nucleobase vibrations and double helical structures [41] were easily observed. With the same experimental conditions, no signal from DNA was observed on the PAP surface (Fig. 7A). Ink patterned PDP layer was submitted to DNA deposition. After FTIR mapping and spectral integration at 1700–1630 cm^{-1} and 1280–1230 cm^{-1} range, DNA is only present on PDP plots (Fig. 7B).

In the same way, GOD was dissolved in water and a self-adhesive surface of gold conductive or insulating material (PP) (Fig. 8A) was subjected to this protein solution for 10 min. After desorption procedures, IR analyses exhibited characteristic GOD amide bands at 1645 cm^{-1} for Amide I and at 1530 cm^{-1} for Amide II on PDP layer but not on PAP film where the mean peak remained at 1614 cm^{-1}. Same results were obtained on ink patterned PDP layer which was subjected to GOD (Fig. 8B).

These results suggest a covalent grafting of biomolecules on PDP layers. Moreover, in all experiments, specific diazonium band at 2270 cm^{-1} was not observed after biological functionalization. In other technologies, immobilization process may lead to partial or complete loss of biological molecule activity, due to random orientation and structural deformation. In order to study the influence of immobilization by self-adhesive surface on biological activity, the biological activity of GOD immobilized on a gold/PDP surface was measured.

3.5. GOD activity detection

Glucose oxidase (GOD) is an enzyme that catalyses the oxidation of beta-D-glucose into D-glucono-1,5-lactone, which then hydrolyzes to gluconic acid and hydrogen peroxide. The GOD modified surface was evaluated electrochemically through the detection of hydrogen peroxide generated through their usual catalytic activity [42–45].

The monitoring of H_2O_2 was then performed by cyclic voltammetry at scan rate of 20 mV s^{-1}. To determine the most efficient

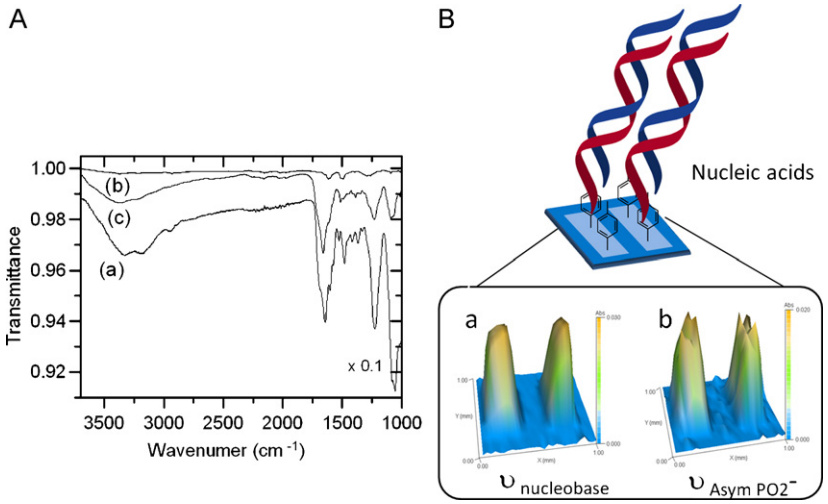

Fig. 7. (A) Grafting of DNA salmon sperm on a gold self-adhesive modified surface: (a) IR spectrum for neat DNA salmon sperm sodium salt product, (b) IR spectrum after sonication (10 min) in BPS buffer showing desorption of deposited DNA layer on PAP, (c) IR spectra after sonication (10 min) in BPS buffer showing persistence of deposited DNA layer on PDP. (B) 3D mapping of patterned-PDP layer functionalized with DNA of salmon sperm. 3D view acquired on mapping IR mode obtained by integration of the (a) 1700–1630 cm^{-1} range (nucleobase and double helical structure vibrations) and (b) the 1280–1230 cm^{-1} range (asymmetric PO_2^- stretching mode).

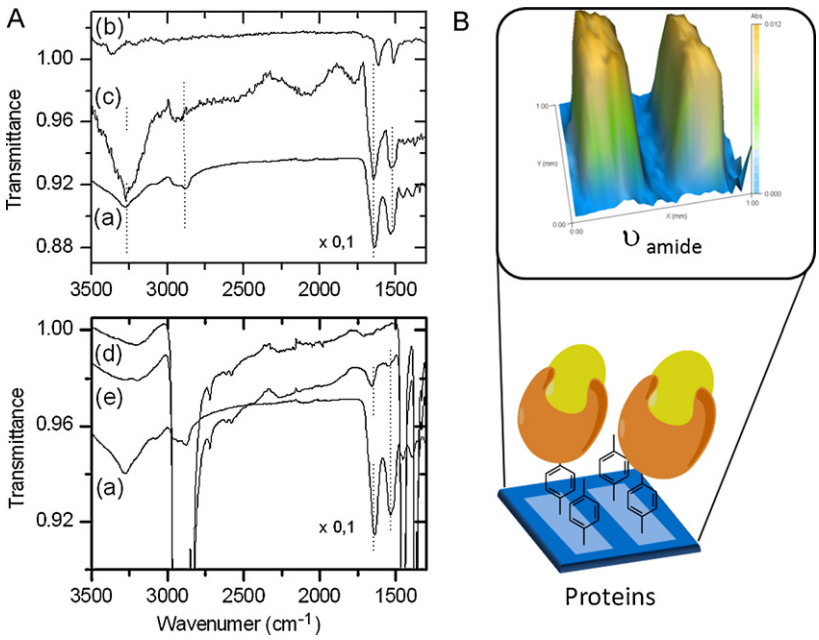

Fig. 8. (A) Grafting of GOD on gold self-adhesive modified surface (top) and on polypropylene self-adhesive modified surface (bottom): (a) IR spectrum for neat GOD product, (b) and (d) IR spectrum after sonication (10 min) in water showing desorption of deposited GOD layer on PAP, (c) and (e) IR spectrum after sonication (10 min) in water showing persistence of deposited GOD layer on PDP. (B) 3D mapping of patterned-PDP layer functionalized with glucose oxidase (GOD). 3D view acquired on mapping IR mode obtained by integration of the 1692–1635 cm^{-1} range (Amide I bond adsorption shows up at 1645 cm^{-1}).

electrochemical potential for detection, H_2O_2 electrochemical activity was calibrated in our experimental conditions by cyclic voltammetry on bare gold surface. Results are given in Fig. 9A and show the electrochemical response of 0.1 M phosphate buffer saline solution (PBS) pH 7 between −0.6 and 1.0 V vs SCE. An oxidation onset is observed at 0.9 V whereas no activity was observed in the cathodic part. When H_2O_2 was added at 3×10^{-2} M a pronounced activity both at positive and negative polarisation was noticed on

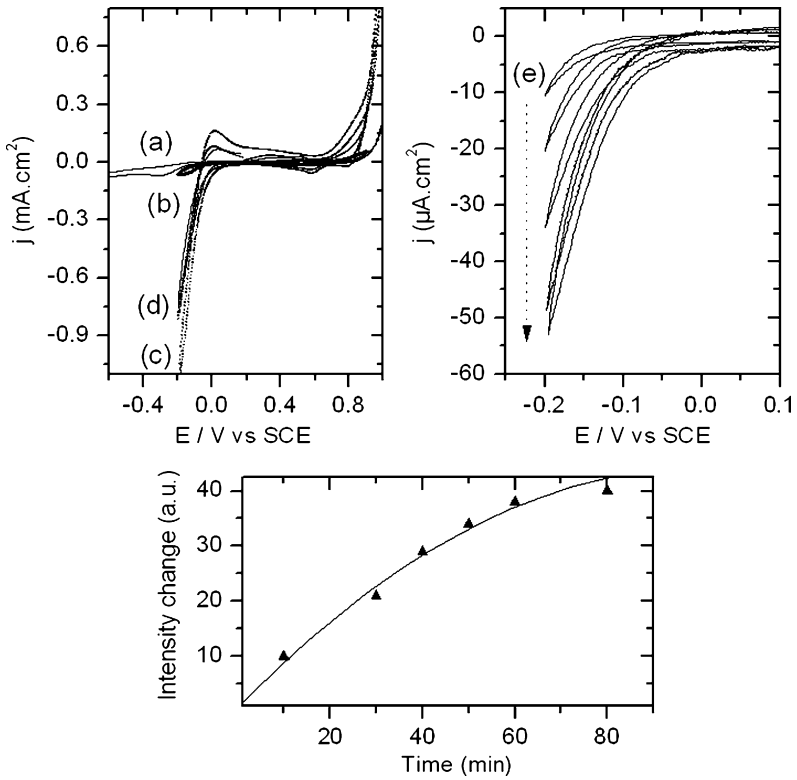

Fig. 9. (A) Cyclic voltammetry registered at 20 mV s^{-1}: (a) PBS 0.1 M solution on gold surface, (b) PBS 0.1 M and glucose 0.1 M solution on gold surface, (c) PBS 0.1 M and H_2O_2 3×10^{-2} M solution on gold surface, (d) PBS 0.1 M and H_2O_2 3×10^{-2} M solution on gold PAP modified surface. (e) Cyclic voltammetry registered at 20 mV s^{-1} during time, measured on glucose oxidase grafted PDP modified gold surface with addition of 7.69×10^{-3} M of glucose in 0.1 M PBS buffer. (B) Kinetic activity of a GOD modified gold electrode represented by the variation of intensity of the generated H_2O_2 electrochemically detected during time when glucose was added in cell. The initial rate of H_2O_2 production follows pseudo-first order appearance kinetics. First order rate constant k_{obs} is 0.016 ± 0.003 a.u./min and intensity of current density change is 59.4 ± 7.7 a.u.

the raw gold surface and on the PAP modified gold surface (Fig. 9A). The cathodic side was preferred because of its flat shape which is favourable to detect a very small quantity of generated H_2O_2. Furthermore, in the potential range of H_2O_2, no glucose electrochemical activity was measured (Fig. 9A).

$$\text{Current density}\,(t) = \text{Current density}_{\max}(1 - \exp(-k_{\text{obs}}t)) \quad (1)$$

A solution of glucose at 7.69×10^{-3} M was added to a cell containing PBS and GOD modified gold electrode. Voltammetry was carried out at different delay times. For clarity, only a few curves registered with glucose are reported in Fig. 9A. In agreement with minimal quantities of biological immobilized material usually used in microarray format, Faradic currents remain in the microampere range. However the rise with delay time of the H_2O_2 electrochemical activity was clearly observed in Fig. 9A. The initial rate of glucose hydrolysis or H_2O_2 appearance was monitored by the increase in current density during time. The change observed in the intensity of H_2O_2 reduction peak can be used to characterize enzyme activity. First order rate constant, k_{obs}, was determined from the progress curve of H_2O_2 appearance (Fig. 9B) by fitting the current density; time data points to Eq. (1). The initial rate of H_2O_2 production follows pseudo-first order appearance kinetics. First order rate constant k_{obs} is 0.016 ± 0.003 a.u./min and intensity of current density change is 59.4 ± 7.7 a.u. This first rate constant is consistent with the literature data (0.012 a.u./min) in solution conditions [46]. These results highlight that grafting by PDP layers did not alter the activity of GOD and therefore its three-dimensional structure.

4. Conclusion

The need for multianalyte chem/biosensors can be met by using a robust surface chemistry that allows the selective patterning of conducting or insulating materials with diverse biomolecules as proteins or nucleic acids. We have shown that material modifications by diazonium chemical grafting lead to a spontaneous adhesive primer which can be patterned by cheap and easy methods as ink or UV masking. Activation and surface modification by biomolecules takes place within few minutes and without harsh chemical conditions. A proof of concept for the covalently immobilization of biological models as low molecular weight DNA and glucose oxidase was performed. Because of the narrow range of operation of the biomolecules, we have studied the stability of self-adhesive surfaces under a pH 7 ± 1. Results show a decrease kinetic of diazonium amount compatible with the immobilization time of biomolecules. No effect of this new immobilization method on biological activity of glucose oxidase was found. This "universal toolset" provides a powerful alternative for the development of bioelectronic devices and biosensors.

References

[1] F. Rusmini, Z.Y. Zhong, J. Feijen, Protein immobilization strategies for protein biochips, Biomacromolecules 8 (2007) 1775.
[2] R. Mukhopadhyay, The versatility of microarrayers, Anal. Chem. 78 (2006) 5969.
[3] K.A. Heyries, C.A. Mandon, L. Ceriotti, J. Ponti, P. Colpo, L.J. Blum, C.A. Marquette, Macromolecules to PDMS transfer as a general route for PDMS biochips, in: International Workshop on GPCRs, Elsevier Advanced Technology, Elsevier, Berlin, 2009.
[4] D. Collard, S. Takeuchi, H. Fujita, MEMS technology for nanobio research, Drug Discovery Today 13 (2008) 989.
[5] P. Jonkheijm, D. Weinrich, H. Schroder, C.M. Niemeyer, H. Waldmann, Chemical strategies for generating protein biochips, Angew. Chem. Int. Ed. 47 (2008) 9618.
[6] A. Sassolas, B.D. Leca-Bouvier, L.J. Blum, DNA biosensors and microarrays, Chem. Rev. 108 (2008) 109.
[7] S. Cagnin, M. Caraballo, C. Guiducci, P. Martini, M. Ross, M. SantaAna, D. Danley, T. West, G. Lanfranchi, Overview of electrochemical DNA biosensors: new approaches to detect the expression of life, Sensors 9 (2009) 3122.
[8] B.P. Corgier, C.A. Marquette, L.J. Blum, Diazonium–protein adducts for graphite electrode microarrays modification: direct and addressed electrochemical immobilization, J. Am. Chem. Soc. 127 (2005) 18328.
[9] M. Pellissier, D. Zigah, F. Barriere, P. Hapiot, Optimized preparation and scanning electrochemical microscopy analysis in feedback mode of glucose oxidase layers grafted onto conducting carbon surfaces, Langmuir 24 (2008) 9089.
[10] B.P. Corgier, C.A. Marquette, D. Juncker, Microfabricated electrochemical probe for the rapid detection of proteins released by cells, in: Proceedings of the 35th Annual Northeast Bioengineering Conference, IEEE, Cambridge, 2009.
[11] R.E. Fernandez, E. Bhattacharya, A. Chadha, Covalent immobilization of *Pseudomonas cepacia* lipase on semiconducting materials, Appl. Surf. Sci. 254 (2008) 4512.
[12] F. Vianello, L. Zennaro, A. Rigo, Microfabricated electrochemical probe for the rapid detection of proteins released by cells, Biosens. Bioelectron. 22 (2007) 2694.
[13] M. Darder, K. Takada, F. Pariente, E. Lorenzo, H.D. Abruna, Dithiobissuccinimidyl propionate as an anchor for assembling peroxidases at electrodes surfaces and its application in a H_2O_2 biosensor, Anal. Chem. 71 (1999) 5530.
[14] S. Cosnier, Biomolecule immobilization on electrode surfaces by entrapment or attachment to electrochemically polymerized films. A review, Biosens. Bioelectron. 14 (1999) 443.
[15] T. Livache, E. Maillart, N. Lassalle, P. Mailley, B. Corso, P. Guedon, A. Roget, Y. Levy, Polypyrrole based DNA hybridization assays: study of label free detection processes versus fluorescence on microchips, J. Pharmaceut. Biomed. 32 (2003) 687.
[16] C.R. Toh, T.A. Fraterman, D.A. Walker, R.C. Bailey, Direct biophotolithographic method for generating substrates with multiple overlapping biomolecular patterns and gradients, Langmuir 25 (2009) 8894.
[17] C.B. Herbert, T.L. McLernon, C.L. Hypolite, D.A. Adams, L. Pikus, C.C. Huang, G.B. Fields, P.C. Letourneau, M.D. Distefano, W.S. Hu, Micropatterning gradients and controlling surface densities of photoactivatable biomolecules on self-assembled monolayers of oligo(ethylene glycol) alkanethiolates, Chem. Biol. 4 (1997) 731.
[18] R. Polsky, J.C. Harper, D.R. Wheeler, S.M. Dirk, D.C. Arango, S.M. Brozik, Electrically addressable diazonium-functionalized antibodies for multianalyte electrochemical sensor applications, Biosens. Bioelectron. 23 (2008) 757.
[19] J.J. Gooding, Advances in interfacial design for electrochemical biosensors and sensors: aryl diazonium salts for modifying carbon and metal electrodes, Electroanalysis 20 (2008) 573.
[20] J.C. Harper, R. Polsky, D.R. Wheeler, S.M. Brozik, Maleimide-activated aryl diazonium salts for electrode surface functionalization with biological and redox-active molecules, Langmuir 24 (2008) 2206.
[21] R. Polsky, J.C. Harper, S.M. Dirk, D.C. Arango, D.R. Wheeler, S.M. Brozik, Diazonium-functionalized horseradish peroxidase immobilized via addressable electrodeposition: direct electron transfer and electrochemical detection, Langmuir 23 (2007) 364.
[22] J. Wang, J.A. Carlisle, Covalent immobilization of glucose oxidase on conducting ultrananocrystalline diamond thin films, Diamond Relat. Mater. 15 (2006) 279.
[23] M.C. Liu, Y. Qi, G.H. Zhao, Carboxyphenyl covalent immobilization of heme proteins and its favorable biocompatible electrochemical and electrocatalytic characteristics, Electroanalysis 20 (2008) 900.
[24] C.A. Marquette, F. Bouteille, B.P. Corgier, A. Degiuli, L.J. Blum, Disposable screen-printed chemiluminescent biochips for the simultaneous determination of four point-of-care relevant proteins, Anal. Bioanal. Chem. 393 (2009) 1191.
[25] V. Mevellec, S. Roussel, L. Tessier, J. Chancolon, M. Mayne-L'Hermite, G. Deniau, P. Viel, S. Palacin, Grafting polymers on surfaces: a new powerful and versatile diazonium salt-based one-step process in aqueous media, Chem. Mater. 19 (2007) 6323.
[26] P. Viel, French Patent FR2929618 (2008).
[27] P. Viel, X.T. Le, V. Huc, J. Bar, A. Benedetto, A. Le Goff, A. Filoramo, D. Alamarguy, S. Noel, L. Baraton, S. Palacin, Covalent grafting onto self-adhesive surfaces based on aryldiazonium salt seed layers, J. Mater. Chem. 18 (2008) 5913.
[28] T. Berthelot, V. Huc, X.T. Le, S. Roussel, P. Viel, PCT/EP2009/053977-FR2929619 (2009).
[29] A.E. Radi, X. Munoz-Berbel, M. Cortina-Ping, J.L. Marty, Novel protocol for covalent immobilization of Horseradish peroxidase on gold electrode surface, Electroanalysis 21 (2009) 696.
[30] C. Galli, Radical reactions of arenediazonium ions: an easy entry into the chemistry of the aryl radical, Chem. Rev. 88 (1988) 765.
[31] D.S. Wulfman, Synthetic Applications of Diazonium Ions, in the Chemistry of Diazonium and Diazo Groups, Wiley, New York, 1978.
[32] H. Zollinger, Diazo Chemistry I, Aromatic and Heteroaromatic Compounds, Weinheim, 1994.
[33] J.H. Phillips, S.A. Robrish, C. Bates, High efficiency coupling of diazonium ions to proteins and amino acids, J. Biol. Chem. 240 (1965) 699.
[34] C. Combellas, M. Delamar, F. Kanoufi, J. Pinson, F.I. Podvorica, Spontaneous grafting of iron surfaces by reduction of aryldiazonium salts in acidic or neutral aqueous solution. Application to the protection of iron against corrosion, Chem. Mater. 17 (2005) 3968.
[35] H.H. Weetall, Immobilized enzymes: analytical applications, Anal. Chem. 46 (1974) 602A.
[36] J.H. Phillips, S.A. Robrish, C.H. Bates, High efficiency coupling of diazonium ions to proteins and amino acids, J. Biol. Chem. 240 (1965) 699.
[37] T. Akasaka, K. Matsuura, N. Emi, K. Kobayashi, Conjugation of plasmid DNAs with lactose via diazocoupling enhances resistance to restriction enzymes and

acquires binding affinity to galactose-specific lectin, Biochem. Biophys. Res. Commun. 260 (1999) 323.
[38] A. Chin, M.-H. Hung, L.M. Stock, Reactions of benzenediazonium ions with adenine and its derivatives, J. Org. Chem. 46 (1981) 2203.
[39] A.R. Murphy, P.S. John, D.L. Kaplan, Modification of silk fibroin using diazonium coupling chemistry and the effects on hMSC proliferation and differentiation, Biomaterials 29 (2008) 2829.
[40] R. Buchta, M. Fridkin, Introduction of the dansyl group into histidine and tyrosine residues in peptides and proteins, Biochem. Biophys. Res. Commun. 130 (1985) 350.
[41] M. Banyay, M. Sarkar, A. Graslund, A library of IR band of nucleic acids in solution, Biophys. Chem. 104 (2003) 477.
[42] M.M. Barsan, J. Klincar, M. Batic, C.M.A. Brett, Design and application of a flow cell for carbon-film based electrochemical enzyme biosensors, Talanta 71 (2007) 1893.
[43] C. Bourdillon, M. Delamar, C. Demaille, R. Hitmi, J. Moiroux, J. Pinson, Immobilization of glucose-oxidase on a carbon surface derivatized by electrochemical reduction of diazonium salts, J. Electroanal. Chem. 336 (1992) 113.
[44] R. Pauliukaite, M.E. Ghica, M. Barsan, C.M.A. Brett, Characterisation of poly(neutral red) modified carbon film electrodes; application as a redox mediator for biosensors, J. Solid State Electrochem. 11 (2007) 899.
[45] C.P. Remirez, D.J. Caruana, Immobilisation of glucose oxidase in electrodeposited copper, Electrochem. Commun. 8 (2006) 450.
[46] E.O. Odebunmi, S.O. Owalude, Kinetic and thermodynamic studies of glucose oxidase catalysed oxidation reaction of glucose, J. Appl. Sci. Environ. Manage. 11 (2007) 95.

Appendix B: Piezoelectric Self-Sensing Scanning Probe and Diazonium Salt Chemistry: a Toolset for Characterization of Proteins

J. Polesel-Maris*, J. Legrand, T. Berthelot, A. Garcia, P. Viel, S. Palacin, Tuning fork scanning probe and diazonium salt chemistry: a toolset for characterization of proteins, submitted

Tuning fork scanning probe and diazonium salt chemistry: a toolset for characterization of proteins.

By *Jérôme Polesel-Maris* [*], *Jérémy Legrand, Thomas Berthelot, Alexandre Garcia, Pascal Viel and Serge Palacin*

CEA, IRAMIS, SPCSI Chemistry of Surfaces and Interfaces Grp, F-91191, Gif-sur-Yvette, France

EMAIL ADRRESS: jerome.polesel@cea.fr

KEYWORDS: Tuning Fork, Diazonium chemistry, Proteins, AFM, Force interactions

ABSTRACT

A tuning fork AFM (Atomic Force Microscope) scanning probe has been used to study the specific chemical grafting between a functionnalized tip and BSA (Bovine Serum Albumin) protein. Specific unfolding signatures of the protein have been observed, using amplitude modulation (AM-AFM) control of the probe. Our results demonstrate the great potential of this new probe combined with the diazonium salt chemistry to analyse biological materials.

INTRODUCTION

Systems based on AFM (Atomic Force Microscope) scanning probes for force measurement open ultrafine analysis opportunities for nanomedecine and personalized diagnosis [1-4]. For instance, AFM technique allows to refine our understanding of the destabilization of proteins implied in the neurodegeneratives diseases and the mechanisms by which some molecules bind and modulate the transmembrane receivers of the cells [5]. The characterization of cell-cell interactions implied in pathologies like cancer, and also the interactions with the disease-causing agents are other research fields where the measuring instruments of force to local probes can bring answers [6]. These force nanosensors [4] allow to diagnose by recognition of specific donor-acceptors molecular interactions, with applications concerning pharmacological engineering or the detection of biomarkers in blood samples. The use of a process with AFM scanning probe for the generation and the characterization of biochips with DNA represents, as showed by the Hermann Gaub team [7], a decisive step in terms of sensitivity of diagnosis compared to the traditional techniques of amplification of the DNA. It demonstrates that single molecule is necessary to obtain a sufficient signal-to-noise ratio of a clear DNA hybridization signature.

AFM techniques have already demonstrated their capabilities to reveal the molecular structures of proteins crystals [8], or isolated proteins [9, 10] with a very light preparation of the sample to analyze. Most of the commercial AFM systems use the standard optical lever method proposed by G. Meyer et al. [11] to detect the deflection of a cantilever by means of a laser reflection on the rear side of the beam. These cantilevers are microfabricated in silicon based materials with a sharp tip of tens of nanometers radius. Beside of this AFM scheme, some scientific teams tried to implement alternative scanning probes on AFM instead of silicon cantilevers. Hence, self-sensing scanning probes have an increasing interest to characterize the matter at the nanometer scale [12-21]. F. J. Giessibl demonstrated the use of piezoelectric tuning fork scanning probes to reveal atomic resolution of materials in Ultra High vacuum [22]. Atomic handling has also recently demonstrated with this kind of probes [22]. Molecular resolution at the air/liquid interface has been performed on self assembled alkane monolayers showing very high sensitivity comparable with standard AFM cantilevered instruments [23]. For biology aims, Rensen et al. used a tuning fork probe to image cells in air but also in water [24]. Another great challenge for molecular biology is to quantify specific interaction of

proteins by AFM force spectroscopy [25] where M. Hofer et al. applied recently a tuning fork sensor in shear mode configuration to perform avidin and lysozyme antibody recognition [14].

We propose the development of an innovative chemistry between a functionalized tip of a piezoelectric tuning fork self-sensing scanning probe and proteins. These tips make it possible in biological environment to interact in a strong and specific way with biological materials. The image of a molecular harpoon allows to visualize our approach. The objective is handling and analysis by AFM spectroscopy of a BSA (Bovine Serum Albumin) [26] protein by means of a new kind of scanning probe we recently developed. The BSA with the HSA (Human Serum Albumin) proteins are the principal carriers of fatty acids and other hydrophobic molecules such as lysolecithin, bilirubin and bile salts in circulating plasma, and these proteins are also capable of binding with metals, hormones and a broad spectrum of therapeutic drugs. Studies on interactions of small molecules with these proteins have attracted much attention for understanding many biological systems, as well as immobilization of proteins in biotechnology.

The tuning fork sensor simplifies the implementation of various commercial or home-built AFM microscopes, with the possibility to fix any kind of material or shape for the tip [22]. Furthermore, the absence of any light source, compared to standard AFM systems equipped with a detection laser, can be a great advantage to study photosensitive systems in a total obscurity, and even the only alternative to characterize samples immersed in non-transparent solutions. In this work, we propose a new method to use a tuning fork scanning probe as a specific chemical interaction sensor. We take advantage of the piezoelectric tuning fork probe to fix a tip optimized for the shape but also for the materials.

EXPERIMENTAL SECTION

Chemicals. All standard chemicals and solvents were of research grade, purchased from Sigma Aldrich and used as received. *p*-Diazo-*N*,*N*-diethyl-*m*-toluidine hemi(zinc chloride) salt, 4 aminophenol and 1,4-Phenylenediamine dihydrochloride are used as received. Cathodic electrophoretic painting (GY85-0030) was purchased from BASF Coatings GmbH, Muenster, Germany. Electrically conductive silver epoxy EPO-TEK H21D glue was purchased from Epoxy Technology. 50 micrometers diameter platinum/iridium Pt90/Ir10 wire, Muscovite mica samples, 10 micrometers diameter carbon fiber and TEFLON sheet were purchased from

Goodfellow, Cambridge Ltd – Huntingdon. Acetone removable varnish (BLOCJELT Rouge) was purchased from ITW Spraytec, Asnières sur Seine, France. Iron particles were purchased from VWR (98%, mean particle size 45–100 mm). Gold substrates were obtained by successive metallic evaporation of 5 nm of chromium underlayer (BALZERS BAK600, Switzerland) and 200 nm of gold as top coat on microscopic glass slide or Muscovite mica samples. Bovine Serum Albumine (BSA) was purchased from Sigma-Aldrich and used as received.

FTIR characterization. Infrared spectra were recorded on a Bruker Vertex 70 spectrometer controlled by OPUS software. ATR mono-reflexion Pike-Miracle and Hyperion 2000 microscope accessories were implemented. The detector was for both accessories MCT working at liquid nitrogen temperature. For ATR spectra acquisition were obtained at 2 cm^{-1} resolution after 256 scans.

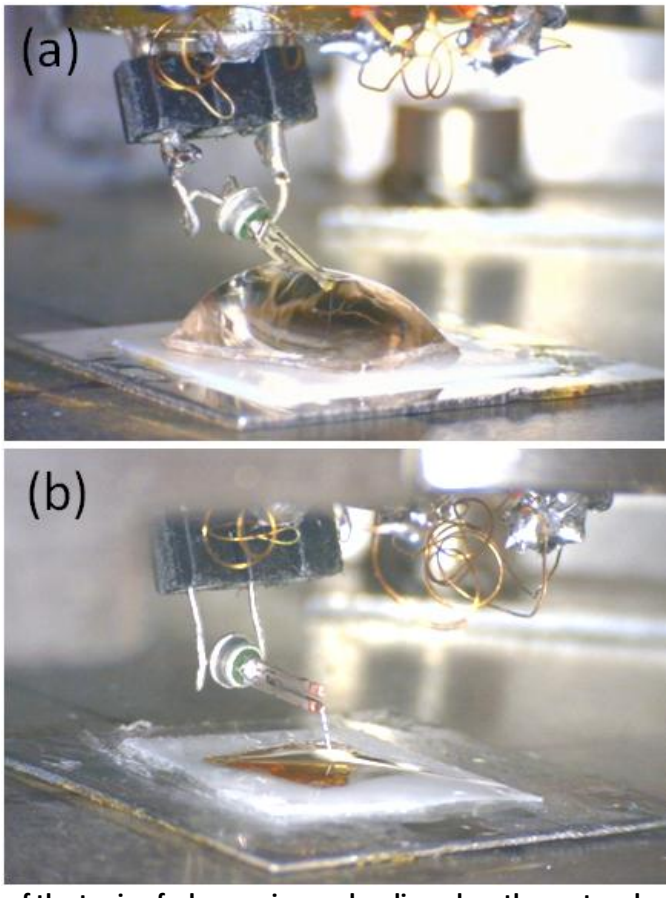

Figure 1: Close view of the tuning fork scanning probe clipped on the custom home built AFM head, and scanning the mica surface by its high aspect ratio platinum/iridium-carbon terminated tip. a) Configuration with the whole probe immersed in the buffer droplet and scanning the surface, b) configuration with only the tip kept immersed in the buffer droplet and scanning the surface.

Atomic force microscopy measurements. We used a custom home built AFM microscope to drive the tuning fork probe in AM-AFM (Amplitude Modulation AFM, also called Tapping AFM) mode to approach and scan the surface (Figure 1). As depicted in **Figure 1**; the probe is clipped by a holder to the piezotube scanner (PT130.24, Physik Instrumente (PI) GmbH, Karlsruhe, Germany) of our custom home built AFM. The piezotube scanner control is performed via a home built XYZ high voltage amplifier driven by the RC4 and SC4 modules of the SPM controller from NANONIS-SPECS [27]. The stepper motor (VEXTA PX245M-03AA, Interinar Electronics LLC) of our AFM is also driven by the same SPM controller to do the auto approach of the probe to the surface. During operation, the tuning fork probe's oscillation is maintained at constant excitation and is electrically excited at its free resonance frequency. The amplitude and the phase shift during approach/withdrawn spectroscopy curves are demodulated by the OC4 lock-in amplifier of the SPM controller from NANONIS-SPECS [27]. All the AFM spectroscopy measurements were realized in buffer solution composed of Tris(hydroxymethyl)aminomethan (TRIS at 10mM, KCl at 10mM and $MgCl_2$ at 10mM, with a pH of 8.2. For each point of the amplitude and phase approach curves, a series of five to ten acquisitions were performed using the same experimental conditions but in different locations of the surface to ensure the reproducibility of the results. The approach and withdrawn speed have been swept between 30nm/s to 300nm/s.

Tuning fork scanning probe fabrication. EPSON TOYOCOM C-001R tuning fork quartz resonators (EPSON Europe Electronics GmbH, Munich, Germany) with a free resonance frequency of 32.768 kHz and removed from their canister were used. The stiffness of the tuning fork was estimated equal to 2'161 N/m using the dimensions of the tuning fork measured under an optical microscope and using the spring constant definition introduced by Karraï et al. [28]. To work in aqueous solution, the tuning fork sensors have been coated with a cathodic electrophoretic painting diluted at 40% in MilliQ water. The tuning fork was first cleaned in an ultrasonic bath in isopropanol followed by MilliQ water rinsing and dried under nitrogen. Then, the electrophoretic coating of the sensor was performed using a very slow voltage ramp (3.4 Volt/minute) from 0 to 17 Volts. After an annealing at 140°C during 15 minutes, we performed another time the same process. This procedure allows to obtain a thin passivation layer on the tuning fork electrodes and it avoids a meniscus polymerization between the prongs, that can dramatically reduces the oscillation performance of the resonator. Electrically conductive silver epoxy EPO-TEK H21D glue has been used to fix the

platinum/iridium wire to one tuning fork prong with a curing temperature of 100°C during 45 minutes. The same glue has been also added to the other prong to compensate the tip weight which allows to increase the quality factor [29].

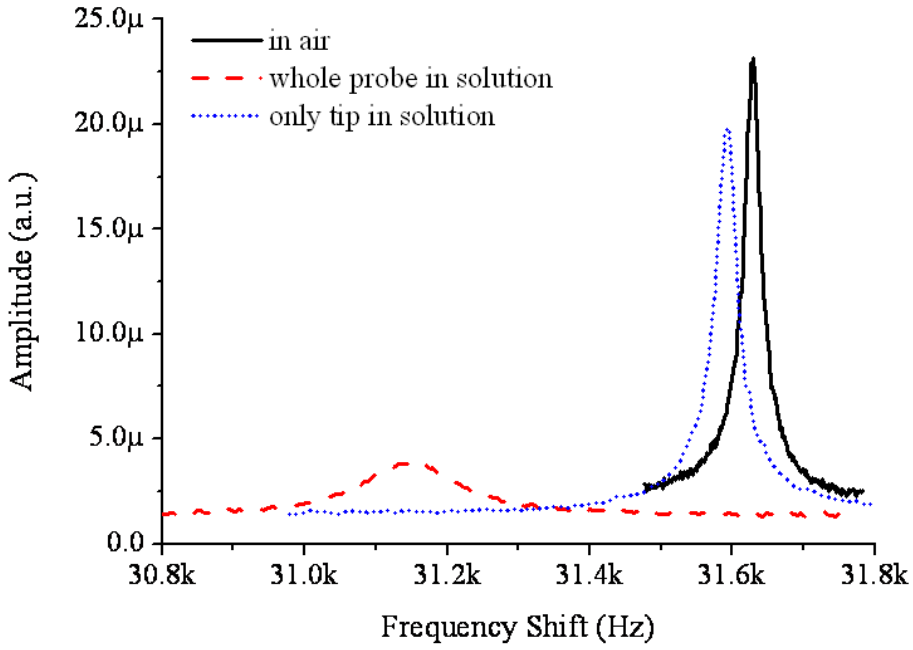

Figure 2: Resonance curves obtained for three different configurations of the tuning fork probe: in air (black filled curve), only the tip immersed in the buffer droplet as depicted on figure 1b) (blue dotted curve), and the whole tuning fork scanning probe immersed in the buffer droplet as depicted on figure 1a) (red dashed curve).

Quality factor in the order of 1'800 was routinely obtained after mass compensation, and frequency detuning of the resonance towards the low frequencies due to the added mass of the tip is also observed around 31.63 kHz in air (**Figure 2**). For the tip, a 50 micrometers diameter platinum/iridium Pt90/Ir10 wire was glued to one free prong of the tuning fork's end (**Figure 3a)**). The wire was electrochemically cut to the dimension of 1.5 to 2 mm long in a $CaCl_2$ aqueous solution [30]. Then, a 10 micrometers diameter carbon fiber was glued with the EPO-TEK H21D at the end of the platinum/iridium wire using two micromanipulators (Research Instruments Inc., UK). A sharp apex of the carbon tip was realized by electrochemical etching in a $NaHCO_3$ aqueous solution [30] using the reverse etching geometry proposed by M. Fotino [31] but with a carbon counterelectrode. The AC voltage applied for the electrochemical etching of the carbon tip was 16 Volts peak-to-peak amplitude with a sinusoidal waveform of 46Hz frequency. Tip radii below 1 micrometer, characterized by optical microscopy, are

routinely obtained (Figure 3b)). Subsequently, the probe was rinsed in ethanol, MilliQ water and dried under nitrogen before to be functionalized.

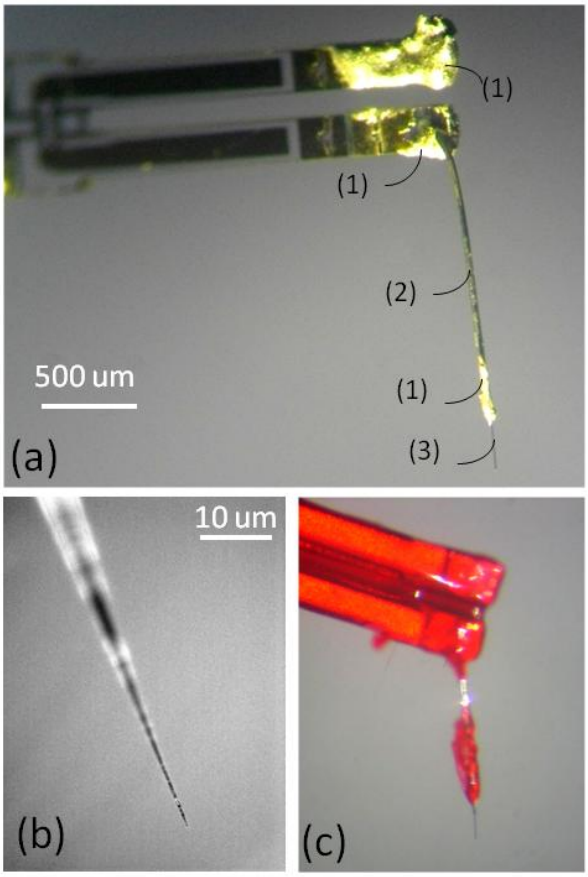

Figure 3: Views of prepared tuning fork scanning probe for approach/withdrawn amplitude and phase spectroscopy. a) General view of the complete probe with the platinum/iridium wire (2) glued (1) on the tuning fork prong. The carbon tip (3) is glued (1) at the end of the platinum/iridium wire (2). For the mass compensation, a drop of glue (1) is also put on the opposite prong of the tuning fork. b) Close view of the carbon tip end after electrochemical etching. c) View of the tuning fork probe tip area covered by a varnish coating to prevent any attack of the glue or electrode corrosion during the chemical functionnalization of the carbon tip.

Tip functionnalization materials. In order to protect the tuning fork probe from the reactive bath used for the functionalization by diazonium salts of the carbon tip, an acetone removable varnish was manually deposited on the tuning fork body and also on the glued areas as illustrated on **figure 3c)**. Two different methods were used to functionalize the carbon tip (**Scheme 1**): Method (A) based on the *in situ* synthesis of diazonium salts from a precursor followed by their reduction in solution and method (B) based on the reduction in solution of commercial diazonium salts. For each experiment, an Au/Cr coated glass slide was introduced in each reactive bath in the same time than Tuning forks functionalized with a carbon tip to check the chemical process. Each gold slides were analyzed by infrared spectroscopy.

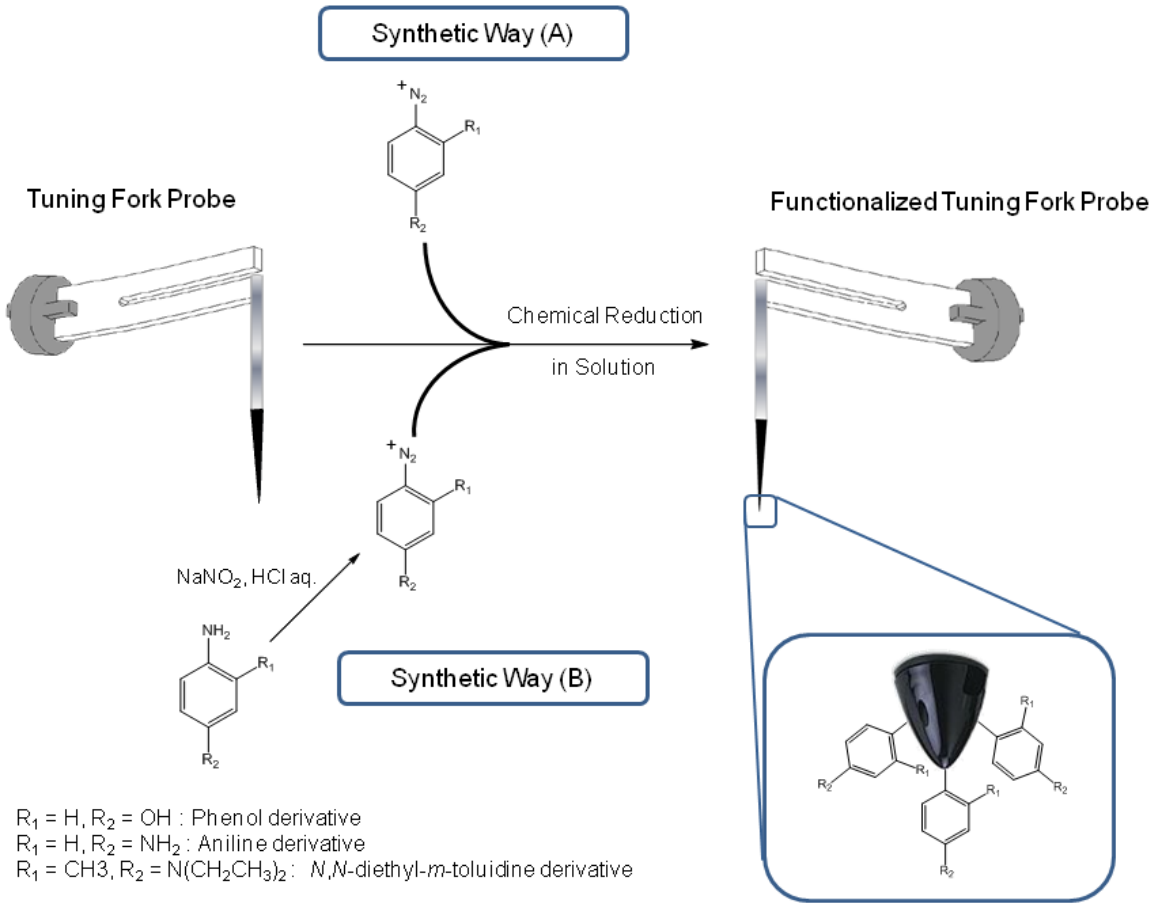

Scheme 1:

***Synthetic way (A): p*-Diazo-*N*,*N*-diethyl-*m*-toluidine hemi(zinc chloride) salt (0.294 g, 1 mmol) was dissolved in MilliQ water (20 mL) under vigourous stirring. After complete dissolution, Iron powder (200 mg) was then added to reduce the aryldiazonium salt in solution and start the overall grafting and growing chemical process. Tuning forks functionalized with a carbon tip were then introduced in the reactive bath for 15 min at room temperature. Afterwards, they were rinsed with acetone and ethanol and dried under N_2.**

***Synthetic way (B):* 4 aminophenol (1.08g, 9.96 mmol) or 1,4-Phenylenediamine dihydrochloride (1.81g, 9.96 mmol) were dissolved in a solution of HCL 0.5 N (100 mL). To 10 mL of these solutions, 10 mL of a 0.1 N $NaNO_2$ solution were added dropwise under magnetic agitation. Iron powder (200 mg) was then added to reduce the aryldiazonium salt in solution and start the overall grafting and growing chemical process. Tuning forks functionalized with a carbon tip were then introduced in the reactive bath for 15 min at 40 °C. Afterwards, they were rinsed with acetone and ethanol and dried under N_2.**

Surface functionnalization materials. Muscovite mica samples were cut in squares of 1cm², cleaved and gold coated by pulverisation in a vacuum chamber. According to the process summarized here and detailed in previous papers [32-34], addition of sodium nitrite (1 eq.) to an acidic solution (HCl 0.25 N) of *p*-phenylenediamine followed by addition of iron powder (200 mg) start the overall grafting and growing chemical process. Then gold coated micas were introduced and left in the solution for 15 min at 40°C. Afterwards, samples were rinsed with

deionized water and acetone in an ultrasonic bath for 5 min. The resulting polyaminophenylene (PAP) film on gold coated mica was analyzed by ATR FTIR. The diazotisation of the grafted PAP layer on substrates was performed in aqueous medium. The PAP layer was soaked 60 sec with acidic nitrite sodium solution in the same way that the first diazotisation, rinsed with dry acetone then finally dried with a flow of nitrogen. Diazotisation of PAP layer was confirmed by ATR FTIR spectra. 200 µl of a solution of 0.9 mM Bovine Serum Albumin (BSA) in MilliQ water was deposited on the activated mica and after 15 min, the resulting sample was rinsed with a 10 mM TRIS solution. Surface grafting of BSA was confirmed by infrared spectroscopy.

Sample preparation. BSA coated mica pieces are glued on a TEFLON surface clamped on stainless steel holders specially designed to fit to our custom home built AFM (**Figure 1**). The hydrophobic TEFLON area is larger than the mica sample area to confine the buffer droplet and avoiding liquid leakages [35]. LOCTITE 770 polyolefin primer combined with the LOCTITE 406 glue allows to obtain a good adhesion of the mica on TEFLON.

RESULTS AND DISCUSSIONS

AFM spectroscopy was used in this study to reveal the physiochemical interactions of proteins during adhesion to various substrates. Measurements involved two preliminary chemical immobilizing steps: 1) proteins immobilization on surface, and 2) grafting of a specific chemical function on tips of the AFM tuning fork probe, which were then used to probe substrates of interest in physiological buffer.

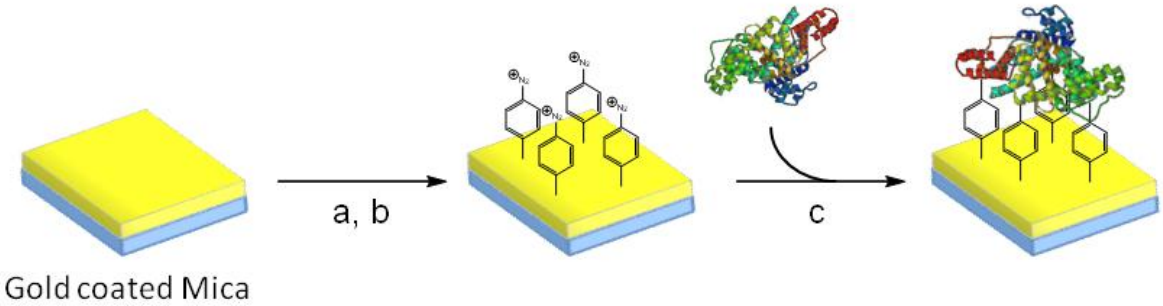

Scheme 2: Chemical functionalization of gold coated mica by GrafFast© process and BSA immobilization on activated surface. a) 1,4 phenylenediamine dihydrochloride, $NaNO_2$, HCl 0.25N, Iron powder, 15 min., 40°C. b) $NaNO_2$, HCl 0.25N, 60 s rt. c) BSA in MilliQ water r.t.

Protein Immobilization on surface and Characterization by FTIR. In previous works [32-34], we have described an innovative synthetic way to covalently graft biomolecules as proteins or nucleic acids on any kind of surface without conventional chemical activation and without release of side products. We used this process based on aryldiazonium salt chemistry to graft in random orientations Bovine Serum Albumin on gold coated mica as depicted in **Scheme 2**. Resulting BSA functionalized micas were analyzed by ATR FTIR and amide bonds of BSA were observed at 1655 and 1540 cm^{-1} (Figure 4).

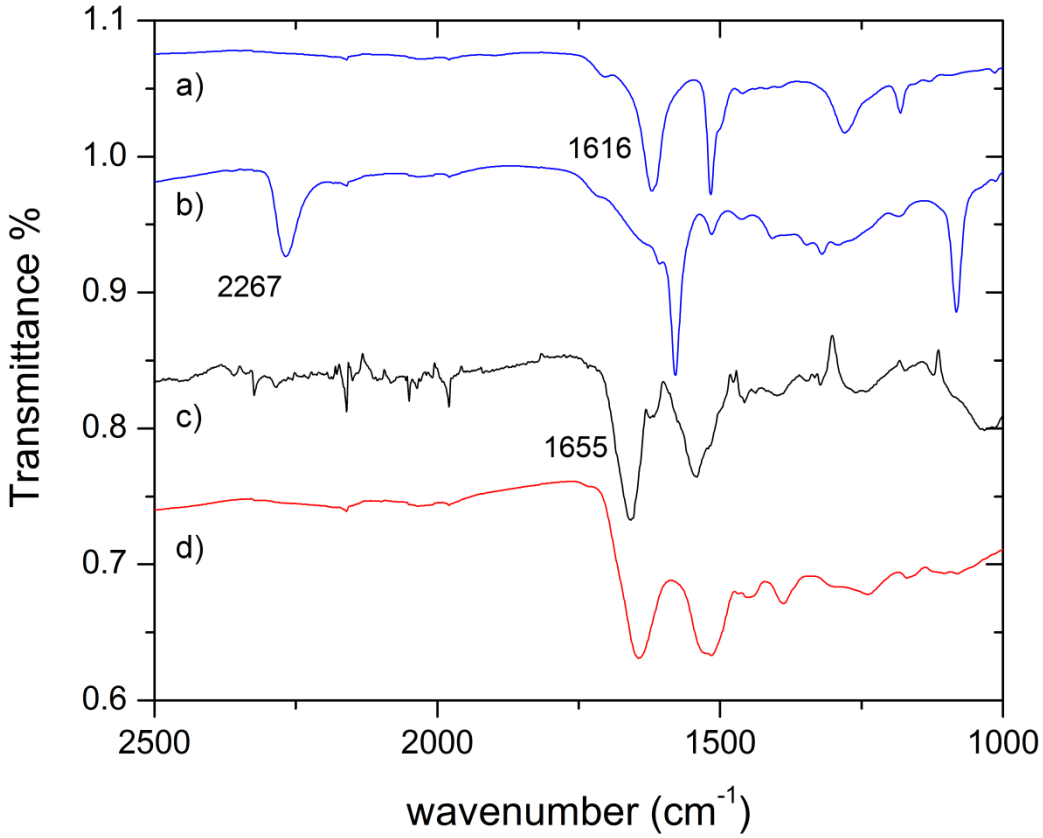

Figure 4: **ATR FTIR spectra of a) PAP layer on gold coated mica (NH_2 vibrational band 1616 cm^{-1}), b) rediazotization of PAP layer on gold coated mica (diazonium vibrational band 2267 cm^{-1}) obtained on a gold coated mica surface, c) BSA grafting on activated surface (Amide I vibrational band 1655 cm^{-1}) and d) IR spectrum of neat BSA product.**

Tip functionnalization. Currently, functionalized tips for conventional AFM are based i) on silane chemistry for silicone tips [36] or ii) on thiol layer on gold coated tips [37]. These strategies present a major drawback: the chemistry used for tip functionalization depends on the surface nature. To overcome this drawback, we focused our chemical approach on a versatile surface chemistry developed in our team and named GraftFast© [38, 39] to

functionalize in a one-step procedure a wide range of tips. By this process based on diazonium salt chemistry, we create a covalent and stable bond between the tip surface and the organic layer. To reach this goal, we applied our process, named GraftFast© [38, 39], based on a chemical reduction in solution of aryldiazonium salt to modify any kind of surfaces and a long Pt/Ir tip terminated with a short carbon tip end as depicted on figure 3a). This combined tip insures a sufficient mechanical stiffness avoiding the bending of the tip during the immersion in the droplet as illustrated on figure 1. It is well known that aryldiazonium salts react with carbon materials to create a covalent C-C bond [40-44]. The carbon tips were functionalized with *p*-diazo-*N*,*N*-diethyl-*m*-toluidine, 4-diazo-phenol and 1-diazo-,4-Phenyleneamine hydrochloride regarding to protocols previously published to afford different tips bearing hydroxyl, amino or methyl groups. In order to protect the tuning fork of surface modification and mass uptake which can alter the resonance frequency and quality factor, an acetone removable varnish was manually deposited on the tuning fork body and also on the glued areas as illustrated on figure 3c). Because of high absorption of carbon materials, ATR FTIR analysis of carbon tips cannot be done. To overcome this drawback, we performed ATR FTIR analyses on gold glass slide substrates introduced at the same time as functionalized tuning fork by carbon tip. These indirect analyses allow us to inform us about the bath reactivity and on the subsequent surface modification.

AFM amplitude and phase spectroscopy. To characterize the chemical interaction behaviour on the proteins coated mica surface, we performed dynamical AFM spectroscopy and recorded simultaneously the amplitude and phase signals during the approach of the tip in the surface. The oscillation amplitude is modified by the constant excitation driving voltage injected in the probe and by the surface forces acting on the tip end. Also, the surface forces probed by the tip induce a phase shift between the sinusoidal excitation waveform and the response of the tuning fork probe. This produces the phase curves giving information about the chemical interactions with the surface, but also the elastic and viscoelastic properties of the surface materials.

For all the AFM spectroscopy measurements shown in this work, we privilege the configuration with the tip only immersed in the buffer solution rather than the complete probe immersed to keep the highest quality factor as illustrated on the resonance curves of figure 2. The higher is the quality factor, the higher is the detection sensitivity of the probe during AFM

spectroscopy operation. When the tip is only immersed in the solution, we find quality factor of 1'200, to compare with the complete probe immersed in the buffer with a quality factor of 304.

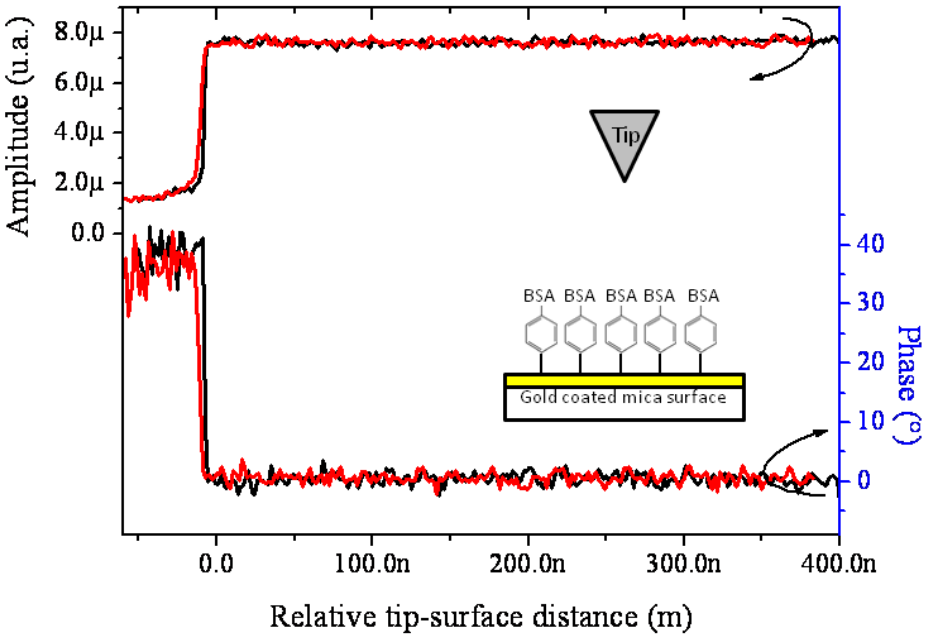

Figure 5: **Approach/withdrawn amplitude and phase spectroscopy result with a non-functionnalized carbon tip on a gold coated mica surface with grafted BSA proteins.**

Figure 5 displays spectroscopy curves obtained with clean carbon tip onto the BSA grafted surface. Approach (black curves) and withdrawn (red curves) curves show three distinct domains as the oscillating probe penetrates the surface. In the first domain, the tip is far from the surface with a constant amplitude oscillation and a phase shift equal to zero. In a second domain, the tip is very close to the surface with a fast decreasing of the oscillation amplitude, and an increasing of the phase shift due to a net repulsive interaction of the tip with surface. In the third domain, the hard compression of the tip to the surface stops the oscillation amplitude with a low residual plateau value corresponding to the detection noise level of the electronics. For this third domain, the phase shift curve becomes noisier and starts to decrease, because the phase shift analysis by the SPM controller is based on the oscillation signal which is stopped here. So, the phase shift signal has no significance in this domain. Based on these considerations, in the frame of this work, we consider that quantitative or qualitative analysis won't be done in the third domain of the spectroscopy curves when the oscillation amplitude is stopped. By the same, we point the reproducible behaviour of the amplitude or phase curves during the approach and the withdrawn of the tip.

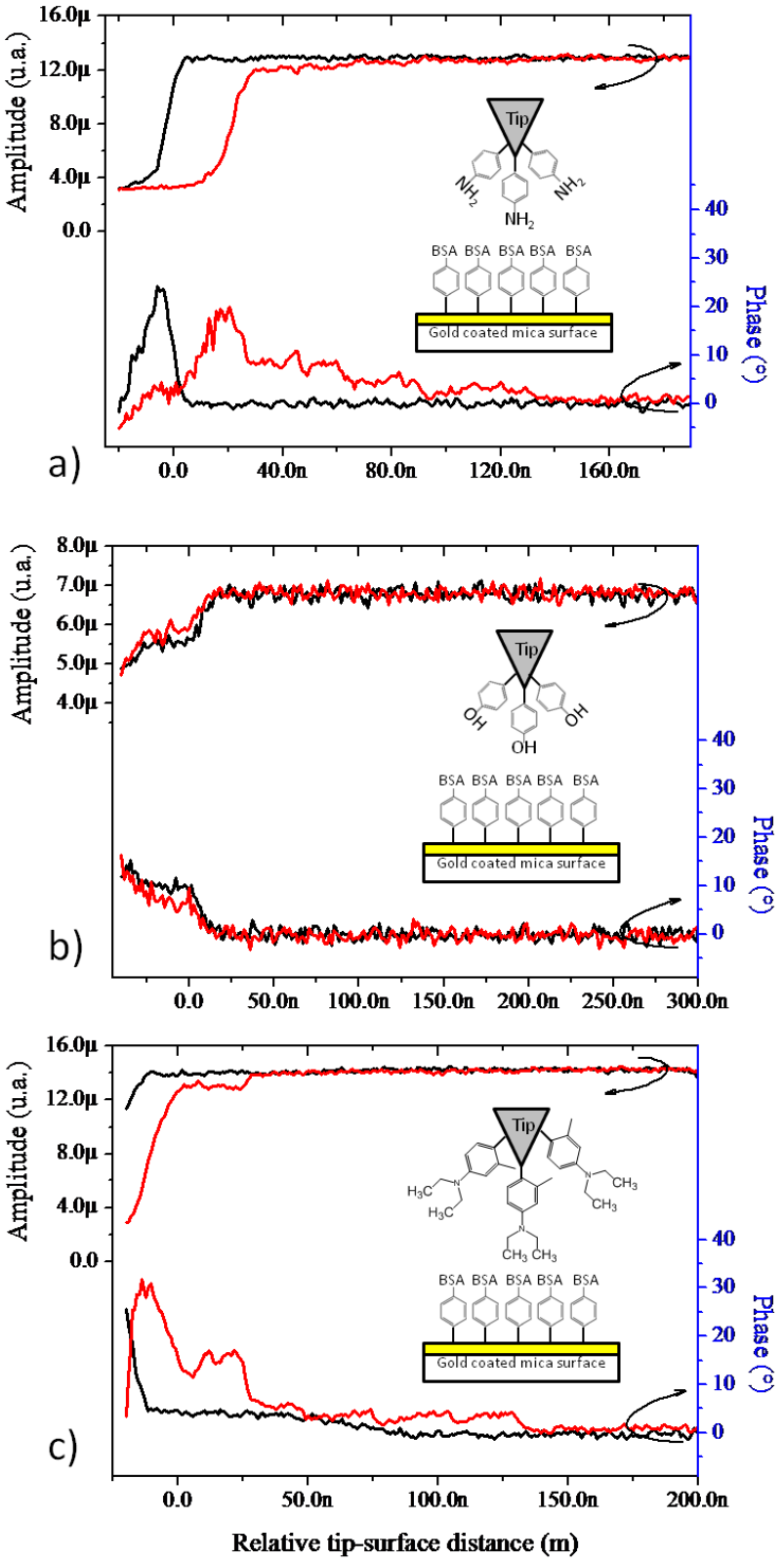

Figure 6: Approach/withdrawn amplitude and phase spectroscopy results obtained for three different functionalization of the carbon tip on a gold coated mica surface with grafted BSA proteins: a) amine terminated tip, b) hydroxyl terminated tip and c) methyl terminated tip.

Different approach and withdrawn spectroscopy curves in amplitude and phase using the three different kind of chemically terminated carbon tips have been performed on the same BSA grafted surface used previously, as illustrated on **figure 6**. The approach curves topology is similar for amine and methyl terminated tips to the case of the clean carbon tip of **figure 5**. The reduction of the oscillation amplitude and the increasing of the phase shift value, due to the tip compression on the surface, are also illustrated for the hydroxyl terminated tip but with a short plateau region during the tip compression. We incriminate steric interactions of the hydrophilic tip with the hydrophobic BSA proteins.

The clear signature of protein grafting is present on the withdrawn curves in amplitude and even more on the phase shift. Amine and methyl terminated tips exhibit wild changes in the first and the second domain, as defined previously, and four to five pulloff plateaux appeared clearly in the phase curve before the probe returns to the original oscillation amplitude far from the surface with a phase shift equal to zero. That is the revealing of strong interactions between the functionalized tip and the proteins fixed on the surface. The retraction portion of the curve highlights the pulloff force or the force required to break short-range (van der Waals or hydrophobic) interactions or specific binding events. The almost equal magnitude pulloff forces for amine and methyl terminated tips on BSA was already showed by M. S. Wang et al. [45], but for the case of standard cantilevered AFM with optical lever detection. The withdrawn curve of the phenol terminated tip shows also changes compare to the approach curve but only in the second domain. The hydroxyl chemical interaction with BSA in the buffer solution appears weak compare to amine or methyl interaction. Considering the hydrophobic sites on BSA [26], in the buffer solution of pH=8.2, it appears a reasonable assumption that the CH_3 and NH_2 terminated tips would have strong *hydrophobic-hydrophobic* interactions with the hydrophobic binding sites of BSA. In the case of the hydrophilic phenol terminated tip, the presence of the phenyl group above the hydroxyl termination could explain the weak grafting observed on the withdrawn AFM curves, due to aromatic interactions some amino acids of BSA. We can note that the presence of cations (K^+, Mg^{2+}) in the buffer solution used in this work could have an influence to inhibit these aromatic interactions by cations-π interactions.

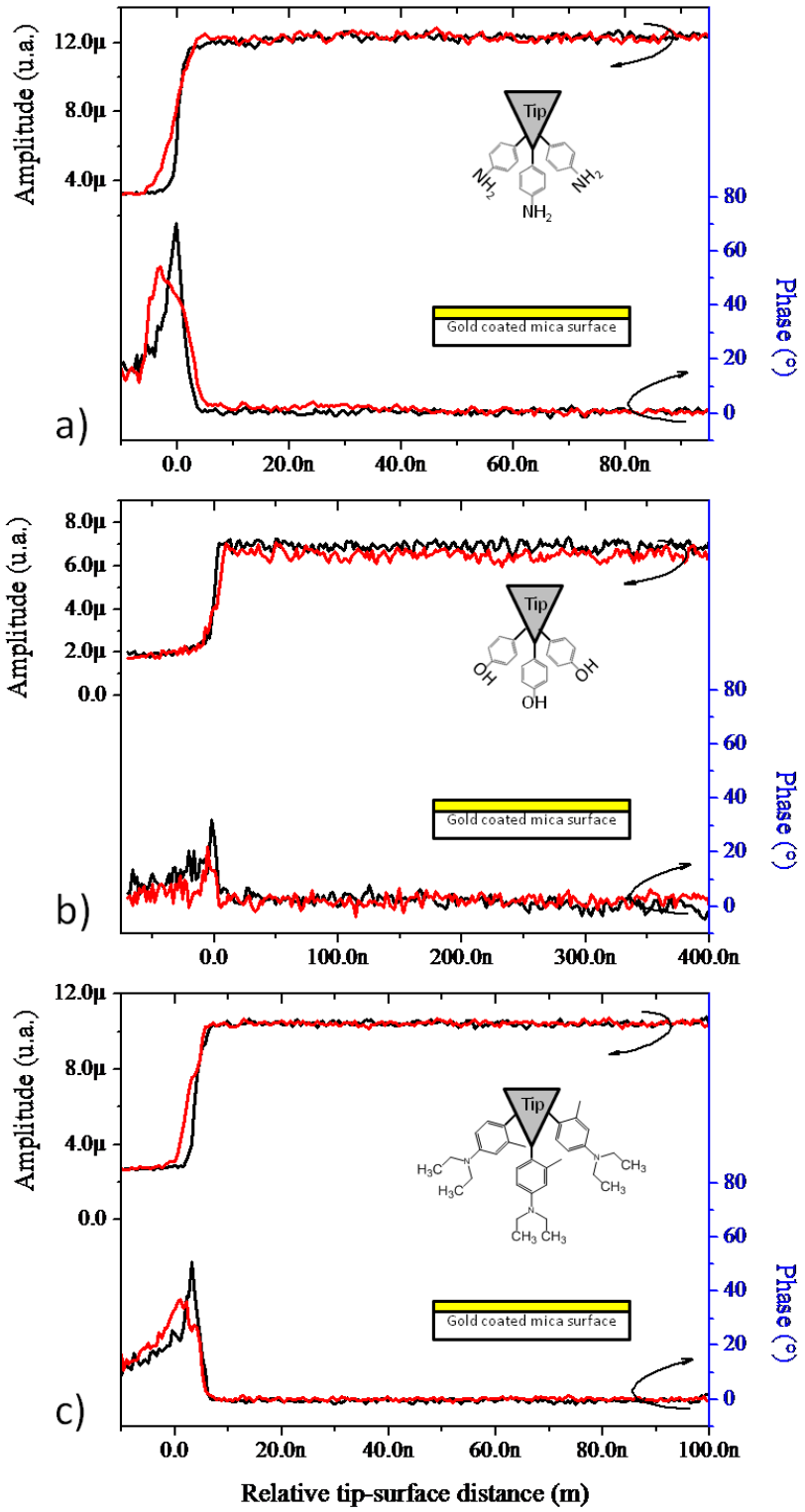

Figure 7: **Approach/withdrawn amplitude and phase spectroscopy results obtained for three different functionalization of the carbon tip on a clean gold coated mica surface: a) amine terminated tip, b) hydroxyl terminated tip and c) methyl terminated tip.**

Reference measurements of approach and withdrawn spectroscopy curves in amplitude and phase using the three different kind of chemically terminated carbon tips have been realized but on a clean gold coated mica surface, as depicted on Figure 7. The curves exhibit standard amplitude and phase shift behaviour as the tip goes to the surface as for curves of figure 5, without signature of specific grafting in the withdrawn curves. The combination of the spectroscopy reference tests of figure 5 and figure 7 allow us to confirm that the specific interaction detected on the withdraw spectroscopy curves of figure 6 are due to interaction between chemical function grafted on the tip end to BSA protein hydrophobic sites.

CONCLUSION

The goal of this work was to demonstrate the application of a non conventional chemistry to functionalize an AFM scanning probe. Furthermore, we used piezoelectric self-sensing scanning probe to provide detailed information about interactions of small molecules with proteins. Specifically, the AFM spectroscopy can provide unique information on the magnitude of adhesion forces that can be used to guide the development of adhesion resistant materials, to analyze protein patterned biochips… In this sense, we consider that this work can contribute to the development of a new kind of protein nanosensors with strong implications for molecular diagnosis or nanomedecine aims.

Acknowledgements:

We are indebted to Carlos Caldas, François Thoyer, Christophe Lubin and Sylvain Foucquart concerning the mechanical design and preamplifier electronics fabrication of the custom home built AFM microscope. We acknowledge Ali Makky, Jacques Cousty, and Laurent Pham Van for fruitful discussions. This work has been financially supported by the Region Ile-de-France in the framework of C'Nano IdF. C'Nano IdF is the nanoscience competence center of Paris Region, supported by CNRS, CEA, MESR and Region Ile-de-France.

REFERENCES

1. Eaton, M. *Nat. Mater.* **2007,** *6*, 251-253.

2. Engel, A.; Lyubchenko, Y.; Muller, D. *Trends Cell Biol.* **1999,** *9*, 77-80.

3. Hood, L.; Heath, J. R.; Phelps, M. E.; Lin, B. Y. *Science* **2004,** *306*, 640-643.

4. Muller, D. J.; Dufrene, Y. F. *Nat. Nanotechnol.* **2008,** *3*, 261-269.

5. Muller, D. J. *Biochemistry* **2008,** *47*, 7986-7998.

6. Cross, S. E.; Jin, Y.-S.; Rao, J.; Gimzewski, J. K. *Nat. Nanotechnol.* **2007,** *2*, 780-783.

7. Kufer, S. K.; Puchner, E. M.; Gumpp, H.; Liedl, T.; Gaub, H. E. *Science* **2008,** *319*, 594-596.

8. Möller, C.; Allen, M.; Elings, V.; Engel, A.; Müller, D. J. *Biophys. J.* **1999,** *77*, 1150-1158.

9. San Paulo, A.; García, R. *Biophys. J.* **2000,** *78*, 1599-1605.

10. Thomson, N. H. *Ultramicroscopy* **2005,** *105*, 103-110.

11. Meyer, G.; Amer, N. M. *Appl. Phys. Lett.* **1988,** *53*, 1045-1047.

12. Arlett, J. L.; Maloney, J. R.; Gudlewski, B.; Muluneh, M.; Roukes, M. L. *Nano Lett.* **2006,** *6*, 1000-1006.

13. Higuchi, S.; Kuramochi, H.; Kubo, O.; Masuda, S.; Shingaya, Y.; Aono, M.; Nakayama, T. *Rev. Sci. Instrum.* **2011,** *82*, 043701.

14. Hofer, M.; Adamsmaier, S.; van Zanten, T. S.; Chtcheglova, L. A.; Manzo, C.; Duman, M.; Mayer, B.; Ebner, A.; Moertelmaier, M.; Kada, G.; Garcia-Parajo, M. F.; Hinterdorfer, P.; Kienberger, F. *Ultramicroscopy* **2010,** *110*, 605-611.

15. Koopman, M.; de Bakker, B. I.; Garcia-Parajo, M. F.; van Hulst, N. F. *Appl. Phys. Lett.* **2003,** *83*, 5083-5085.

16. Macpherson, J. V.; Unwin, P. R. *Eur. Biophys. J.* **2000,** *29*, 385.

17. Polesel-Maris, J.; Aeschimann, L.; Meister, A.; Ischer, R.; Bernard, E.; Akiyama, T.; Giazzon, M.; Niedermann, P.; Staufer, U.; Pugin, R.; de Rooij, N. F.; Vettiger, P.; Heinzelmann, H. *J. Phys. Conf. Ser.* **2007,** *61*, 955-9.

18. Polesel-Maris, J.; Lubin, C.; Thoyer, F.; Cousty, J. *J. Appl. Phys.* **2011,** *109*, 074320.

19. Rogers, B.; Sulchek, T.; Murray, K.; York, D.; Jones, M.; Manning, L.; Malekos, S.; Beneschott, B.; Adams, J. D.; Cavazos, H.; Minne, S. C. *Rev. Sci. Instrum.* **2003,** *74*, 4683-4686.

20. Trevethan, T.; Watkins, M.; Shluger, A. L.; Polesel-Maris, J.; Gauthier, S.; Kantorovich, L. N. *Nanotechnology* **2007,** *18*, 84017.

21. Zhang, J.; O'Shea, S. *Sensor Actuat. B-Chem.* **2003,** *94*, 65-72.

22. Giessibl, F. J. *Rev. Mod. Phys.* **2003,** *75*, 949-983.

23. Pham Van, L.; Kyrylyuk, V.; Polesel-Maris, J.; Thoyer, F.; Lubin, C.; Cousty, J., *Langmuir* **2009,** *25*, 639-642.

24. Rensen, W. H. J.; van Hulst, N. F.; Kammer, S. B. *Appl. Phys. Lett.* **2000,** *77*, 1557-1559.

25. Hinterdorfer, P.; Dufrene, Y. F. *Nat. Methods* **2006,** *3*, 347-355.

26. Kalpana, H. N.; Channu, B. C.; Dass, C.; Houghton, P. J.; Thimmaiah, K. N. *Proc. Indian Acad. Sci. (Chem. Sci.)* **2000,** *112*, 51-61.

27. Technoparkstrasse 1 NANONIS-SPECS Zurich GmbH, Z., Switzerland., in http://www.specszurich.com/en/SPM-Control-System.html.

28. Karraï, K.; Grober, R. D. *Ultramicroscopy* **1995,** *61*, 197-205.

29. Castellanos-Gomez, A.; Agraït, N.; Rubio-Bollinger, G. *Nanotechnology* **2009,** *20*, 215502.

30. Nam, A. J.; Teren, A.; Lusby, T. A.; Melmed, A. J. *J. Vac. Sci. Technol. B* **1995,** *13*, 56.

31. Fotino, M., *Appl. Phys. Lett.* **1992,** *60*, 2935.

32. Berthelot, T.; Deniau, G.; Huc, V.; Le Xuan, T.; Nekelson, F.; Roussel, S.; Viel, P., **2009,** PCT/EP2009/053977, (WO/2009/121944).

33. Berthelot, T.; Garcia, A.; Le, X. T.; Morsli, J. E.; Jégou, P.; Palacin, S.; Viel, P. *Appl. Surf. Sci.* **2010,** *257*, 3538-3546.

34. Viel, P.; Le, X. T.; Huc, V.; Bar, J.; Benedetto, A.; Le Goff, A.; Filoramo, A.; Alamarguy, D.; Noel, S.; Baraton, L.; Palacin, S. *J. Mater. Chem.* **2008,** *18*, 5913-5920.

35. Muller, D. J.; Engel, A. *Nat. Protocols* **2007,** *2*, 2191-2197.

36. Riener, C. K.; Stroh, C. M.; Ebner, A.; Klampfl, C.; Gall, A. A.; Romanin, C.; Lyubchenko, Y. L.; Hinterdorfer, P.; Gruber, H. J. *Anal. Chim. Acta* **2003,** *479*, 59-75.

37. Berquand, A.; Xia, N.; Castner, D. G.; Clare, B. H.; Abbott, N. L.; Dupres, V.; Adriaensen, Y.; Dufrène, Y. F. *Langmuir* **2005,** *21*, 5517-5523.

38. Mevellec, V.; Roussel, S.; Palacin, S.; Berthelot, T.; Baudin, C.; Trenggono, A.; Deniau, G. **2008,** PCT/FR2007/052556, (WO/2008/078052).

39. Mevellec, V.; Roussel, S.; Tessier, L.; Chancolon, J.; Mayne-L'Hermite, M.; Deniau, G.; Viel, P.; Palacin, S. *Chem. Mater.* **2007,** *19*, 6323-6330.

40. Baranton, S.; Bélanger, D. *J. Phys. Chem. B* **2005,** *109*, 24401-24410.

41. Garrett, D. J.; Flavel, B. S.; Shapter, J. G.; Baronian, K. H. R.; Downard, A. J. *Langmuir* **2009,** *26*, 1848-1854.

42. Kariuki, J. K.; McDermott, M. T. *Langmuir* **2001,** *17*, 5947-5951.

43. Saby, C.; Ortiz, B.; Champagne, G. Y.; Bélanger, D. *Langmuir* **1997,** *13*, 6805-6813.

44. Toupin, M.; Belanger, D. *Langmuir* **2008,** *24*, 1910-1917.

45. Wang, M. S.; Palmer, L. B.; Schwartz, J. D.; Razatos, A. *Langmuir* **2004,** *20*, 7753-7759.